



UNIVERSITÀ DI PISA  
DIPARTIMENTO DI INGEGNERIA DELL'INFORMAZIONE  
ELETTRONICA, INFORMATICA, TELECOMUNICAZIONI

**STATISTICAL ANALYSIS OF REAL  
POLARIMETRIC CLUTTER DATA AT DIFFERENT  
RANGE RESOLUTIONS**

**PART I: AVERAGE BEHAVIOR**

Fulvio Gini, Maria S. Greco

and

Muralidhar Rangaswamy\*

*\*collaborating engineer from the Air Force Research  
Laboratory*

**Pisa, April 2005**

This work has been funded by AFOSR grant FA8655-04-1-3059 on "High resolution clutter analysis and modelling for advanced target detection strategies".

**REPORT DOCUMENTATION PAGE**

Form Approved OMB No. 0704-0188

Public reporting burden for this collection of information is estimated to average 1 hour per response, including the time for reviewing instructions, searching existing data sources, gathering and maintaining the data needed, and completing and reviewing the collection of information. Send comments regarding this burden estimate or any other aspect of this collection of information, including suggestions for reducing the burden, to Department of Defense, Washington Headquarters Services, Directorate for Information Operations and Reports (0704-0188), 1215 Jefferson Davis Highway, Suite 1204, Arlington, VA 22202-4302. Respondents should be aware that notwithstanding any other provision of law, no person shall be subject to any penalty for failing to comply with a collection of information if it does not display a currently valid OMB control number.

**PLEASE DO NOT RETURN YOUR FORM TO THE ABOVE ADDRESS.**

<b>1. REPORT DATE (DD-MM-YYYY)</b> 18-11-2005			<b>2. REPORT TYPE</b> Final Report		<b>3. DATES COVERED (From – To)</b> 26 July 2004 - 26-Jul-05	
<b>4. TITLE AND SUBTITLE</b>  High Resolution Radar Clutter Analysis and Modelling for Advanced Target Detection Strategies				<b>5a. CONTRACT NUMBER</b> FA8655-04-1-3059		
				<b>5b. GRANT NUMBER</b>		
				<b>5c. PROGRAM ELEMENT NUMBER</b>		
<b>6. AUTHOR(S)</b>  Professor Fulvio Gini				<b>5d. PROJECT NUMBER</b>		
				<b>5d. TASK NUMBER</b>		
				<b>5e. WORK UNIT NUMBER</b>		
<b>7. PERFORMING ORGANIZATION NAME(S) AND ADDRESS(ES)</b> University of Pisa Via Caruso, 14 Pisa 56122 Italy				<b>8. PERFORMING ORGANIZATION REPORT NUMBER</b>  N/A		
<b>9. SPONSORING/MONITORING AGENCY NAME(S) AND ADDRESS(ES)</b>  EOARD PSC 802 BOX 14 FPO 09499-0014				<b>10. SPONSOR/MONITOR'S ACRONYM(S)</b>		
				<b>11. SPONSOR/MONITOR'S REPORT NUMBER(S)</b> Grant 04-3059		
<b>12. DISTRIBUTION/AVAILABILITY STATEMENT</b>  Approved for public release; distribution is unlimited.						
<b>13. SUPPLEMENTARY NOTES</b>  Two part report. Both reports are included in this submission for total of 188 pages						
<b>14. ABSTRACT</b>  This report results from a contract tasking University of Pisa as follows: The research is divided in two phases. In the first phase, we consider modeling and estimating the texture time/spatial variation in high resolution non-Gaussian clutter from RAR and SAR. We will investigate as well non-stationary and possible non-Gaussianity of the speckle component. The speckle distribution will be analyzed by both fitting to the data non-Gaussian distributions accounting for speckle non-Gaussianity, and by direct analysis of speckle through estimation of the I/Q ratio statistics (which decouples from the texture effects). The analyses of high resolution RAR clutter will be performed by processing complex clutter data collected in November 1993 and in winter 1998 with the high resolution IPIX radar, provided by McMaster University. The analyses of high resolution SAR clutter will be performed by processing clutter data (single-look complex) collected at Kohala Coast, Hawaii, on 1996 with the high resolution AIRSAR airborne radar platform, provided by NASA/Jet Propulsion Laboratory. An accurate characterization of the high resolution radar clutter allows a more adequate design of the radar detector of targets. This detector needs to be adaptive to the data and should have the ability to comply with the non-homogeneous nature of the clutter interference. This aspect of the problem will be discussed in a preliminary fashion in the second phase of this study. A more detailed analysis of the problem, which encompasses the design of the detector and the evaluation of its performance in operationally meaningful environment, will be tackled in a future phase of the study to be separately funded after this research.						
<b>15. SUBJECT TERMS</b> EOARD, Electromagnetics, radar, Antennas						
<b>16. SECURITY CLASSIFICATION OF:</b>			<b>17. LIMITATION OF ABSTRACT</b> UL	<b>18, NUMBER OF PAGES</b>  188	<b>19a. NAME OF RESPONSIBLE PERSON</b> MICHAEL KJ MILLIGAN, Lt Col, USAF	
<b>a. REPORT</b> UNCLAS	<b>b. ABSTRACT</b> UNCLAS	<b>c. THIS PAGE</b> UNCLAS			<b>19b. TELEPHONE NUMBER (Include area code)</b> +44 (0)20 7514 4955	



# *Abstract*

*The work developed and described in this technical report deals with the problem of providing a statistical model of the backscattering from sea surface for low-grazing angle and high resolution radar systems. Based on the electromagnetic two-scale model, we analyzed both the amplitude and frequency modulations induced on the small-scale Bragg resonant waves by the large-scale surface tilt and advection, due to the swell presence. Evidence of sea clutter non-stationarity and the relationship between the variations of clutter spectral features, like texture, Doppler centroid and bandwidth, have been investigated by processing real recorded data. The data used for the research activity have been recorded by the IPIX radar of McMaster University in Grimsby, Ontario, Canada.*

*In the first part of this technical report, we describe our statistical analyses of high-resolution polarimetric data characterized by different range resolutions (60 m, 30 m, 15 m, 9 m, 3 m), in order to highlight possible statistical differences due to changes of both resolution and polarization.*

*The second part of this technical report will be devoted to the description of the analysis of clutter non-stationarity performed by processing the same data. The relation between texture changes, spectrum bandwidth and Doppler centroid will be highlighted with the aim of proving that a hybrid AM7FM modulated process is more suitable than a stationary process to model the sea high resolution clutter.*

**Keywords:** *Radar clutter, non-Gaussian clutter, phenomenological modeling, statistical analysis, model parameter estimation, high-resolution radar, compound model.*

*This work has been funded by AFOSR grant FA8655-04-1-3059 on “High resolution clutter analysis and modeling for advanced target detection strategies.”*



# CONTENTS

<b>SECTION 1</b> .....	<b>1</b>
<b>RADAR AND DATA DESCRIPTION</b> .....	<b>1</b>
1.1 INTRODUCTION.....	1
<b>SECTION 2</b> .....	<b>4</b>
<b>STATISTICAL ANALYSIS</b> .....	<b>4</b>
2.1 INTRODUCTION .....	4
2.2.1 Range resolution of 60 m.....	7
2.2.2 Range resolution of 30 m.....	17
2.2.3 Range resolution of 15 m.....	27
2.2.4 Range resolution of 9 m.....	40
2.2.5 Range resolution of 3 m.....	54
2.3 CUMULANT DOMAIN ANALYSIS.....	70
2.4 CONCLUSIONS.....	74
<b>SECTION 3</b> .....	<b>75</b>
<b>FREQUENCY ANALYSIS</b> .....	<b>75</b>
3.1 CORRELATION ANALYSIS AND POWER SPECTRUM ESTIMATION.....	75
3.1.1 Estimation of $R_{x_i}$ and $R_{x_i x_Q}$ .....	75
3.1.2 Estimation of the texture correlation function.....	76
3.1.3 Mean range texture auto-covariance .....	108
3.2 CONCLUSIONS .....	110
<b>REFERENCES</b> .....	<b>111</b>



# Section 1

## Radar and Data Description

### 1.1 Introduction

The clutter data we processed were collected at Grimsby, Ontario, with McMaster University IPIX radar. IPIX is an experimental X-band search radar, capable of dual polarized and frequency agile operation. The characteristic features of the IPIX radar are summarized in [Far97] and in Table 1.1.

The radar site was located at east of the “Place Polonaise” at Grimsby, Ontario (Latitude 43.2114° N, Longitude 79.5985° W), looking at lake Ontario from a height of 20 m. Figure 1.1 reports the map of the area. The nearest shore on the far side of the lake is more than 20 Km away. The city on the left is Hamilton, 50 Km east of Niagara Falls.



Figure 1.1 - Map of the recording area.

The data of the OHGR database are stored in 222 files, as 10 bits integers. There are like polarizations, HH and VV (Lpol), and cross-polarizations, HV and VH (Xpol), coherent reception, leading to a quadruplet of I and Q values for Lpol and Xpol.

<b>Transmitter</b>	<b>Receiver</b>	<b>Parabolic dish antenna</b>
TWT peak power:8 Kw	2 receivers	Diameter: 2.4 m
Dual frequency simultaneous transmission: 8.9-9.4 GHz	Outputs: Linear, I and Q	Pencil beam width (azimuth resolution): 1.1°
H-V polarization, agile	Receiving polarizations: H-V	Antenna gain: 45.7 dB
Pulse width (PW): 20 ns to 5000 ns (real) 5000 ns (expanded) 32 ns (compressed)	<b>Data acquisition:</b> Sample rate from 0 to 50 MHz Outputs: Linear, I and Q	Cross polarization isolation: 30 dB
PRF: from 0 to 20 KHz	Quantization: 10 bit- up to 16 bit effective with H/W decimation	Double polarization with central feeder

**Table 1.1** - Characteristics of the radar.

In this work, we analyzed 5 files recorded on February 4 1998 at about 22.30. Unfortunately, we have no data available regarding the wind and wave observations. The operational conditions are summarized in Tables 1.2 and 1.3.

It is important to observe that in each file the range resolution is different, and that at 30 m range resolution the illuminated zone is different with respect to the that illuminated at 60 m, 15 m, 9 m, e 3 m range resolution. These files were chosen to highlight the differences due to the change of the resolution.

It is important to observe that the IPIX receiver has two operational modes depending upon the selected RF pulse width (PW). For  $PW \geq 200 \text{ ns}$ , a 5 MHz filter is used to limit the receiver bandwidth to approximately 5 MHz. For  $PW < 200 \text{ ns}$ , this filter is by-passed, so the bandwidth of the receiver becomes about 50 MHz to match the minimum 20 ns pulse width. Therefore, for files when  $PW < 200 \text{ ns}$ , the noise floor is about 10 dB higher than for  $PW \geq 200 \text{ ns}$  [Cur03].

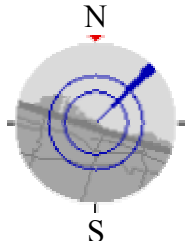
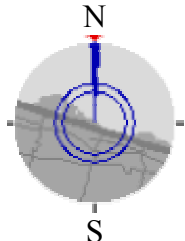
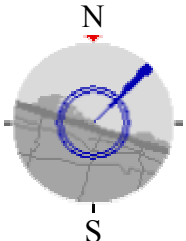
<b>Name of the data set</b>	19980204_223753_ANTSTEP	19980204_220849_ANTSTEP	19980204_223220_ANTSTEP
<b>Date, time of acquisition</b>	02/04/1998 22:37:53	02/04/1998 22:08:49	02/04/1998 22:32:20
<b>#Range cells</b>	28	28	28
<b>Start range</b>	3201 m	3201 m	3201 m
<b>Range resolution</b>	60 m	30 m	15 m
<b>Pulse width</b>	400 ns	200 ns	100 ns
<b>Total # sweep</b>	60000	60000	60000
<b>Sample for cell</b>	60000 Sampled at 60 m	60000 Sampled at 30 m	60000 Sampled at 15 m
<b>PRF</b>	1 KHz	1 KHz	1 KHz
<b>Frequency RF</b>	9.39 GHz	9.39 GHz	9.39 GHz
<b>Radar and wave geometry</b>			

Table 1.2 - Characteristics of the analyzed files.

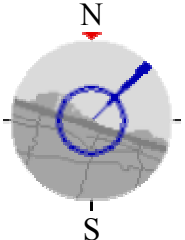
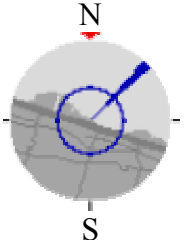
<b>Name of the data set</b>	19980204_224024_ANTSTEP	19980204_223506_ANTSTEP
<b>Date, time of acquisition</b>	02/04/1998 22:40:24	02/04/1998 22:35:06
<b>#Range cells</b>	28	27
<b>Start range</b>	3201 m	3321 m
<b>Range resolution</b>	9 m	3 m
<b>Pulse width</b>	60 ns	20 ns
<b>Total # sweep</b>	60000	60000
<b>Sample for cell</b>	60000 Sampled at 9 m	60000 Sampled at 3 m
<b>PRF</b>	1 KHz	1 KHz
<b>Frequency RF</b>	9.39 GHz	9.39 GHz
<b>Radar and wave geometry</b>		

Table 1.3 - Characteristics of the analyzed files.

# Section 2

## Statistical Analysis

### 2.1 Introduction

The first analyzed file is “19980204\_223753\_antstep.cdf “ with a range resolution of 60 m. Many distributions have been proposed in the literature to model the amplitude probability density function (PDF) of high resolution non-Gaussian clutter (see [Bar96], [Con87], [Fay77], [Far97], [Jak76] [War90], [Ran93], [Ran95a], [Ran95b], [Ran97], [Ran98], and references therein). Here, we compare the empirical PDF with log-normal (LN), Weibull (W), K, and Generalized K (GK) PDFs. The expressions of these PDFs and their moments are reported below [Far97], where  $R = |z[i]|$  denotes the clutter amplitude:

#### Log-normal model (LN)

$$\text{PDF:} \quad P_R(r) = \frac{1}{r\sqrt{2\pi\sigma^2}} \exp\left(-\frac{1}{2\sigma^2} \left[ (\ln r - \ln \delta)^2 \right] \right) u(r) \quad (2.1)$$

$$\text{Moments:} \quad E\{R^n\} = \delta^n \exp(\delta^2 \sigma^2 / 2) \quad (2.2)$$

where  $\sigma$  is the *shape parameter*, and  $\delta$  is the *scale parameter*.

#### Weibull model (W)

$$\text{PDF:} \quad P_R(r) = \frac{c}{b^c} r^{c-1} \exp\left[-(r/b)^c\right] u(r) \quad (2.3)$$

$$\text{Moments:} \quad E\{R^n\} = b^n \Gamma\left(\frac{n}{c+1}\right) \quad (2.4)$$

where  $c$  is the *shape parameter* and  $b$  is the *scale parameter*. Rayleigh PDF is a particular case of the Weibull PDF for  $c=2$ .

### K-model (K)

$$\text{PDF: } P_R(r) = \frac{\sqrt{2\nu/\mu}}{2^{\nu-1}\Gamma(\nu)} \left( \sqrt{\frac{2\nu}{\mu}} r \right)^\nu K_{\nu-1} \left( \sqrt{\frac{2\nu}{\mu}} r \right) u(r) \quad (2.5)$$

$$\text{Moments: } E\{R^n\} = \left( \frac{2\mu}{\nu} \right)^{\frac{n}{2}} \frac{\Gamma(\nu + \frac{n}{2})\Gamma(1 + \frac{n}{2})}{\Gamma(\nu)} \quad (2.6)$$

where  $\Gamma(\cdot)$  is the gamma function,  $K_{\nu-1}(\cdot)$  is the modified Bessel function of the third kind of order  $\nu-1$ ,  $\nu$  is the *shape parameter*, and  $\mu$  is the *scale parameter*.

### Generalized K model (log-normal texture) (LNT)

$$\text{PDF: } P_R(r) = \frac{r}{\sqrt{2\pi\sigma^2}} \int_0^\infty \frac{2}{\tau^2} \exp\left[ \frac{r^2}{\tau} - \frac{1}{2\sigma^2} \left[ \ln\left(\frac{\tau}{2m}\right) \right]^2 \right] d\tau \quad (2.7)$$

$$\text{Moments: } E\{R^n\} = (2m)^{\frac{n}{2}} \Gamma\left(1 + \frac{n}{2}\right) \exp\left(\frac{n^2\sigma^2}{8}\right) \quad (2.8)$$

### Generalized K model (Generalized Gamma texture) (GK)

$$\text{PDF: } P_R(r) = \frac{2br}{\Gamma(\nu)} \left( \frac{\nu}{\mu} \right) \int_0^\infty \tau^{\nu b-2} \exp\left[ \frac{r^2}{\tau} - \left( \frac{\nu}{\mu} \tau \right)^b \right] d\tau \quad (2.9)$$

$$\text{Moments: } E\{R^n\} = \left( \frac{\mu}{\nu} \right)^{\frac{n}{2}} \frac{\Gamma(\nu + \frac{n}{2})\Gamma(1 + \frac{n}{2})}{2b\Gamma(\nu)} \quad (2.10)$$

Apart from Log-normal model, the other models proposed here are particular cases of the so-called compound-Gaussian family because obtained from the composition of two random variables; texture and speckle. According to this model, the samples of the complex envelope of the sea-clutter process can be written as the product of two components:

$$z(n) = \sqrt{\tau(n)}x(n) \quad (2.11)$$

The term  $x(n) = x_I(n) + jx_Q(n)$  is a stationary complex Gaussian process, usually called *speckle*, which accounts for local backscattering;  $x_I(n)$  e  $x_Q(n)$  are the in-phase and quadrature components of  $x(n)$ . They satisfy the property  $E\{x_I(n)\} = E\{x_Q(n)\} = 0$ , with  $E\{x_I^2(n)\} = E\{x_Q^2(n)\} = 1/2$  and thus  $E\{|x(n)|^2\} = 1$ . Factor  $\tau(n)$  is a non-negative real random process, usually called *texture*.

Once fixed the PDFs of speckle and texture, it is possible to obtain the amplitude PDF:

$$z(n) = \sqrt{\tau(n)}x(n) \Rightarrow |z(n)| = R = \sqrt{\tau(n)}|x(n)| \quad (2.12)$$

$$f_R(r) = \int_{-\infty}^{+\infty} f_R(r|\tau) f_\tau(\tau) d\tau. \quad (2.13)$$

The characteristic parameters of the log-normal, Weibull, K and generalized K with log-normal texture (LNT) theoretical PDFs were estimated by the classical method of moments (MoM), by equating the first and second experimental and theoretical moments [Far97], estimated as:

$$\hat{E}\{R^n\} = \hat{m}_R(n) = \sum_{i=1}^{N_s} |z(i)|^n \quad (2.14)$$

$N_s$  denotes the sample size; we processed  $N_s = 60,000$  samples. As concerning the parameters of the GK-PDF, we encountered several numerical problems with the above approach. Thus, in this case we used a number of empirical moments greater than the number of unknowns; the parameters  $\nu$  and  $b$  were estimated as

$$(\hat{\nu}, \hat{b}) = \arg \min_{(\nu, b)} J(\nu, b) = \arg \min_{(\nu, b)} \sum_{n=2}^5 \left| \frac{\hat{m}_R(n) - m_R(n)}{m_R(n)} \right|^2 \quad (2.15)$$

where  $m_R(n) \triangleq E\{R^n\}/E^n\{R\}$  is the normalized  $n$ th order moment (which does not depend on  $\mu$ ) and  $\hat{m}_R(n)$  denotes its sample estimate. The absolute minimum of the quantity in (2.15) was found by two successive two-dimensional searches. A first coarse grid search

was carried out to prevent convergence to local minima. Then, a fine search was performed to find the absolute minimum around the one found by the previous coarse search. The fine search uses the Nelder-Mead simplex (direct search) method. Once  $\nu$  and  $b$  have been estimated,  $\hat{\mu}$  is obtained from an estimate of the first order moment,  $\hat{E}\{R\}$ .

### 2.2.1 Range resolution of 60 m

Figure 2.1 shows the behavior of the average clutter power as a function of the cell number. The behavior versus the cells is similar in all polarizations. The results of the histogram and moments analysis have been reported in figures 2.2, 2.4, 2.6, and in figures 2.3, 2.5, and 2.7 respectively for the 15<sup>th</sup> range cell. The results show that a very good fitting is obtained by the GK-PDF, both for like- and cross-polarized data. Therefore, the analyzed lake clutter process, at a range resolution of 60 m, can be accurately modeled by a compound-Gaussian process with Generalized K-PDF. The results for the other range cells are very similar.

The parameters estimated for each theoretical PDF (see Tables. 2.1, 2.2, 2.3, 2.4, 2.5 and 2.6) show that, on the average, HH component is spikier ( $\bar{c} = 1.2261$ ) than both VV ( $\bar{c} = 1.2927$ ) and VH ( $\bar{c} = 1.2900$ ) components; different polarization have been compared with respect to the mean value of the  $c$  parameter in Weibull distribution because the meaning of this parameter is very easy to understand.

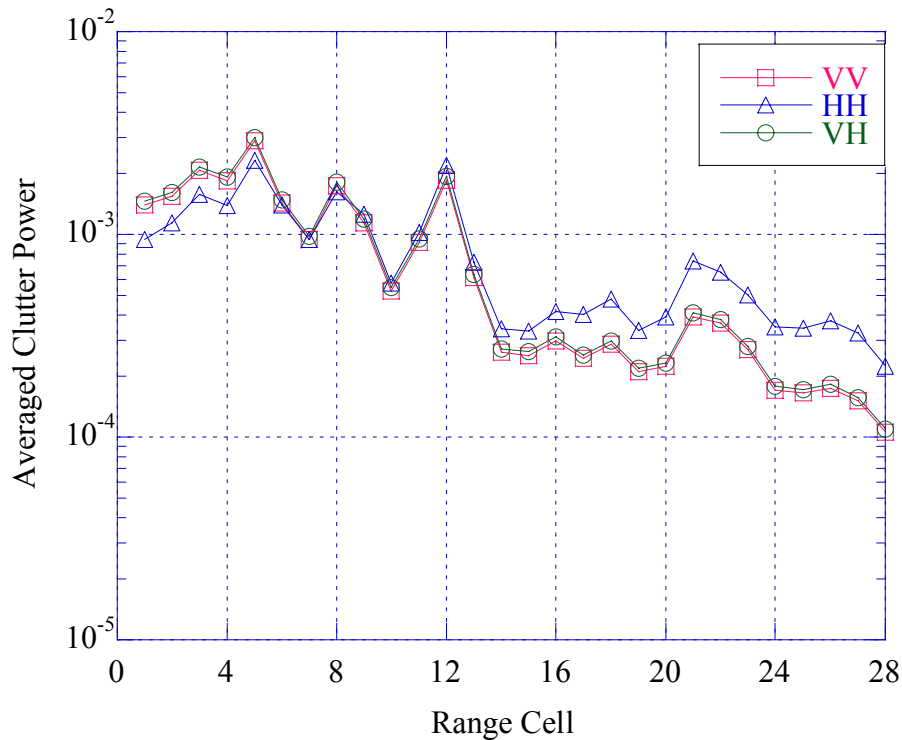


Figure 2.1 - Average backscattered power vs range cell number.

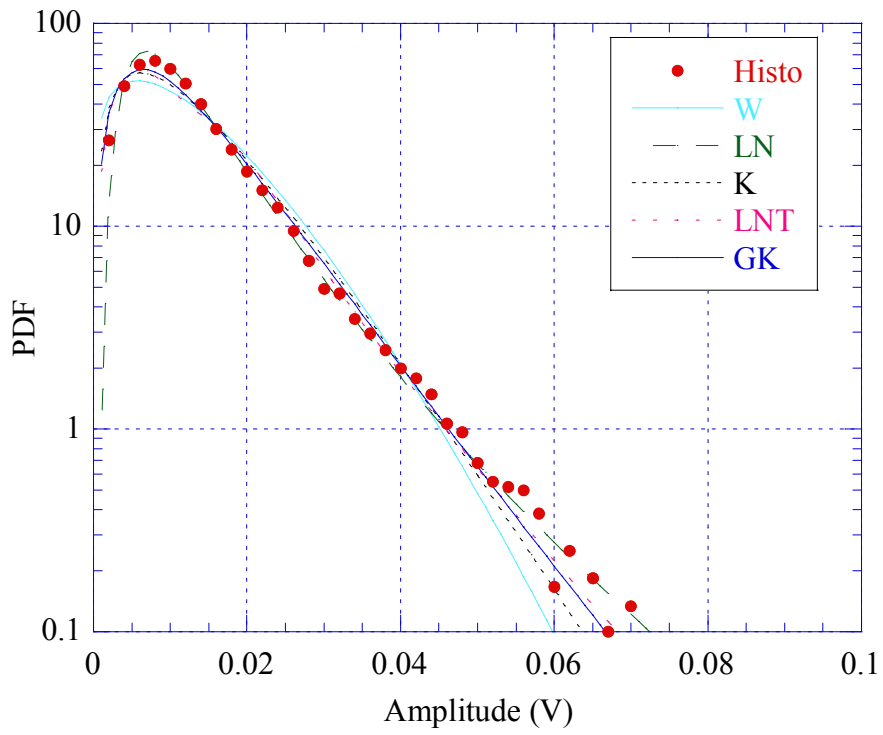


Figure 2. 2 – Clutter amplitude PDF, VV polarization, 15<sup>th</sup> range cell.

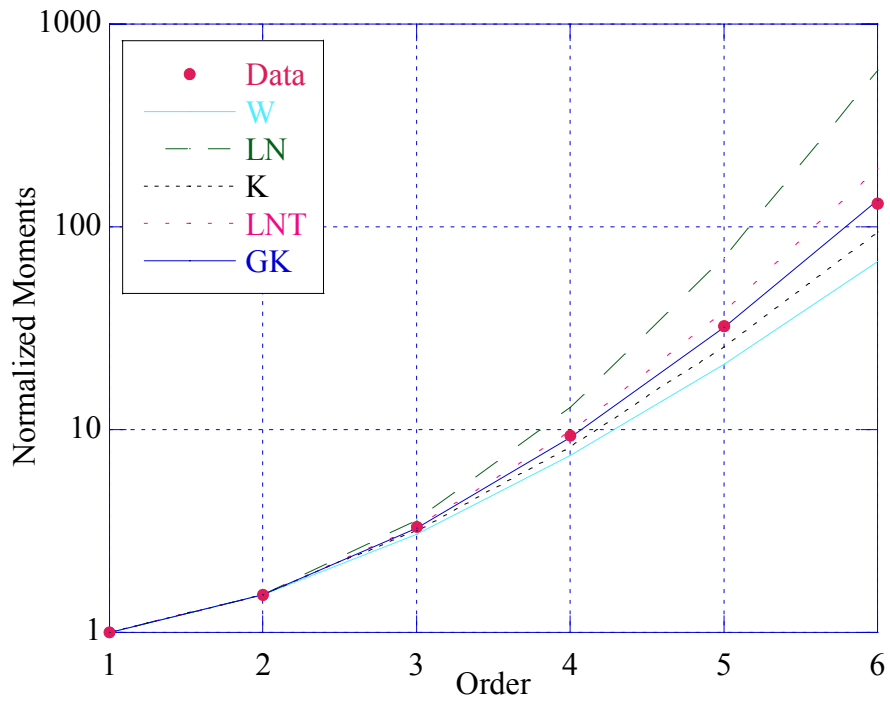


Figure 2. 3 - Normalized clutter moments, VV polarization, 15<sup>th</sup> range cell.

Cell	W		LN		K	
	$\hat{c}$	$\hat{b}$	$\hat{\sigma}$	$\hat{\delta}$	$\hat{\nu}$	$\hat{\mu}$
1	1.5200	0.034494	0.60950	0.025820	1.9036	0.00070076
2	1.1850	0.031786	0.73541	0.022891	0.79437	0.00077275
3	1.0475	0.033507	0.80507	0.023788	0.56454	0.0010343
4	1.2080	0.035099	0.72501	0.025342	0.84054	0.00091880
5	1.0758	0.040507	0.78956	0.028835	0.60632	0.0014464
6	1.1236	0.029421	0.76484	0.021046	0.68283	0.00071352
7	1.2574	0.025739	0.70371	0.018690	0.94938	0.00047024
8	1.0521	0.030878	0.80247	0.021931	0.57124	0.00087184
9	1.4166	0.030168	0.64323	0.022317	1.4255	0.00056968
10	1.3350	0.019907	0.67277	0.014587	1.1532	0.00026304
11	1.1983	0.024609	0.72936	0.017749	0.82073	0.00045642
12	1.0412	0.031525	0.80857	0.022369	0.55569	0.00092497
13	1.3724	0.021751	0.65889	0.016008	1.2692	0.00030530
14	1.4137	0.014472	0.64422	0.010702	1.4147	0.00013134
15	1.3905	0.014096	0.65237	0.010396	1.3305	0.00012658
16	1.2927	0.014731	0.68925	0.010741	1.0366	0.00014917
17	1.4643	0.014206	0.62717	0.010567	1.6235	0.00012261
18	1.3978	0.015044	0.64979	0.011105	1.3563	0.00014346
19	1.4320	0.013029	0.63797	0.0096551	1.4856	0.00010520
20	1.4901	0.013651	0.61886	0.010184	1.7455	0.00011154
21	1.2305	0.016404	0.71516	0.011875	0.88830	0.00019609
22	1.1379	0.015029	0.75779	0.010767	0.70729	0.00018278
23	1.1781	0.013237	0.73861	0.0095248	0.78093	0.00013506
24	1.2864	0.011114	0.69178	0.0080974	1.0205	8.5375e-05
25	1.2987	0.010988	0.68689	0.0080174	1.0521	8.2576e-05
26	1.4255	0.011841	0.64016	0.0087686	1.4601	8.7252e-05
27	1.4077	0.010933	0.64630	0.0080798	1.3923	7.5265e-05
28	1.5188	0.0094769	0.60988	0.0070929	1.8967	5.2930e-05

**Table 2.1** - Estimated parameters, VV polarization.

Cell	LNT		GK		
	$\hat{\sigma}^2$	$\hat{m}$	$\hat{v}$	$\hat{\mu}$	$\hat{b}$
1	0.51969	0.00054040	2.7405	0.0010499	0.80795
2	1.1970	0.00042472	1.9355	0.00075764	0.59008
3	1.6263	0.00045868	9.4774	4.3318e-07	0.22479
4	1.1363	0.00052056	0.87289	0.0018062	0.95366
5	1.5273	0.00067395	4.5522	8.7781e-05	0.33906
6	1.3736	0.00035902	56.449	6.0461e-19	0.10413
7	1.0146	0.00028315	9.8372	2.2771e-06	0.28886
8	1.6096	0.00038987	7.2833	2.9721e-06	0.25812
9	0.68874	0.00040371	4.5449	0.00026235	0.53665
10	0.84421	0.00017247	52.472	1.6450e-14	0.14265
11	1.1616	0.00025534	2.3092	0.00035718	0.55452
12	1.6489	0.00040558	0.57015	0.0018380	0.95000
13	0.77026	0.00020771	0.83295	0.00064125	1.2749
14	0.69382	9.2839e-05	1.6356	0.00024008	0.89814
15	0.73611	8.7602e-05	5.4991	2.7977e-05	0.46105
16	0.93402	9.3508e-05	67.651	7.2347e-20	0.10640
17	0.60712	9.0506e-05	68.868	1.5526e-15	0.14240
18	0.72263	9.9957e-05	10.142	2.8699e-06	0.34715
19	0.66176	7.5562e-05	68.239	6.5954e-16	0.13894
20	0.56572	8.4061e-05	30.489	1.6504e-09	0.22786
21	1.0795	0.00011430	13.030	1.1400e-07	0.24961
22	1.3307	9.3967e-05	7.5384	1.2683e-06	0.28235
23	1.2159	7.3537e-05	1.4774	0.00018303	0.67369
24	0.94800	5.3147e-05	4.0910	2.6797e-05	0.46961
25	0.92101	5.2103e-05	19.736	2.6065e-09	0.21849
26	0.67294	6.2323e-05	8.8679	4.0704e-06	0.38165
27	0.70458	5.2917e-05	68.637	1.3554e-16	0.13373
28	0.52156	4.0780e-05	46.108	1.3163e-11	0.19634

**Table 2.2** - Estimated parameters, VV polarization.

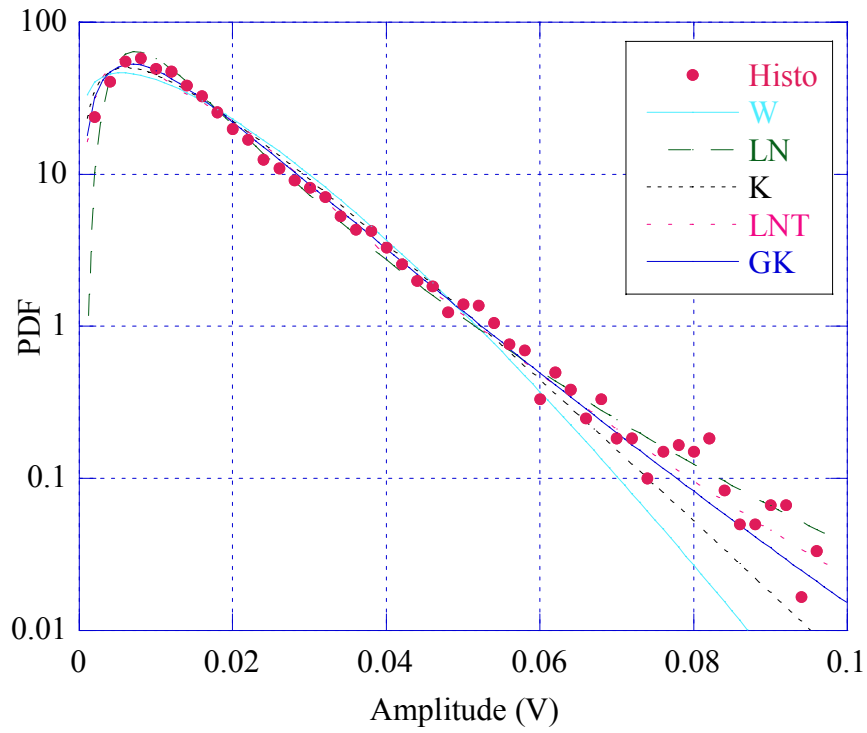


Figure 2.4 - Clutter amplitude PDF, HH polarization, 15<sup>th</sup> range cell.

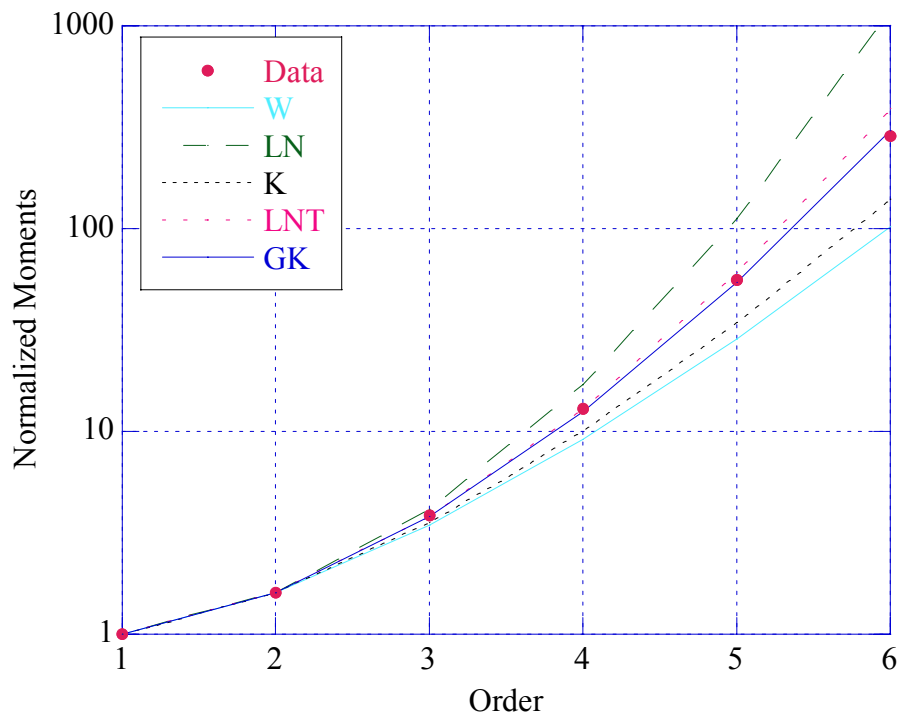


Figure 2.5 - Normalized clutter moments, HH polarization, 15<sup>th</sup> range cell.

Cell	W		LN		K	
	$\hat{c}$	$\hat{b}$	$\hat{\sigma}$	$\hat{\delta}$	$\hat{\nu}$	$\hat{\mu}$
1	1.4399	0.027611	0.63528	0.020480	1.5181	4.70094e-04
2	1.1013	0.025864	0.77618	0.018458	0.64606	5.68366e-04
3	0.98564	0.027673	0.84128	0.019547	0.48168	7.86789e-04
4	1.2169	0.030612	0.72109	0.022125	0.85906	6.92409e-04
5	1.0611	0.035894	0.79751	0.025516	0.58437	1.16150e-03
6	1.0021	0.026474	0.83128	0.018723	0.50276	6.98106e-04
7	1.2009	0.025031	0.72822	0.018058	0.82585	4.70903e-04
8	1.0881	0.030597	0.78303	0.021807	0.62524	8.10455e-04
9	1.3130	0.030470	0.68124	0.022269	1.0908	6.27313e-04
10	1.2922	0.020462	0.68948	0.014918	1.0352	2.87951e-04
11	1.1903	0.025962	0.73302	0.018707	0.80463	5.12507e-04
12	1.0155	0.033518	0.82337	0.023730	0.52036	1.09248e-03
13	1.3053	0.023133	0.68428	0.016892	1.0697	3.63927e-04
14	1.3250	0.015961	0.67658	0.011682	1.1244	1.70454e-04
15	1.3242	0.015796	0.67692	0.011560	1.1219	1.67072e-04
16	1.2890	0.017362	0.69075	0.012654	1.0270	2.07903e-04
17	1.3616	0.017602	0.66283	0.012938	1.2343	2.01514e-04
18	1.3149	0.018849	0.68051	0.013780	1.0959	2.39705e-04
19	1.3478	0.016025	0.66795	0.011760	1.1914	1.68778e-04
20	1.3664	0.017365	0.66108	0.012771	1.2496	1.95450e-04
21	1.1286	0.021285	0.76234	0.015234	0.69136	3.71023e-04
22	1.1015	0.019590	0.77606	0.013981	0.64643	3.25959e-04
23	1.0987	0.017187	0.77753	0.012262	0.64187	2.51902e-04
24	1.1630	0.014942	0.74571	0.010734	0.75237	1.75199e-04
25	1.2048	0.015173	0.72644	0.010952	0.83394	1.72302e-04
26	1.3310	0.016767	0.67431	0.012280	1.1414	1.87213e-04
27	1.3235	0.015627	0.67717	0.011435	1.1200	1.63585e-04
28	1.4385	0.013440	0.63577	0.0099672	1.5120	1.11481e-04

**Table 2.3** - Estimated parameters, HH polarization

Cell	LNT		GK		
	$\hat{\sigma}^2$	$\hat{m}$	$\hat{\nu}$	$\hat{\mu}$	$\hat{b}$
1	0.64804	3.39989e-04	3.2763	4.46566e-04	0.65262
2	1.4436	2.76162e-04	2.1566	3.58957e-04	0.49939
3	1.8647	3.09699e-04	4.1112	3.21681e-05	0.30910
4	1.1136	3.96773e-04	0.84706	1.37935e-03	0.98792
5	1.5778	5.27718e-04	2.2024	6.07104e-04	0.46863
6	1.7978	2.84137e-04	26.314	1.67124e-13	0.12970
7	1.1550	2.64321e-04	3.3623	1.61376e-04	0.45835
8	1.4863	3.85465e-04	10.959	2.26087e-07	0.22492
9	0.89009	4.01978e-04	1.7723	9.24844e-04	0.74666
10	0.93525	1.80398e-04	13.319	3.11253e-07	0.26556
11	1.1830	2.83669e-04	2.0165	4.90353e-04	0.58871
12	1.7455	4.56448e-04	0.48726	2.18530e-03	1.0074
13	0.90669	2.31275e-04	1.3626	6.55524e-04	0.86545
14	0.86480	1.10617e-04	4.5612	4.87975e-05	0.47041
15	0.86663	1.08322e-04	6.0103	1.88775e-05	0.40773
16	0.94227	1.29792e-04	67.986	1.63504e-18	0.11431
17	0.79112	1.35680e-04	23.430	4.42032e-09	0.22129
18	0.88612	1.53907e-04	5.7957	2.89782e-05	0.40967
19	0.81839	1.12100e-04	35.770	1.23539e-11	0.17583
20	0.78186	1.32208e-04	58.339	4.09491e-15	0.14028
21	1.3584	1.88119e-04	2.6974	1.61669e-04	0.46540
22	1.4428	1.58437e-04	6.4131	4.27946e-06	0.29377
23	1.4520	1.21883e-04	3.0067	7.28340e-05	0.42494
24	1.2581	9.33995e-05	3.0814	6.57839e-05	0.46028
25	1.1446	9.72163e-05	66.569	1.49350e-19	0.10760
26	0.85252	1.22240e-04	68.237	1.25577e-17	0.12126
27	0.86798	1.05990e-04	7.0555	1.00037e-05	0.37855
28	0.65055	8.05256e-05	4.1858	6.86213e-05	0.57891

**Table 2.4** - Estimated parameters, HH polarization.

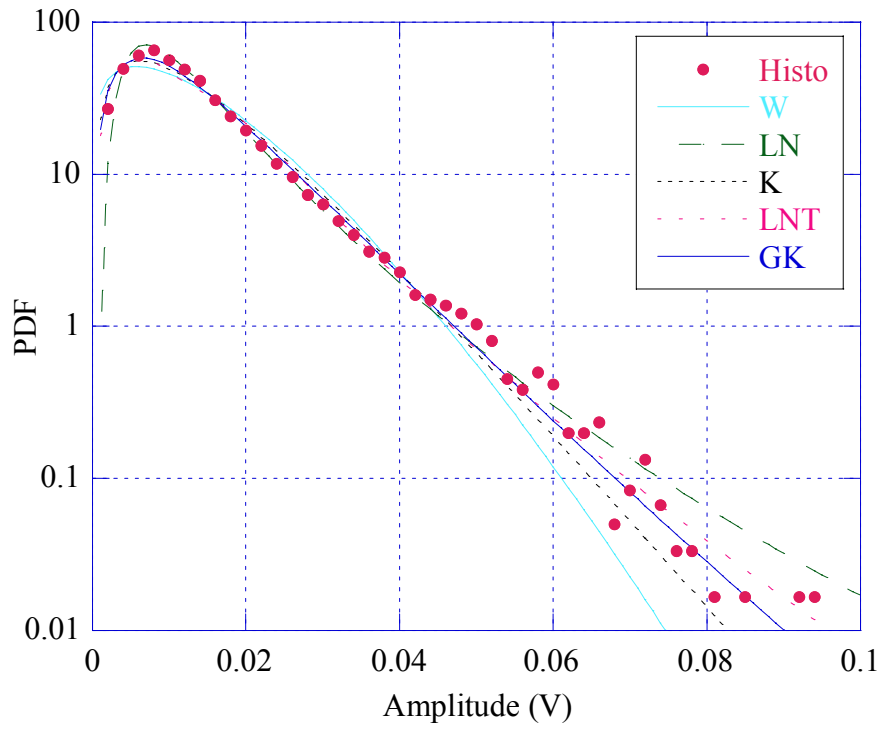


**Figure 2.6** - Clutter amplitude PDF, VH polarization, 15<sup>th</sup> range cell.

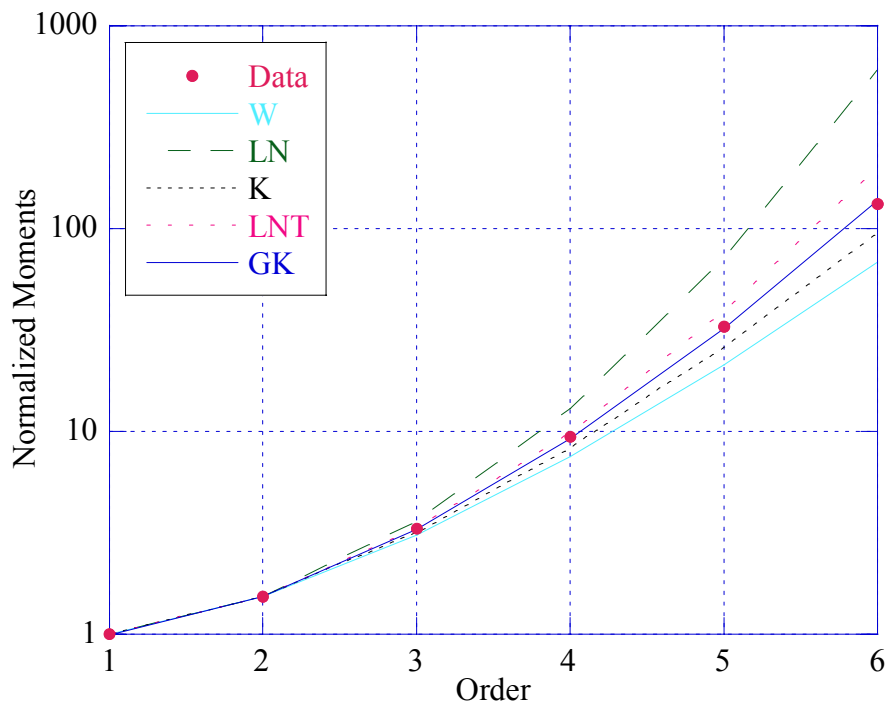


**Figure 2.7** - Normalized clutter moments, VH polarization, 15<sup>th</sup> range cell.

Cell	W		LN		K	
	$\hat{c}$	$\hat{b}$	$\hat{\sigma}$	$\hat{\delta}$	$\hat{\nu}$	$\hat{\mu}$
1	1.5197	0.035189	0.60958	0.026340	1.9022	7.29366e-04
2	1.1856	0.032453	0.73515	0.023372	0.79545	8.05008e-04
3	1.0506	0.034247	0.80332	0.024321	0.56904	1.07510e-03
4	1.2069	0.035809	0.72550	0.025852	0.83828	9.57496e-04
5	1.0762	0.041344	0.78936	0.029432	0.60689	1.50597e-03
6	1.1243	0.030059	0.76452	0.021504	0.68391	7.44168e-04
7	1.2565	0.026253	0.70408	0.019061	0.94726	4.89634e-04
8	1.0535	0.031532	0.80173	0.022398	0.57318	9.07201e-04
9	1.4163	0.030834	0.64334	0.022809	1.4243	5.95206e-04
10	1.3326	0.020279	0.67371	0.014855	1.1460	2.73507e-04
11	1.1993	0.025122	0.72894	0.018120	0.82261	4.75149e-04
12	1.0406	0.032181	0.80891	0.022833	0.55483	9.64803e-04
13	1.3709	0.022210	0.65942	0.016343	1.2644	3.18668e-04
14	1.4170	0.014771	0.64308	0.010928	1.4273	1.36535e-04
15	1.3862	0.014378	0.65390	0.010599	1.3157	1.32098e-04
16	1.2909	0.015051	0.69000	0.010972	1.0318	1.55976e-04
17	1.4619	0.014480	0.62797	0.010768	1.6126	1.27566e-04
18	1.3941	0.015333	0.65109	0.011313	1.3433	1.49401e-04
19	1.4319	0.013283	0.63800	0.0098434	1.4853	1.09348e-04
20	1.4908	0.013921	0.61865	0.010386	1.7488	1.15959e-04
21	1.2312	0.016750	0.71483	0.012126	0.88995	2.04296e-04
22	1.1385	0.015343	0.75746	0.010993	0.70844	1.90353e-04
23	1.1768	0.013491	0.73919	0.0097063	0.77852	1.40502e-04
24	1.2895	0.011364	0.69057	0.0082824	1.0282	8.90235e-05
25	1.2965	0.011190	0.68776	0.0081627	1.0464	8.57998e-05
26	1.4246	0.012095	0.64049	0.0089555	1.4563	9.10909e-05
27	1.4065	0.011145	0.64675	0.0082351	1.3876	7.82760e-05
28	1.5157	0.0096406	0.61084	0.0072129	1.8795	5.48630e-05

**Table 2.5** - Estimated parameters, VH polarization.

Cell	LNt		GK		
	$\hat{\sigma}^2$	$\hat{m}$	$\hat{v}$	$\hat{\mu}$	$\hat{b}$
1	0.52008	5.62356e-04	2.6643	0.0011234	0.81995
2	1.1955	4.42782e-04	1.9259	0.00079653	0.59216
3	1.6150	4.79453e-04	9.2207	5.8973e-07	0.22864
4	1.1392	5.41719e-04	0.83801	0.0018992	0.97486
5	1.5261	7.02154e-04	4.6107	8.6917e-05	0.33723
6	1.3717	3.74809e-04	51.396	7.4510e-18	0.10890
7	1.0167	2.94511e-04	9.8644	2.3068e-06	0.28815
8	1.6048	4.06653e-04	7.3848	2.8744e-06	0.25696
9	0.68929	4.21686e-04	4.4500	0.00028774	0.54218
10	0.84926	1.78877e-04	43.730	4.7733e-13	0.15575
11	1.1592	2.66146e-04	2.3045	0.00037452	0.55595
12	1.6511	4.22579e-04	0.57434	0.0019152	0.94501
13	0.77307	2.16505e-04	0.81027	0.00066769	1.2947
14	0.68793	9.67974e-05	1.7192	0.00024310	0.87787
15	0.74411	9.10572e-05	5.3408	3.1226e-05	0.46531
16	0.93813	9.75765e-05	67.634	6.5582e-20	0.10602
17	0.61111	9.39794e-05	68.856	1.4354e-15	0.14185
18	0.72939	1.03746e-04	8.9849	5.2749e-06	0.36657
19	0.66190	7.85383e-05	68.767	5.9063e-16	0.13848
20	0.56464	8.74365e-05	29.743	2.3055e-09	0.23112
21	1.0777	1.19191e-04	12.292	1.8928e-07	0.25692
22	1.3287	9.79547e-05	7.6216	1.2464e-06	0.28117
23	1.2194	7.63658e-05	1.4658	0.00019158	0.67554
24	0.94129	5.56041e-05	4.5411	2.1114e-05	0.44825
25	0.92578	5.40077e-05	16.908	1.1714e-08	0.23492
26	0.67466	6.50092e-05	8.7084	4.5597e-06	0.38441
27	0.70688	5.49706e-05	68.633	1.3608e-16	0.13358
28	0.52623	4.21707e-05	40.412	7.3223e-11	0.20896

**Table 2.6** - Estimated parameters, VH polarization.

## 2.2.2 Range resolution of 30 m

The second analyzed file is “19980204\_220849\_antstep.cdf “ at a range resolution of 30 m. The expressions of the used PDF and their moments are the same as those used at 60 m range resolution. The results of the histogram and moment analysis, reported in figures 2.9, 2.10, 2.11, 2.12, 2.13, and 2.14 for the 1<sup>st</sup> range cell, show that, also with this range resolution, a very good fitting is obtained by the GK-PDF.

Figure 2.8, plotting the average backscattered power versus range, shows that with this resolution, both VV and VH powers overcome HH power; let’s notice that both 7<sup>th</sup> and 8<sup>th</sup> cells are not important for our clutter analysis because containing a target with strong power particularly in HH data (for further information you can visit the web site <http://soma.ece.mcmaster.ca/ipix/>). The other analyzed files did not show the target because of their different illuminated zone, as indicated in Tables 1.2 and 1.3.

Estimated parameters show that on the average (Tables 2.7, 2.8, 2.9, 2.10, 2.11 and 2.12), data clutter are spikier at 30 m range resolution than at 60 m in all polarizations. Both VV component ( $\bar{c} = 1.1148$ ) and VH component ( $\bar{c} = 1.1153$ ) are spikier than HH component ( $\bar{c} = 1.1900$ ).

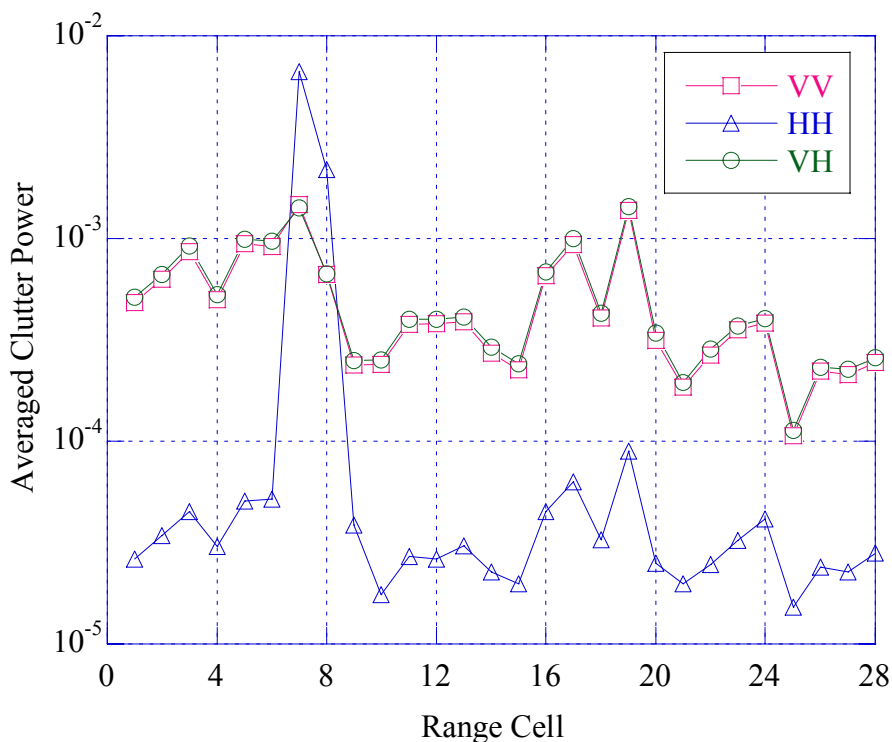


Figure 2.8 - Average backscattered power vs range cell number.

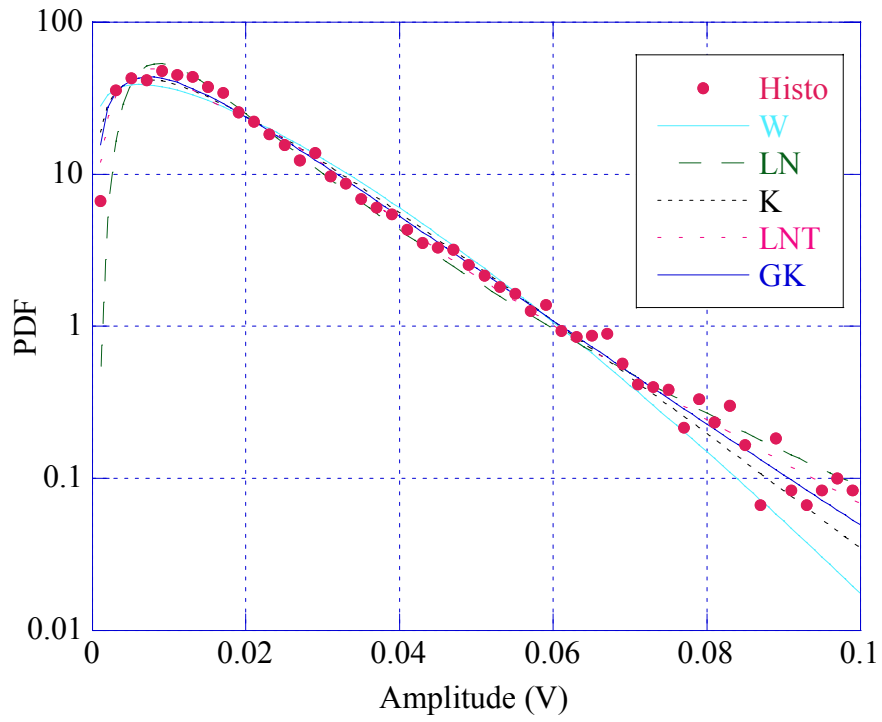


Figure 2.9 - Clutter amplitude PDF, VV polarization, 1<sup>st</sup> range cell.

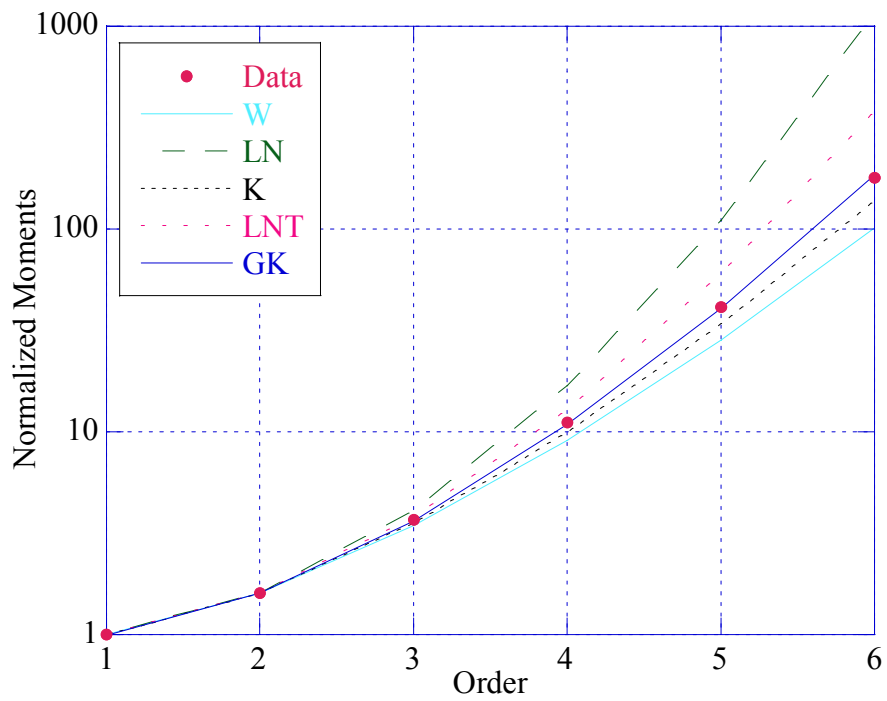


Figure 2.10 - Normalized clutter moments, VV polarization, 1<sup>st</sup> range cell.

Cell	W		LN		K	
	$\hat{c}$	$\hat{b}$	$\hat{\sigma}$	$\hat{\delta}$	$\hat{\nu}$	$\hat{\mu}$
1	1.3006	0.018815	0.68612	0.013731	1.0572	2.41710e-04
2	1.1686	0.020138	0.74306	0.014476	0.76283	3.16121e-04
3	0.98441	0.020478	0.84203	0.014463	0.48014	4.31872e-04
4	1.1323	0.017527	0.76055	0.012549	0.69755	2.50393e-04
5	1.2188	0.025299	0.72023	0.018289	0.86320	4.71964e-04
6	1.2255	0.024964	0.71732	0.018061	0.87745	4.56424e-04
9	1.2905	0.013122	0.69017	0.0095650	1.0308	1.18596e-04
10	1.1903	0.012546	0.73298	0.0090404	0.80478	1.19675e-04
11	1.0384	0.014211	0.81015	0.010081	0.55175	1.88828e-04
12	1.0452	0.014322	0.80633	0.010166	0.56134	1.89671e-04
13	1.2511	0.016483	0.70634	0.011960	0.93474	1.94009e-04
14	1.1455	0.013057	0.75409	0.0093619	0.72064	1.36653e-04
15	1.0484	0.011071	0.80452	0.0078609	0.56594	1.12748e-04
16	0.84143	0.014987	0.94144	0.010535	0.32357	3.26665e-04
17	0.99783	0.021584	0.83386	0.015260	0.49720	4.67759e-04
18	1.1345	0.015798	0.75945	0.011314	0.70140	2.02858e-04
19	0.67653	0.015575	1.0946	0.011201	0.18788	6.89038e-04
20	0.95985	0.012055	0.85745	0.0085006	0.45008	1.57207e-04
21	1.3271	0.011774	0.67579	0.0086198	1.1303	9.26050e-05
22	0.91112	0.010521	0.88995	0.0074012	0.39454	1.33509e-04
23	0.89920	0.011936	0.89832	0.0083933	0.38174	1.76915e-04
24	1.0214	0.014087	0.81994	0.0099784	0.52826	1.91005e-04
25	1.3321	0.0089411	0.67390	0.0065493	1.1446	5.31887e-05
26	0.91626	0.0096553	0.88640	0.0067933	0.40016	1.11066e-04
27	1.1810	0.011773	0.73728	0.0084747	0.78648	1.06504e-04
28	1.2162	0.012886	0.72139	0.0093127	0.85763	1.22781e-04

**Table 2. 7** - Estimated parameters, VV polarization.

Cell	LNT		GK		
	$\hat{\sigma}^2$	$\hat{m}$	$\hat{v}$	$\hat{\mu}$	$\hat{b}$
1	0.91680	1.52832e-04	2.4530	0.00023316	0.61895
2	1.2423	1.69859e-04	4.3843	3.7054e-05	0.37995
3	1.8698	1.69563e-04	1.0807	0.00055216	0.59540
4	1.3475	1.27649e-04	60.852	4.7852e-20	0.10190
5	1.1087	2.71122e-04	1.0558	0.00087248	0.86521
6	1.0920	2.64396e-04	7.7420	7.3753e-06	0.31644
9	0.93906	7.41578e-05	46.365	2.1635e-14	0.14460
10	1.1828	6.62463e-05	2.1617	0.00010011	0.56179
11	1.6591	8.23735e-05	3.7264	1.9121e-05	0.35379
12	1.6344	8.37714e-05	2.2389	8.5293e-05	0.44753
13	1.0294	1.15954e-04	5.0253	2.5515e-05	0.40258
14	1.3084	7.10420e-05	1.3833	0.00018636	0.66629
15	1.6228	5.00877e-05	8.5959	7.7955e-08	0.22947
16	2.5790	8.99672e-05	0.44289	0.00063435	0.78399
17	1.8150	1.88754e-04	0.49535	0.00093397	0.96674
18	1.3408	1.03762e-04	4.5539	1.6659e-05	0.35806
19	3.8267	1.01690e-04	0.46164	0.0010617	0.55146
20	1.9746	5.85716e-05	3.1976	1.5348e-05	0.33741
21	0.86049	6.02255e-05	1.0738	0.00018591	1.0081
22	2.2018	4.44011e-05	5.0867	6.6740e-07	0.24608
23	2.2616	5.71025e-05	1.6203	8.7924e-05	0.42401
24	1.7229	8.07076e-05	6.0227	1.8957e-06	0.27891
25	0.85028	3.47682e-05	68.353	8.9331e-18	0.12450
26	2.1765	3.74068e-05	3.8744	2.8294e-06	0.28308
27	1.2081	5.82156e-05	67.325	3.4544e-21	0.099688
28	1.1153	7.02970e-05	23.062	8.6880e-11	0.17955

**Table 2. 8** - Estimated parameters, VV polarization.

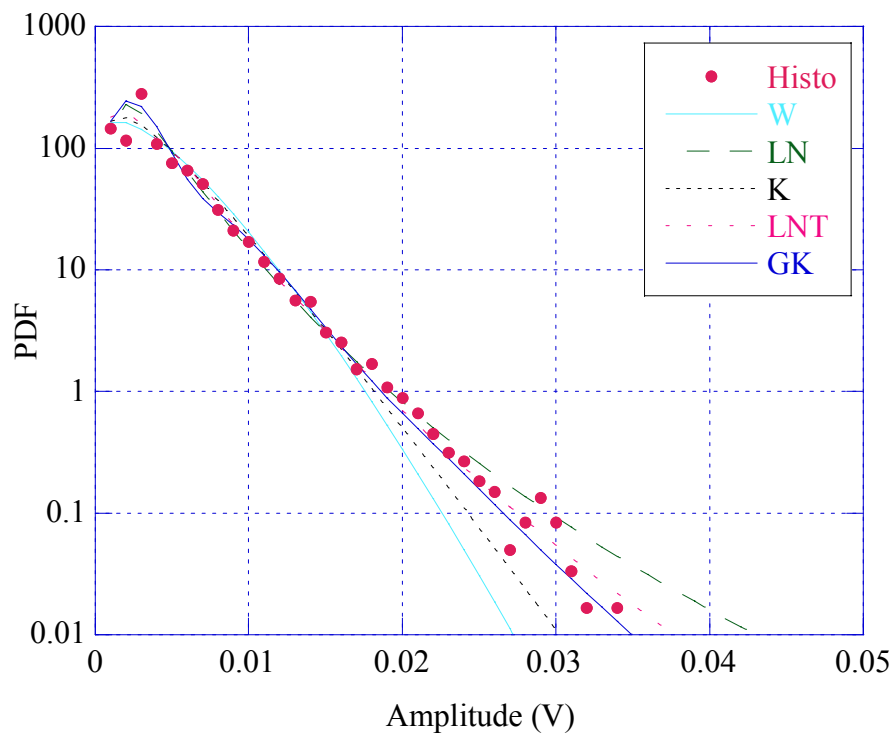


Figure 2.11 - Clutter amplitude PDF, HH polarization, 1<sup>st</sup> range cell.

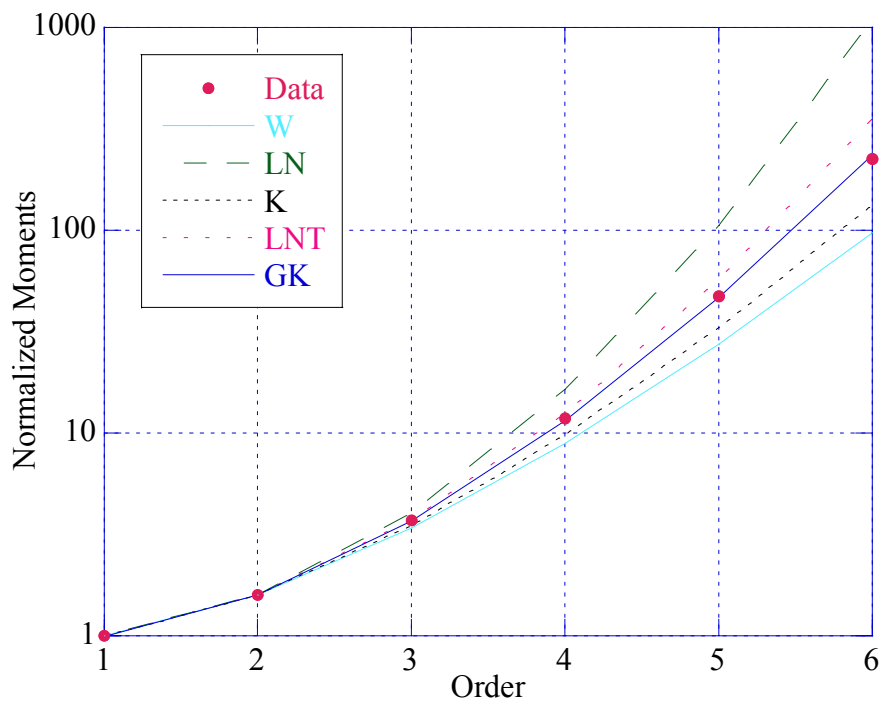


Figure 2.12 - Normalized clutter moments, HH polarization, 1<sup>st</sup> range cell.

Cell	W		LN		K	
	$\hat{c}$	$\hat{b}$	$\hat{\sigma}$	$\hat{\delta}$	$\hat{\nu}$	$\hat{\mu}$
1	1.3095	0.0044027	0.68263	0.0032165	1.0810	1.31364e-05
2	1.2178	0.0048202	0.72067	0.0034842	0.86108	1.71509e-05
3	1.0468	0.0049380	0.80545	0.0035055	0.56357	2.24889e-05
4	1.1899	0.0044591	0.73318	0.0032130	0.80394	1.51252e-05
5	1.2655	0.0060034	0.70034	0.0043634	0.96865	2.53882e-05
6	1.2202	0.0059250	0.71963	0.0042839	0.86613	2.58500e-05
9	1.2973	0.0053150	0.68745	0.0038774	1.0484	1.93438e-05
10	1.3874	0.0037123	0.65348	0.0027369	1.3197	8.79843e-06
11	1.1374	0.0040904	0.75803	0.0029303	0.70643	1.35486e-05
12	1.2488	0.0042761	0.70731	0.0031020	0.92948	1.30853e-05
13	1.2503	0.0046275	0.70668	0.0033574	0.93291	1.53020e-05
14	1.2629	0.0040163	0.70139	0.0029183	0.96253	1.13902e-05
15	1.2338	0.0036931	0.71373	0.0026744	0.89554	9.90598e-06
16	0.98122	0.0046617	0.84400	0.0032917	0.47614	2.25191e-05
17	1.0645	0.0059358	0.79567	0.0042208	0.58934	3.15980e-05
18	1.2408	0.0047496	0.71073	0.0034422	0.91116	1.62706e-05
19	0.77359	0.0049412	0.99835	0.0034871	0.26274	4.46297e-05
20	1.1880	0.0040518	0.73407	0.0029188	0.80007	1.25153e-05
21	1.4762	0.0040468	0.62332	0.0030143	1.6781	9.88104e-06
22	1.1430	0.0039200	0.75530	0.0028099	0.71622	1.23558e-05
23	1.0937	0.0043499	0.78013	0.0031020	0.63392	1.62513e-05
24	1.1119	0.0049665	0.77076	0.0035483	0.66326	2.06546e-05
25	1.5981	0.0036577	0.58640	0.0027617	2.4273	7.58552e-06
26	1.1474	0.0038691	0.75313	0.0027748	0.72417	1.19700e-05
27	1.4210	0.0042671	0.64171	0.0031582	1.4425	1.13641e-05
28	1.3718	0.0046599	0.65910	0.0034293	1.2672	1.40188e-05

**Table 2.9** - Estimated parameters, HH polarization.

Cell	LNT		GK		
	$\hat{\sigma}^2$	$\hat{m}$	$\hat{\nu}$	$\hat{\mu}$	$\hat{b}$
1	0.89768	8.38590e-06	8.2564	3.2062e-07	0.34037
2	1.1112	9.83996e-06	9.1023	9.0862e-08	0.28646
3	1.6287	9.96072e-06	2.6410	6.6957e-06	0.41389
4	1.1839	8.36781e-06	57.505	1.4635e-19	0.11126
5	0.99563	1.54324e-05	2.0493	2.8657e-05	0.64551
6	1.1052	1.48755e-05	11.651	2.6973e-08	0.25656
9	0.92410	1.21864e-05	0.44279	3.4977e-05	1.6817
10	0.74190	6.07161e-06	21.713	4.8461e-10	0.23200
11	1.3322	6.96009e-06	5.2485	5.6107e-07	0.32989
12	1.0349	7.79941e-06	9.1631	8.5228e-08	0.29390
13	1.0313	9.13693e-06	33.841	1.1646e-13	0.15701
14	1.0016	6.90309e-06	9.8692	5.5916e-08	0.28953
15	1.0714	5.79753e-06	67.282	2.2534e-22	0.098871
16	1.8831	8.78290e-06	0.91382	3.3810e-05	0.64933
17	1.5661	1.44405e-05	0.65213	6.1721e-05	0.90064
18	1.0543	9.60432e-06	67.813	3.5689e-20	0.11054
19	3.0205	9.85647e-06	0.66764	6.0547e-05	0.54519
20	1.1892	6.90571e-06	67.056	4.3722e-23	0.094767
21	0.58784	7.36468e-06	54.627	2.6723e-14	0.16564
22	1.3157	6.39992e-06	66.742	3.2136e-24	0.089609
23	1.4682	7.79967e-06	5.5558	3.6002e-07	0.30439
24	1.4100	1.02055e-05	35.988	7.7994e-16	0.12982
25	0.40919	6.18201e-06	69.413	9.1513e-15	0.16785
26	1.3026	6.24084e-06	66.503	4.3418e-25	0.086056
27	0.68089	8.08505e-06	68.399	2.8113e-18	0.12592
28	0.77141	9.53239e-06	30.918	8.0828e-12	0.18914

**Table 2.10** - Estimated parameters, HH polarization.

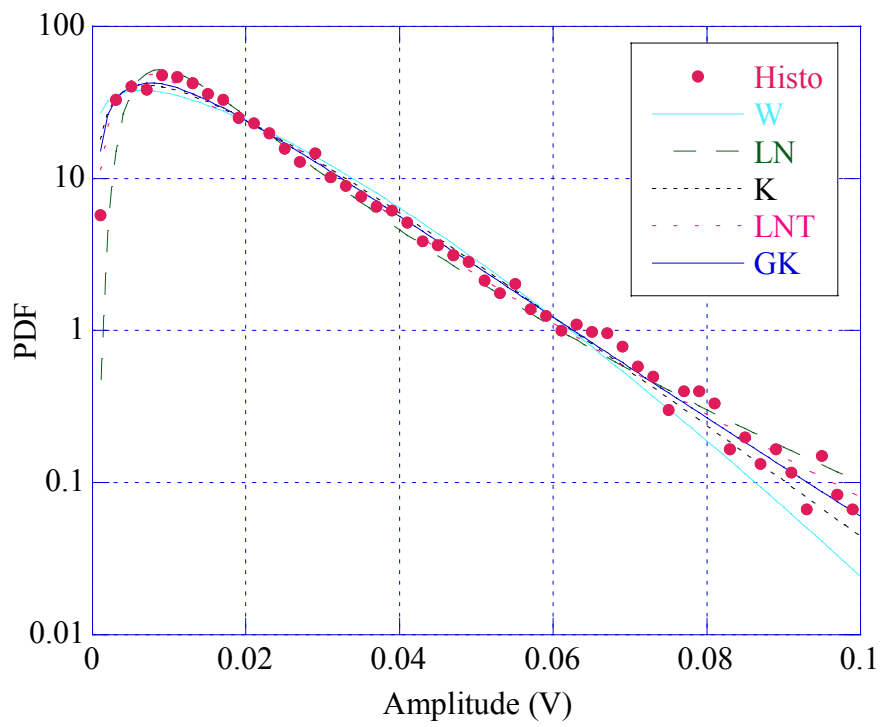


Figure 2.13 - Clutter amplitude PDF, VH polarization, 1<sup>st</sup> range cell.

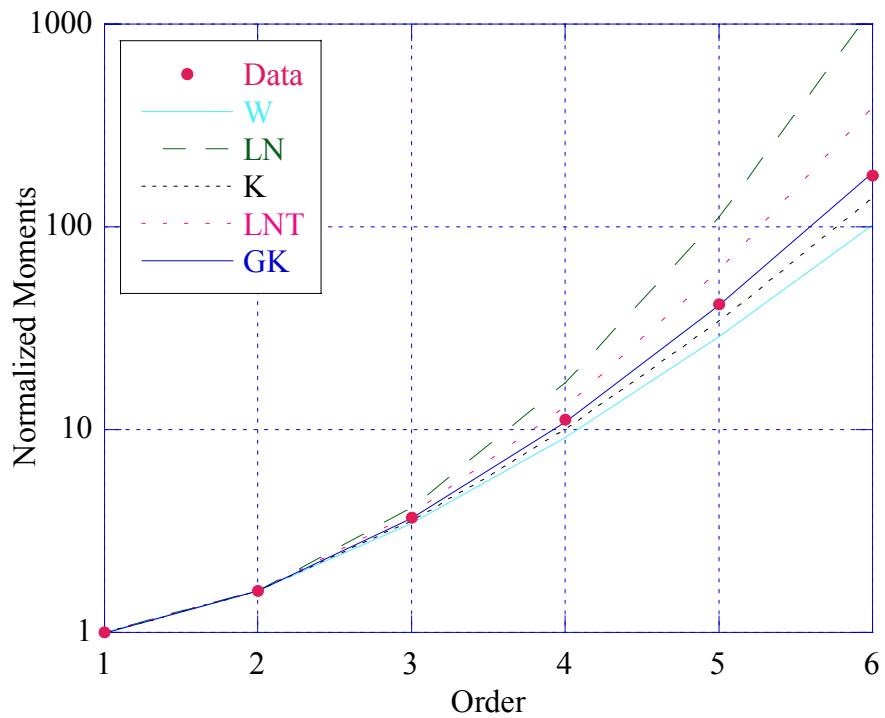


Figure 2.14 - Normalized clutter moments, VH polarization, 1<sup>st</sup> range cell.

Cell	W		LN		K	
	$\hat{c}$	$\hat{b}$	$\hat{\sigma}$	$\hat{\delta}$	$\hat{\nu}$	$\hat{\mu}$
1	1.2980	0.019382	0.68715	0.014141	1.0504	2.57067e-04
2	1.1738	0.020725	0.74064	0.014906	0.77262	3.32792e-04
3	0.98441	0.021148	0.84203	0.014936	0.48014	4.60589e-04
4	1.1331	0.018065	0.76011	0.012935	0.69908	2.65684e-04
5	1.2214	0.026001	0.71909	0.018802	0.86872	4.97176e-04
6	1.2246	0.025730	0.71772	0.018613	0.87547	4.85319e-04
9	1.2854	0.013473	0.69219	0.0098154	1.0179	1.25590e-04
10	1.1949	0.012914	0.73091	0.0093101	0.81386	1.26156e-04
11	1.0358	0.014600	0.81166	0.010355	0.54804	2.00200e-04
12	1.0433	0.014715	0.80743	0.010443	0.55856	2.00845e-04
13	1.2510	0.016970	0.70640	0.012313	0.93445	2.05652e-04
14	1.1451	0.013456	0.75425	0.0096479	0.72005	1.45202e-04
15	1.0432	0.011391	0.80743	0.0080839	0.55854	1.20360e-04
16	0.84287	0.015373	0.94031	0.010806	0.32495	3.42229e-04
17	0.99513	0.022271	0.83549	0.015742	0.49373	5.00501e-04
18	1.1345	0.016254	0.75946	0.011641	0.70139	2.14739e-04
19	0.67788	0.016013	1.0932	0.011511	0.18883	7.23050e-04
20	0.95084	0.012469	0.86326	0.0087874	0.43941	1.71388e-04
21	1.3210	0.012047	0.67814	0.0088127	1.1129	9.74150e-05
22	0.90912	0.010824	0.89134	0.0076133	0.39238	1.41971e-04
23	0.89986	0.012257	0.89785	0.0086190	0.38244	1.86245e-04
24	1.0226	0.014498	0.81919	0.010270	0.53000	2.01851e-04
25	1.3236	0.0091914	0.67713	0.0067261	1.1204	5.65900e-05
26	0.91580	0.0098682	0.88672	0.0069430	0.39965	1.16147e-04
27	1.1715	0.012079	0.74169	0.0086852	0.76833	1.13330e-04
28	1.2183	0.013251	0.72048	0.0095789	0.86201	1.29562e-04

**Table 2.11** - Estimated parameters, VH polarization.

Cell	LNT		GK		
	$\hat{\sigma}^2$	$\hat{m}$	$\hat{v}$	$\hat{\mu}$	$\hat{b}$
1	0.92246	1.62083e-04	2.2923	0.00027144	0.63815
2	1.2279	1.80110e-04	4.4203	3.9259e-05	0.38124
3	1.8698	1.80837e-04	1.1220	0.00056462	0.58403
4	1.3448	1.35625e-04	57.332	3.1099e-19	0.10529
5	1.1021	2.86540e-04	1.0425	0.00092655	0.87482
6	1.0942	2.80813e-04	9.0093	3.2938e-06	0.29414
9	0.95027	7.80918e-05	37.903	7.4108e-13	0.15902
10	1.1707	7.02591e-05	2.2275	0.00010191	0.55723
11	1.6689	8.69090e-05	3.8195	1.8157e-05	0.34856
12	1.6415	8.83921e-05	2.1425	9.9221e-05	0.45627
13	1.0297	1.22894e-04	4.8672	3.0218e-05	0.40881
14	1.3093	7.54492e-05	1.4062	0.00019461	0.66030
15	1.6415	5.29696e-05	8.3605	9.5407e-08	0.23078
16	2.5705	9.46547e-05	0.44729	0.00066325	0.78147
17	1.8259	2.00868e-04	0.50740	0.00099735	0.94902
18	1.3408	1.09838e-04	4.3694	2.0897e-05	0.36588
19	3.8137	1.07405e-04	0.46718	0.0011073	0.54999
20	2.0146	6.25903e-05	2.8412	2.4338e-05	0.35302
21	0.87324	6.29512e-05	1.0513	0.00019586	1.0118
22	2.2117	4.69823e-05	4.9214	8.5091e-07	0.24920
23	2.2583	6.02147e-05	1.6139	9.3890e-05	0.42562
24	1.7180	8.54999e-05	5.8867	2.3257e-06	0.28262
25	0.86775	3.66700e-05	67.380	1.4083e-17	0.12558
26	2.1788	3.90740e-05	3.6749	3.8061e-06	0.28997
27	1.2342	6.11428e-05	67.291	2.7694e-21	0.099035
28	1.1101	7.43745e-05	22.857	1.0864e-10	0.18086

**Table 2.12** - Estimated parameters, VH polarization.

### 2.2.3 Range resolution of 15 m

The results of the histograms and moments analysis obtained by focusing on the file “19980204\_223220\_antstep.cdf” with a range resolution of 15 m show new features. We observed, for co-polarizations, the presence of some longer tailed cells as shows in Figures 2.18 (7<sup>th</sup> cell) and 2.23 (24<sup>th</sup> cell).

Considering that the data clutter are always recorded in presence of additive white Gaussian noise (AWGN), mostly originated by the receiver, and that the clutter power loses 6 dB as resolution doubles with respect to the thermal noise that does not depend on the radar resolution, we started to compare the amplitude histograms also to the Rayleigh (R) PDF (Weibull where  $c=2$ ), whose expression is:

$$\text{PDF:} \quad f_R(r) = \frac{2r}{\sigma^2} \exp\left[-\left(\frac{r}{\sigma}\right)^2\right] u(r) \quad (2.19)$$

$$\text{Moments:} \quad E\{R^n\} = \sigma^n \Gamma\left(\frac{n}{2}\right) \quad (2.20)$$

The parameter  $\sigma^2$  was estimated by equating the second experimental and theoretical moment. The results are shown in Figure 2.19 for the 7<sup>th</sup> range cell. The fitting with the Rayleigh model is not good.

Figure 2.15 reports the mean backscattered power behavior versus range cells. With a range resolution of 30 m we observed that HH component was the weakest one. This time both HH polarization and VV polarization exhibit the same behavior although VV component keeps on being the most powerful one; VH component is weaker than the others.

Figures 2.16, 2.17, 2.21 and 2.22 show the histograms in two cells where a very good fitting is still obtained by the GK-PDF. Also in cross-polarizations the GK-PDF keeps on showing a good fitting with the histogram (Figures 2.25, and 2.26).

Estimated parameters confirm that when resolution increases clutter gets spikier. We also notice that on the average HH component is spikier ( $\bar{c} = 0.87$ ) than both VV component ( $\bar{c} = 0.93$ ) and VH component ( $\bar{c} = 1.01$ ).

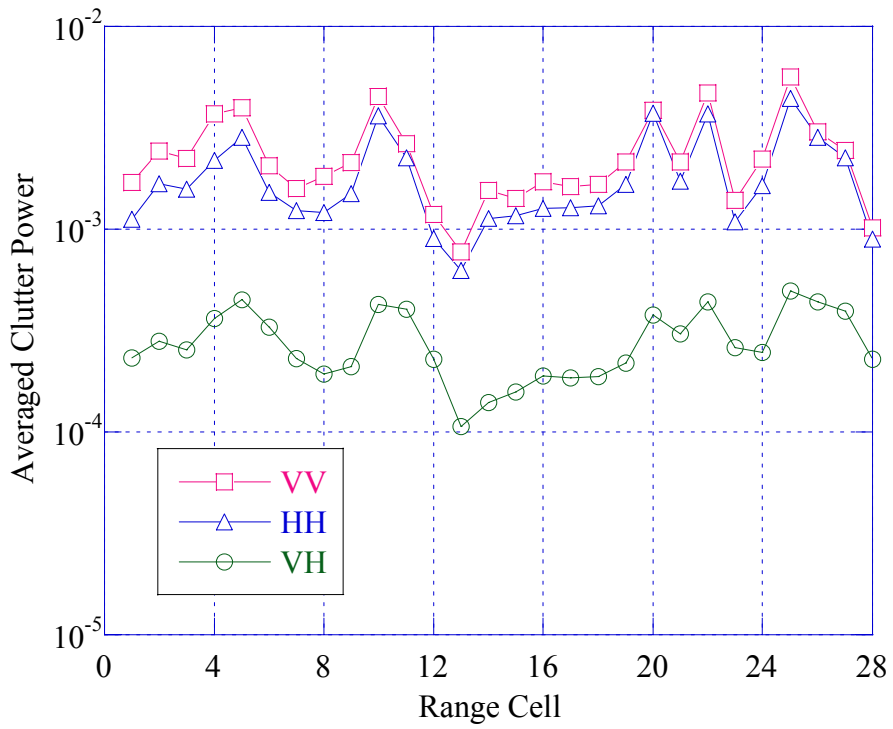


Figure 2.15 - Average backscattered power vs range cell number.

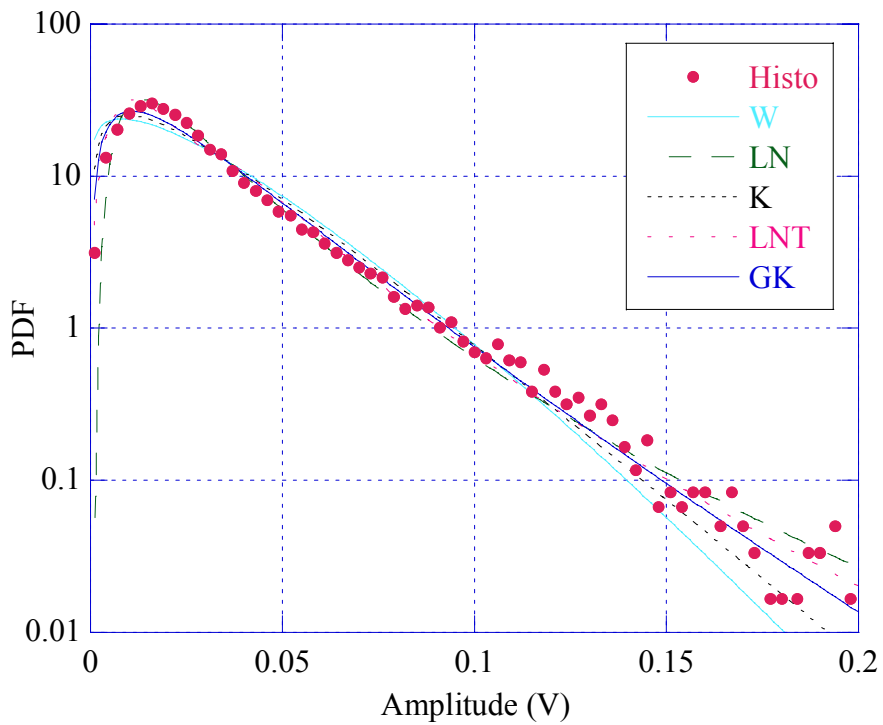


Figure 2.16 - Clutter amplitude PDF, VV polarization, 15th range cell.

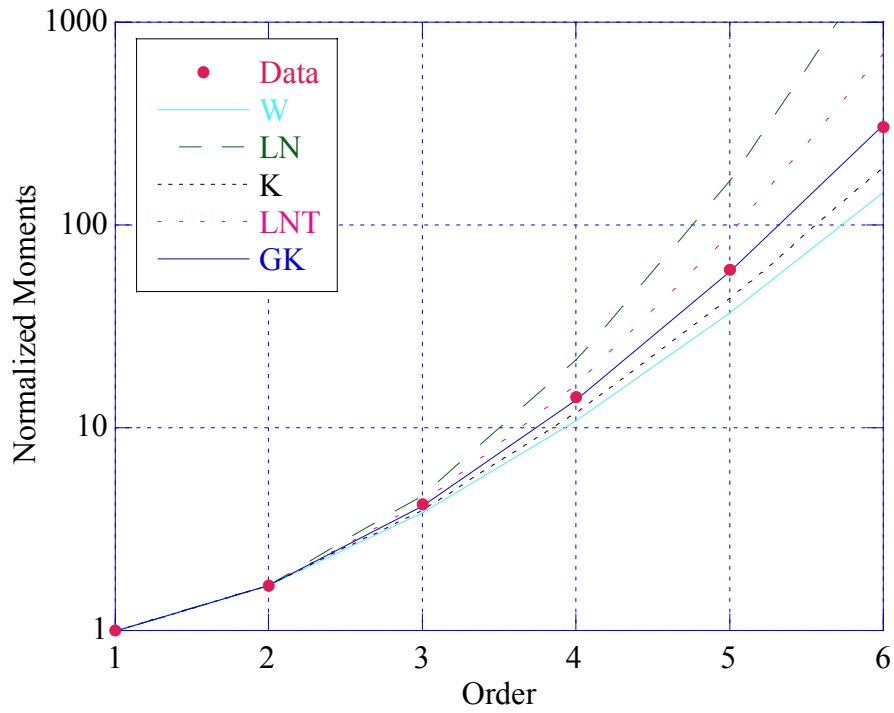


Figure 2.17 - Normalized clutter moments, VV polarization, 15th range cell.

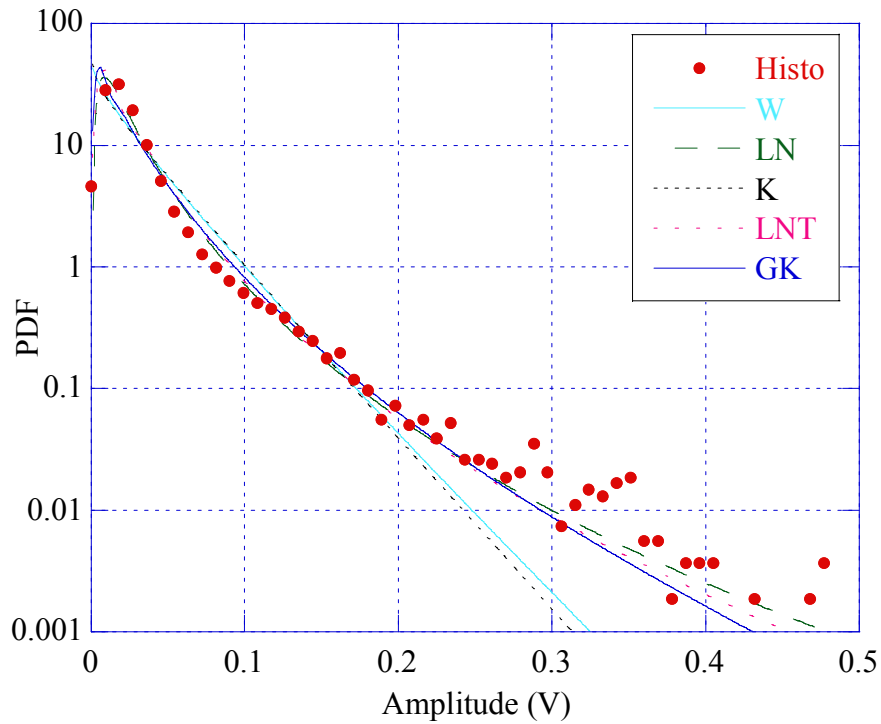


Figure 2.18 - Clutter amplitude PDF, VV polarization, 7th range cell.

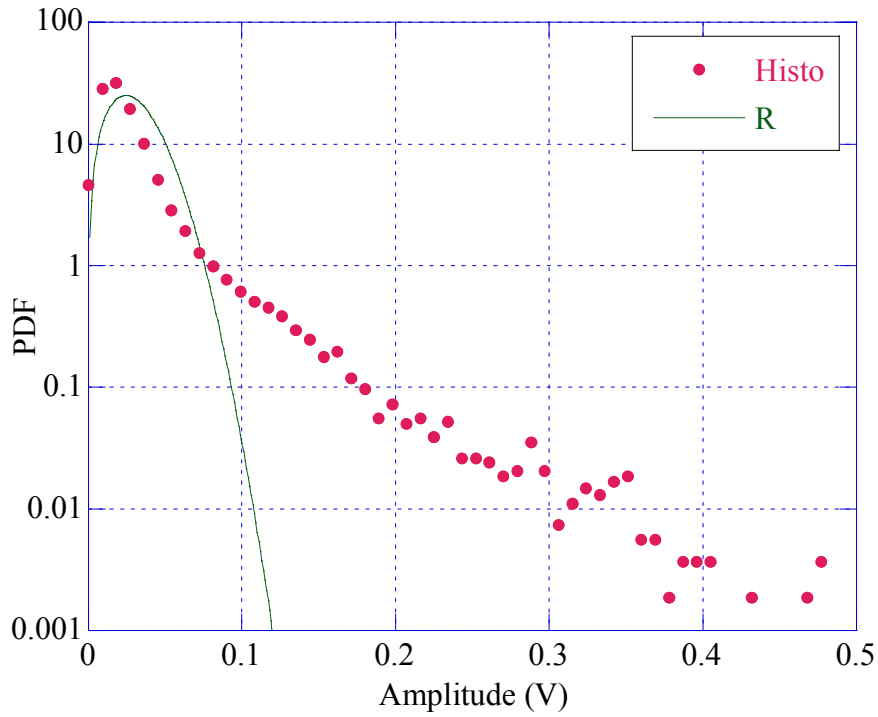


Figure 2.19 - Clutter amplitude PDF, VV polarization, 7th range cell.

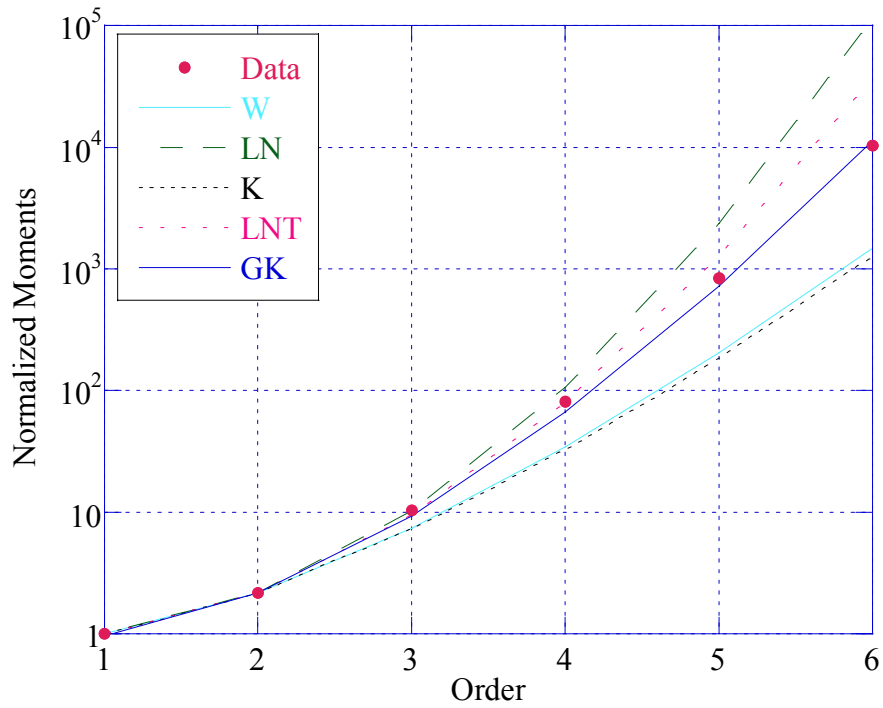


Figure 2.20 - Normalized clutter moments, VV polarization, 7th range cell.

Cell	W		LN		K	
	$\hat{c}$	$\hat{b}$	$\hat{\sigma}$	$\hat{\delta}$	$\hat{v}$	$\hat{\mu}$
1	1.1231	0.032150	0.76511	0.022997	0.68190	0.00085266
2	0.85872	0.029667	0.92807	0.020851	0.34033	0.0012171
3	0.97708	0.032746	0.84657	0.023116	0.47101	0.0011202
4	0.76662	0.031474	1.0046	0.022229	0.25691	0.0018597
5	0.73361	0.030440	1.0356	0.021598	0.23028	0.0019925
6	0.89616	0.028632	0.90048	0.020132	0.37852	0.0010258
7	0.92410	0.026099	0.88103	0.018369	0.40883	0.00079679
8	0.93018	0.028118	0.87692	0.019795	0.41564	0.00091204
9	0.91398	0.029902	0.88797	0.021037	0.39766	0.0010711
10	0.71029	0.030729	1.0589	0.021903	0.21241	0.0022585
11	0.78357	0.027363	0.98951	0.019292	0.27122	0.0013188
12	1.1521	0.027274	0.75089	0.019570	0.73250	0.00059141
13	1.4061	0.024801	0.64686	0.018325	1.3865	0.00038768
14	1.1489	0.031241	0.75243	0.022408	0.72676	0.00077901
15	1.2313	0.031229	0.71482	0.022608	0.89002	0.00071010
16	1.0460	0.030523	0.80591	0.021667	0.56238	0.00086044
17	1.0507	0.029772	0.80326	0.021143	0.56920	0.00081231
18	1.0477	0.030099	0.80496	0.021370	0.56481	0.00083440
19	0.86710	0.028207	0.92173	0.019825	0.34864	0.0010748
20	0.75395	0.031315	1.0163	0.022151	0.24649	0.0019358
21	0.97522	0.032094	0.84773	0.022653	0.46872	0.0010800
22	0.66383	0.027774	1.1088	0.020057	0.17905	0.0023518
23	1.0607	0.027774	0.79777	0.019742	0.58365	0.00069596
24	0.85314	0.028054	0.93233	0.019718	0.33486	0.0011059
25	0.59692	0.024337	1.1910	0.018138	0.13594	0.0028069
26	0.79266	0.029795	0.98159	0.020992	0.27909	0.0015134
27	0.69169	0.021570	1.0782	0.015445	0.19870	0.0012200
28	1.1714	0.025583	0.74175	0.018395	0.76810	0.00050849

**Table 2.13** - Estimated parameters, VV polarization.

Cell	LNT		GK			R
	$\hat{\sigma}^2$	$\hat{m}$	$\hat{\nu}$	$\hat{\mu}$	$\hat{b}$	$\hat{\sigma}^2$
1	1.3753	0.00042867	2.7593	0.00032511	0.44934	0.0012594
2	2.4790	0.00035240	0.82769	0.0015744	0.55780	0.0017977
3	1.9005	0.00043313	2.3119	0.00034978	0.40467	0.0016545
4	3.0709	0.00040051	0.76127	0.0021112	0.49991	0.0027468
5	3.3239	0.00037812	0.60024	0.0026562	0.52309	0.0029429
6	2.2772	0.00032853	3.5398	3.4656e-05	0.28852	0.0015151
7	2.1386	0.00027349	5.7680	2.1086e-06	0.23692	0.0011768
8	2.1097	0.00031761	4.5134	1.1388e-05	0.26684	0.0013471
9	2.1877	0.00035872	2.0608	0.00031385	0.38562	0.0015819
10	3.5185	0.00038886	0.46151	0.0036737	0.58256	0.0033357
11	2.9502	0.00030168	1.2518	0.00064267	0.39353	0.0019478
12	1.2891	0.00031043	2.4250	0.00033270	0.49330	0.00087350
13	0.70744	0.00027218	36.960	7.3521e-11	0.18537	0.00057260
14	1.2984	0.00040701	2.3010	0.00049254	0.50812	0.0011506
15	1.0776	0.00041431	3.0865	0.00034465	0.49864	0.0010488
16	1.6317	0.00038053	2.2346	0.00039925	0.45189	0.0012708
17	1.6146	0.00036234	2.3189	0.00035194	0.44638	0.0011998
18	1.6256	0.00037015	1.9347	0.00051279	0.48013	0.0012324
19	2.4321	0.00031857	2.3815	0.00014268	0.33217	0.0015875
20	3.1651	0.00039771	0.50102	0.0032262	0.61286	0.0028592
21	1.9083	0.00041596	1.3895	0.00097381	0.51830	0.0015952
22	3.9517	0.00032607	0.49828	0.0031065	0.49629	0.0034736
23	1.5795	0.00031593	12.542	2.0156e-08	0.19572	0.0010279
24	2.5107	0.00031514	0.70016	0.0016477	0.59824	0.0016333
25	4.7076	0.00026668	0.20246	0.0057243	0.69179	0.0041458
26	2.8878	0.00035717	0.26033	0.0030455	0.96981	0.0022353
27	3.6842	0.00019335	0.63279	0.0012385	0.44849	0.0018019
28	1.2345	0.00027429	5.6430	2.0879e-05	0.33555	0.00075103

**Table 2.14** - Estimated parameters, VV polarization.

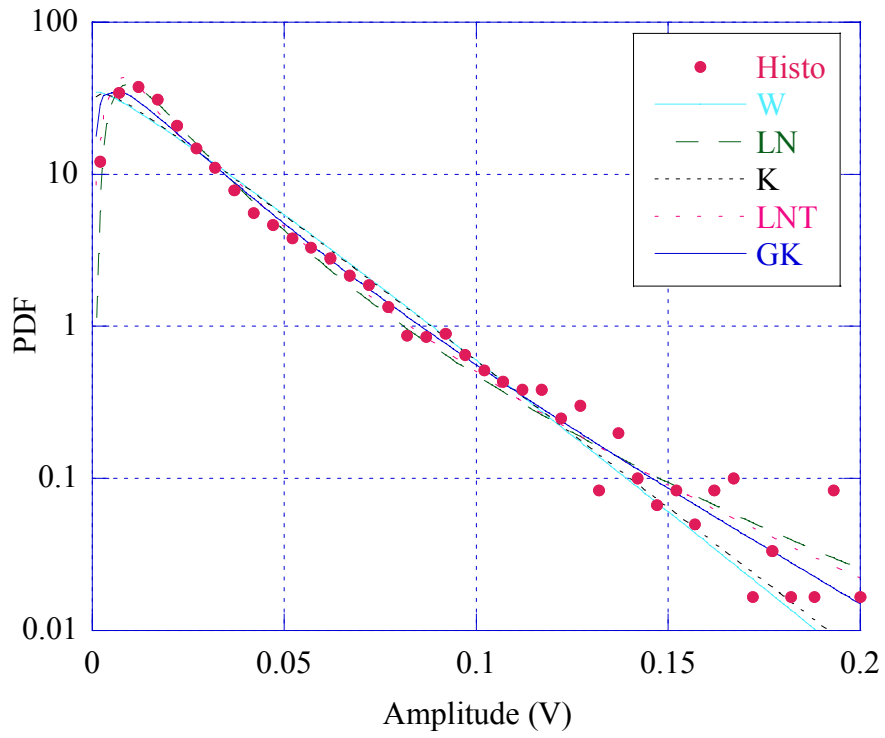


Figure 2.21 - Clutter amplitude PDF, HH polarization, 1<sup>st</sup> range cell.

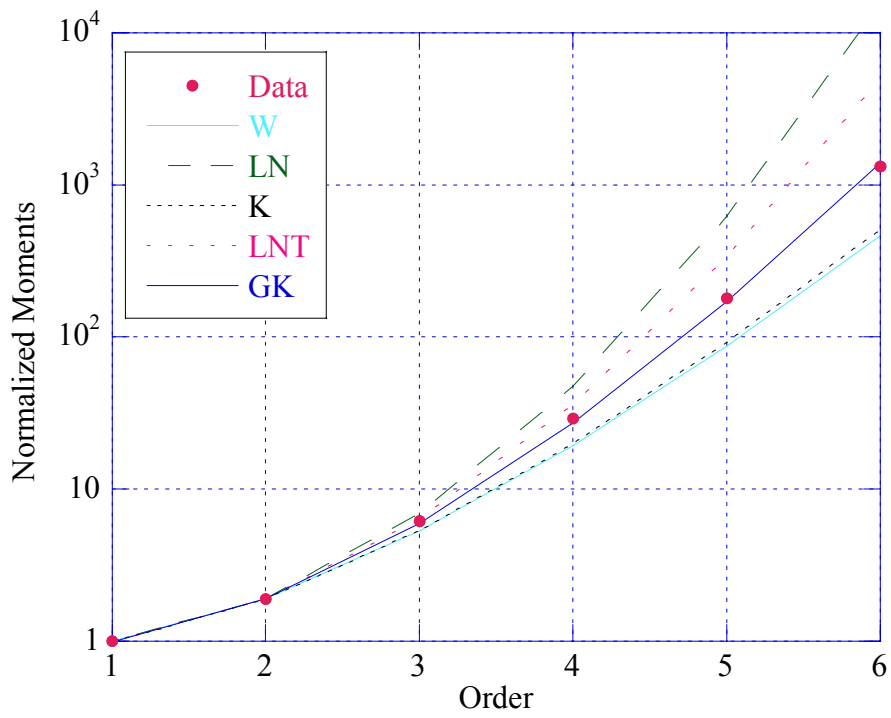


Figure 2.22 - Normalized clutter moments, HH polarization, 1<sup>st</sup> range cell.

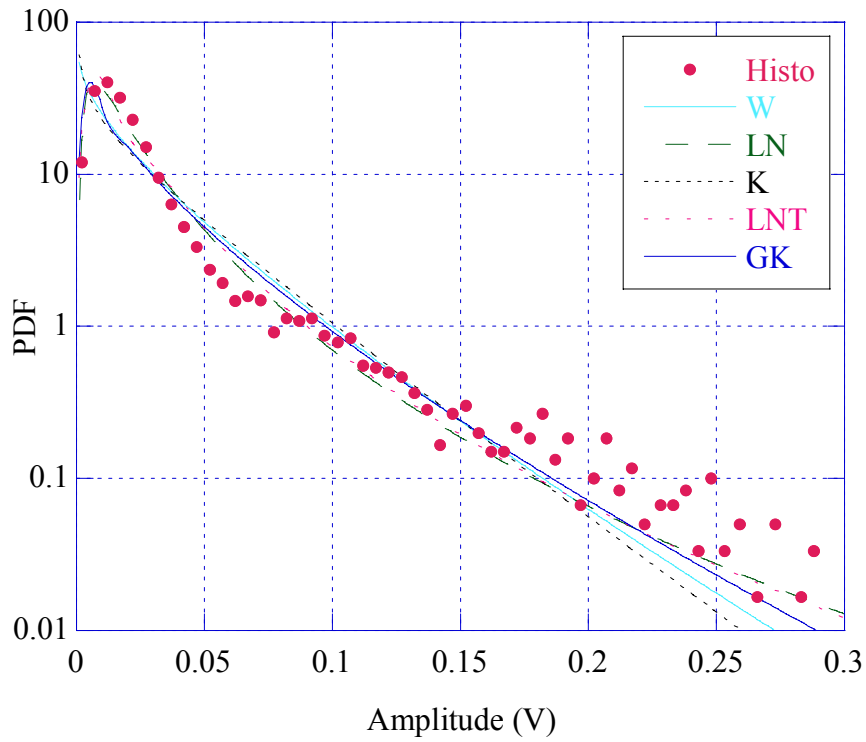


Figure 2.23 - Clutter amplitude PDF, HH polarization, 24<sup>th</sup> range cell.

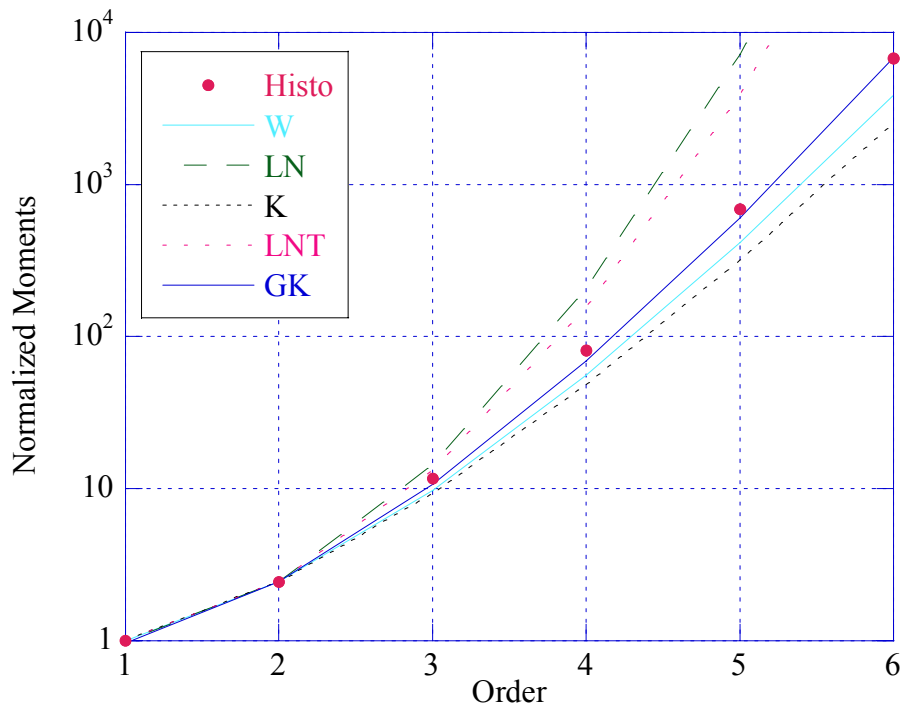


Figure 2.24 - Normalized clutter moments, HH polarization, 24<sup>th</sup> range cell.

Cell	W		LN		K	
	$\hat{c}$	$\hat{b}$	$\hat{\sigma}$	$\hat{\delta}$	$\hat{\nu}$	$\hat{\mu}$
1	1.0530	0.024817	0.80197	0.017628	0.57254	5.62339e-04
2	0.78998	0.022077	0.98391	0.015557	0.27675	8.38825e-04
3	0.86118	0.024008	0.92620	0.016873	0.34275	7.91578e-04
4	0.76273	0.023968	1.0082	0.016935	0.25369	1.09489e-03
5	0.67859	0.022537	1.0924	0.016197	0.18933	1.42669e-03
6	0.85248	0.023248	0.93285	0.016340	0.33421	7.60862e-04
7	0.81729	0.019878	0.96085	0.013984	0.30105	6.19668e-04
8	0.89973	0.022078	0.89794	0.015525	0.38230	6.04492e-04
9	0.88311	0.024021	0.90989	0.016885	0.36490	7.46613e-04
10	0.66576	0.024522	1.1066	0.017696	0.18037	1.81330e-03
11	0.71907	0.022124	1.0500	0.015740	0.21905	1.12350e-03
12	1.0613	0.022328	0.79741	0.015872	0.58462	4.49297e-04
13	1.1941	0.020337	0.73128	0.014660	0.81224	3.13154e-04
14	1.0765	0.025308	0.78920	0.018017	0.60734	5.64034e-04
15	1.1056	0.026279	0.77396	0.018763	0.65302	5.83273e-04
16	1.0263	0.025726	0.81710	0.018230	0.53492	6.31610e-04
17	0.98998	0.025047	0.83862	0.017698	0.48717	6.39229e-04
18	1.0165	0.025915	0.82278	0.018349	0.52170	6.51927e-04
19	0.82724	0.023403	0.95275	0.016458	0.31021	8.32048e-04
20	0.67872	0.025811	1.0922	0.018550	0.18942	1.87011e-03
21	0.95076	0.028016	0.86332	0.019745	0.43931	8.65440e-04
22	0.65534	0.024087	1.1185	0.017447	0.17325	1.85837e-03
23	1.0050	0.023439	0.82956	0.016580	0.50651	5.44351e-04
24	0.84006	0.023718	0.94252	0.016673	0.32227	8.21498e-04
25	0.59248	0.021255	1.1969	0.015886	0.13328	2.21507e-03
26	0.74145	0.026189	1.0281	0.018558	0.23646	1.42590e-03
27	0.65627	0.018794	1.1175	0.013609	0.17388	1.12521e-03
28	1.0760	0.022511	0.78948	0.016025	0.60654	4.46628e-04

**Table 2.15** - Estimated parameters, HH polarization.

Cell	LNT		GK			R
	$\hat{\sigma}^2$	$\hat{m}$	$\hat{\nu}$	$\hat{\mu}$	$\hat{b}$	$\hat{\sigma}^2$
1	1.6064	2.51870e-04	3.2986	9.32213e-05	0.37995	0.00083056
2	2.9061	1.96169e-04	0.47355	1.50673e-03	0.67000	0.0012389
3	2.4651	2.30781e-04	1.9071	2.22038e-04	0.37335	0.0011691
4	3.0994	2.32456e-04	0.82456	1.11778e-03	0.48033	0.0016171
5	3.8070	2.12644e-04	1.0862	5.78346e-04	0.35880	0.0021072
6	2.5146	2.16409e-04	1.2574	5.29974e-04	0.44902	0.0011238
7	2.7267	1.58512e-04	3.2392	1.49631e-05	0.26828	0.00091523
8	2.2589	1.95377e-04	4.7160	4.60247e-06	0.25362	0.00089282
9	2.3453	2.31109e-04	2.1894	1.59195e-04	0.36133	0.0011027
10	3.9324	2.53841e-04	0.48544	2.56424e-03	0.51878	0.0026782
11	3.4436	2.00821e-04	0.71510	1.15548e-03	0.46507	0.0016594
12	1.5772	2.04195e-04	2.5644	1.56157e-04	0.42888	0.00066360
13	1.1728	1.74216e-04	46.194	1.54797e-15	0.12772	0.00046252
14	1.5251	2.63111e-04	1.8932	4.12122e-04	0.51163	0.00083307
15	1.4298	2.85363e-04	1.8116	5.11107e-04	0.54873	0.00086148
16	1.7044	2.69373e-04	1.0459	9.11275e-04	0.64947	0.00093287
17	1.8469	2.53873e-04	2.3450	2.10213e-04	0.41217	0.00094413
18	1.7416	2.72904e-04	0.72818	1.18491e-03	0.77763	0.00096288
19	2.6647	2.19547e-04	2.1718	1.18478e-04	0.32910	0.0012289
20	3.8057	2.78908e-04	0.34295	3.49701e-03	0.65210	0.0027621
21	2.0150	3.15997e-04	0.81405	1.36923e-03	0.66326	0.0012782
22	4.0382	2.46741e-04	0.45275	2.67584e-03	0.51753	0.0027448
23	1.7864	2.22825e-04	6.6402	1.66754e-06	0.24931	0.00080399
24	2.5871	2.25331e-04	0.78925	1.07835e-03	0.55654	0.0012133
25	4.7644	2.04555e-04	0.28184	3.95775e-03	0.57589	0.0032716
26	3.2615	2.79160e-04	0.27888	2.90109e-03	0.84324	0.0021060
27	4.0286	1.50116e-04	0.71211	8.47477e-04	0.40227	0.0016619
28	1.5268	2.08159e-04	2.5956	1.60519e-04	0.43448	0.00065966

**Table 2.16** - Estimated parameters, HH polarization.

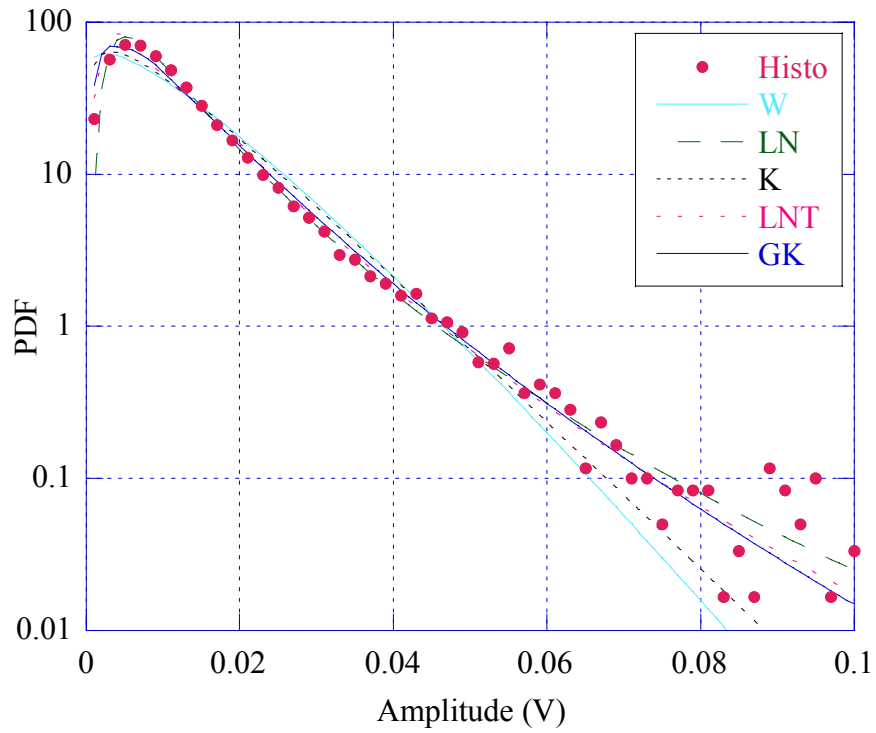


Figure 2.25 - Clutter amplitude PDF, VH polarization, 1<sup>st</sup> range cell.

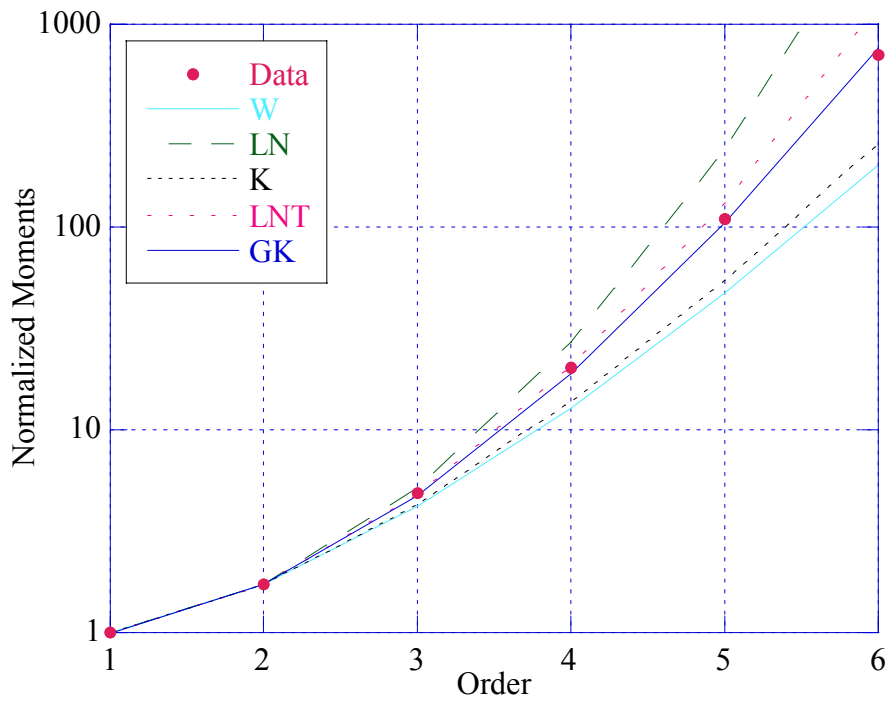


Figure 2.26 - Normalized clutter moments, VH polarization, 1<sup>st</sup> range cell.

Cell	W		LN		K	
	$\hat{c}$	$\hat{b}$	$\hat{\sigma}$	$\hat{\delta}$	$\hat{\nu}$	$\hat{\mu}$
1	1.1731	0.012249	0.74092	0.0088093	0.77146	1.16326e-04
2	1.0155	0.012028	0.82337	0.0085154	0.52036	1.40679e-04
3	1.0860	0.012121	0.78415	0.0086374	0.62193	1.27592e-04
4	0.91906	0.012383	0.88447	0.0087135	0.40324	1.81486e-04
5	0.86373	0.012815	0.92426	0.0090068	0.34529	2.23931e-04
6	0.95075	0.012230	0.86332	0.0086190	0.43930	1.64916e-04
7	0.99957	0.010727	0.83281	0.0075850	0.49944	1.15162e-04
8	1.0445	0.010246	0.80671	0.0072720	0.56037	9.71712e-05
9	1.0838	0.010995	0.78535	0.0078332	0.61844	1.05333e-04
10	0.82491	0.011789	0.95463	0.0082909	0.30806	2.12683e-04
11	0.85909	0.012085	0.92778	0.0084933	0.34069	2.01738e-04
12	1.0133	0.010832	0.82463	0.0076672	0.51749	1.14525e-04
13	1.4650	0.0093752	0.62695	0.0069742	1.6266	5.33782e-05
14	1.3264	0.010209	0.67607	0.0074731	1.1282	6.96592e-05
15	1.3933	0.011138	0.65138	0.0082174	1.3403	7.88830e-05
16	1.3051	0.011785	0.68436	0.0086054	1.0692	9.44736e-05
17	1.2231	0.011244	0.71834	0.0081325	0.87242	9.28157e-05
18	1.2625	0.011532	0.70157	0.0083789	0.96155	9.39426e-05
19	1.0217	0.010673	0.81977	0.0075602	0.52865	1.09585e-04
20	0.86559	0.011777	0.92286	0.0082773	0.34714	1.88151e-04
21	1.0074	0.012454	0.82816	0.0088116	0.50960	1.53040e-04
22	0.82529	0.011991	0.95432	0.0084328	0.30841	2.19769e-04
23	0.94295	0.010757	0.86842	0.0075775	0.43022	1.29741e-04
24	0.98369	0.010930	0.84248	0.0077193	0.47923	1.23201e-04
25	0.68669	0.0095926	1.0836	0.0068778	0.19510	2.47595e-04
26	0.80102	0.011502	0.97444	0.0080991	0.28643	2.19076e-04
27	0.72096	0.0093150	1.0481	0.0066248	0.22049	1.97450e-04
28	0.82843	0.0086912	0.95179	0.0061116	0.31132	1.14324e-04

**Table 2.17** - Estimated parameters, VH polarization.

Cell	LNT		GK			R
	$\hat{\sigma}^2$	$\hat{m}$	$\hat{\nu}$	$\hat{\mu}$	$\hat{b}$	$\hat{\sigma}^2$
1	1.2296	6.29032e-05	12.186	3.99333e-08	0.23474	0.00017181
2	1.7455	5.87761e-05	1.7059	9.99138e-05	0.49165	0.00020778
3	1.4933	6.04721e-05	1.2749	1.69678e-04	0.64051	0.00018845
4	2.1629	6.15419e-05	4.1802	3.86250e-06	0.28130	0.00026805
5	2.4508	6.57557e-05	0.92957	2.56157e-04	0.52999	0.00033074
6	2.0150	6.02146e-05	1.3792	1.36387e-04	0.49620	0.00024358
7	1.8081	4.66333e-05	1.7539	7.27535e-05	0.47258	0.00017009
8	1.6369	4.28645e-05	3.8849	7.48454e-06	0.33956	0.00014352
9	1.5008	4.97357e-05	4.1084	9.01712e-06	0.35139	0.00015557
10	2.6790	5.57179e-05	1.5948	7.84685e-05	0.38439	0.00031413
11	2.4769	5.84717e-05	0.95783	2.18525e-04	0.51697	0.00029796
12	1.7538	4.76502e-05	5.9829	7.81120e-07	0.26590	0.00016915
13	0.60599	3.94252e-05	2.5306	7.49860e-05	0.76678	7.8838e-05
14	0.86200	4.52686e-05	4.7880	1.57476e-05	0.44875	0.00010289
15	0.73093	5.47347e-05	4.4953	3.22888e-05	0.51700	0.00011651
16	0.90712	6.00248e-05	15.851	2.80806e-08	0.24644	0.00013954
17	1.0978	5.36093e-05	3.7269	2.60019e-05	0.44530	0.00013709
18	1.0025	5.69072e-05	2.1589	9.76270e-05	0.62434	0.00013875
19	1.7218	4.63300e-05	19.795	3.92859e-12	0.14965	0.00016185
20	2.4404	5.55355e-05	0.64708	3.10089e-04	0.65105	0.00027789
21	1.7771	6.29366e-05	0.47202	3.06090e-04	1.0041	0.00022604
22	2.6767	5.76413e-05	2.6515	1.49881e-05	0.30060	0.00032459
23	2.0504	4.65417e-05	5.3800	7.93733e-07	0.25551	0.00019162
24	1.8728	4.82993e-05	0.64768	2.29052e-04	0.78744	0.00018197
25	3.7304	3.83436e-05	0.74459	2.14549e-04	0.43160	0.00036569
26	2.8319	5.31692e-05	0.61917	3.40980e-04	0.60308	0.00032357
27	3.4277	3.55745e-05	0.52093	2.95805e-04	0.55442	0.00029163
28	2.6573	3.02762e-05	2.6949	6.67246e-06	0.29381	0.00016885

**Table 2.18** - Estimated parameters, VH polarization.

## 2.2.4 Range resolution of 9 m

Looking at the histograms obtained by analyzing the file “19980204\_224024\_antstep.cdf” at a resolution of 9 m, it comes obvious to notice that the received clutter power and the statistical characteristic of the backscattered echoes strictly depend on the illuminated cell. To have an idea of the phenomenon it is sufficient to compare figure 2.28 to figure 2.31, reporting the amplitude histograms of the 9<sup>th</sup> and of the 5<sup>th</sup> cell, for VV polarization. In the 5<sup>th</sup> cell the histogram presents a longer tail than the one presented by 9<sup>th</sup> cell; this means that the received power is very different in each case. This is because the number of scatters decreases as resolution increases and, it is not true anymore that local conditions are similar in each cell; as well known, the characteristics of the backscattering depend on local conditions. Received power is influenced by the number of scatterers per cell, by their position, and by the looking direction of the radar.

We also noticed that both cells present a peak in the histogram for low values of the amplitude whose shape and extension (0.1 V about) are different with respect to those shown at 60 m and 30 m of resolution. We can suppose that “the peak” or the “bell-shaped” part of the histogram is mostly originated by the thermal noise contribution. In the 9<sup>th</sup> cell (Figure 2.28), we can notice that the peak can be well modeled by the Rayleigh-PDF.

Figures 2.33, 2.34, 2.35, 2.36, and 2.37 show that all the results found for VV polarization can be extended to HH polarization.

To conclude, looking at the results, we can state that none of the proposed distributions can be used to model the data clutter for co-polarizations.

On the contrary, figures 2.38 and 2.39 show that for cross-polarizations, the clutter process can be accurately modeled by a compound-Gaussian process with Generalized K-PDF.

Figure 2.27 shows that also at 9 m range resolution, the highest backscattered power levels are measured for VV polarization. Both HH and VV polarizations have the same behavior while VH polarization is the weakest one.

Estimated parameters show, like at both 60 m and 15 m range resolution, that HH component is the spikiest one (HH:  $\bar{c} = 0.99$ , VV:  $\bar{c} = 1.0985$ , VH:  $\bar{c} = 1.1700$ , see Tables 2.19-2.24).

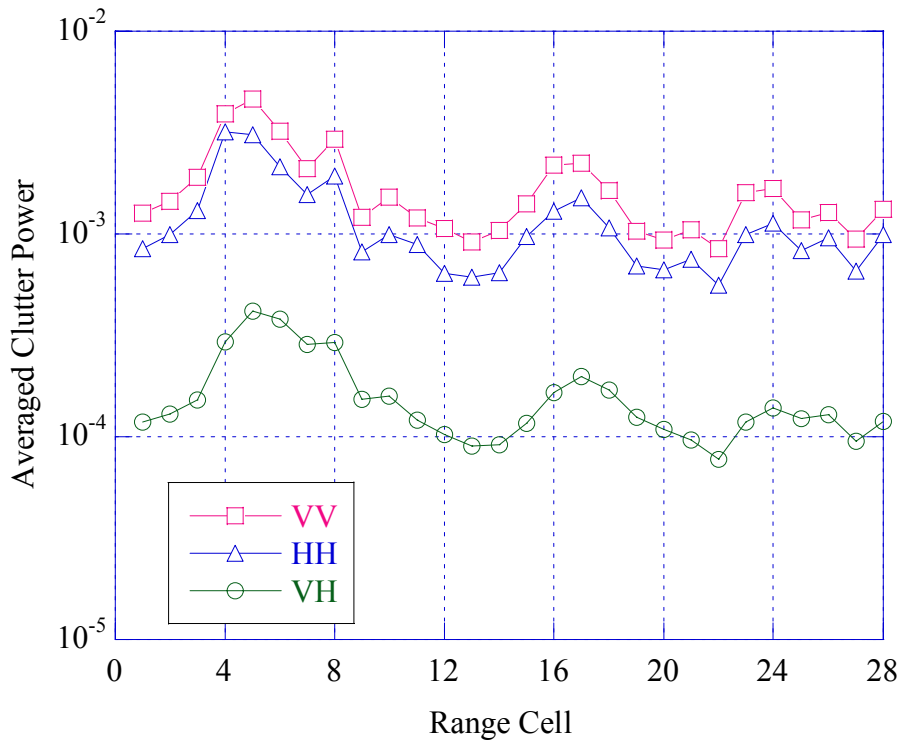


Figure 2.27 - Average backscattered power vs range cell number..

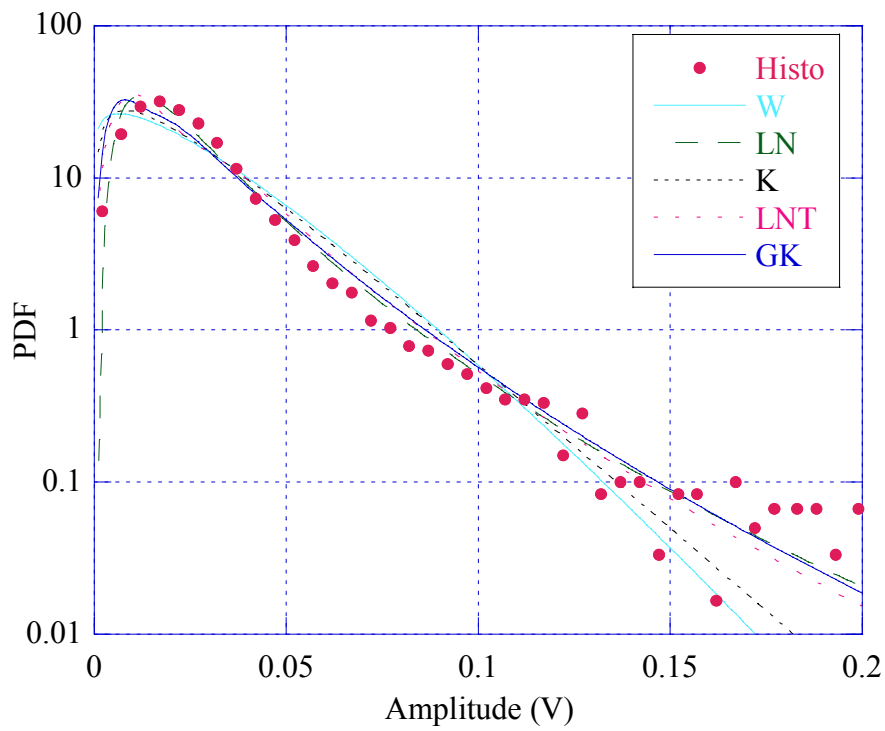


Figure 2.28 - Clutter amplitude PDF, VV polarization, 9th range cell.

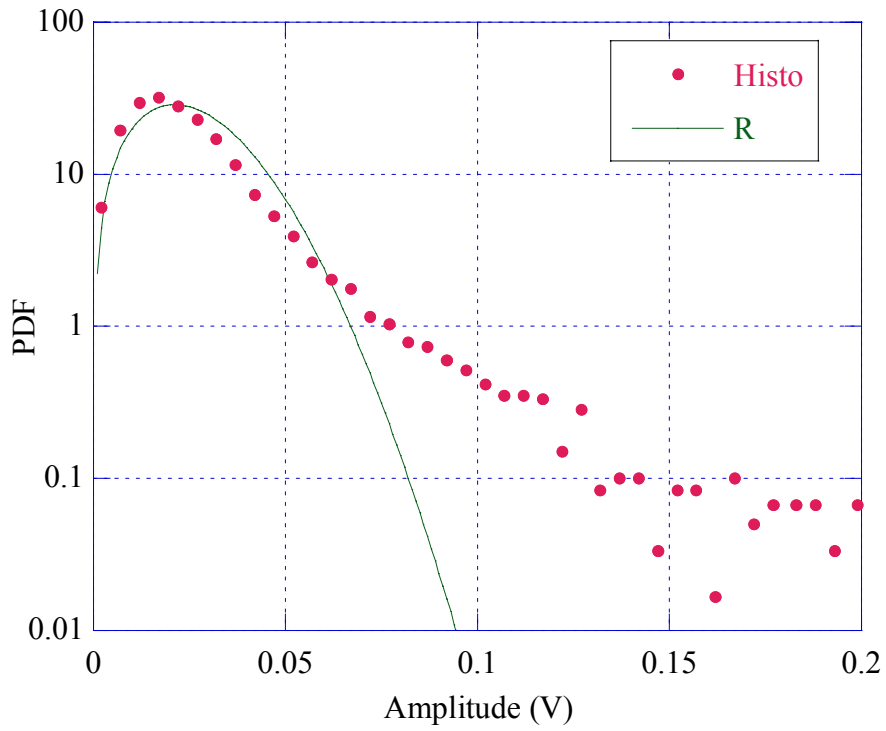


Figure 2.29 - Clutter amplitude PDF, VV polarization, 9th range cell.

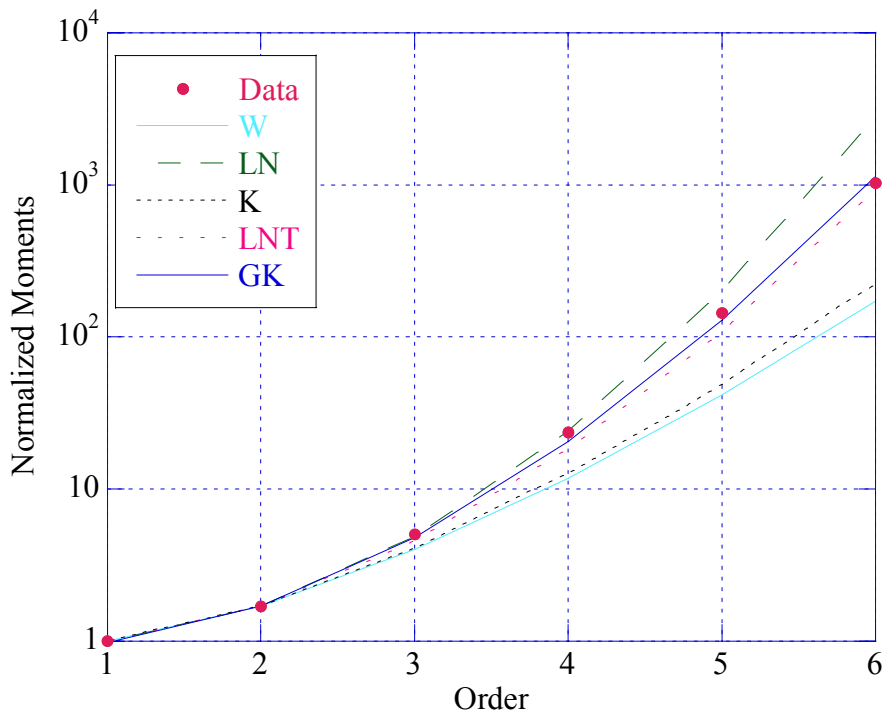


Figure 2.30 - Normalized clutter moments, VV polarization, 9th range cell.

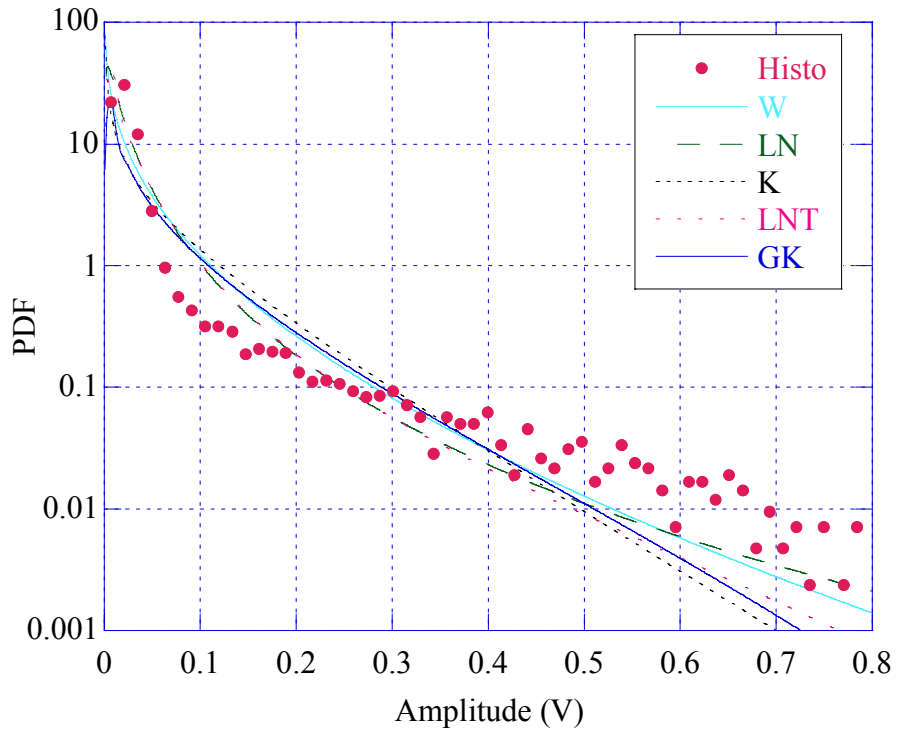


Figure 2.31 - Clutter amplitude PDF, VV polarization, 5th range cell.

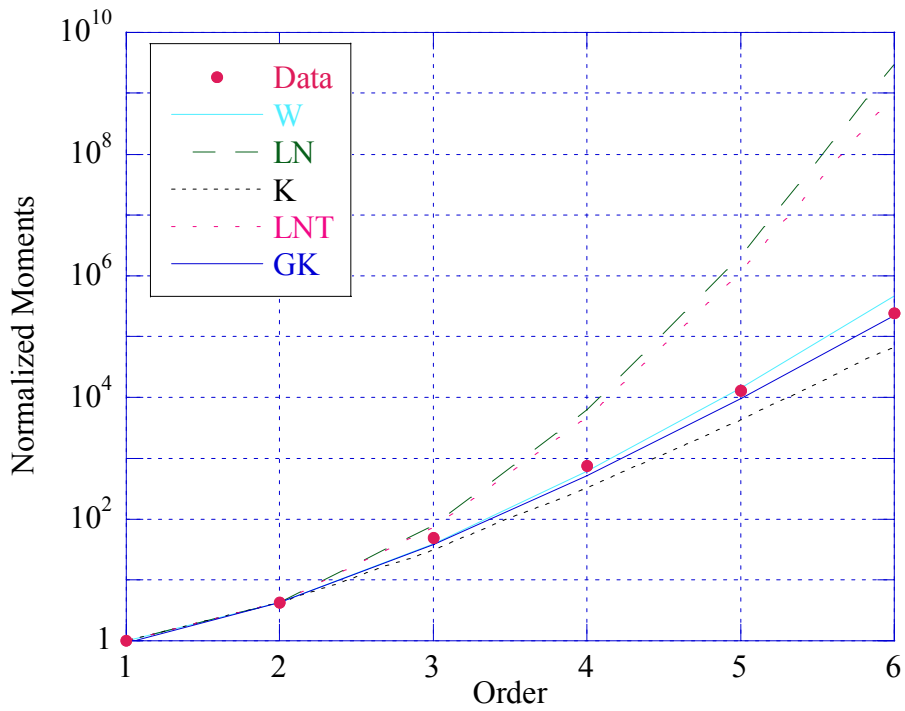


Figure 2.32 - Normalized clutter moments, VV polarization, 5th range cell.

Cell	W		LN		K	
	$\hat{c}$	$\hat{b}$	$\hat{\sigma}$	$\hat{\delta}$	$\hat{\nu}$	$\hat{\mu}$
1	1.0268	0.025826	0.81677	0.018302	0.53571	0.00063592
2	0.94365	0.025438	0.86797	0.017920	0.43103	0.00072448
3	0.89185	0.027483	0.90356	0.019322	0.37399	0.00095545
4	0.61444	0.021708	1.1682	0.016017	0.14668	0.0019651
5	0.58511	0.021082	1.2070	0.015833	0.12892	0.0023090
6	0.73606	0.027442	1.0333	0.019464	0.23219	0.0016023
7	0.91203	0.029594	0.88932	0.020819	0.39553	0.0010540
8	0.70509	0.024482	1.0642	0.017471	0.20853	0.0014700
9	1.2011	0.028407	0.72813	0.020494	0.82627	0.00060636
10	1.0533	0.028855	0.80182	0.020497	0.57295	0.00075992
11	1.1864	0.028073	0.73479	0.020220	0.79702	0.00060185
12	1.2517	0.027311	0.70610	0.019818	0.93610	0.00053231
13	1.5315	0.028004	0.60596	0.020990	1.9700	0.00045911
14	1.4108	0.028761	0.64525	0.021262	1.4035	0.00051977
15	1.0966	0.028707	0.77862	0.020478	0.63853	0.00070489
16	0.99777	0.032963	0.83389	0.023304	0.49712	0.0010910
17	0.96040	0.032197	0.85710	0.022704	0.45074	0.0011201
18	0.93425	0.026806	0.87420	0.018875	0.42025	0.00082137
19	1.3525	0.028040	0.66620	0.020588	1.2057	0.00051488
20	1.3957	0.027137	0.65055	0.020026	1.3486	0.00046747
21	1.1876	0.026199	0.73424	0.018873	0.79935	0.00052350
22	1.4981	0.026672	0.61631	0.019916	1.7862	0.00042393
23	0.96048	0.027242	0.85705	0.019210	0.45082	0.00080173
24	1.0270	0.029670	0.81667	0.021026	0.53595	0.00083905
25	1.3334	0.029760	0.67337	0.021802	1.1486	0.00058860
26	1.2139	0.029337	0.72240	0.021196	0.85282	0.00063790
27	1.5113	0.028261	0.61221	0.021134	1.8554	0.00047258
28	1.2409	0.030285	0.71067	0.021949	0.91149	0.00066145

**Table 2.19** - Estimated parameters, VV polarization

Cell	LNT		GK			R
	$\hat{\sigma}^2$	$\hat{m}$	$\hat{\nu}$	$\hat{\mu}$	$\hat{b}$	$\hat{\sigma}^2$
1	1.7022	0.00027150	20.863	4.8779e-12	0.14142	0.00093924
2	2.0472	0.00026030	6.9437	3.4996e-07	0.21085	0.0010700
3	2.2994	0.00030262	2.3681	0.00013835	0.33783	0.0014112
4	4.4921	0.00020794	0.30924	0.0033557	0.55656	0.0029024
5	4.8608	0.00020320	0.21612	0.0045520	0.63768	0.0034104
6	3.3043	0.00030707	0.89647	0.0012283	0.42795	0.0023666
7	2.1973	0.00035132	2.3154	0.00019955	0.35654	0.0015568
8	3.5639	0.00024742	0.91691	0.00081217	0.38016	0.0021712
9	1.1544	0.00034044	64.343	1.5011e-19	0.10366	0.00089557
10	1.6054	0.00034054	7.6349	1.1225e-06	0.23947	0.0011224
11	1.1934	0.00033140	67.280	1.3586e-20	0.098853	0.00088892
12	1.0280	0.00031837	67.570	1.3165e-19	0.10464	0.00078621
13	0.50252	0.00035711	68.927	9.3752e-15	0.14470	0.00067809
14	0.69915	0.00036643	68.581	5.9187e-16	0.13184	0.00076769
15	1.4587	0.00033991	66.582	4.9291e-23	0.087208	0.0010411
16	1.8153	0.00044021	1.4404	0.00095696	0.51634	0.0016114
17	1.9722	0.00041781	5.4600	7.5102e-06	0.25927	0.0016543
18	2.0906	0.00028878	13.159	5.5786e-10	0.15769	0.0012131
19	0.80905	0.00034358	67.807	9.1822e-19	0.10996	0.00076047
20	0.72659	0.00032507	68.121	1.1326e-17	0.11786	0.00069044
21	1.1902	0.00028871	67.177	6.1766e-21	0.097386	0.00077319
22	0.55311	0.00032151	68.649	8.4241e-16	0.13414	0.00062614
23	1.9719	0.00029911	7.4109	4.3620e-07	0.21652	0.0011841
24	1.7015	0.00035835	4.9607	1.8433e-05	0.29533	0.0012392
25	0.84745	0.00038530	68.181	2.8064e-17	0.12009	0.00086935
26	1.1212	0.00036416	44.947	4.3167e-15	0.12831	0.00094216
27	0.53293	0.00036204	68.706	1.5202e-15	0.13619	0.00069800
28	1.0539	0.00039051	67.617	2.4249e-19	0.10566	0.00097694

**Table 2.20** - Estimated parameters, VV polarization.

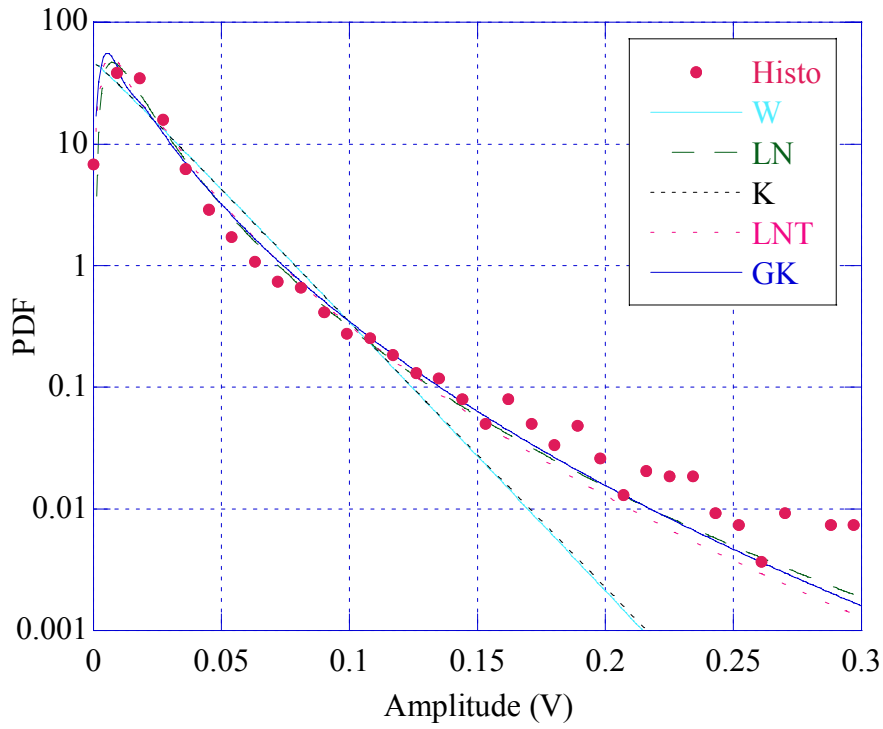


Figure 2.33 - Clutter amplitude PDF, HH polarization, 9th range cell.

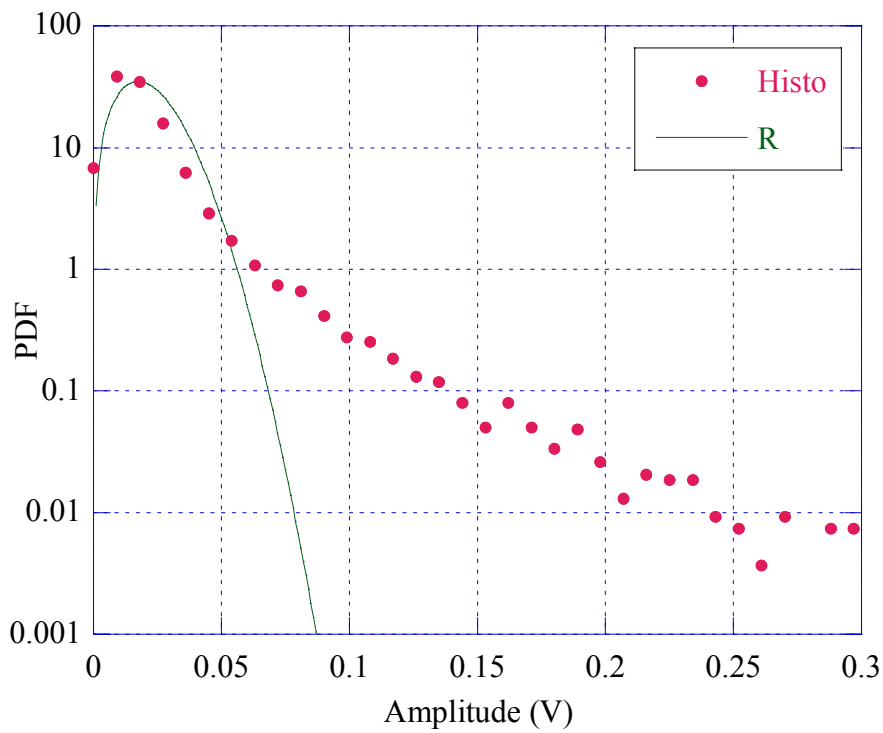


Figure 2.34 - Clutter amplitude PDF, HH polarization, 9th range cell.

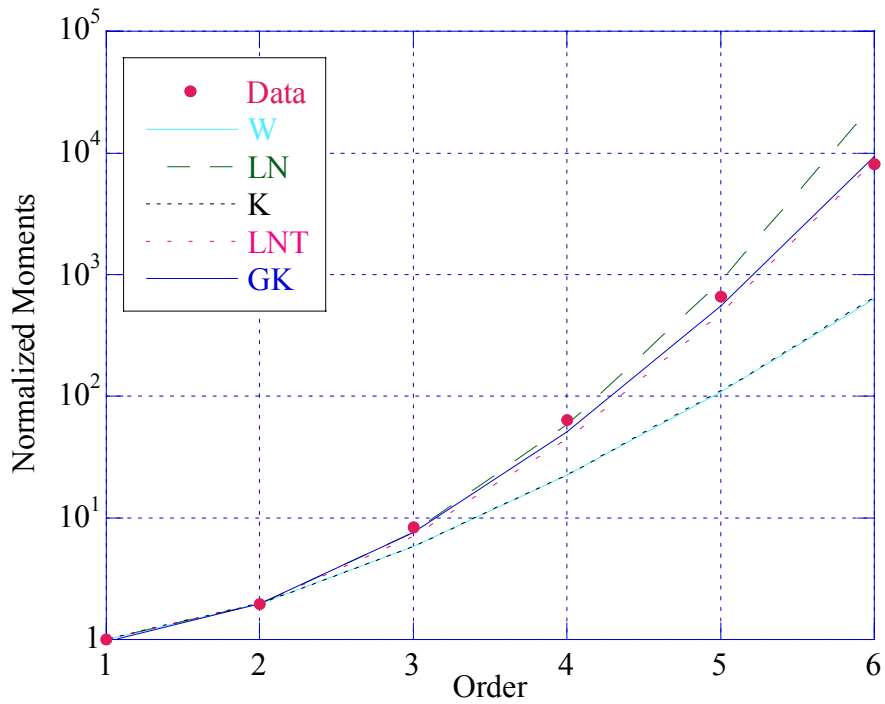


Figure 2.35 - Normalized clutter moments, HH polarization, 9th range cell.

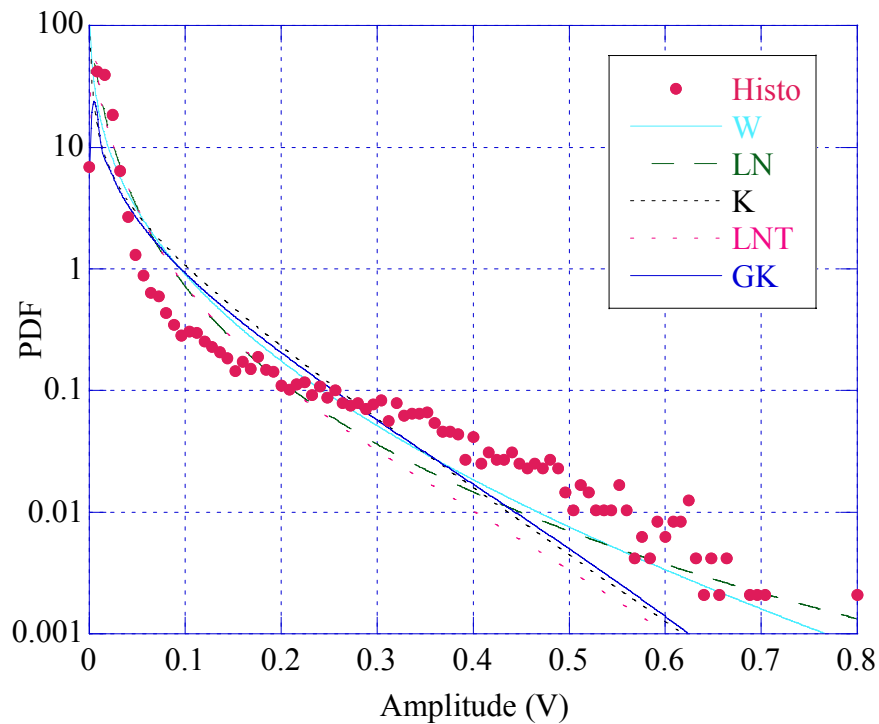
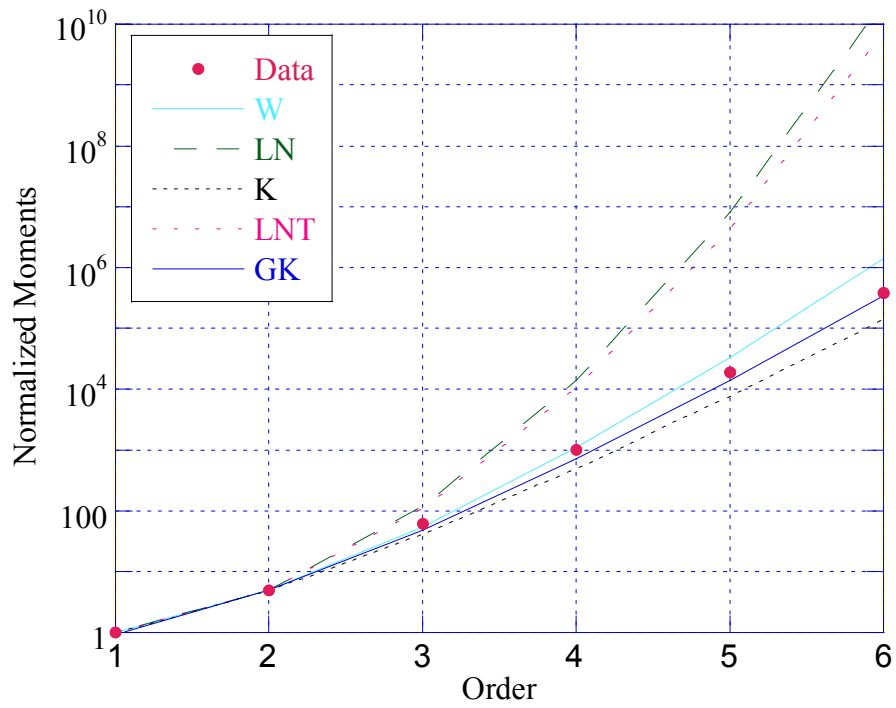


Figure 2.36 - Clutter amplitude PDF, HH polarization, 5th range cell.



**Figure 2.37** - Normalized clutter moments, HH polarization, 5th range cell.

Cell	W		LN		K	
	$\hat{c}$	$\hat{b}$	$\hat{\sigma}$	$\hat{\delta}$	$\hat{\nu}$	$\hat{\mu}$
1	0.85084	0.017344	0.93411	0.012190	0.33262	0.00042550
2	0.78819	0.016954	0.98547	0.011949	0.27520	0.00049789
3	0.77594	0.018994	0.99625	0.013401	0.26473	0.00065364
4	0.54485	0.014712	1.2653	0.011414	0.10627	0.0016014
5	0.54765	0.014647	1.2611	0.011334	0.10778	0.0015452
6	0.68620	0.019960	1.0841	0.014313	0.19474	0.0010747
7	0.79057	0.021332	0.98340	0.015032	0.27727	0.00078157
8	0.66555	0.017893	1.1069	0.012913	0.18023	0.00096652
9	1.0152	0.020502	0.82352	0.014515	0.52001	0.00040893
10	0.96480	0.021523	0.85430	0.015182	0.45602	0.00049604
11	0.98073	0.020683	0.84430	0.014604	0.47554	0.00044370
12	1.1903	0.020503	0.73301	0.014774	0.80468	0.00031963
13	1.3215	0.021372	0.67793	0.015635	1.1144	0.00030647
14	1.2876	0.021625	0.69132	0.015758	1.0234	0.00032292
15	0.97588	0.021565	0.84732	0.015222	0.46953	0.00048697
16	0.96585	0.024658	0.85363	0.017394	0.45729	0.00064963
17	0.89789	0.024564	0.89925	0.017273	0.38034	0.00075175
18	0.89094	0.020591	0.90422	0.014476	0.37302	0.00053761
19	1.2067	0.021564	0.72561	0.015567	0.83778	0.00034730
20	1.2136	0.021149	0.72253	0.015280	0.85219	0.00033164
21	1.0353	0.019990	0.81191	0.014177	0.54743	0.00037556
22	1.3775	0.020829	0.65703	0.015339	1.2862	0.00027893
23	0.94380	0.021100	0.86787	0.014864	0.43120	0.00049829
24	0.96115	0.022880	0.85662	0.016135	0.45163	0.00056476
25	1.1989	0.023492	0.72911	0.016944	0.82185	0.00041566
26	1.1033	0.023772	0.77517	0.016969	0.64922	0.00047886
27	1.4107	0.022846	0.64528	0.016889	1.4033	0.00032796
28	1.1387	0.024799	0.75738	0.017768	0.70875	0.00049715

**Table 2.21** - Estimated parameters, HH polarization.

Cell	LNt		GK			Rayleigh
	$\hat{\sigma}^2$	$\hat{m}$	$\hat{\nu}$	$\hat{\mu}$	$\hat{b}$	$\hat{\sigma}^2$
1	2.5240	0.00012045	2.7028	2.4227e-05	0.29280	0.00062845
2	2.9183	0.00011573	1.7344	8.7604e-05	0.32534	0.00073538
3	3.0038	0.00014557	0.92624	0.00054056	0.44607	0.00096542
4	5.4380	0.00010560	0.14971	0.0033572	0.70553	0.0023653
5	5.3947	0.00010412	0.14659	0.0032543	0.72748	0.0022822
6	3.7350	0.00016605	0.64084	0.0011771	0.46868	0.0015874
7	2.9020	0.00018315	1.1114	0.00052096	0.42700	0.0011544
8	3.9344	0.00013516	0.77679	0.00064209	0.39074	0.0014275
9	1.7465	0.00017077	38.063	1.9895e-17	0.10694	0.00060398
10	1.9530	0.00018682	5.0274	4.7734e-06	0.26533	0.00073264
11	1.8851	0.00017288	65.751	3.3157e-26	0.076527	0.00065533
12	1.1829	0.00017692	67.262	6.1366e-21	0.098485	0.00047208
13	0.87212	0.00019816	68.113	6.9648e-18	0.11765	0.00045265
14	0.94541	0.00020128	15.624	5.8717e-08	0.23601	0.00047694
15	1.9055	0.00018781	24.111	1.2233e-13	0.12748	0.00071925
16	1.9485	0.00024523	1.0187	0.00083849	0.58988	0.00095950
17	2.2683	0.00024183	2.5849	9.5956e-05	0.33664	0.0011103
18	2.3042	0.00016987	9.6406	8.2995e-09	0.17623	0.00079403
19	1.1398	0.00019643	25.244	3.7948e-11	0.16647	0.00051295
20	1.1219	0.00018925	51.708	8.0440e-17	0.11915	0.00048983
21	1.6705	0.00016291	20.897	5.2684e-12	0.14522	0.00055470
22	0.76049	0.00019070	68.354	4.7217e-17	0.12453	0.00041197
23	2.0465	0.00017910	5.5790	1.8828e-06	0.24412	0.00073596
24	1.9690	0.00021101	3.8518	2.4574e-05	0.30697	0.00083414
25	1.1602	0.00023271	67.128	2.6300e-21	0.096031	0.00061392
26	1.4373	0.00023340	8.4704	9.3105e-07	0.25256	0.00070726
27	0.69927	0.00023120	68.588	3.9361e-16	0.13205	0.00048439
28	1.3282	0.00025590	7.2695	4.2768e-06	0.28723	0.00073428

**Table 2.22** - Estimated parameters, HH polarization.

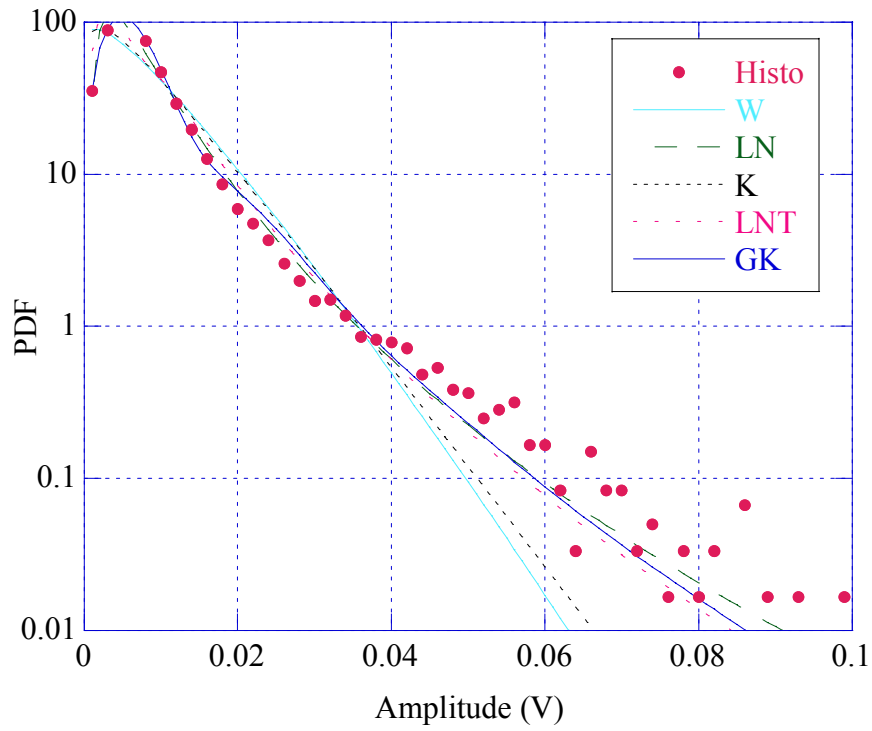


Figure 2.38 - Clutter amplitude PDF, VH polarization, 1<sup>st</sup> range cell.

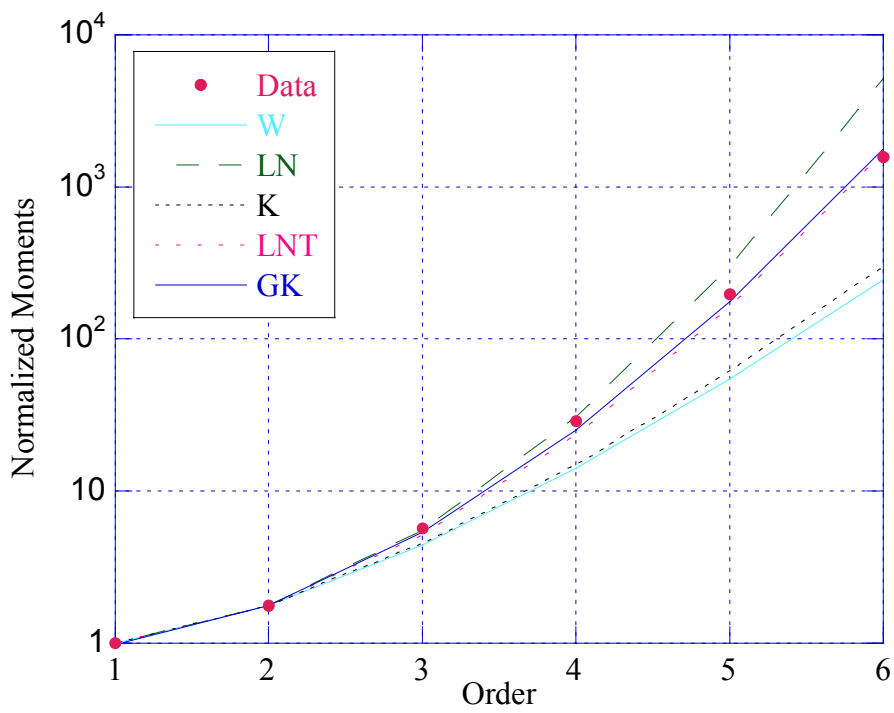


Figure 2.39 - Normalized clutter moments, VH polarization, 1<sup>st</sup> range cell.

Cell	W		LN		K	
	$\hat{c}$	$\hat{b}$	$\hat{\sigma}$	$\hat{\delta}$	$\hat{\nu}$	$\hat{\mu}$
1	1.1426	0.0085673	0.75548	0.0061409	0.71559	5.9044e-05
2	1.0313	0.0082828	0.81420	0.0058719	0.54187	6.4913e-05
3	0.99249	0.0086713	0.83709	0.0061280	0.49035	7.6252e-05
4	0.69983	0.0076419	1.0697	0.0054603	0.20464	0.00014697
5	0.62646	0.0073686	1.1531	0.0054036	0.15427	0.00020853
6	0.71158	0.0089568	1.0575	0.0063824	0.21338	0.00019071
7	0.84564	0.0099581	0.93815	0.0069996	0.32760	0.00014242
8	0.81797	0.0096575	0.96029	0.0067938	0.30168	0.00014594
9	1.1498	0.0098045	0.75198	0.0070332	0.72843	7.6639e-05
10	1.0599	0.0093958	0.79816	0.0066783	0.58261	7.9736e-05
11	1.2482	0.0091980	0.70758	0.0066718	0.92801	6.0581e-05
12	1.3532	0.0088368	0.66593	0.0064890	1.2080	5.1111e-05
13	1.5000	0.0087158	0.61573	0.0065095	1.7957	4.5223e-05
14	1.5424	0.0088575	0.60268	0.0066469	2.0356	4.5677e-05
15	1.2541	0.0090620	0.70509	0.0065777	0.94168	5.8470e-05
16	1.1569	0.010239	0.74861	0.0073504	0.74116	8.2862e-05
17	1.1010	0.010787	0.77634	0.0076979	0.64556	9.8905e-05
18	1.1296	0.010208	0.76187	0.0073065	0.69297	8.5224e-05
19	1.3724	0.0098424	0.65889	0.0072436	1.2692	6.2513e-05
20	1.3326	0.0090375	0.67371	0.0066203	1.1460	5.4321e-05
21	1.3239	0.0084746	0.67702	0.0062017	1.1212	4.8097e-05
22	1.5921	0.0082555	0.58810	0.0062292	2.3803	3.8747e-05
23	1.1307	0.0085042	0.76132	0.0060879	0.69488	5.9066e-05
24	1.1198	0.0091558	0.76677	0.0065467	0.67634	6.9454e-05
25	1.3313	0.0095937	0.67419	0.0070267	1.1423	6.1275e-05
26	1.3438	0.0098602	0.66944	0.0072326	1.1794	6.4093e-05
27	1.6262	0.0091998	0.57851	0.0069673	2.6700	4.7402e-05
28	1.3753	0.0096387	0.65783	0.0070961	1.2788	5.9825e-05

**Table 2.23** - Estimated parameters, VH polarization.

Cell	LNT		GK			R
	$\hat{\sigma}^2$	$\hat{m}$	$\hat{\nu}$	$\hat{\mu}$	$\hat{b}$	$\hat{\sigma}^2$
1	1.3167	3.0567e-05	42.677	5.7346e-17	0.11945	8.7206e-05
2	1.6854	2.7948e-05	12.231	1.0202e-09	0.18672	9.5875e-05
3	1.8366	3.0439e-05	3.1468	8.8229e-06	0.34752	0.00011262
4	3.6104	2.4167e-05	0.70733	0.00013803	0.44282	0.00021707
5	4.3520	2.3668e-05	0.45949	0.00026803	0.47828	0.00030800
6	3.5073	3.3019e-05	0.37039	0.00035351	0.65664	0.00028167
7	2.5542	3.9714e-05	0.73843	0.00020255	0.58244	0.00021036
8	2.7224	3.7412e-05	1.5685	4.9293e-05	0.37313	0.00021555
9	1.2957	4.0096e-05	2.9834	2.5921e-05	0.44285	0.00011319
10	1.5820	3.6151e-05	3.1961	1.2823e-05	0.37425	0.00011777
11	1.0364	3.6081e-05	19.653	5.7583e-10	0.20165	8.9477e-05
12	0.80760	3.4131e-05	38.138	8.4801e-13	0.16648	7.5490e-05
13	0.55023	3.4346e-05	57.840	1.2929e-13	0.16784	6.6794e-05
14	0.48662	3.5812e-05	66.456	4.1629e-14	0.16470	6.7463e-05
15	1.0223	3.5070e-05	67.321	1.8367e-21	0.099614	8.6359e-05
16	1.2754	4.3793e-05	4.8384	5.7029e-06	0.35214	0.00012239
17	1.4446	4.8032e-05	20.711	2.2113e-11	0.16510	0.00014608
18	1.3555	4.3273e-05	67.039	2.5780e-22	0.094465	0.00012587
19	0.77029	4.2531e-05	68.428	3.1444e-17	0.12858	9.2330e-05
20	0.84928	3.5526e-05	68.030	6.1950e-19	0.11546	8.0231e-05
21	0.86715	3.1176e-05	68.075	7.9471e-19	0.11663	7.1038e-05
22	0.41717	3.1452e-05	69.366	3.1312e-14	0.16525	5.7228e-05
23	1.3522	3.0041e-05	66.822	2.9687e-23	0.090863	8.7239e-05
24	1.3855	3.4741e-05	6.3786	9.5671e-07	0.29524	0.00010258
25	0.85188	4.0022e-05	5.8326	7.2817e-06	0.40889	9.0501e-05
26	0.82632	4.2401e-05	23.343	8.4886e-10	0.21390	9.4664e-05
27	0.37242	3.9348e-05	69.590	3.3406e-13	0.18031	7.0011e-05
28	0.76470	4.0816e-05	68.392	1.3884e-17	0.12568	8.8360e-05

**Table 2.24** - Estimated parameters, VH polarization.

### 2.2.5 Range resolution of 3 m

The results obtained at a range resolution of 3 m, for co-polarizations, do not show relevant differences with respect to the results obtained at 9 m. Conversely, VH polarization presents changes. There are cells showing histograms with tails longer than the average length recorded at lower resolutions (Figs. 2.56 and 2.57 ); in these cells the compound PDF can't be used to model the clutter data. The results are reported in figures 2.41-2.58 for all polarizations.

Estimated parameters reported in tables 2.25, 2.26, 2.27, 2.28, 2.29, 2.30 show again that HH component ( $\bar{c} = 1.3068$ ) is more spiky than both VV ( $\bar{c} = 1.4171$ ) and VH ( $\bar{c} = 1.5415$ ) components. Let's notice that with respect to the other resolutions, probably because of thermal noise effect, estimated values of  $\bar{c}$  are a little higher in all polarizations. In some cells, see as instance Figs. 2.45 and 2.48 for the 2<sup>nd</sup> range cell, co-polarized data, the bell-shaped part of the histogram is very similar to the Rayleigh PDF.

Figure 2.40 shows that HH polarization is, in all cells, weaker than VV polarization and, that the behavior versus cell number is very similar in both polarizations.

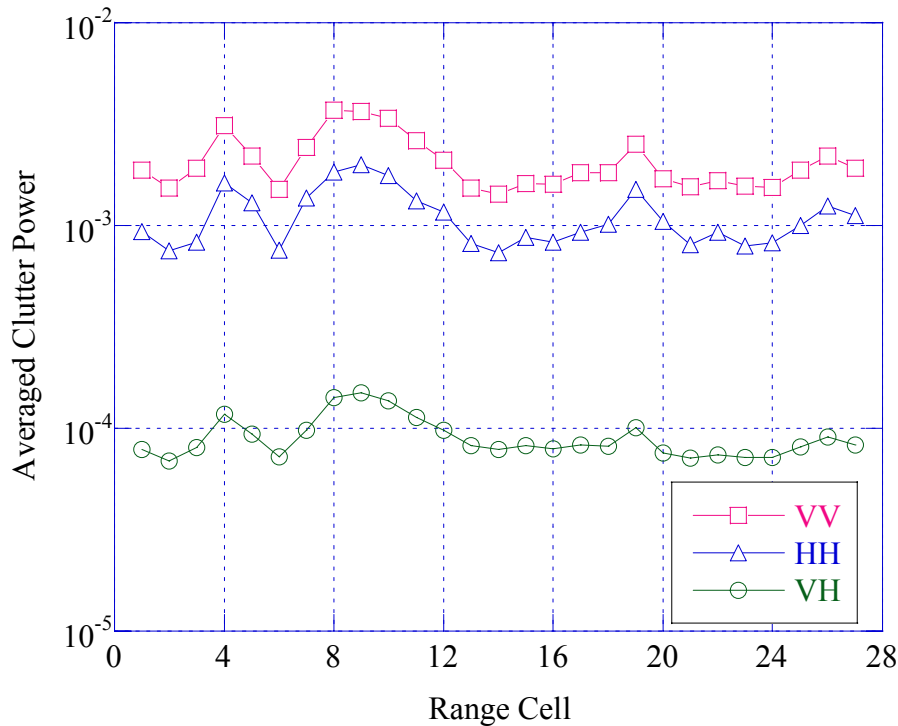


Figure 2.40 - Average backscattered power vs range cell number.

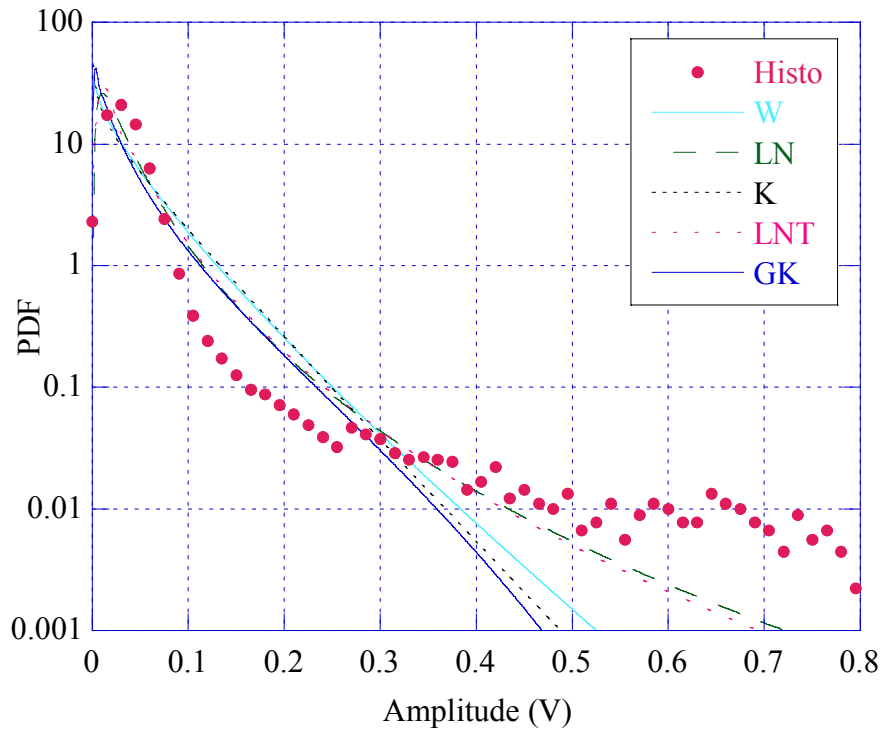


Figure 2.41 - Clutter amplitude PDF, VV polarization, 8th range cell.

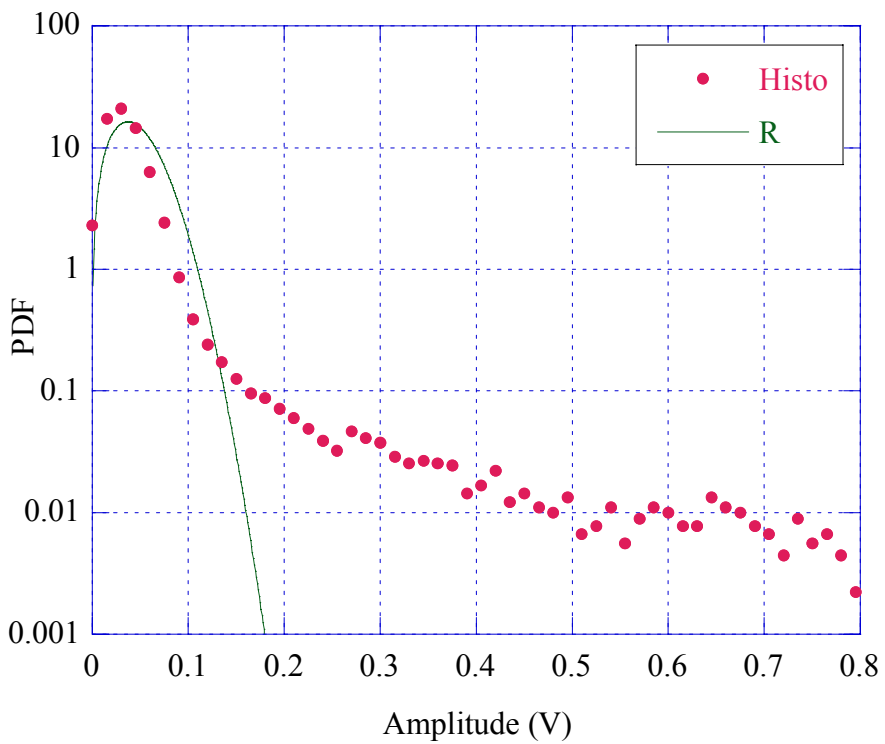


Figure 2.42 - Clutter amplitude PDF, VV polarization, 8th range cell.

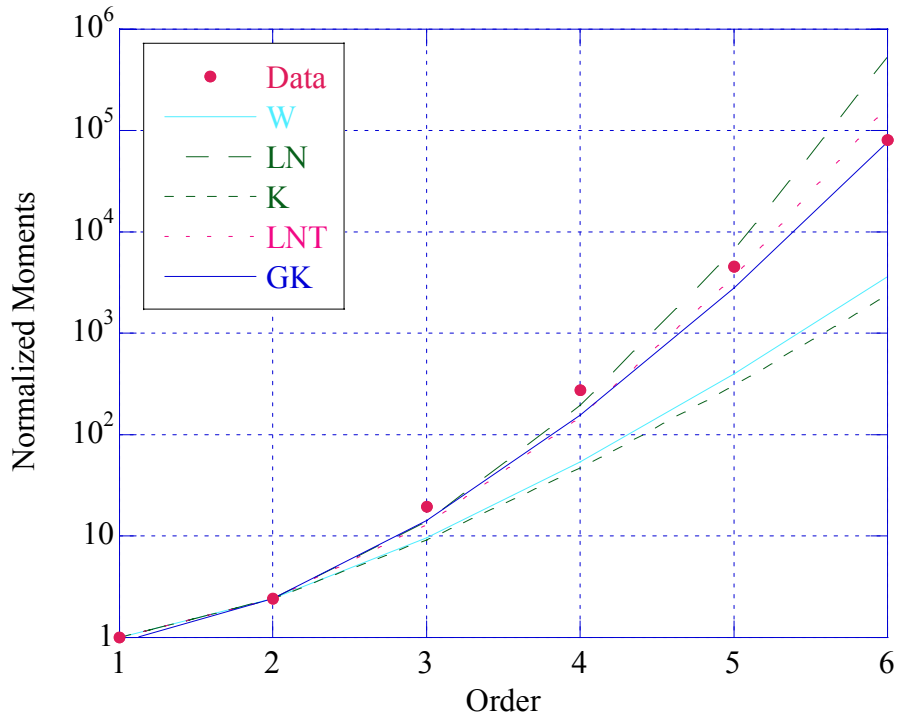


Figure 2.43 - Normalized clutter moments, VV polarization, 8th range cell.

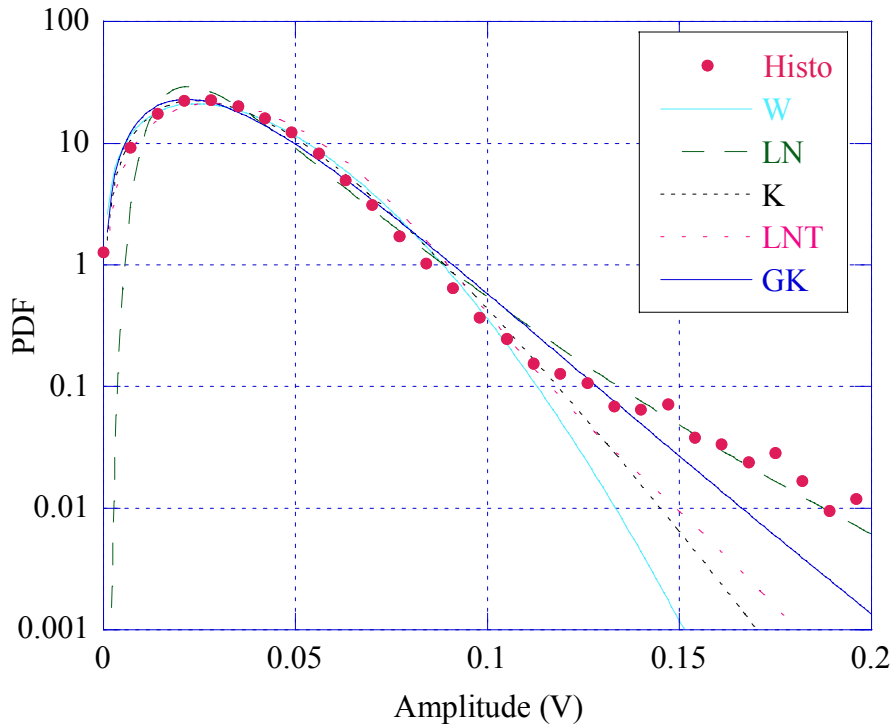


Figure 2.44 - Clutter amplitude PDF, VV polarization, 2nd range cell.

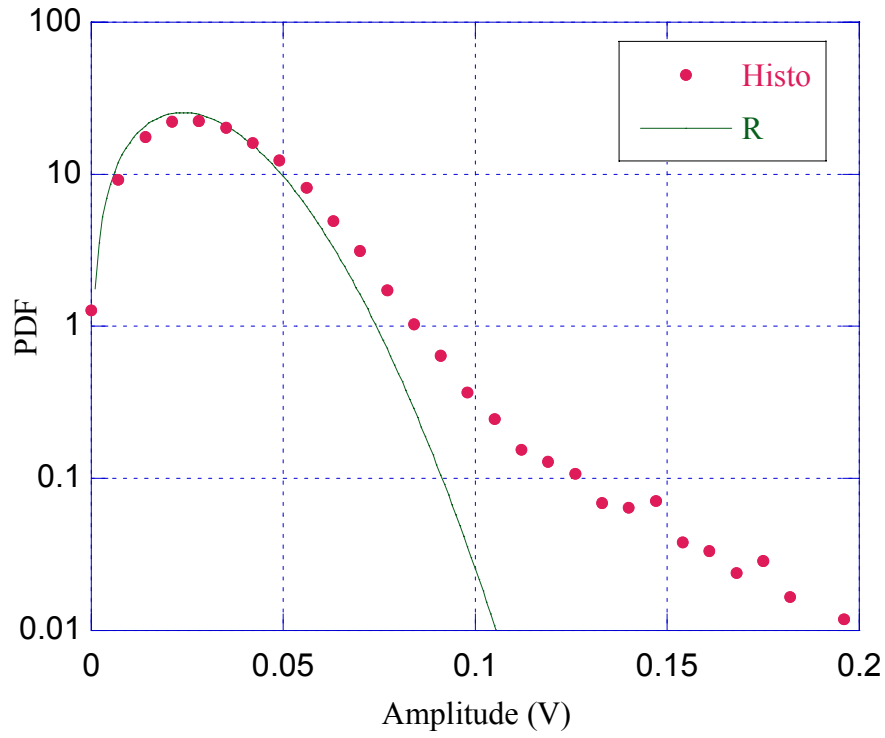


Figure 2.45 - Clutter amplitude PDF, VV polarization, 2nd range cell.

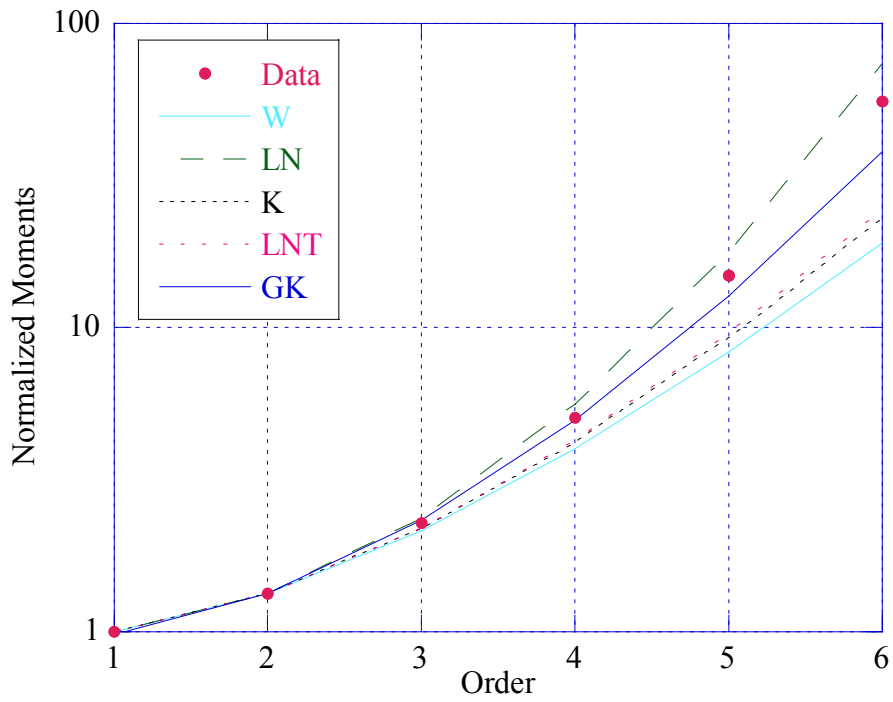


Figure 2.46 - Normalized clutter moments, VV polarization, 2nd range cell.

Cell	W		LN		K	
	$\hat{c}$	$\hat{b}$	$\hat{\sigma}$	$\hat{\delta}$	$\hat{\nu}$	$\hat{\mu}$
1	1.4404	0.038971	0.63513	0.028908	1.5198	0.00093625
2	1.7933	0.038101	0.53593	0.029355	5.4679	0.00076527
3	1.3869	0.038788	0.65367	0.028595	1.3180	0.00096089
4	0.99261	0.039241	0.83702	0.027732	0.49050	0.0015612
5	1.2237	0.038769	0.71808	0.028042	0.87370	0.0011027
6	1.8516	0.038195	0.52256	0.029595	7.9294	0.00075611
7	1.1261	0.038515	0.76360	0.027558	0.68703	0.0012188
8	0.84548	0.035950	0.93827	0.025270	0.32745	0.0018571
9	0.81517	0.033988	0.96260	0.023913	0.29912	0.0018241
10	0.84124	0.034151	0.94160	0.024007	0.32339	0.0016972
11	1.0379	0.037474	0.81046	0.026582	0.55099	0.0013142
12	1.2612	0.038567	0.70213	0.028017	0.95830	0.0010520
13	1.7858	0.038031	0.53770	0.029280	5.2491	0.00076425
14	1.8989	0.037409	0.51224	0.029115	12.003	0.00071630
15	1.6883	0.038457	0.56188	0.029316	3.3594	0.00080801
16	1.7221	0.038470	0.55325	0.029428	3.8641	0.00079867
17	1.4484	0.038501	0.63244	0.028586	1.5536	0.00090929
18	1.4659	0.038817	0.62667	0.028879	1.6304	0.00091461
19	1.0658	0.037622	0.79498	0.026756	0.59121	0.0012669
20	1.5934	0.038764	0.58773	0.029253	2.3902	0.00085380
21	1.7686	0.038267	0.54182	0.029411	4.7988	0.00077799
22	1.6229	0.038552	0.57943	0.029186	2.6393	0.00083357
23	1.7351	0.038111	0.54999	0.029193	4.0936	0.00078028
24	1.7223	0.037877	0.55320	0.028976	3.8674	0.00077422
25	1.4747	0.039441	0.62380	0.029372	1.6711	0.00093936
26	1.2609	0.039387	0.70223	0.028612	0.95773	0.0010975
27	1.3940	0.038932	0.65114	0.028725	1.3427	0.00096330

**Table 2.25** - Estimated parameters, VV polarization.

Cell	LNT		GK			R
	$\hat{\sigma}^2$	$\hat{m}$	$\hat{\nu}$	$\hat{\mu}$	$\hat{b}$	$\hat{\sigma}^2$
1	0.64731	0.00067738	67.758	1.1028e-18	0.10880	0.0013828
2	0.18263	0.00069849	69.906	5.8174e-11	0.20040	0.0011303
3	0.74287	0.00066277	67.461	9.6390e-20	0.10238	0.0014192
4	1.8362	0.00062338	29.719	2.8743e-15	0.11294	0.0023059
5	1.0963	0.00063740	66.499	3.8794e-23	0.086003	0.0016287
6	0.12603	0.00070994	70.521	1.0395e-08	0.26483	0.0011168
7	1.3661	0.00061560	66.243	5.1979e-24	0.082501	0.0018002
8	2.5551	0.00051759	4.3833	4.4718e-06	0.21908	0.0027428
9	2.7402	0.00046349	2.8274	4.1674e-05	0.25724	0.0026942
10	2.5802	0.00046715	3.9349	7.5809e-06	0.22785	0.0025067
11	1.6611	0.00057275	55.010	6.8783e-23	0.083527	0.0019411
12	1.0057	0.00063628	66.686	1.7298e-22	0.088756	0.0015538
13	0.19022	0.00069491	69.916	6.3513e-11	0.20124	0.0011288
14	0.083286	0.00068709	70.863	1.7799e-07	0.32257	0.0010580
15	0.29660	0.00069664	68.919	1.5460e-14	0.14439	0.0011934
16	0.25809	0.00070198	69.150	1.0552e-13	0.15445	0.0011796
17	0.63365	0.00066238	67.372	4.3477e-20	0.10060	0.0013430
18	0.60461	0.00067600	67.657	4.6802e-19	0.10654	0.0013509
19	1.5617	0.00058026	65.805	1.4619e-25	0.077127	0.0018712
20	0.41546	0.00069365	68.627	1.4199e-15	0.13339	0.0012610
21	0.20801	0.00070114	69.671	8.1638e-12	0.18340	0.0011491
22	0.37671	0.00069047	68.235	5.2513e-17	0.12104	0.0012312
23	0.24369	0.00069078	69.039	4.0815e-14	0.14946	0.0011525
24	0.25786	0.00068056	69.099	6.6691e-14	0.15211	0.0011435
25	0.59025	0.00069930	68.088	1.7315e-17	0.11698	0.0013874
26	1.0063	0.00066359	66.942	1.4983e-21	0.092834	0.0016210
27	0.72970	0.00066882	67.302	2.5770e-20	0.099243	0.0014228

**Table 2.26** - Estimated parameters, VV polarization.

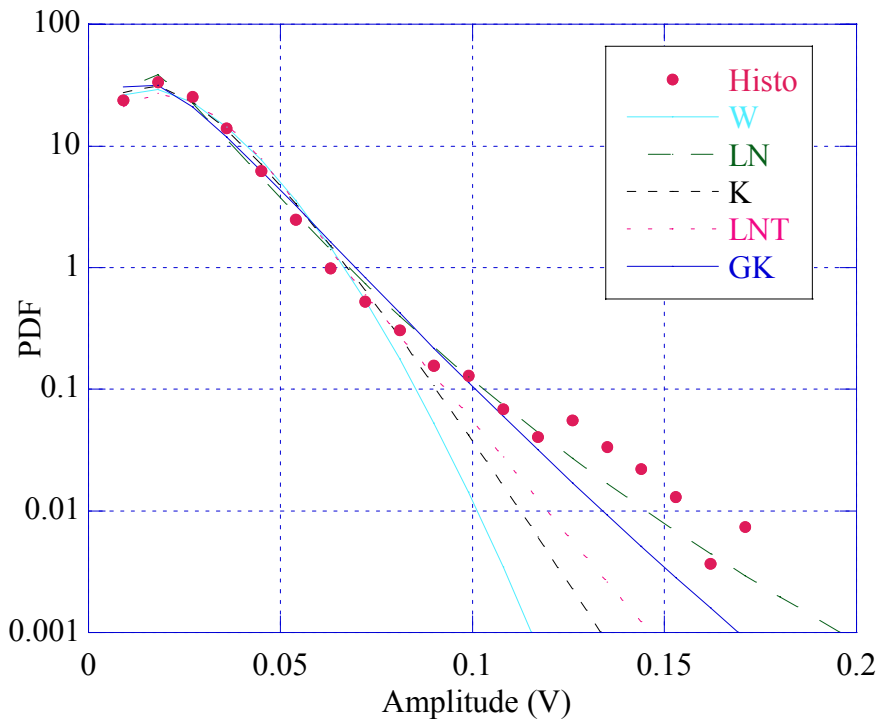


Figure 2.47 - Clutter amplitude PDF, HH polarization, 2nd range cell.

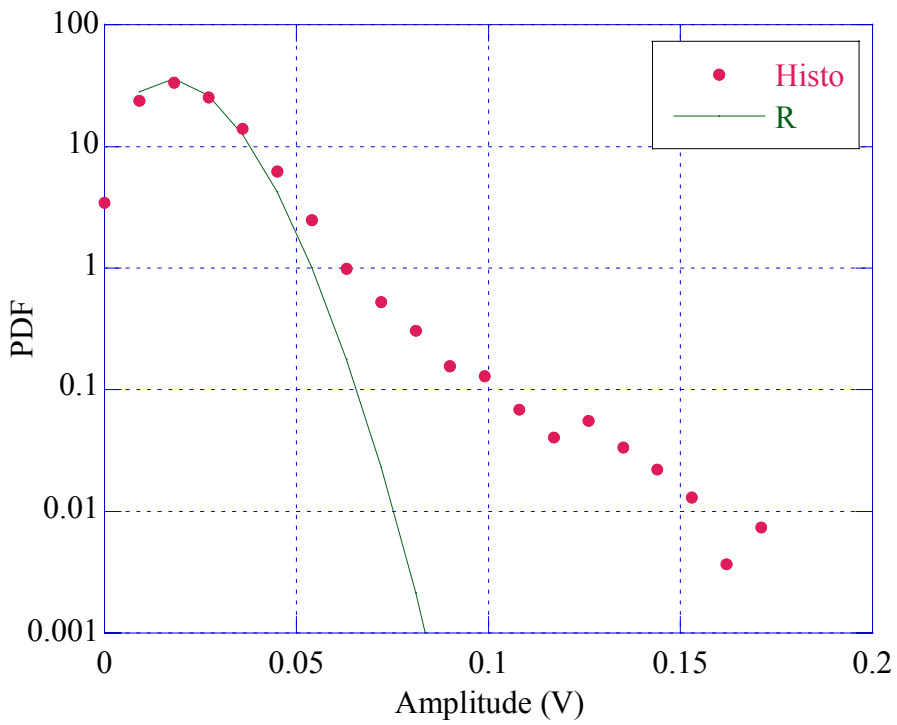


Figure 2.48 - Clutter amplitude PDF, HH polarization, 2nd range cell.

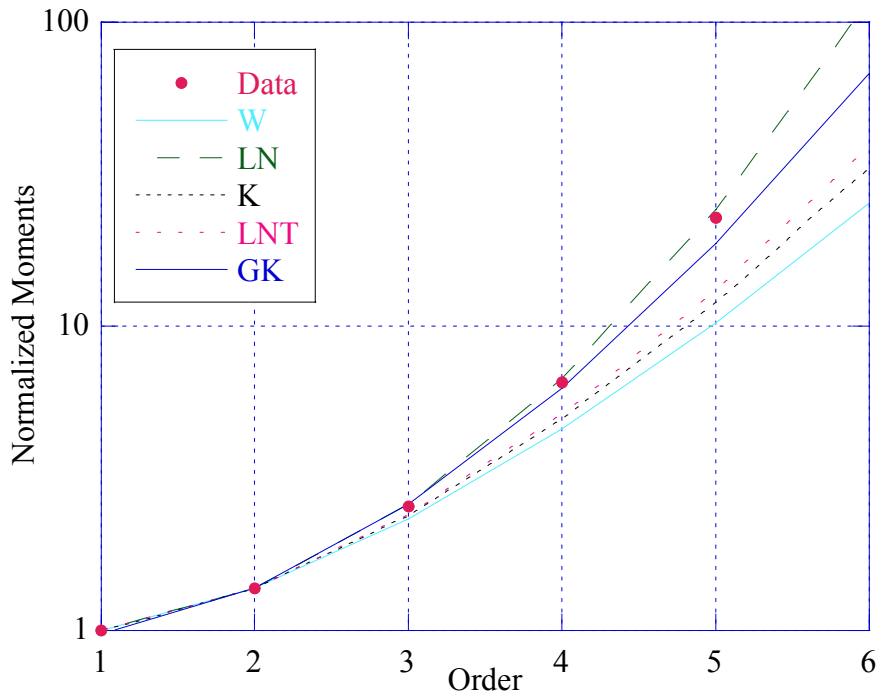


Figure 2.49 - Normalized clutter moments, HH polarization, 2nd range cell.

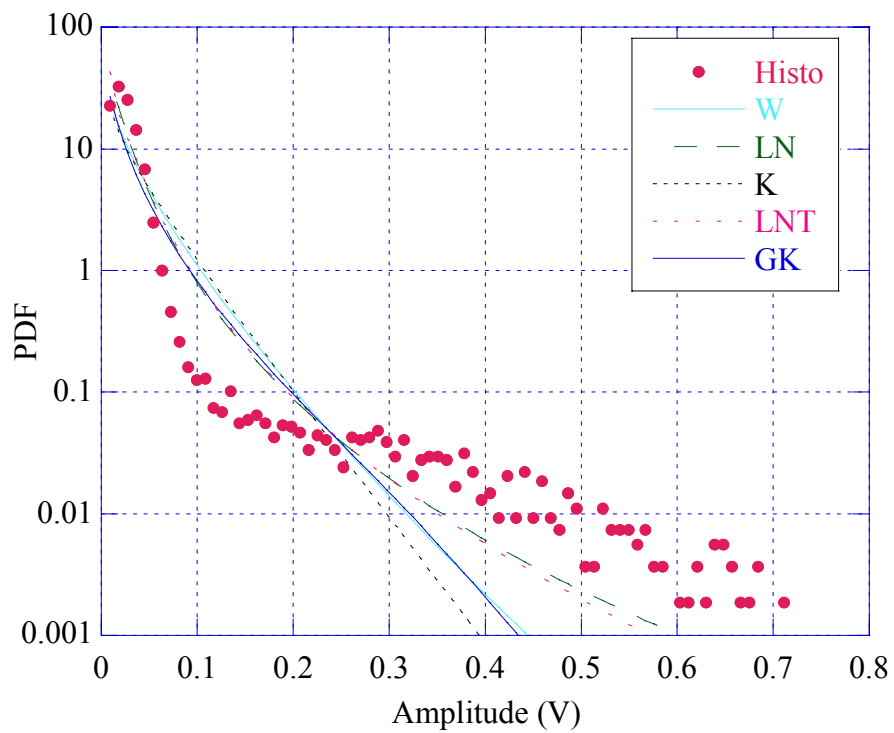


Figure 2.50 - Clutter amplitude PDF, HH polarization, 9th range cell.

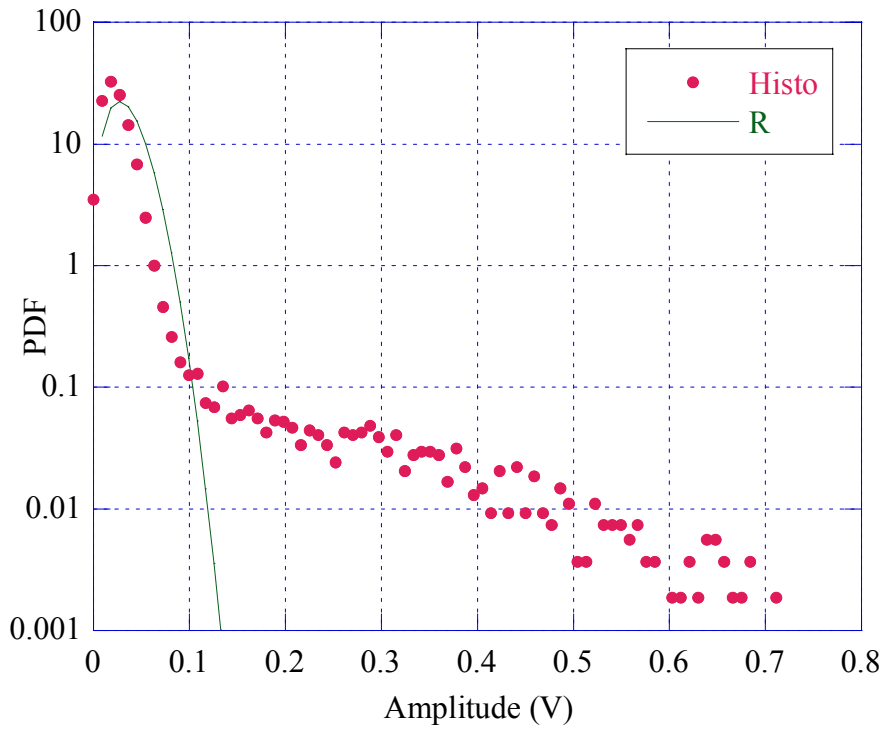


Figure 2.51 - Clutter amplitude PDF, HH polarization, 9th range cell.

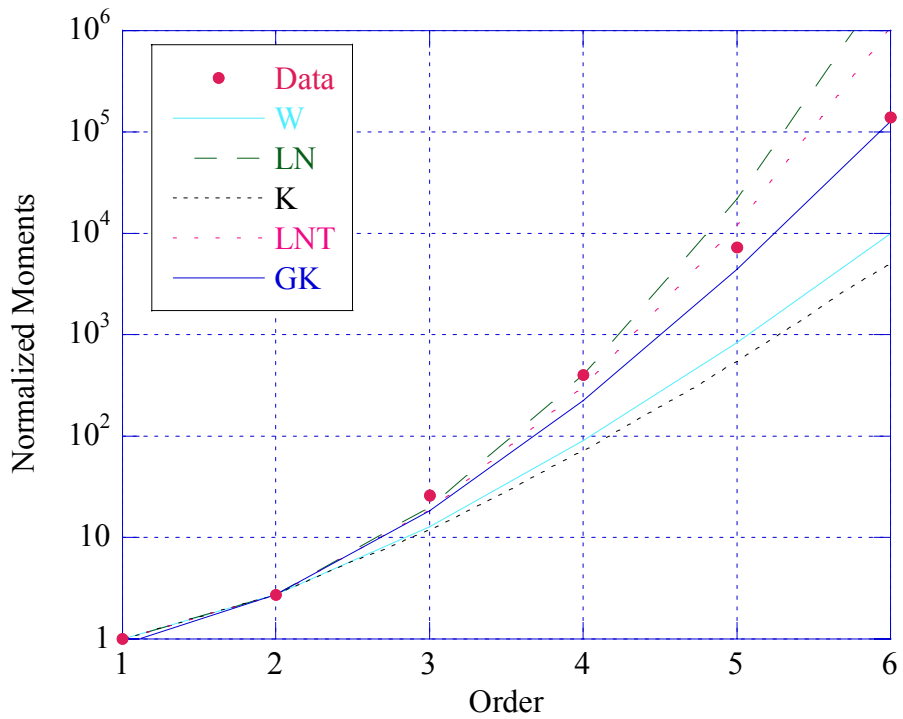


Figure 2.52 Normalized clutter moments, HH polarization, 9th range cell.

Cell	W		LN		K	
	$\hat{c}$	$\hat{b}$	$\hat{\sigma}$	$\hat{\delta}$	$\hat{\nu}$	$\hat{\mu}$
1	1.3712	0.026941	0.65931	0.019825	1.2654	0.00046876
2	1.6784	0.026181	0.56448	0.019937	3.2310	0.00037590
3	1.5002	0.026367	0.61567	0.019693	1.7968	0.00041384
4	0.93914	0.026810	0.87094	0.018883	0.42583	0.00081276
5	1.0407	0.026408	0.80887	0.018737	0.55494	0.00064961
6	1.7264	0.026456	0.55218	0.020247	3.9369	0.00037716
7	0.98135	0.025650	0.84392	0.018113	0.47631	0.00068161
8	0.84870	0.025380	0.93577	0.017839	0.33055	0.00091684
9	0.77153	0.023257	1.0002	0.016416	0.26101	0.00099640
10	0.79590	0.022916	0.97881	0.016141	0.28192	0.00088512
11	1.0308	0.026474	0.81447	0.018768	0.54120	0.00066373
12	1.1310	0.026724	0.76118	0.019132	0.69536	0.00058309
13	1.5829	0.026712	0.59074	0.020135	2.3102	0.00040737
14	1.8034	0.026458	0.53355	0.020405	5.7912	0.00036790
15	1.5311	0.027315	0.60610	0.020472	1.9674	0.00043689
16	1.6185	0.027159	0.58067	0.020551	2.5994	0.00041448
17	1.4045	0.027089	0.64742	0.020011	1.3806	0.00046302
18	1.2814	0.027102	0.69380	0.019735	1.0078	0.00050999
19	0.93129	0.025640	0.87618	0.018052	0.41690	0.00075651
20	1.2303	0.026831	0.71524	0.019422	0.88789	0.00052468
21	1.6384	0.026915	0.57517	0.020410	2.7865	0.00040365
22	1.4377	0.027419	0.63603	0.020333	1.5088	0.00046426
23	1.6841	0.026896	0.56298	0.020494	3.3040	0.00039586
24	1.5717	0.026773	0.59399	0.020156	2.2291	0.00041140
25	1.3750	0.027856	0.65794	0.020507	1.2778	0.00049978
26	1.1727	0.028347	0.74114	0.020386	0.77058	0.00062334
27	1.2072	0.027405	0.72539	0.019785	0.83881	0.00056063

**Table 2.27** - Estimated parameters, HH polarization.

Cell	LNT		GK			R
	$\hat{\sigma}^2$	$\hat{m}$	$\hat{\nu}$	$\hat{\mu}$	$\hat{b}$	$\hat{\sigma}^2$
1	0.77250	0.00031857	67.694	3.2437e-19	0.10734	0.00069235
2	0.30830	0.00032220	69.318	2.0384e-13	0.16275	0.00055520
3	0.54992	0.00031435	67.703	3.0946e-19	0.10755	0.00061123
4	2.0679	0.00028901	4.8620	5.2640e-06	0.25070	0.0012004
5	1.6508	0.00028457	65.639	1.9248e-26	0.075280	0.00095946
6	0.25334	0.00033229	69.777	9.6613e-12	0.19069	0.00055706
7	1.8825	0.00026592	57.282	6.8788e-26	0.074898	0.0010067
8	2.5364	0.00025794	4.3997	2.7148e-06	0.22405	0.0013542
9	3.0353	0.00021844	2.0967	6.1247e-05	0.27834	0.0014717
10	2.8660	0.00021118	3.7622	2.9229e-06	0.21811	0.0013073
11	1.6872	0.00028551	37.560	8.1546e-18	0.10272	0.00098031
12	1.3513	0.00029669	66.261	2.8821e-24	0.082737	0.00086121
13	0.42964	0.00032862	68.679	1.0439e-15	0.13522	0.00060168
14	0.17246	0.00033750	70.242	4.7642e-10	0.23107	0.00054337
15	0.50316	0.00033971	68.476	2.0557e-16	0.12834	0.00064528
16	0.38243	0.00034234	68.829	3.7103e-15	0.14078	0.00061217
17	0.71037	0.00032459	67.499	6.3910e-20	0.10317	0.00068387
18	0.95920	0.00031570	67.128	3.2400e-21	0.096039	0.00075324
19	2.1045	0.00026414	12.462	2.5837e-10	0.15020	0.0011173
20	1.0800	0.00030576	66.407	8.6367e-24	0.084709	0.00077494
21	0.35702	0.00033766	68.973	1.2152e-14	0.14663	0.00059618
22	0.65188	0.00033512	67.758	5.4968e-19	0.10881	0.00068570
23	0.30154	0.00034046	69.263	1.3501e-13	0.15993	0.00058467
24	0.44506	0.00032932	68.242	2.7407e-17	0.12124	0.00060763
25	0.76529	0.00034088	67.683	3.1583e-19	0.10710	0.00073817
26	1.2309	0.00033685	66.424	1.1779e-23	0.084941	0.00092065
27	1.1385	0.00031729	66.109	7.8926e-25	0.080773	0.00082804

**Table 2. 28** - Estimated parameters, HH polarization.

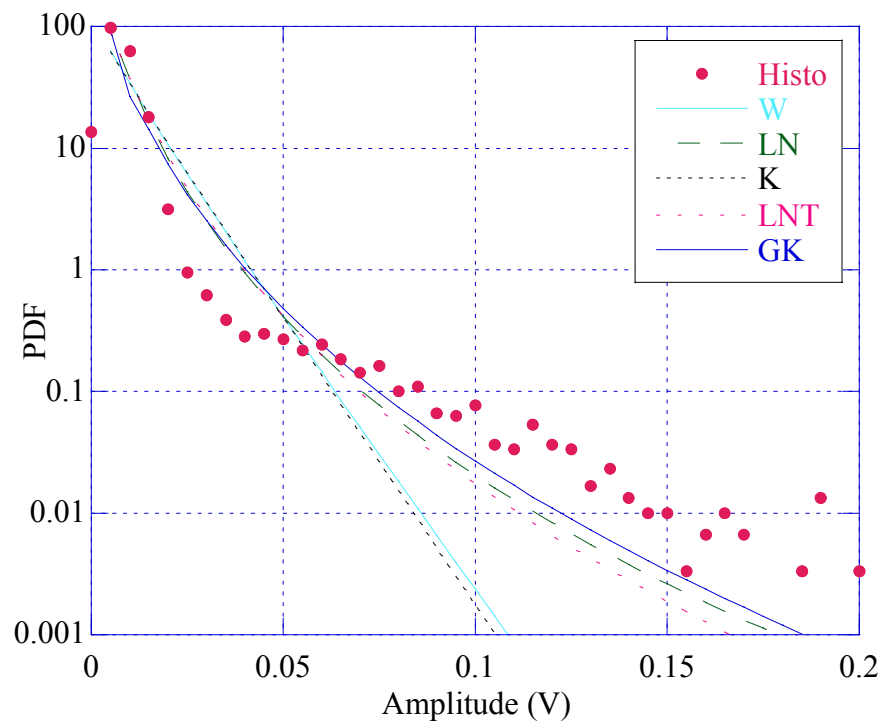


Figure 2.53 - Clutter amplitude PDF, VH polarization, 9<sup>th</sup> range cell.

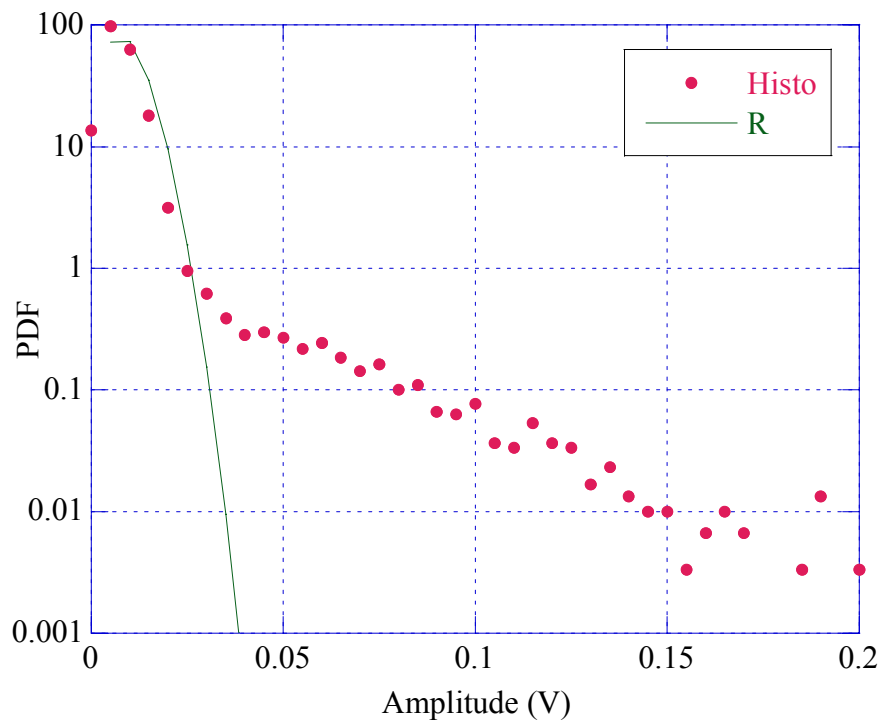


Figure 2.54 - Clutter amplitude PDF, VH polarization, 9<sup>th</sup> range cell.

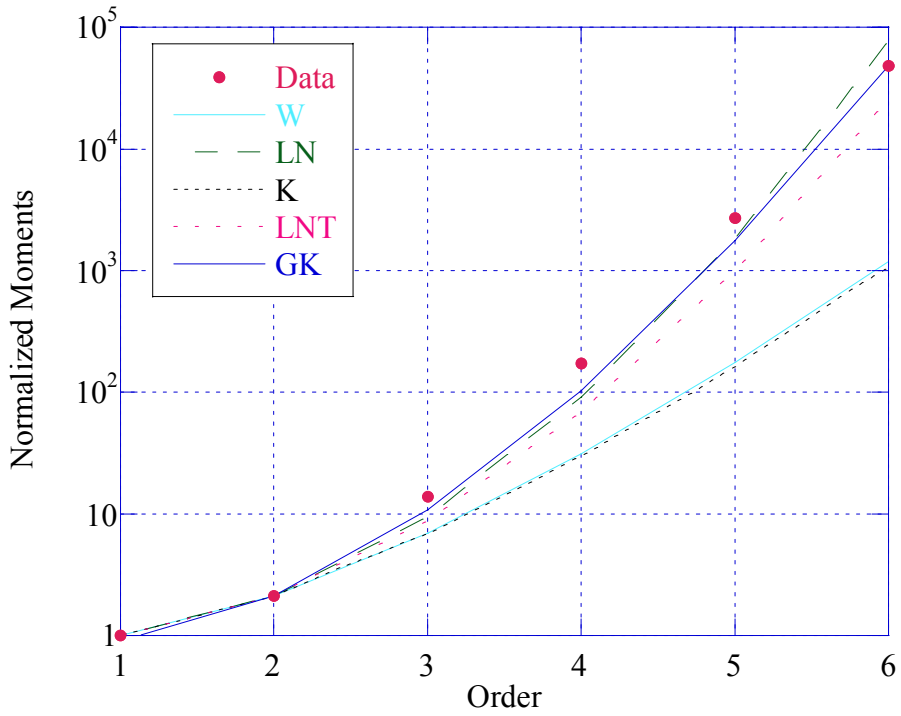


Figure 2.55 - Normalized clutter moments, VH polarization, 9th range cell.

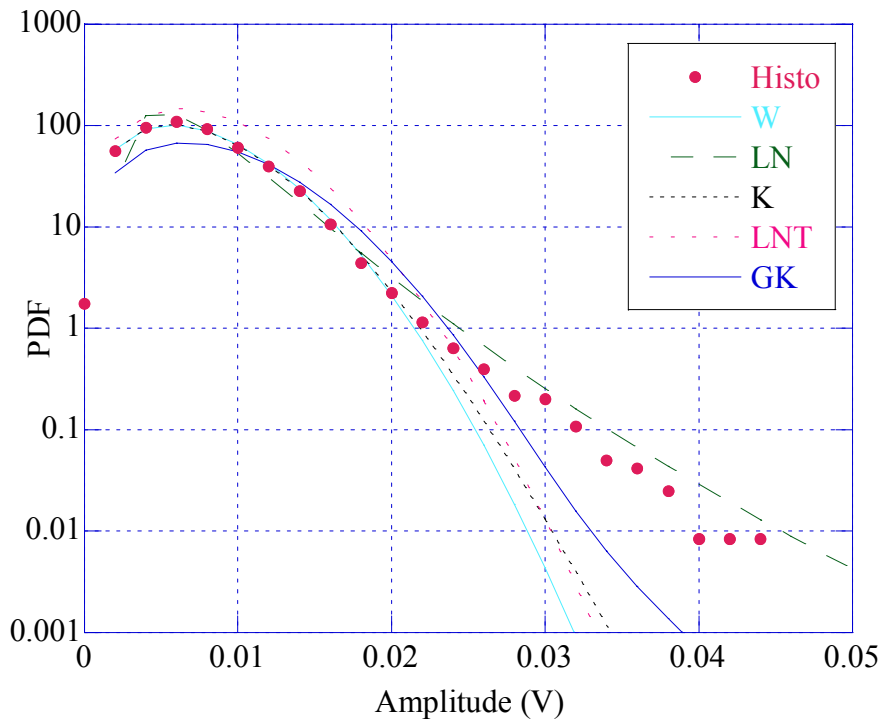


Figure 2.56 - Clutter amplitude PDF, VH polarization, 2<sup>nd</sup> range cell.

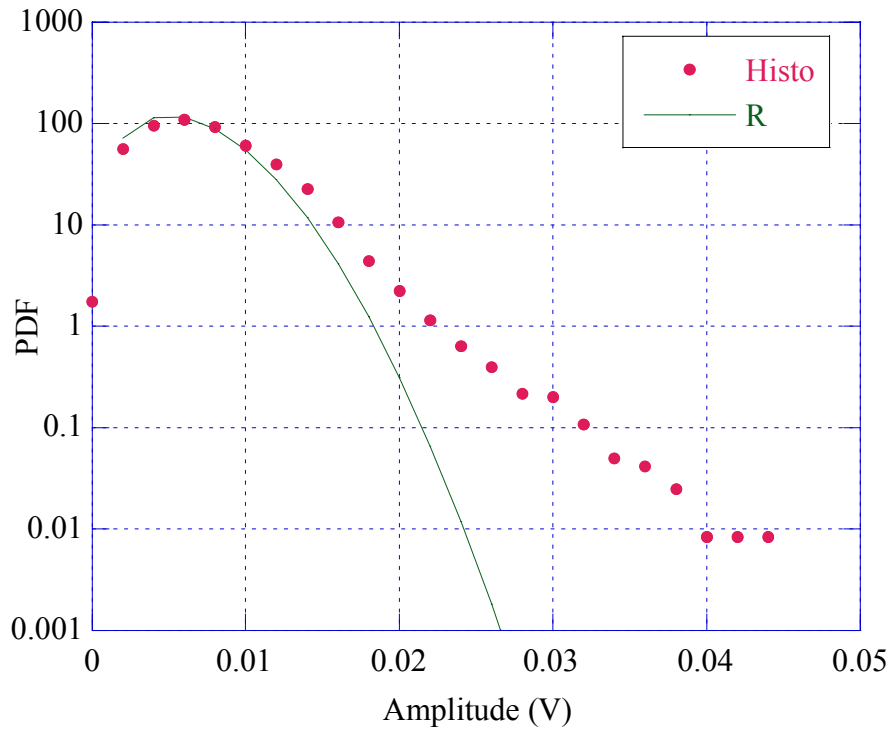


Figure 2.57 - Clutter amplitude PDF, VH polarization, 2<sup>nd</sup> range cell.

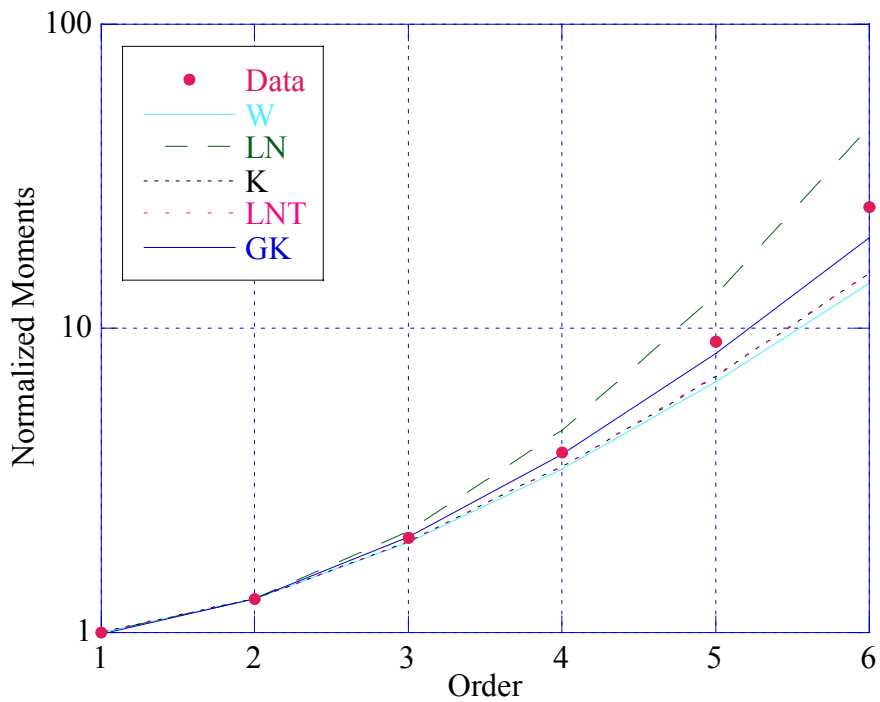


Figure 2.58 - Normalized clutter moments, VH polarization, 2<sup>nd</sup> range cell.

Cell	W		LN		K	
	$\hat{c}$	$\hat{b}$	$\hat{\sigma}$	$\hat{\delta}$	$\hat{\nu}$	$\hat{\mu}$
1	1.6520	0.0084138	0.57149	0.0063896	2.9261	3.9228e-05
2	1.9312	0.0082527	0.50541	0.0064420	18.015	3.4585e-05
3	1.6054	0.0084479	0.58433	0.0063835	2.4870	4.0333e-05
4	1.1774	0.0087325	0.73894	0.0062833	0.77959	5.8833e-05
5	1.4023	0.0086078	0.64821	0.0063572	1.3725	4.6822e-05
6	1.9112	0.0084194	0.50961	0.0065601	13.782	3.6171e-05
7	1.3312	0.0085734	0.67422	0.0062794	1.1421	4.8938e-05
8	0.98862	0.0083496	0.83945	0.0058990	0.48544	7.1220e-05
9	0.94493	0.0081742	0.86713	0.0057589	0.43251	7.4601e-05
10	0.98093	0.0081198	0.84418	0.0057335	0.47578	6.8360e-05
11	1.1843	0.0085814	0.73574	0.0061794	0.79294	5.6370e-05
12	1.3851	0.0087593	0.65430	0.0064561	1.3119	4.9064e-05
13	1.6533	0.0086152	0.57114	0.0065434	2.9400	4.1107e-05
14	1.7101	0.0085158	0.55627	0.0065064	3.6721	3.9303e-05
15	1.6612	0.0086344	0.56903	0.0065635	3.0269	4.1160e-05
16	1.7490	0.0085976	0.54656	0.0065950	4.3640	3.9525e-05
17	1.6054	0.0085696	0.58434	0.0064755	2.4868	4.1504e-05
18	1.6351	0.0085499	0.57606	0.0064813	2.7543	4.0789e-05
19	1.2604	0.0084515	0.70246	0.0061391	0.95645	5.0557e-05
20	1.7446	0.0084158	0.54764	0.0064527	4.2754	3.7927e-05
21	1.8791	0.0083201	0.51650	0.0064634	9.9149	3.5613e-05
22	1.7994	0.0083986	0.53449	0.0064747	5.6592	3.7115e-05
23	1.8622	0.0083417	0.52022	0.0064699	8.5970	3.5960e-05
24	1.8369	0.0082928	0.52586	0.0064165	7.1436	3.5790e-05
25	1.6683	0.0085785	0.56713	0.0065259	3.1092	4.0515e-05
26	1.4722	0.0086734	0.62463	0.0064574	1.6592	4.5496e-05
27	1.5896	0.0085494	0.58882	0.0064491	2.3607	4.1603e-05

**Table 2. 29** - Estimated parameters, VH polarization.

Cell	LNT		GK			R
	$\hat{\sigma}^2$	$\hat{m}$	$\hat{\nu}$	$\hat{\mu}$	$\hat{b}$	$\hat{\sigma}^2$
1	0.34015	3.3093e-05	68.659	8.5033e-17	0.13450	5.7939e-05
2	0.055503	3.3638e-05	70.771	3.9307e-09	0.30462	5.1081e-05
3	0.39950	3.3030e-05	68.353	6.7586e-18	0.12449	5.9571e-05
4	1.2178	3.2001e-05	66.660	7.7834e-24	0.088357	8.6895e-05
5	0.71443	3.2758e-05	67.191	5.0042e-22	0.097174	6.9155e-05
6	0.072543	3.4883e-05	70.631	1.2551e-09	0.28091	5.3424e-05
7	0.85205	3.1961e-05	67.032	1.3998e-22	0.094349	7.2280e-05
8	1.8525	2.8206e-05	37.252	2.7555e-20	0.093892	0.00010519
9	2.0414	2.6883e-05	19.775	2.4175e-14	0.12319	0.00011018
10	1.8843	2.6646e-05	22.329	5.1835e-15	0.12005	0.00010097
11	1.1990	3.0951e-05	66.588	4.1195e-24	0.087286	8.3256e-05
12	0.74619	3.3785e-05	67.547	1.0038e-20	0.10416	7.2466e-05
13	0.33855	3.4706e-05	69.158	5.8063e-15	0.15483	6.0714e-05
14	0.27150	3.4314e-05	69.305	1.9102e-14	0.16207	5.8050e-05
15	0.32892	3.4919e-05	69.162	6.0247e-15	0.15503	6.0793e-05
16	0.22865	3.5255e-05	69.627	2.8627e-13	0.18053	5.8378e-05
17	0.39954	3.3989e-05	68.370	8.0696e-18	0.12503	6.1301e-05
18	0.36114	3.4050e-05	68.561	3.9016e-17	0.13113	6.0244e-05
19	1.0075	3.0549e-05	66.577	3.3731e-24	0.087125	7.4672e-05
20	0.23337	3.3750e-05	69.297	1.7215e-14	0.16165	5.6017e-05
21	0.10082	3.3862e-05	70.429	2.2522e-10	0.25269	5.2599e-05
22	0.17648	3.3980e-05	69.303	1.7711e-14	0.16196	5.4818e-05
23	0.11625	3.3930e-05	70.022	7.3007e-12	0.21006	5.3113e-05
24	0.13987	3.3372e-05	69.805	1.1689e-12	0.19278	5.2861e-05
25	0.32028	3.4520e-05	69.018	1.7699e-15	0.14852	5.9840e-05
26	0.59438	3.3799e-05	67.777	6.3247e-20	0.10926	6.7197e-05
27	0.42058	3.3713e-05	68.192	1.8294e-18	0.11982	6.1446e-05

**Table 2. 30** - Estimated parameters, VH polarization.

## 2.3 Cumulant domain analysis

To perform a deeper analysis of the Gaussian compound model and to verify whether the deviation from the theoretical models is due to the presence of non-negligible thermal noise, we have applied the theory of cumulants to the clutter samples [Far97]. As it is well known, cumulants of order higher than 2 for a Gaussian process are identically zero [Sad94]. Thus, if we consider the clutter process  $z[n] = y[n] + v[n]$ , where  $v[n]$  is a Gaussian process and  $y[n]$  is a non-Gaussian process, independent of  $v[n]$ , we have:

$$\begin{aligned} c_k^z[l_1, \dots, l_{k-1}] &= c_k^y[l_1, \dots, l_{k-1}] + c_k^v[l_1, \dots, l_{k-1}] \\ &= c_k^y[l_1, \dots, l_{k-1}] \end{aligned} \quad \text{for } k > 3 \quad (2.21)$$

so the cumulants of  $y[n]$  can be derived from the cumulants of  $z[n]$ .

In our case the in-phase and quadrature components of the thermal noise are zero mean Gaussian processes, then only non-Gaussian clutter contributes to the 3<sup>rd</sup>, 4<sup>th</sup> and 5<sup>th</sup> order cumulants of the observed coherent data.

We have estimated the 2<sup>nd</sup>, 3<sup>rd</sup> and 5<sup>th</sup> order cumulants, for  $l_1 = l_2 = \dots = l_{k-1} = 0$ , from the data, and we have compared them with the theoretical cumulants of the Gaussian-compound model calculated at the origin. For this model, all the cumulants of odd order calculated at the origin are equal to zero. Then, the cumulants have been normalized with respect to the 2<sup>nd</sup> order cumulant as follows

$$\mu_k = \frac{c_k^I[0, 0, \dots, 0]}{(c_2^I[0])^{k/2}} = \frac{c_k^Q[0, 0, \dots, 0]}{(c_2^Q[0])^{k/2}} \quad (2.22)$$

In figures 2.59, 2.60, 2.61 and 2.62 are reported the normalized cumulants  $\mu_3$  e  $\mu_5$  with respect to the 2<sup>nd</sup> order cumulant.

The results show that at range a resolution of 9 m the compound Gaussian model can be still used to model the clutter process in most cells for VH polarization. The 5<sup>th</sup> order cumulant shows a strong deviation from zero in most cells for both HH e VV polarizations.

At a range resolution of 3 m most cells in all polarizations present estimated values of the cumulants very different from zero then the thermal noise cannot be the cause of the deviation form the Gaussian-compound family.

In order to have further results, we tried to compare the amplitude histogram to the K+Thermal noise model, whose expressions are reported below:

$$\text{PDF: } \frac{(\nu/\mu)^\nu}{\Gamma(\nu)} \int_0^\infty \frac{r\tau^{\nu-1}}{\tau+\sigma^2} \exp\left(-\frac{r^2}{2(\tau+\sigma^2)}\right) \exp\left(-\frac{\nu}{\mu}\tau\right) d\tau \quad (2.23)$$

$$\text{Moments: } \begin{cases} E\{R^2\} = 2\sigma^2(1+CNR) \\ E\{R^4\} = 8\sigma^2\left(1+2CNR+\frac{\nu+1}{\nu}CNR^2\right) \\ E\{R^6\} = 4\sigma^2\left[12+36CNR+37CNR^2\frac{\nu+1}{\nu}+12CNR^3\frac{(\nu+1)(\nu+2)}{\nu}\right] \end{cases} \quad (2.24)$$

where  $CNR = \mu/\sigma^2$ . Unfortunately, we encountered several numerical problems in computing the integral in formula 2.23; then we abandoned the model.

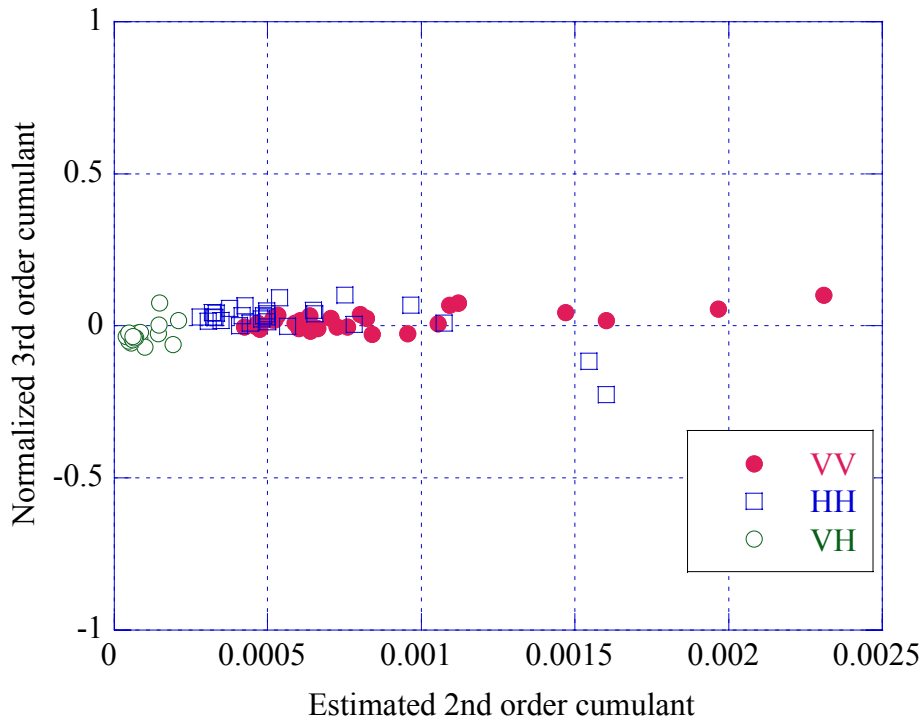


Figure 2. 59 - Normalized 3rd order cumulant versus 2nd order cumulant, 9 m.

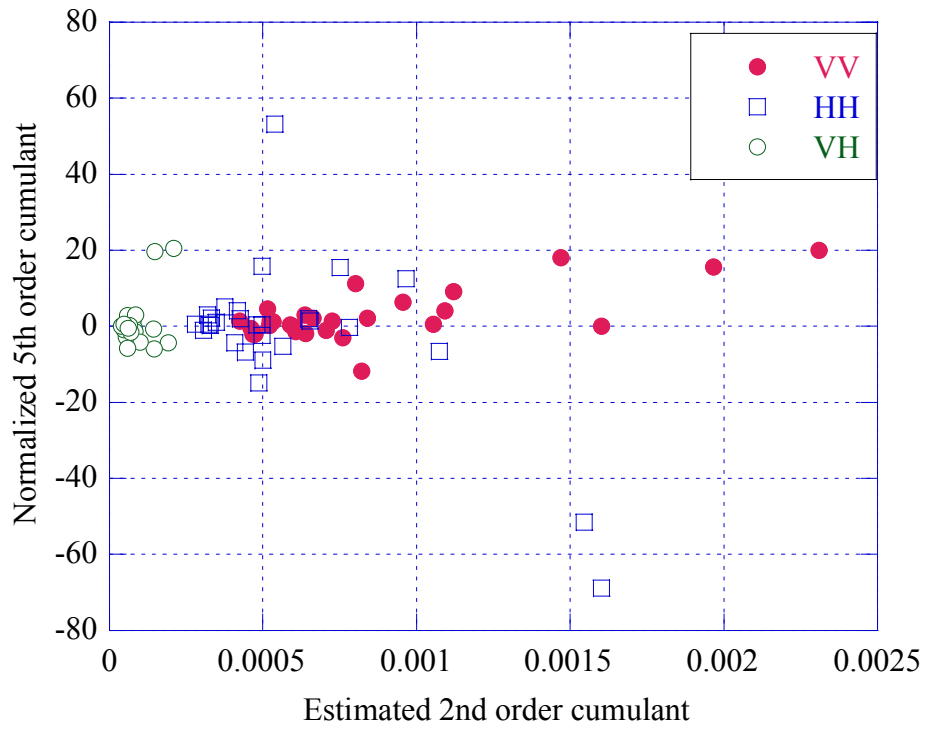


Figure 2.60 - Normalized 5th order cumulant versus 2nd order cumulant, 9 m.

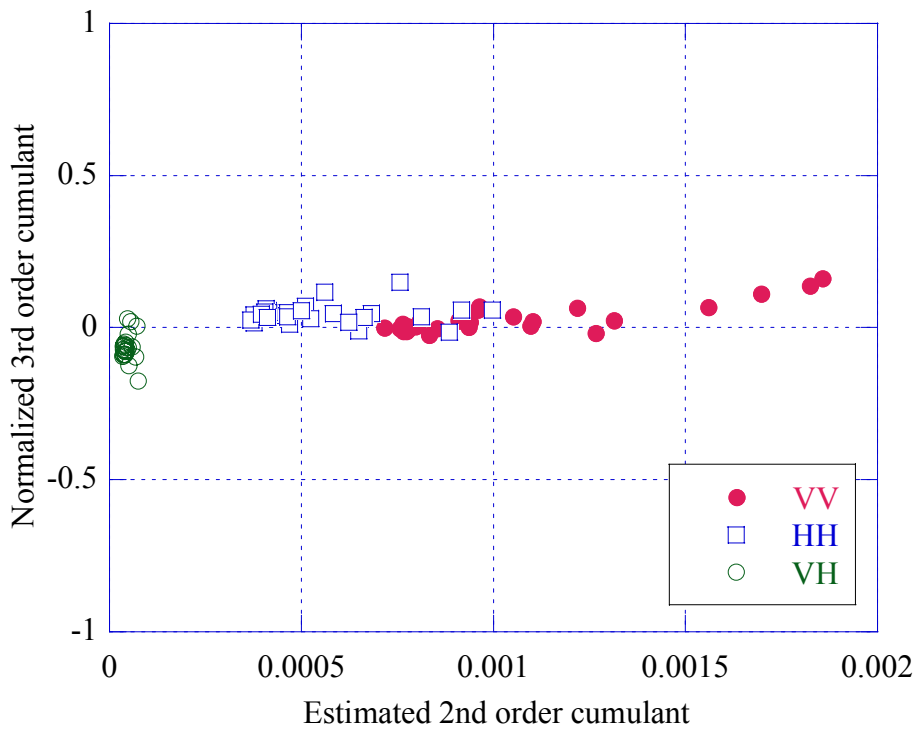
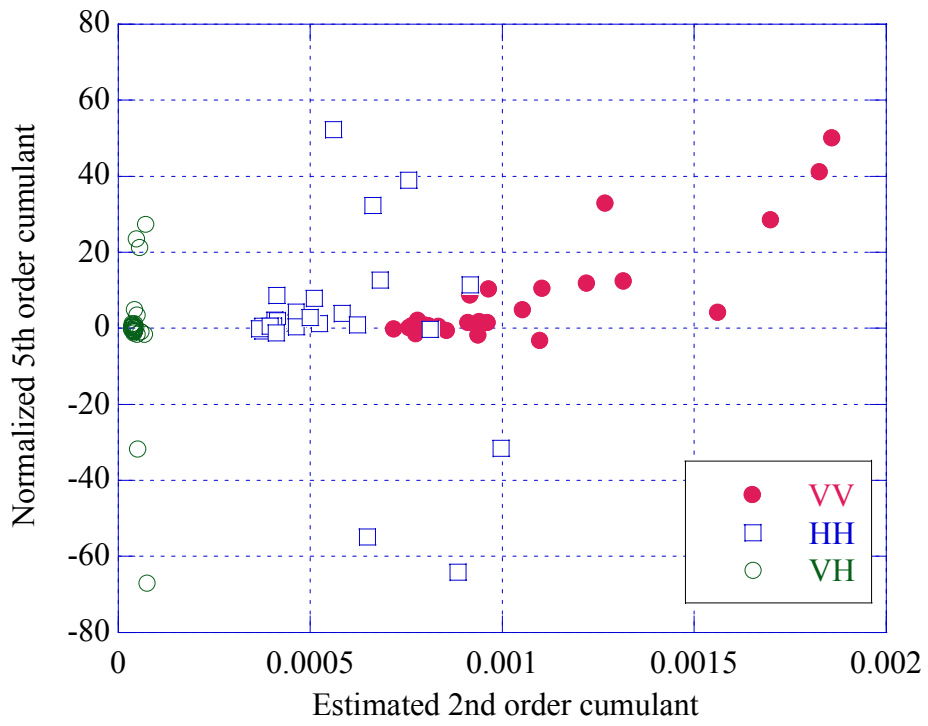


Figure 2.61 - Normalized 3rd order cumulant versus 2nd order cumulant, 3 m.



**Figure 2.62** - Normalized 5th order cumulant versus 2nd order cumulant, 3 m.

## 2.4 Conclusions

Looking at the obtained results, we state that, with resolutions of **60 m** and **30 m**, a very good fitting is obtained by the GK-PDF in all polarizations. Increasing the range resolution up to **15 m**, the model keeps on giving good results in most cells for co-polarizations even if the presence of longer tailed cells with respect to the lower resolutions has been observed. The model is valid for all VH-HV polarized data.

At **9 m** and **3 m** both VV and HH polarizations histograms show very long tails, so that the Gaussian-compound model is not valid anymore. Moreover, at these resolutions the thermal noise contribution becomes very important. The GK model gives a good fitting almost in all cells for VH polarization at 9 m, but at 3 m also the cross-polarizations present long tailed cells and the compound model loses the fitting.

Estimated parameters analysis shows that HH component is the most spiky one at 60 m, 15 m, 9 m, e 3 m range resolution; at a resolution of 30 m, on the average, HH component is less spiky than both VV component and VH component (remind that at 30 m range resolution the illuminated zone is different).

Cumulants domain analysis confirms the results obtained by the histograms analysis. At 9 m range resolution Gaussian-compound model keeps on giving a good fitting in most cells for VH polarization. The 5th order cumulant show a strong deviation from zero in most cells for both HH and VV polarizations.

At 3 m range resolution, most cells in all polarizations present estimated values of the cumulants very different from zero.

# Section 3

## Frequency Analysis

### 3.1 Correlation analysis and power spectrum estimation

The model of clutter we refer to considers the presence of two components, speckle and texture, with very different correlation times (some millisecond for the first component and some seconds for the second one). In fact, if the two components are independent and the model is compound the overall autocorrelation function is the product of the autocorrelation of the two components ([Far97], [Gin02], [Gin01])

$$R_z(m) = E\{z(n)z^*(n+m)\} = R_{\sqrt{f}}(m)R_x(m) = 2R_{\sqrt{f}}(m)\left(R_{Xi}(m) + jR_{XiXQ}(m)\right) \quad (3.1)$$

In practice, the decorrelation time of the signal  $z(n)$ , called coherent signal, is equal to that of the faster component [Far 97].

#### 3.1.1 Estimation of $R_{Xi}$ and $R_{XiXQ}$

Since texture can be considered constant over short time intervals, we can estimate the speckle autocorrelation functions  $R_{Xi}$  and  $R_{XiXQ}$  by using coherent signal samples from such short intervals with or without overlapping.

$$\hat{R}_{Xi}(m) = \frac{1}{N_b} \left[ \sum_{k=1}^{N_b} \frac{1}{2N\hat{\tau}_k} \operatorname{Re} \left\{ \sum_{n=0}^{N-1-m} z_k(n)z_k^*(n+m) \right\} \right] \quad (3.2)$$

$$\hat{R}_{XiXQ}(m) = \frac{1}{N_b} \left[ \sum_{k=1}^{N_b} \frac{1}{2N\hat{\tau}_k} \operatorname{Im} \left\{ \sum_{n=0}^{N-1-m} z_k(n)z_k^*(n+m) \right\} \right] \quad (3.3)$$

$$\hat{\tau}_k = \frac{1}{N} \sum_{n=0}^{N-1} |z_k(n)|^2 \quad (3.5)$$

where  $\hat{\tau}_k$  is the estimated value of the texture in the  $k$ th burst and  $N_b$  is the number of data bursts. We tried three different values of  $N$ ,  $N=64$ ,  $N=128$  and  $N=256$ , with an overlap between bursts of 50%.

Figures 3.2, 3.6, 3.10, 3.14, 3.18, 3.22, 3.26, 3.30, 3.34, 3.38, 3.42, 3.46, 3.50, 3.54, and 3.58 report the real and the imaginary parts of the speckle autocorrelation function. They show that with all resolutions, in all polarizations, the speckle correlation time is about 10 msec long and the behavior is oscillatory. There are not apparent differences in the estimation for  $N=64$ , 128 and 256.

### 3.1.2 Estimation of the texture correlation function

To check the validity of the hypothesis made over the correlation times of the two components, we estimated the texture correlation with the formula

$$R_\tau\left(\frac{Nm}{2}\right) = \frac{1}{N_b} \sum_{k=0}^{N_b-1-|m|} \hat{\tau}(n)\hat{\tau}(n+m), \quad (3.6)$$

and the texture covariance as

$$C_\tau\left(\frac{Nm}{2}\right) = \frac{1}{N_b - |m|} \sum_{k=0}^{N_b-1-|m|} \hat{\tau}(n)\hat{\tau}(n+m) - E^2\{\hat{\tau}\}, \quad (3.7)$$

where  $E\{\hat{\tau}\} = \frac{1}{N_b} \sum_{n=0}^{N_b-1} \hat{\tau}(n)$ . It is useful to observe that with a 50% of overlap, we can estimate the texture correlation and covariance every  $N/2$  lags. In the texture estimation we set  $N=128$ . In the figures we plot the texture autocorrelation and autocovariance coefficients, that is:

$$\rho_\tau\left(\frac{Nm}{2}\right) = R_\tau\left(\frac{Nm}{2}\right) / R_\tau(0) \text{ and } c_\tau\left(\frac{Nm}{2}\right) = C_\tau\left(\frac{Nm}{2}\right) / C_\tau(0).$$

Figures 3.3, 3.4, 3.7, 3.8, 3.11, 3.12, 3.15, 3.16, 3.19, 3.20, 3.23, and 3.24 show the texture autocorrelation and autocovariance coefficients. At the same resolutions and

without differences in the polarizations, the texture correlation time is some seconds long; texture presents periodicities with a period of 8 seconds at a range resolution of 60 m and of 3 seconds at a range resolution of 30 m. The periodicity is particularly evident in the VV polarized data for the resolution of 60 m.

Figs. 3.27, 3.28, 3.31, 3.32, 3.35, 3.36, 3.39, 3.40, 3.43, 3.44, 3.47, 3.48, 3.51, 3.52, 3.55, 3.56, 3.59, and 3.60 show that, with increasing resolution, the texture correlation time get shorter, but still in the order of few seconds and the periodicities tend to disappear, due to the strong contribution of the thermal noise (see Ch.1).

In all analyzed files, the azimuth resolution is constant and equal to 1.1 degrees.

Figures 3.1, 3.5, 3.9, 3.13, 3.17, 3.21, 3.25, 3.29, 3.33, 3.37, 3.41, 3.45, 3.49, 3.53, and 3.57 report the average spectrogram in semi-logarithm scale for each analyzed cell, calculated as

$$P(k) = \frac{1}{N_{seq}} \sum_{r=1}^{N_{seq}} P_r(k) = \frac{1}{N_{seq} N_c} \sum_{r=1}^{N_{seq}} \left| \sum_{n=(r-1)N_c+1}^{rN_c} x(n) e^{-jkn} \right|^2, \quad k = 1, 2, \dots, N_c, \quad (3.8)$$

where  $N_{seq}$  is the number of sequences in which the received vector for each cell has been divided,  $N_c$  is the number of samples per sequence,  $k$  is the normalized frequency and  $P_r(k)$  is the  $k$ th sample of the periodogram of the  $r$ th sequence.

The periodogram shows, for all the polarizations, for all the range resolutions, a peak located around 150 Hz. Moreover, with a resolution of 60 m and 30 m, all the analyzed cells show a bimodal spectrum, particularly evident in HH polarization, and then a second peak near -150 Hz; the power of the second peak is much lower than the power of the main one. From the resolution of 15 m, the IPIX radar seems to add a frequency interfering line in the spectrum at about -220 Hz. The line at 0 Hz is due to a residual of the continuous component. It is evident that, as resolution increases, the thermal noise effect becomes very important. In fact, in the figures it is evident that the clutter-to noise ratio ( $CNR$ ) decreases from  $\approx 20$  dB for a resolution of 60 m and VV data (Fig.3.1) to less than -5 dB for a resolution of 3 m and VH data (Fig. 3.57). The  $CNR$  has been roughly estimated from the spectrum figures reading the value of the noise floor from each figure and calculating the clutter power as the difference between the overall disturbance power and the noise power. The values calculated for each cell is reported in the figure captions.

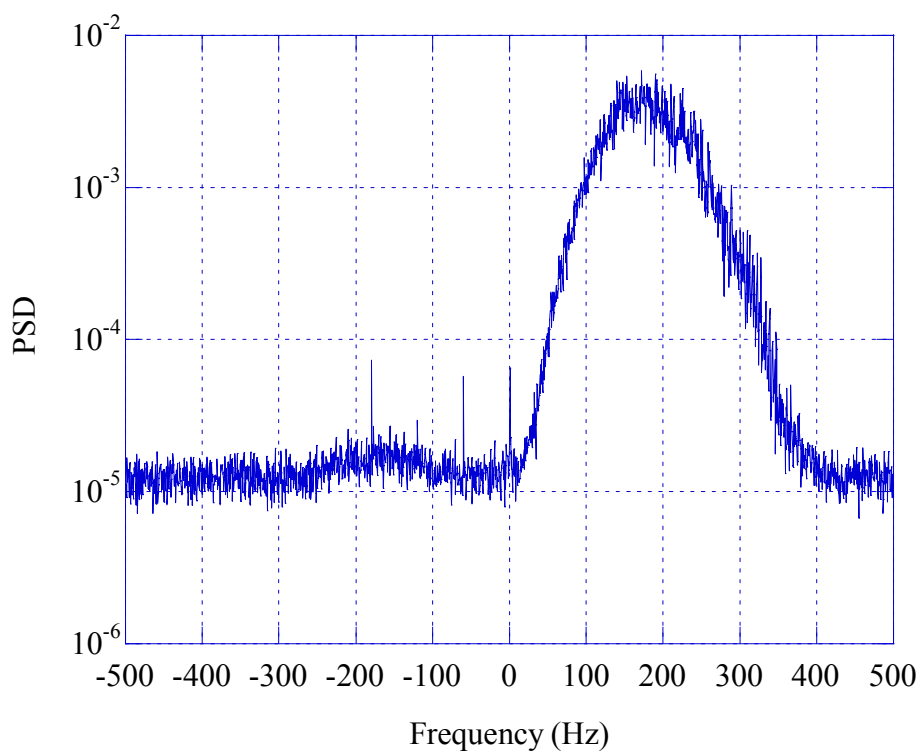


**Figure 3.1** - Average Power Spectral Density, PSD, 15<sup>th</sup> range cell, VV pol., 60 m,  $CNR \approx 17$  dB .

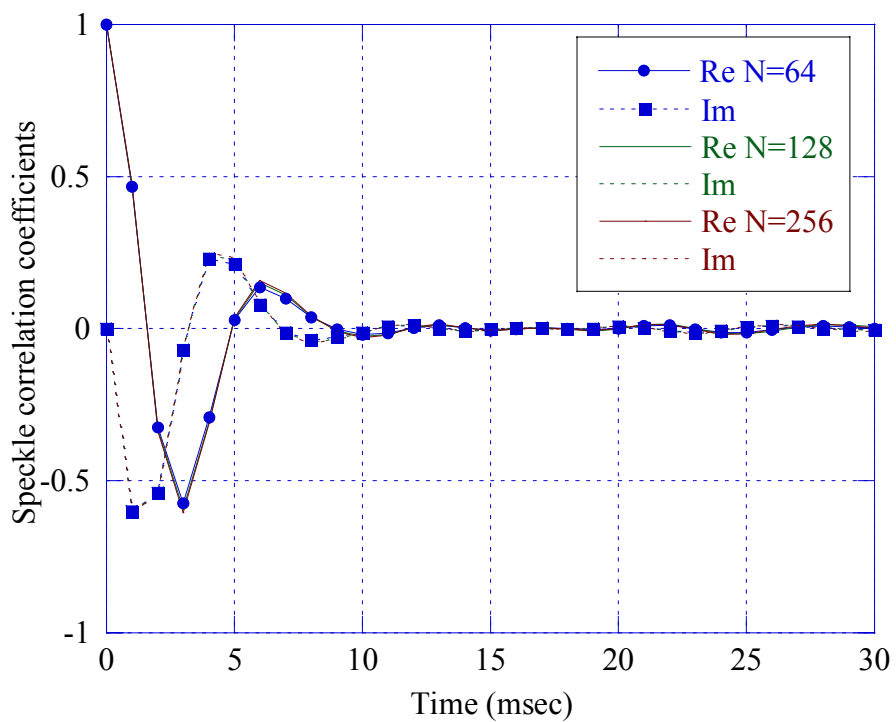


**Figure 3.2** - Speckle correlation coefficients, VV pol., 15<sup>th</sup> range cell, 60 m.

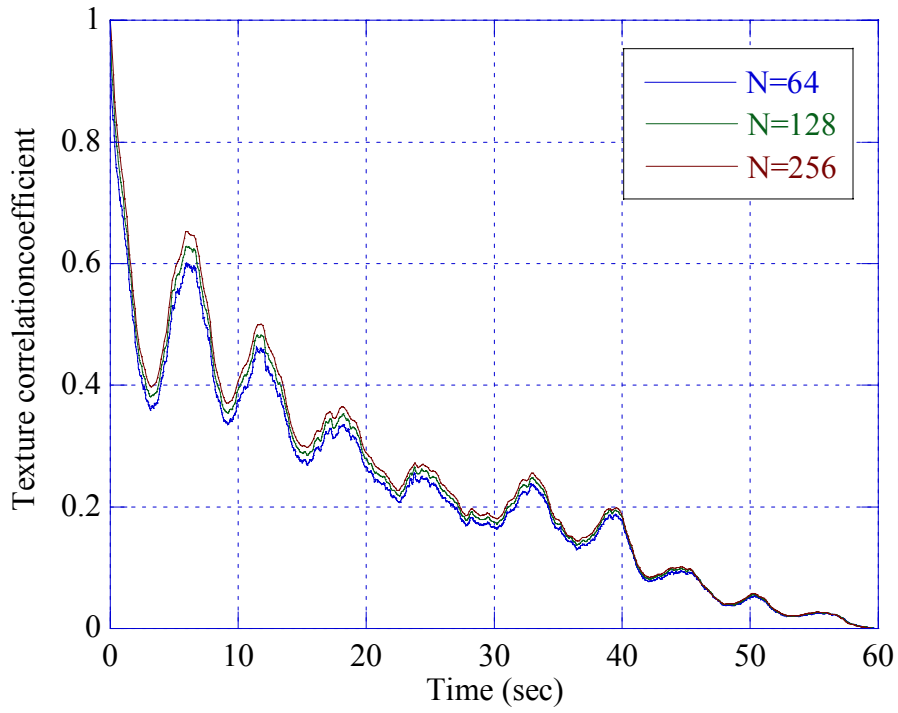


**Figure 3.3** - Texture correlation coefficient, VV pol., 15<sup>th</sup> range cell, 60 m.

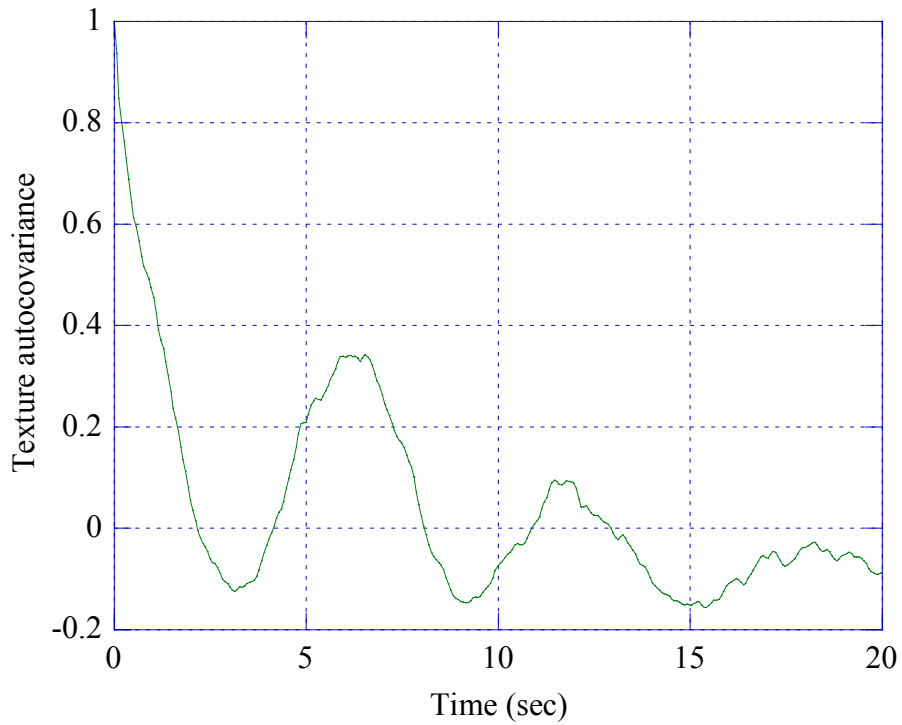


**Figure 3.4** - Texture autocovariance function, VV pol., 15th range cell, N=128, 60 m.

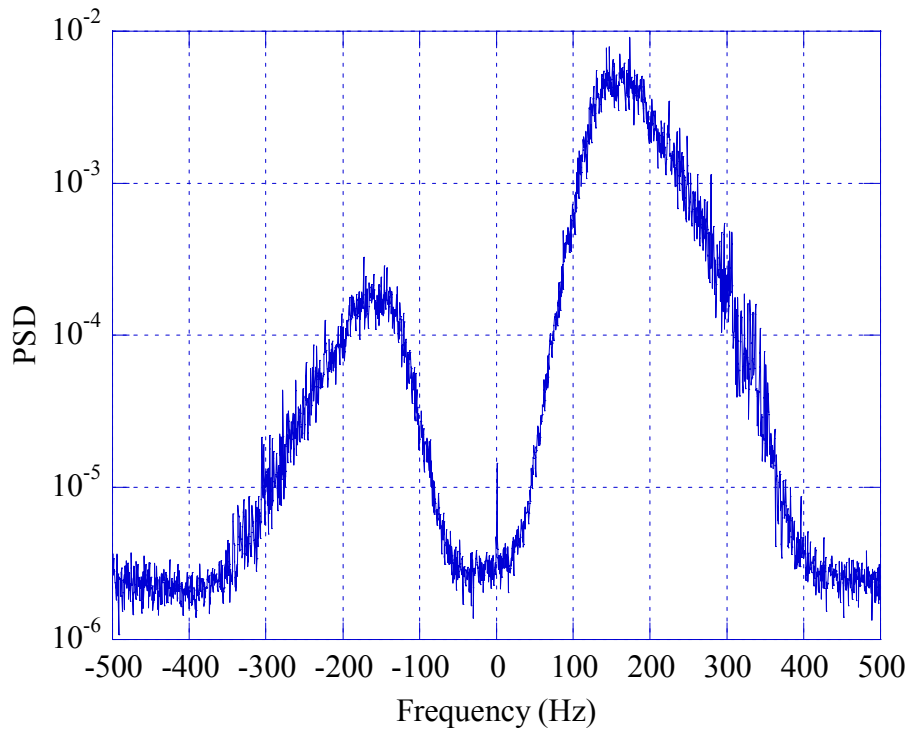


**Figure 3. 5** - Average Power Spectral Density, PSD, 1<sup>st</sup> cell, HH pol., 60 m,  $CNR \approx 24$  dB

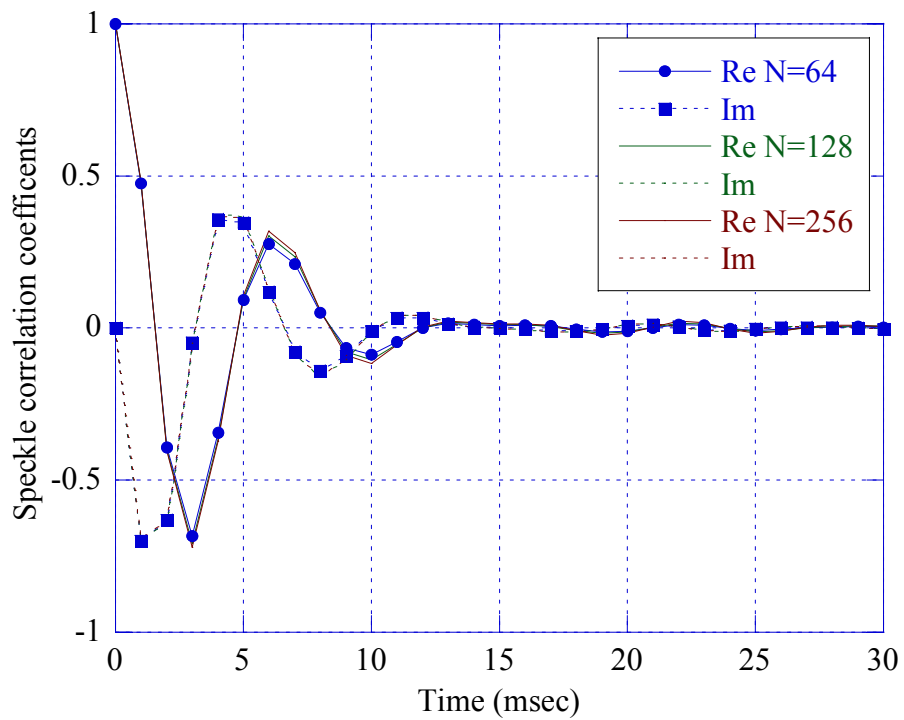


**Figure 3. 6** - Speckle correlation coefficients, HH pol., 1<sup>st</sup> cell, 60 m.

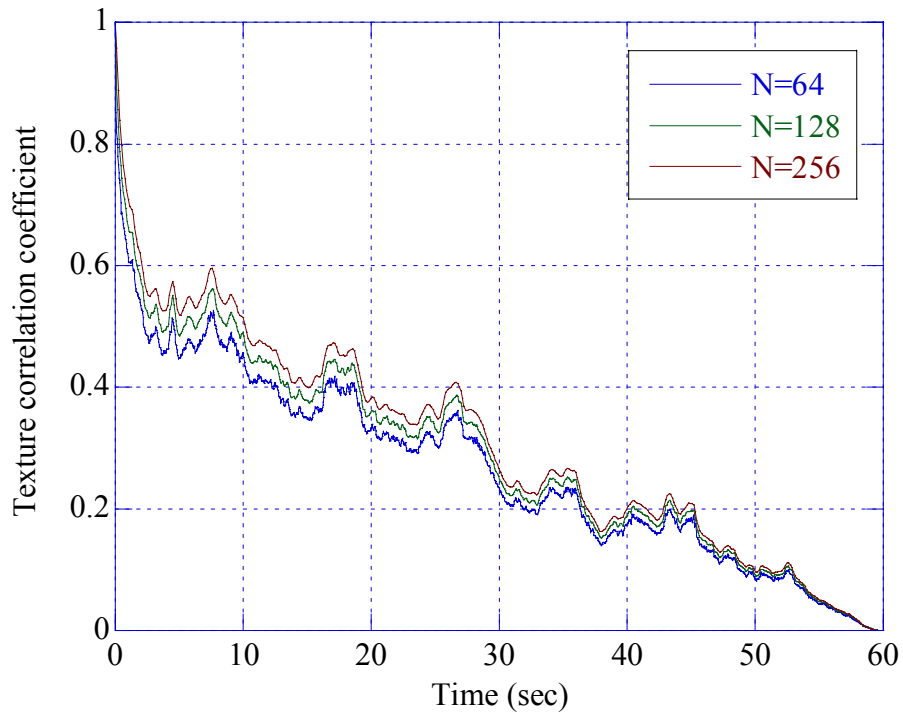


**Figure 3. 7** - Texture correlation coefficient, HH pol., 1<sup>st</sup> cell, 60 m.

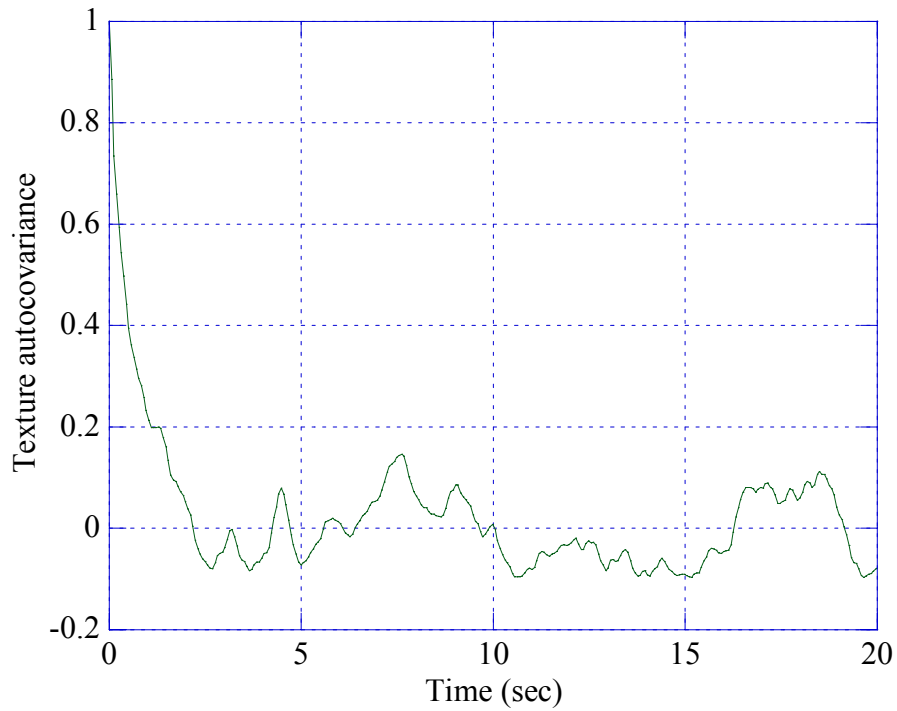


**Figure 3. 8** - Texture autocovariance function, HH pol., 1<sup>st</sup> cell, N=128, 60 m.

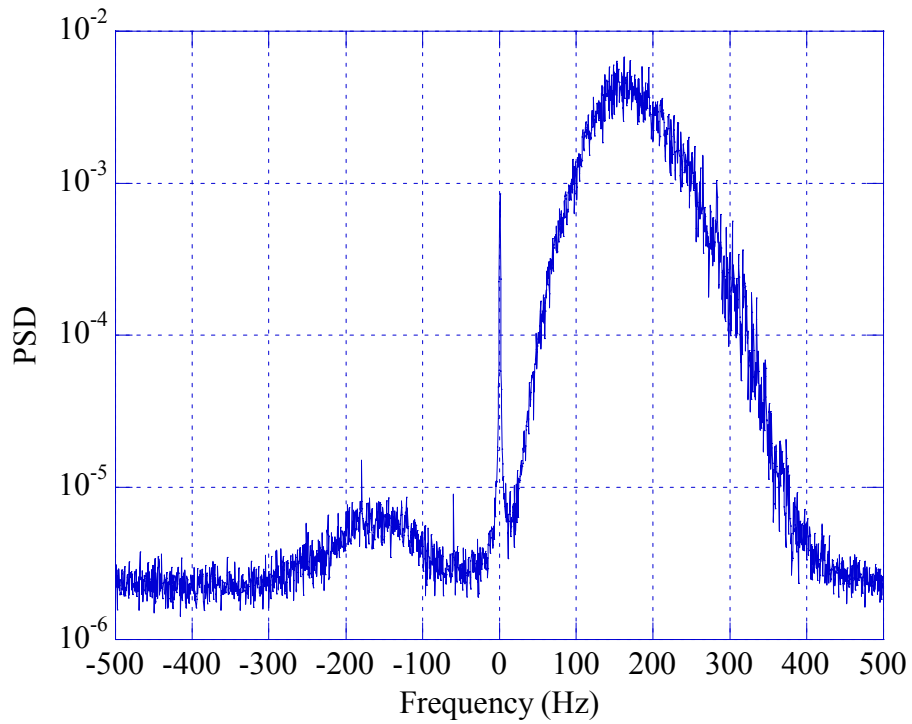


Figure 3. 9 - Average Power Spectral Density, PSD, 1<sup>st</sup> cell, VH pol, 60 m,  $CNR \approx 24$  dB .

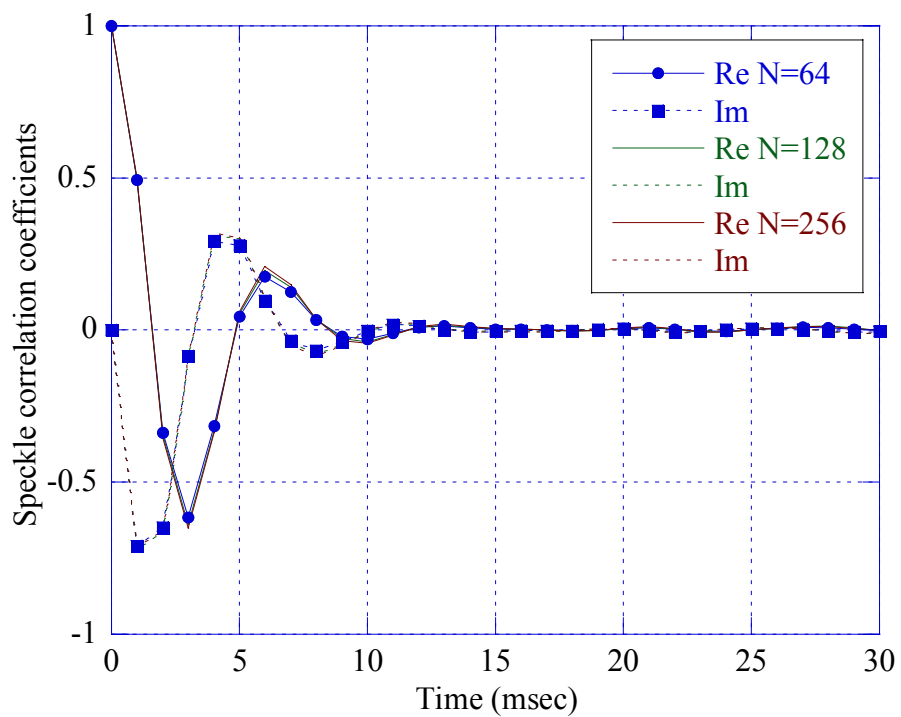
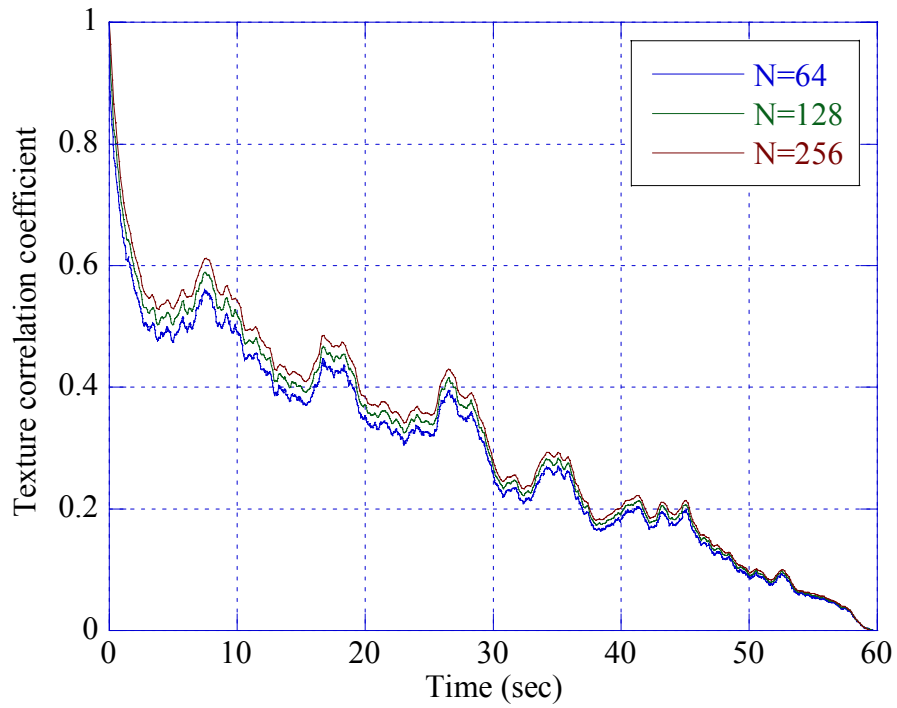
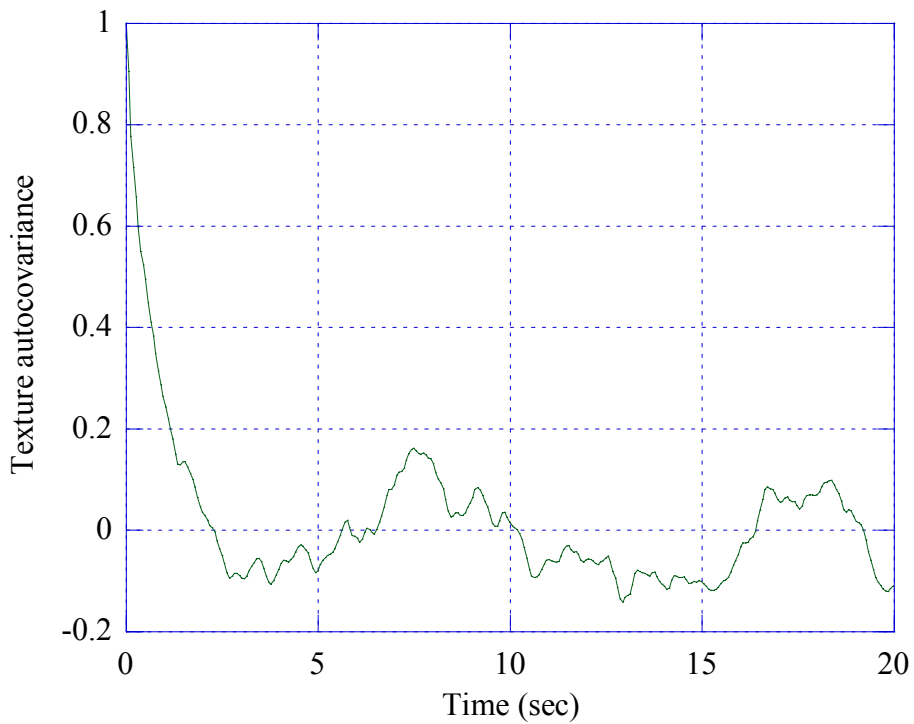


Figure 3. 10 - Speckle correlation coefficients, VH pol., 1st cell, 60 m.



**Figure 3. 11** - Texture correlation coefficient, VH pol., 1st cell, 60 m.



**Figure 3. 12** - Texture auto-covariance function, VH pol., 1st cell, N=128, 60 m.

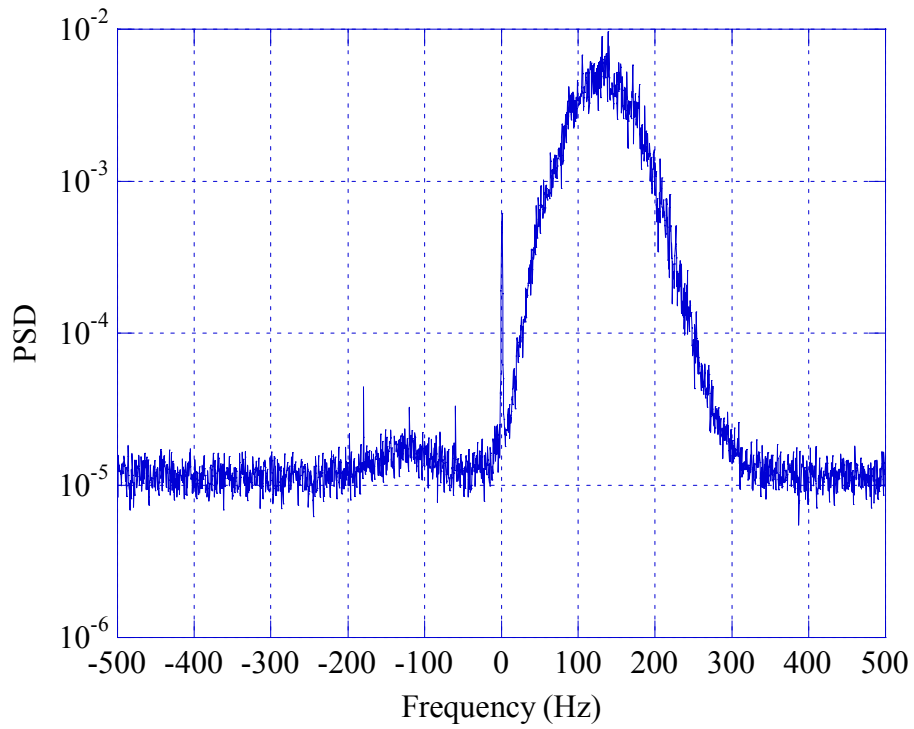


**Figure 3.13** - Average Power Spectral Density, PSD, 1<sup>st</sup> cell, VV pol., 30 m,  $CNR \approx 17$  dB .

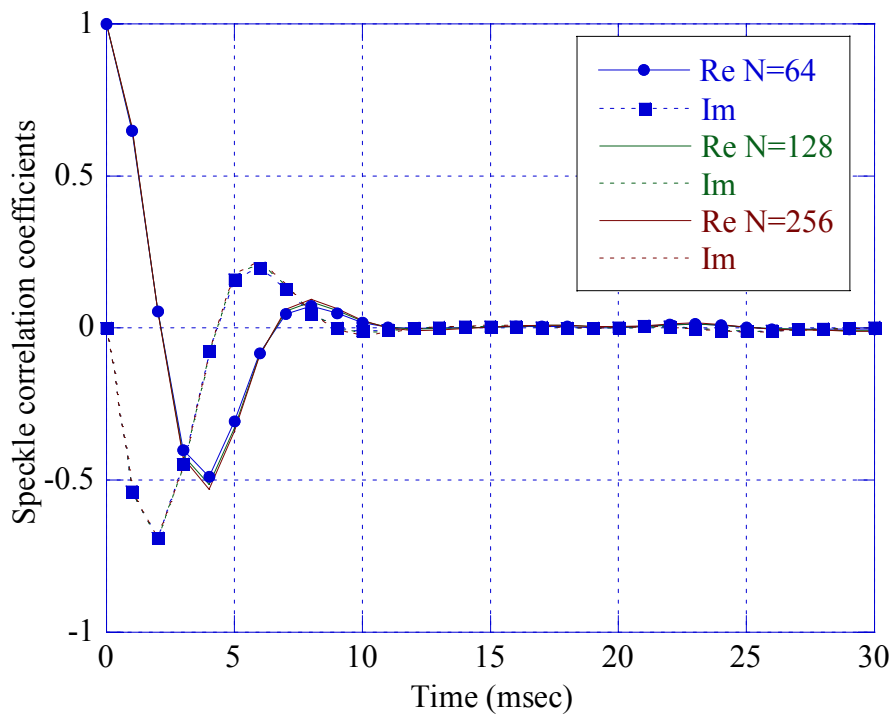


**Figure 3.14** - Speckle correlation coefficients, VV pol., 1<sup>st</sup> cell, 30 m.

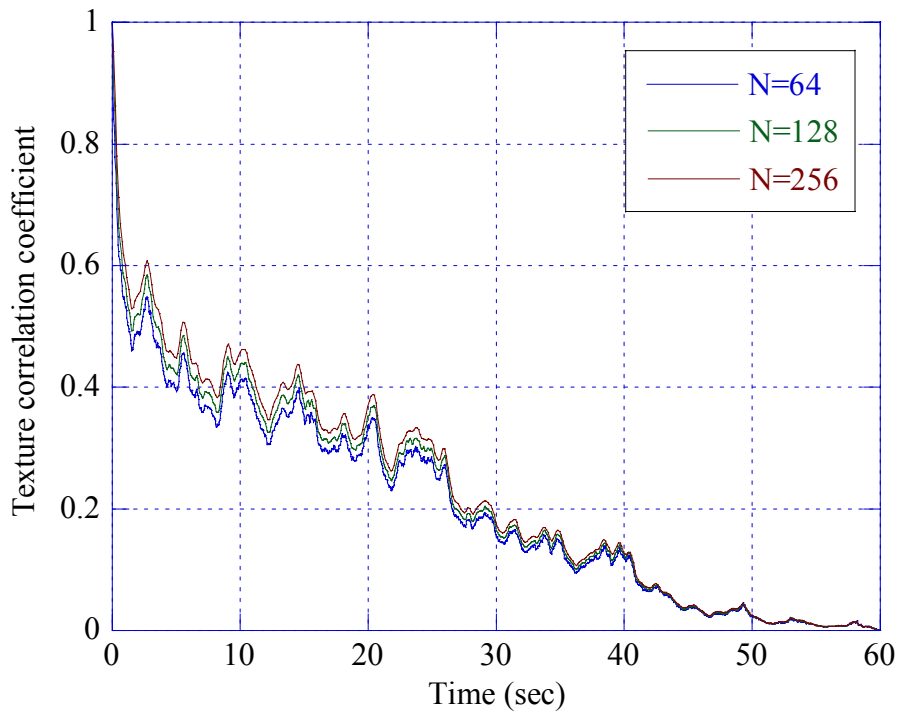


**Figure 3.15** - Texture correlation coefficient, VV pol., 1<sup>st</sup> cell, 30 m.

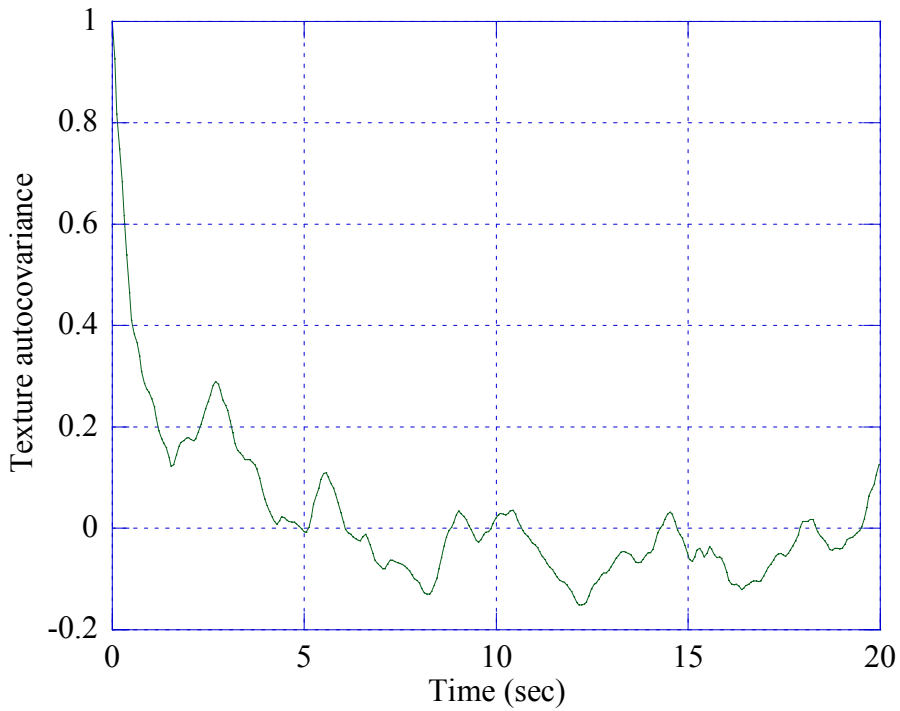


**Figure 3.16** - Texture autocovariance function, VV pol., 1<sup>st</sup> cell, 30 m.

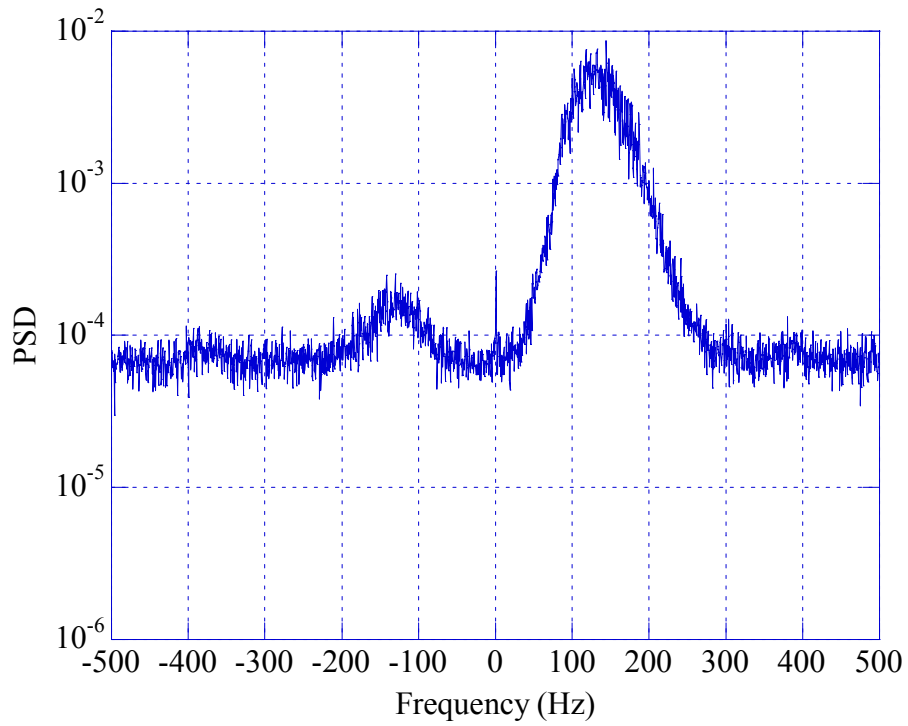


Figure 3.17 - Average Power Spectral Density, PSD, HH pol., 1<sup>st</sup> cell, 30 m,  $CNR \approx 7$  dB .

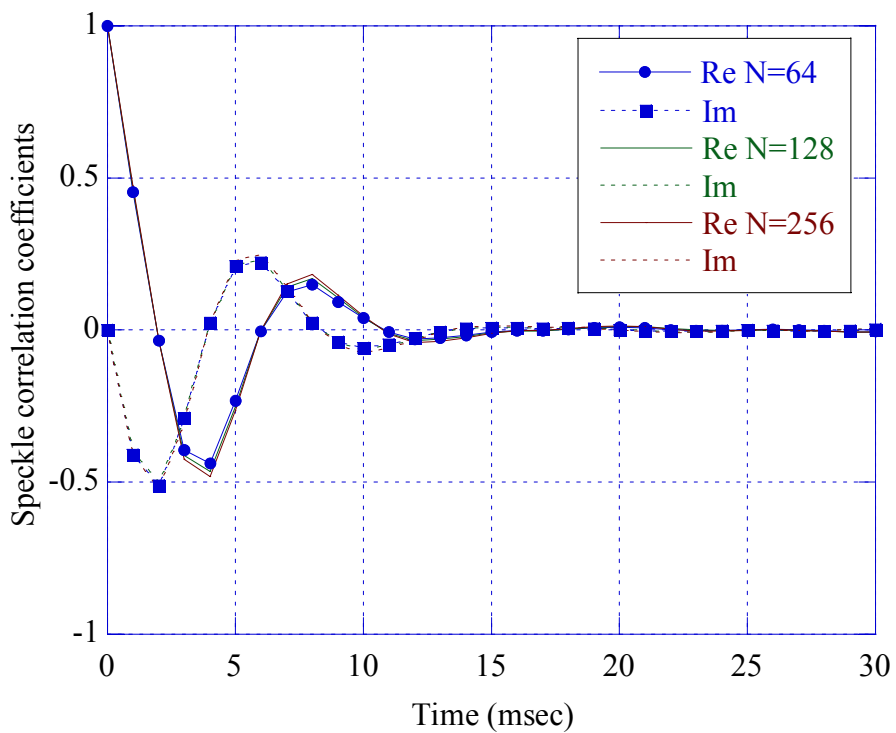
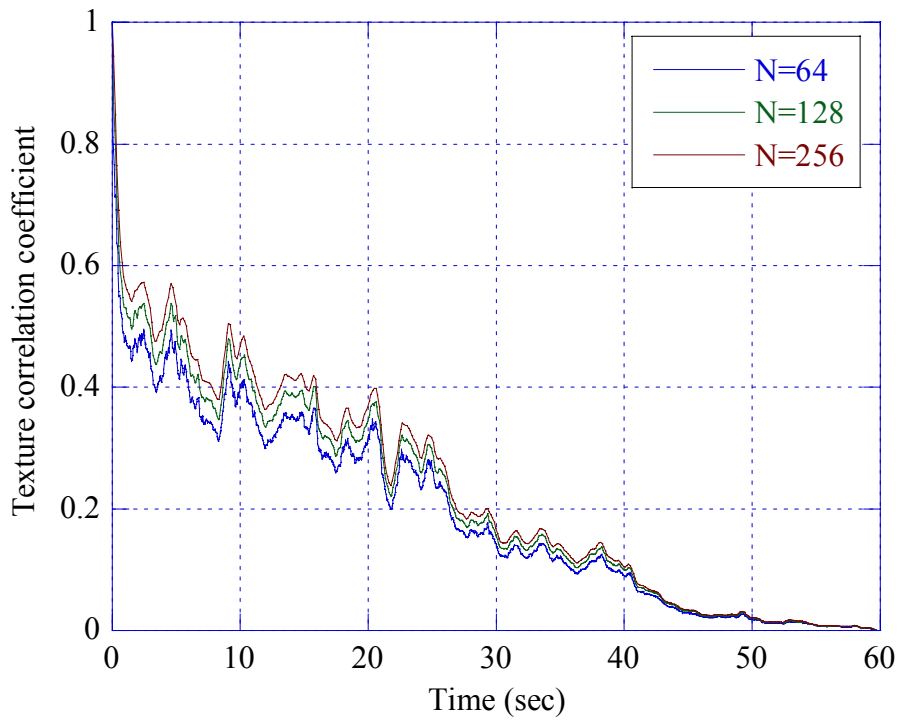
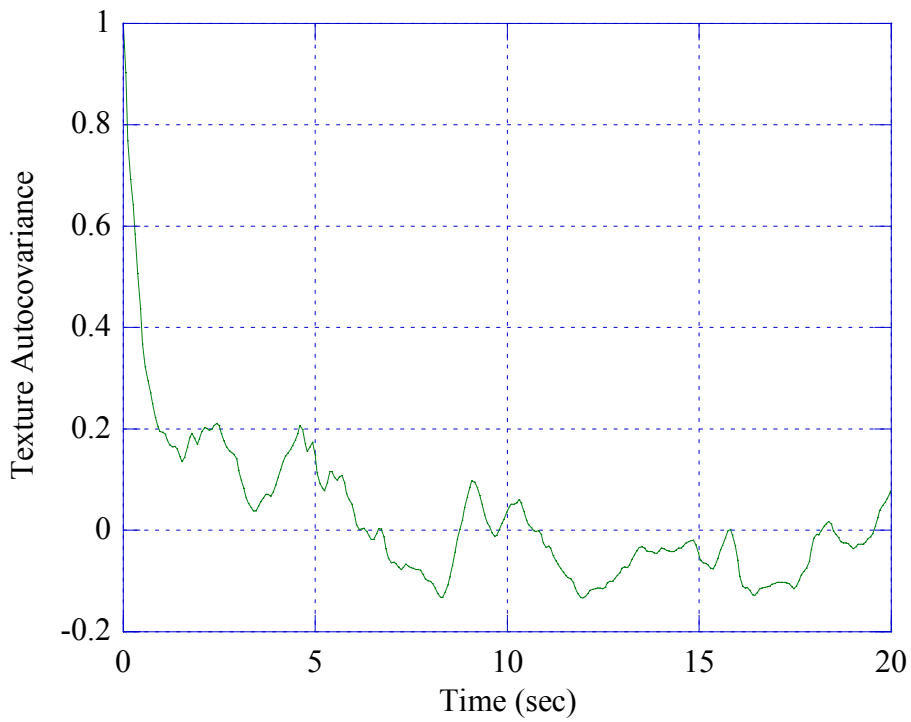


Figure 3.18 - Speckle correlation coefficients, HH pol., 1<sup>st</sup> cell, 30 m.



**Figure 3. 19** - Texture correlation coefficient, HH pol., 1<sup>st</sup> cell, 30 m.



**Figure 3. 20** - Texture autocovariance function, HH pol., 1<sup>st</sup> cell, 30 m.

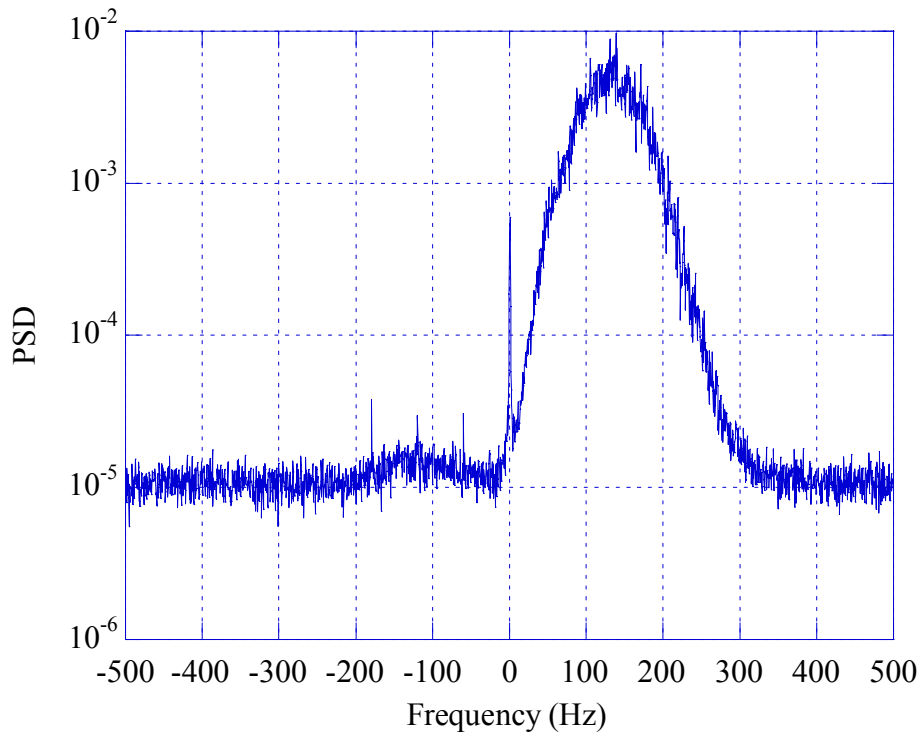


**Figure 3.21** - Average Power Spectral Density, PSD, VH pol., 1<sup>st</sup> cell, 30 m,  $CNR \approx 17$  dB .

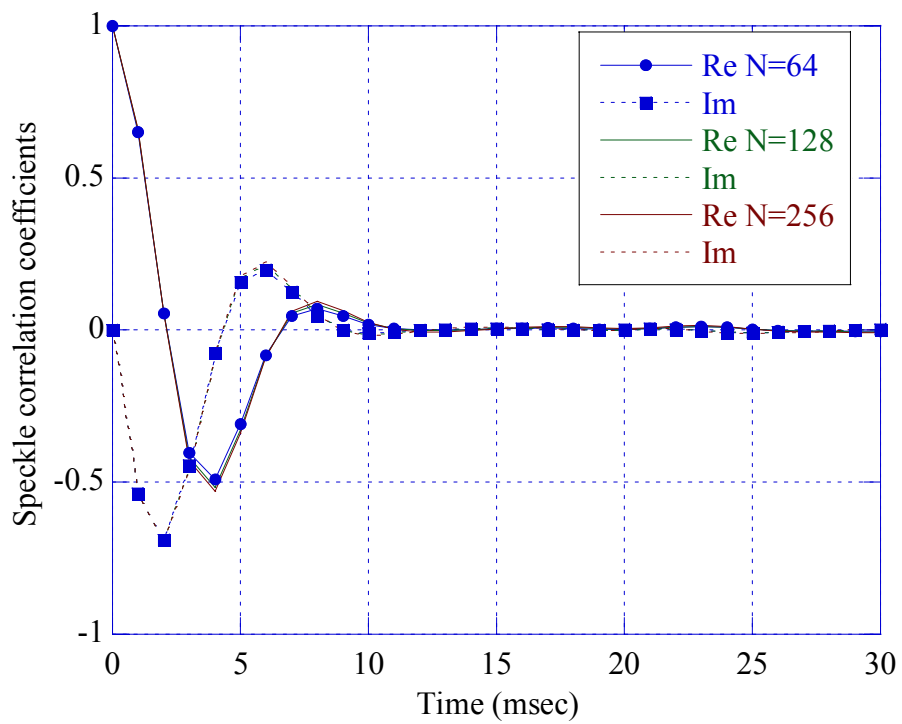


**Figure 3.22** - Speckle correlation coefficients, VH pol., 1<sup>st</sup> cell, 30 m.

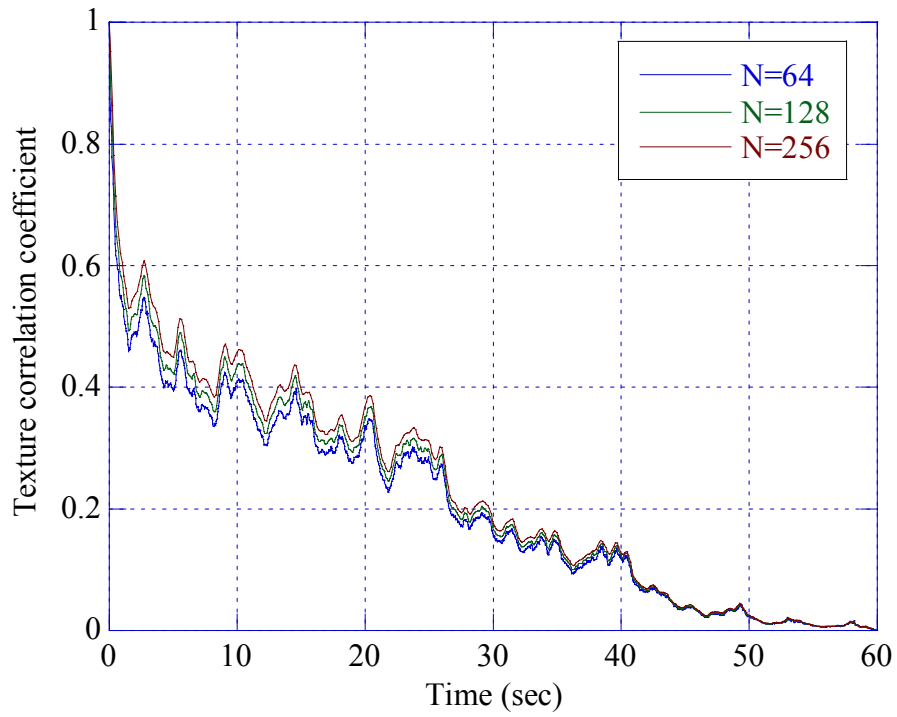


**Figure 3. 23** - Texture correlation coefficient, VH pol., 1<sup>st</sup> cell, 30 m.

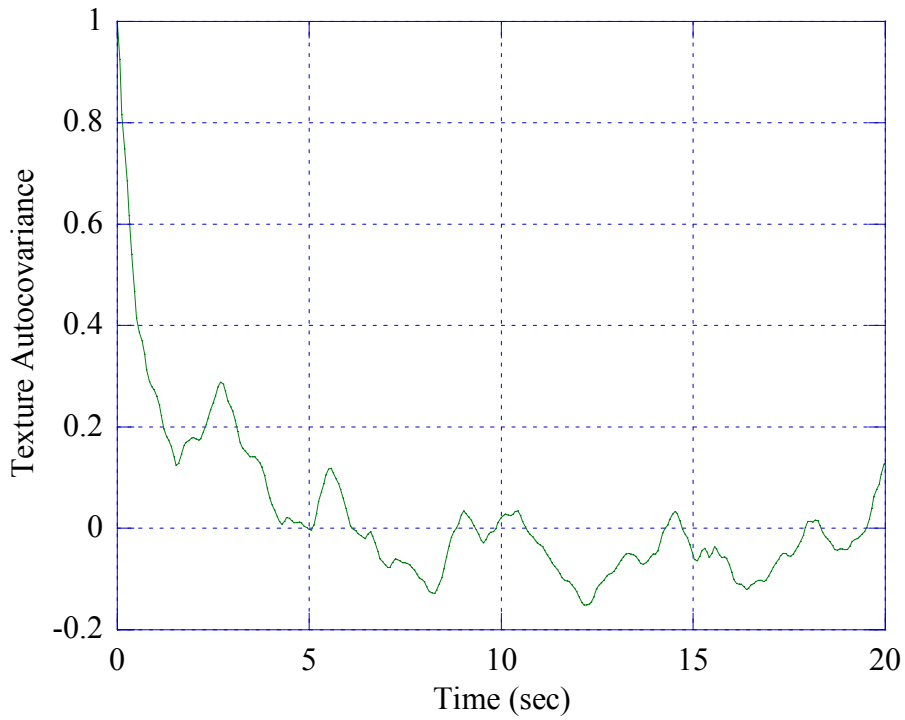


**Figure 3. 24** - Texture auto-covariance function, VH pol., 1<sup>st</sup> cell, 30 m.

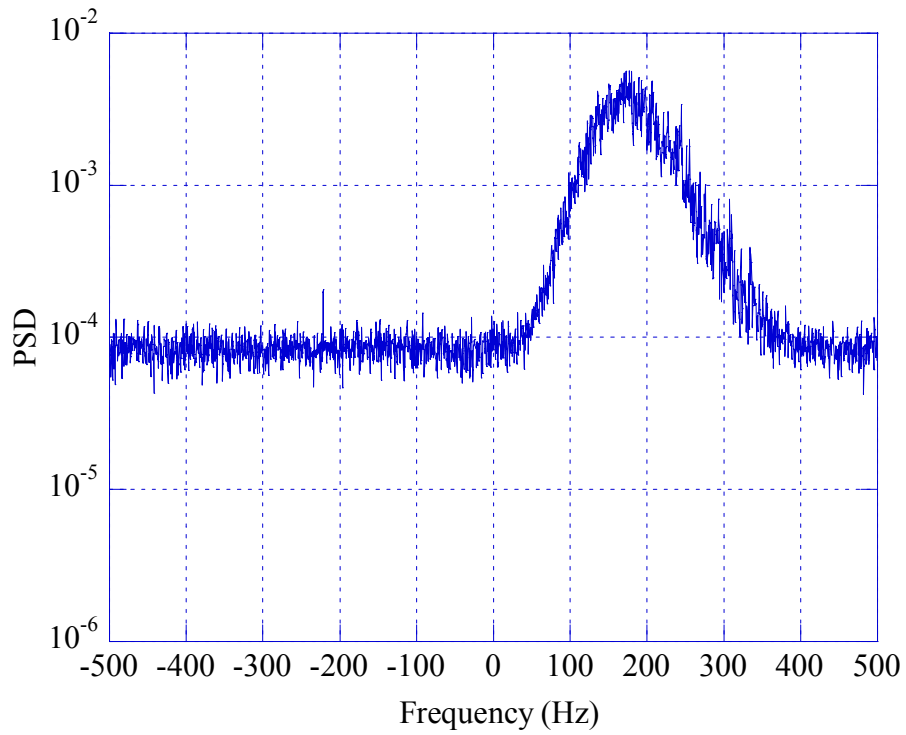


Figure 3. 25 - Average Power Spectral Density, PSD, VV pol., 7<sup>th</sup> cell, 15 m,  $CNR = 6\text{ dB}$  .

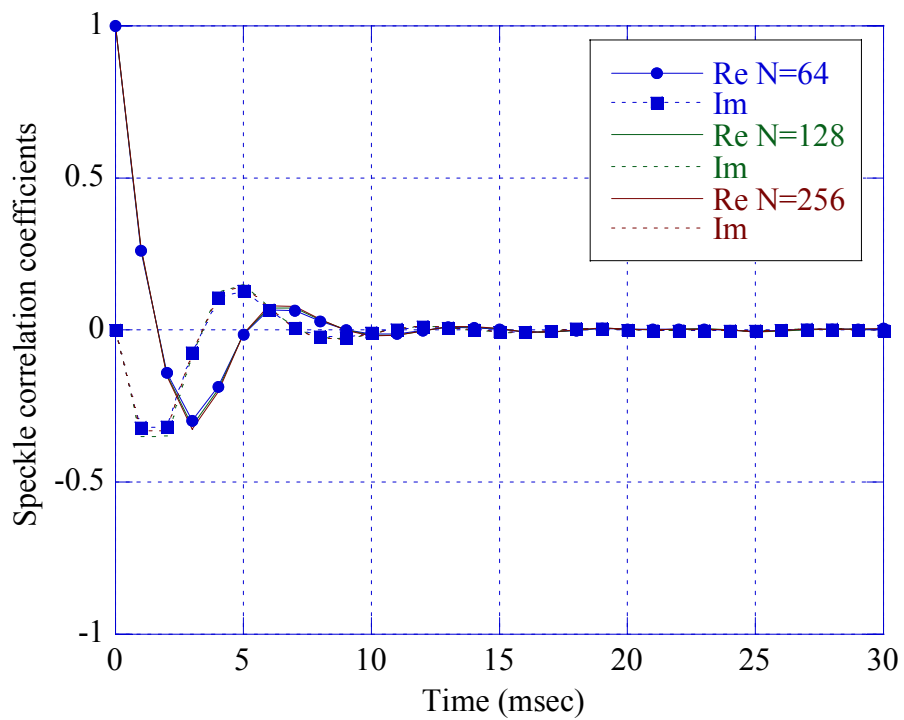
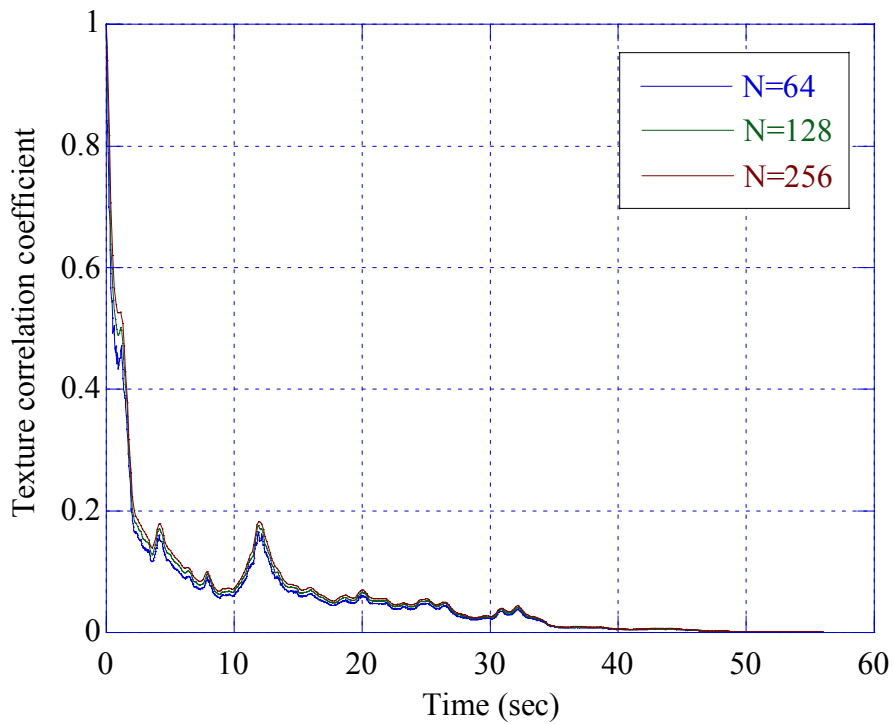
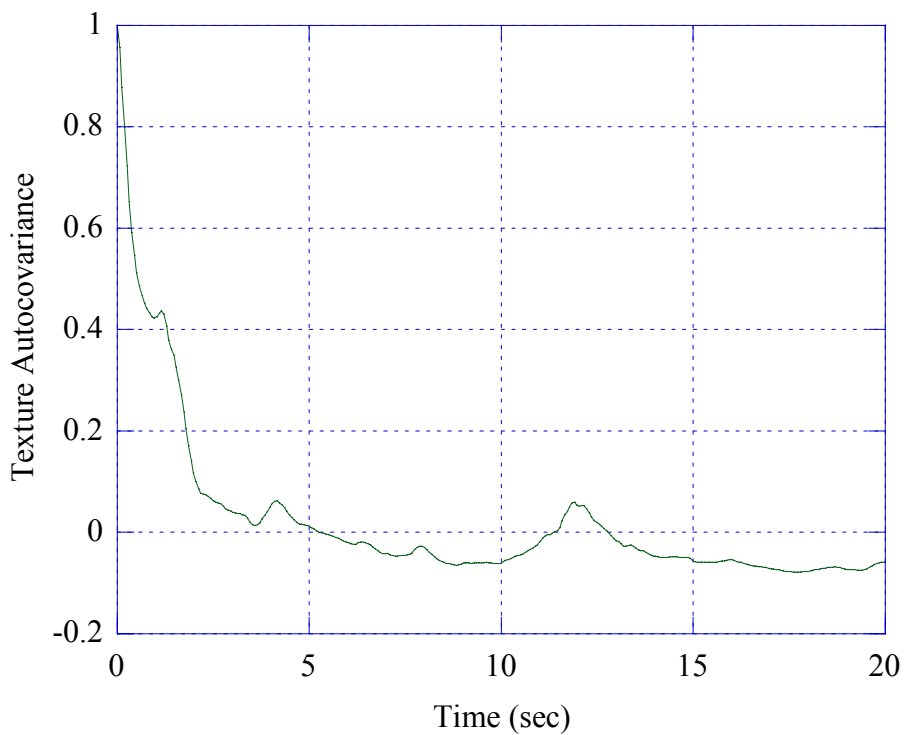


Figure 3. 26 - Speckle correlation coefficients, VV pol., 7<sup>th</sup> cell, 15 m.



**Figure 3. 27** - Texture correlation coefficient, VV pol., 7<sup>th</sup> cell, 15 m.



**Figura 3. 28** - Texture auto-covariance function, VV pol., 7<sup>th</sup> cell, 15 m.

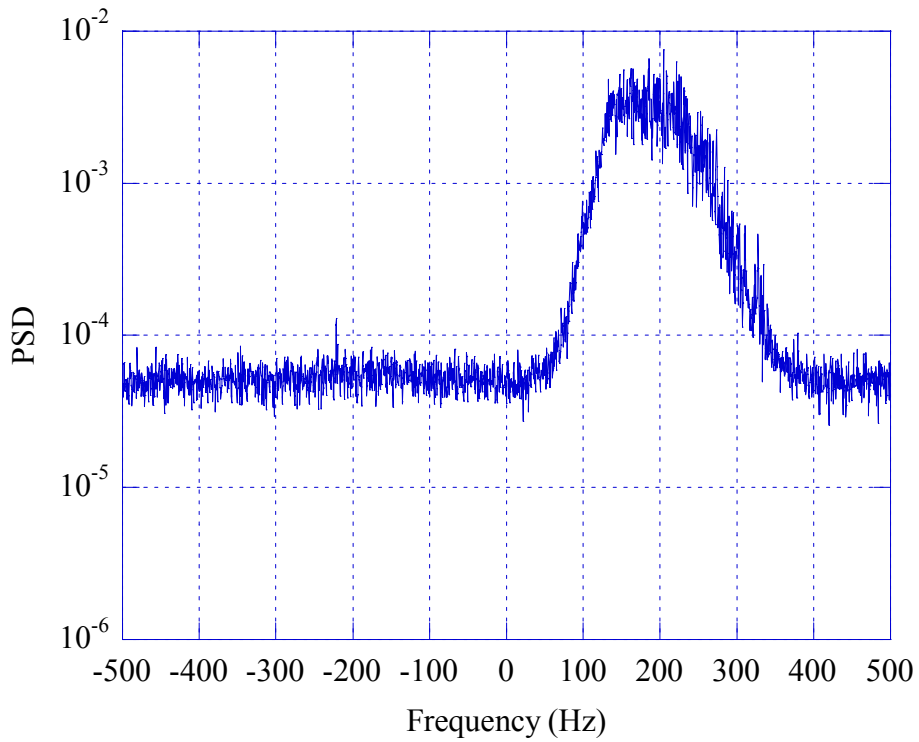


Figure 3.29 - Average Power Spectral Density, PSD, HH pol., 1<sup>st</sup> cell, 15 m,  $CNR \approx 9$  dB.

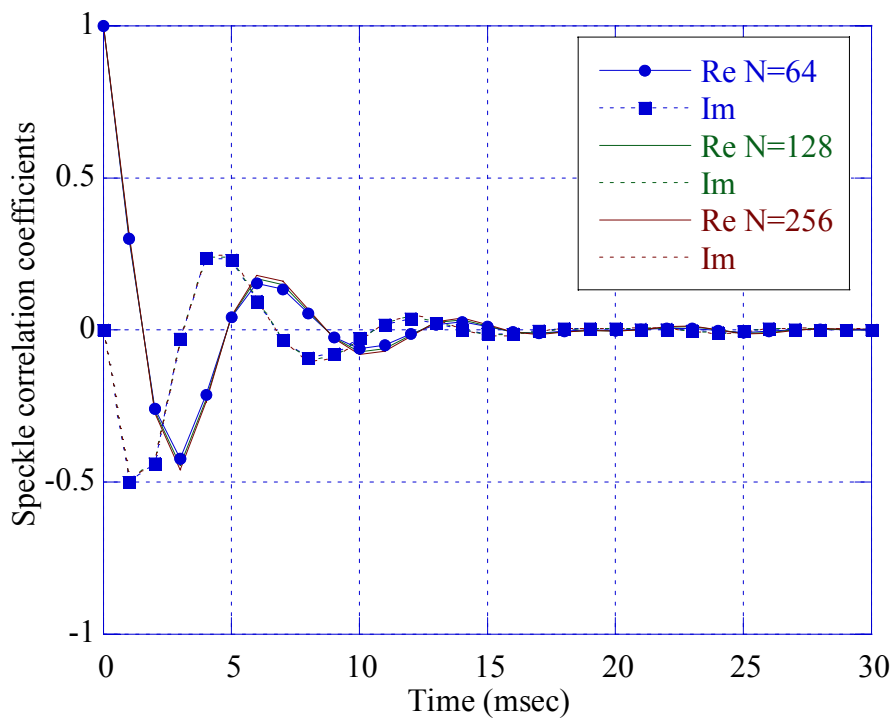
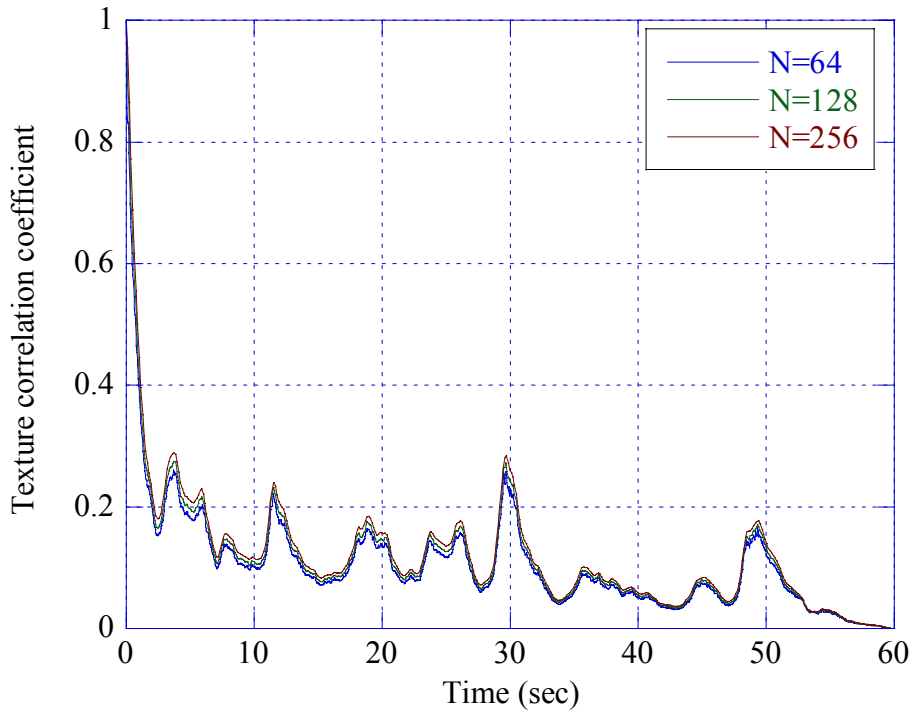
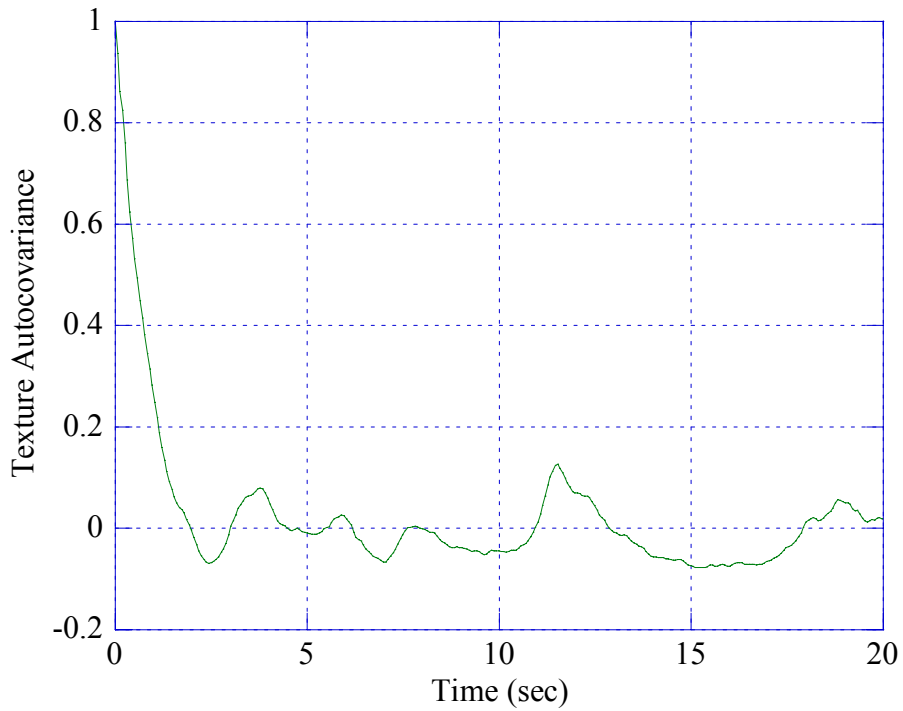


Figure 3.30 - Speckle correlation coefficients, HH pol., 1<sup>st</sup> cell, 15 m.



**Figure 3.31** - Texture correlation coefficient, HH pol., 1<sup>st</sup> cell, 15 m.



**Figure 3.32** - Texture autocovariance function, HH pol., 1<sup>st</sup> cell, 15 m.

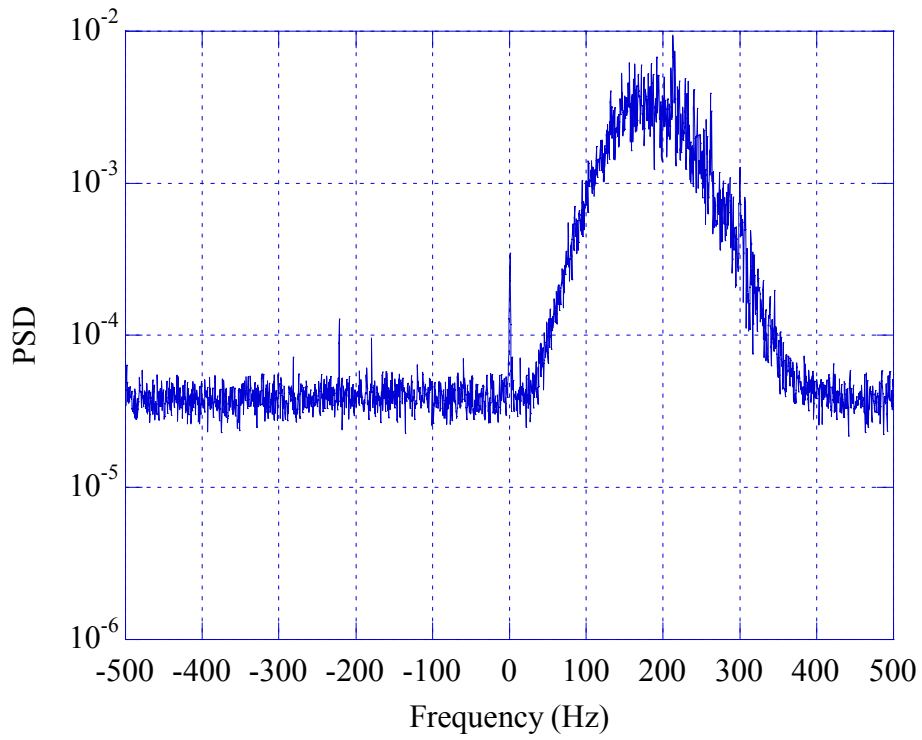


Figure 3.33 - Average Power Spectral Density, PSD, VH pol., 1<sup>st</sup> cell, 15 m,  $CNR \approx 9$  dB.

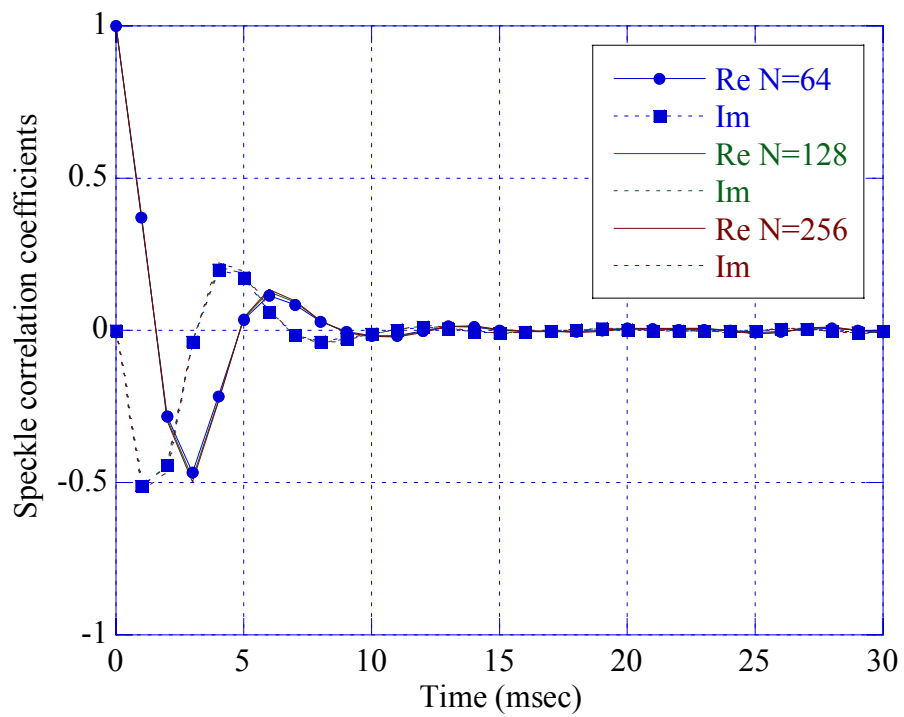
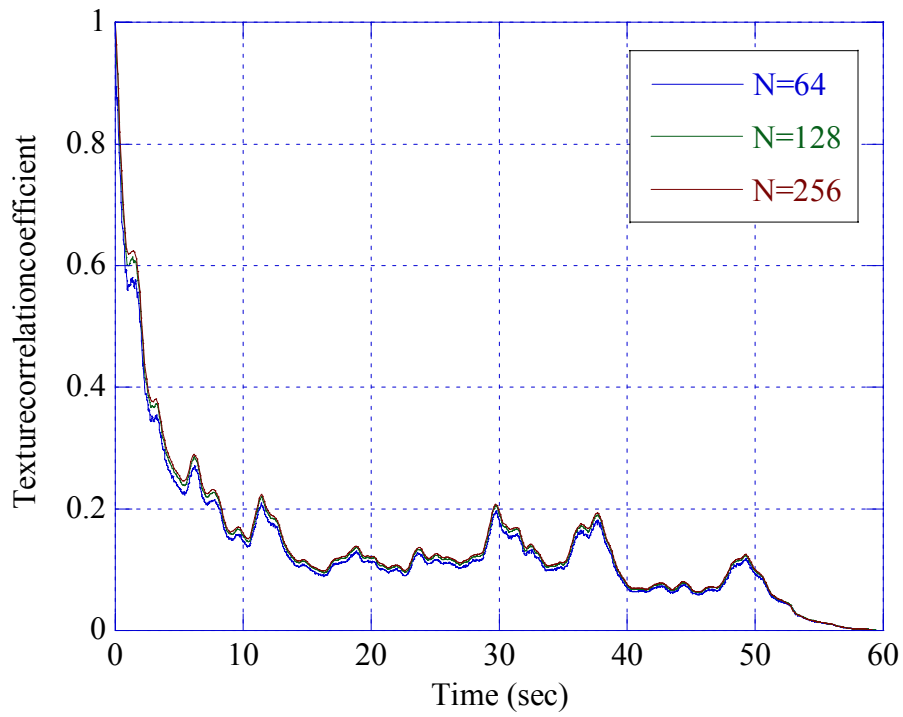
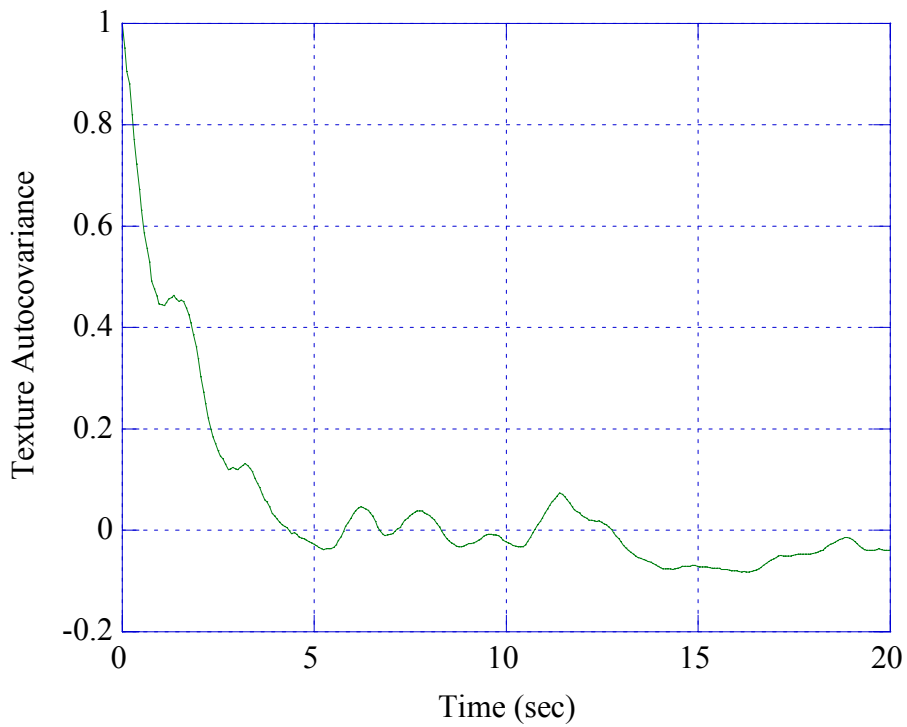


Figure 3.34 - Speckle correlation coefficients, VH pol., 1<sup>st</sup> cell, 15 m.



**Figure 3. 35** - Texture correlation coefficient, VH pol., 1<sup>st</sup> cell, 15 m.



**Figure 3. 36** - Texture autocovariance function, VH pol., 1<sup>st</sup> cell, 15 m.

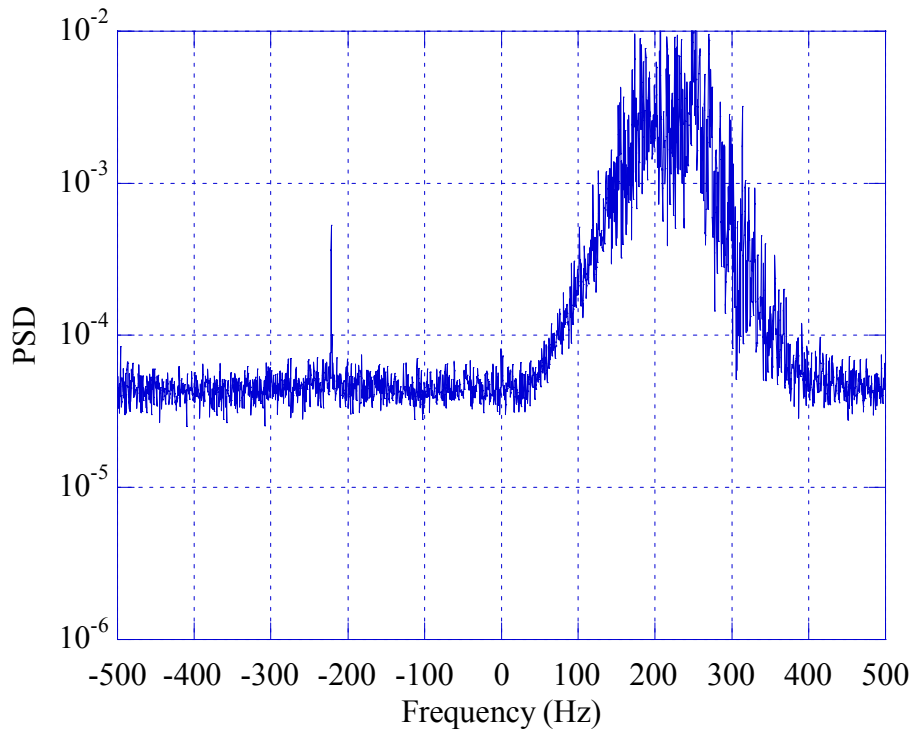


**Figure 3.37** - Average Power Spectral Density, PSD, VV pol., 5<sup>th</sup> cell, 9 m,  $CNR \approx 9$  dB .

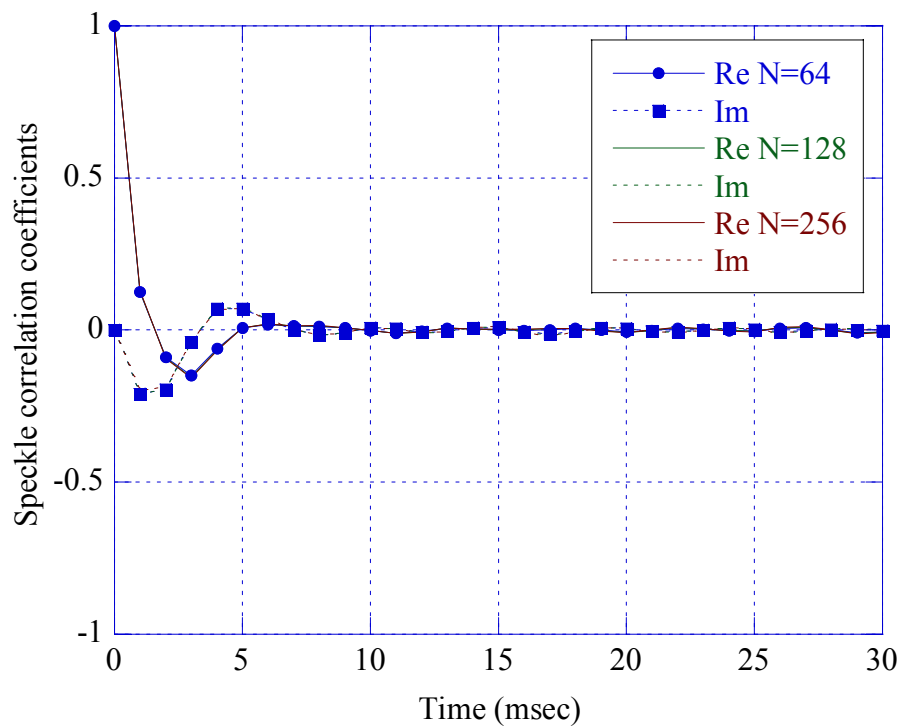


**Figure 3.38** - Speckle correlation coefficients, VV pol., 5<sup>th</sup> cell, 9 m.

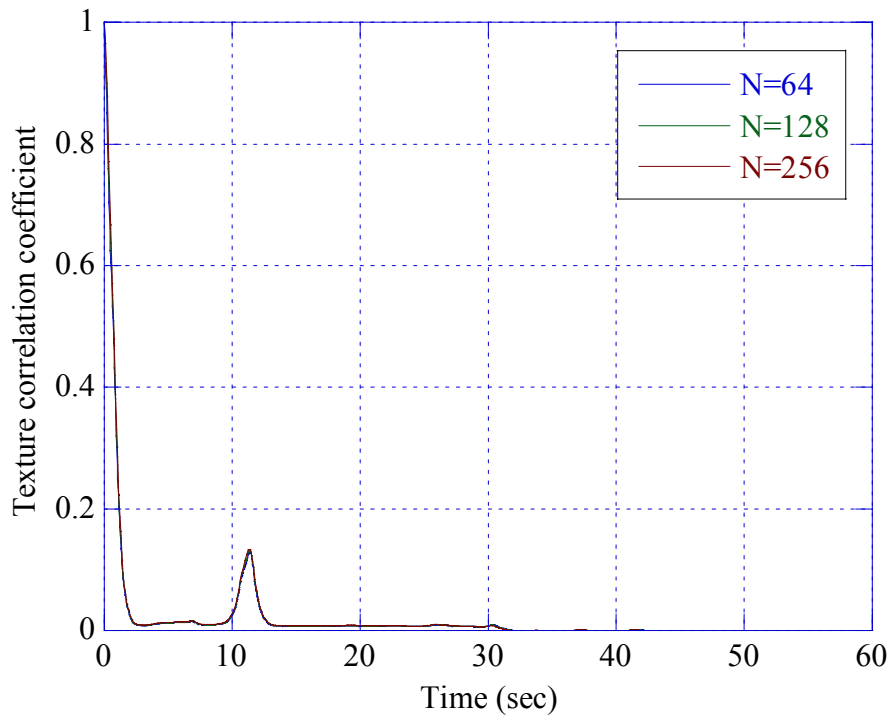


**Figure 3. 39** - Texture correlation coefficient, VV pol., 5<sup>th</sup> cell, 9 m.

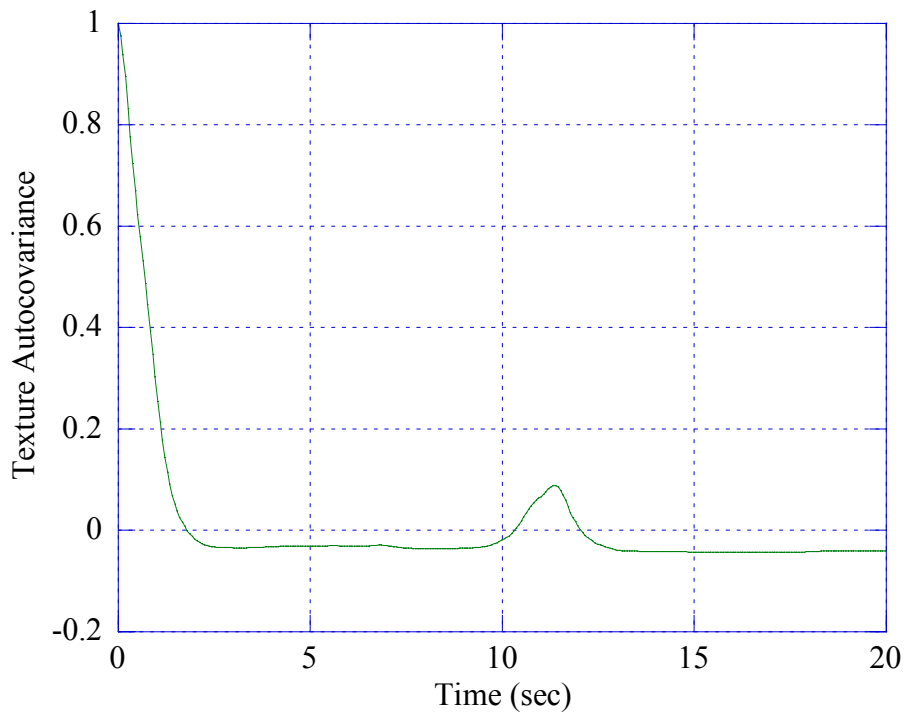


**Figure 3. 40** - Texture auto-covariance function, VV pol., 5<sup>th</sup> cell, 9 m.

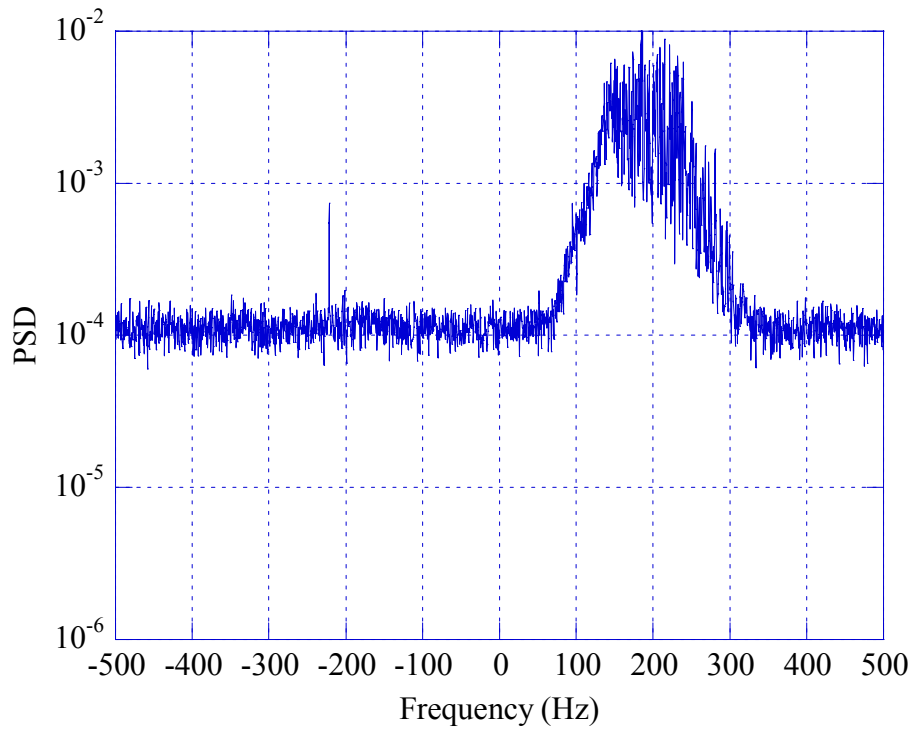


**Figure 3. 41** - Average Power Spectral Density, PSD, HH pol., 1<sup>st</sup> cell, 9 m,  $CNR \approx 6$  dB .

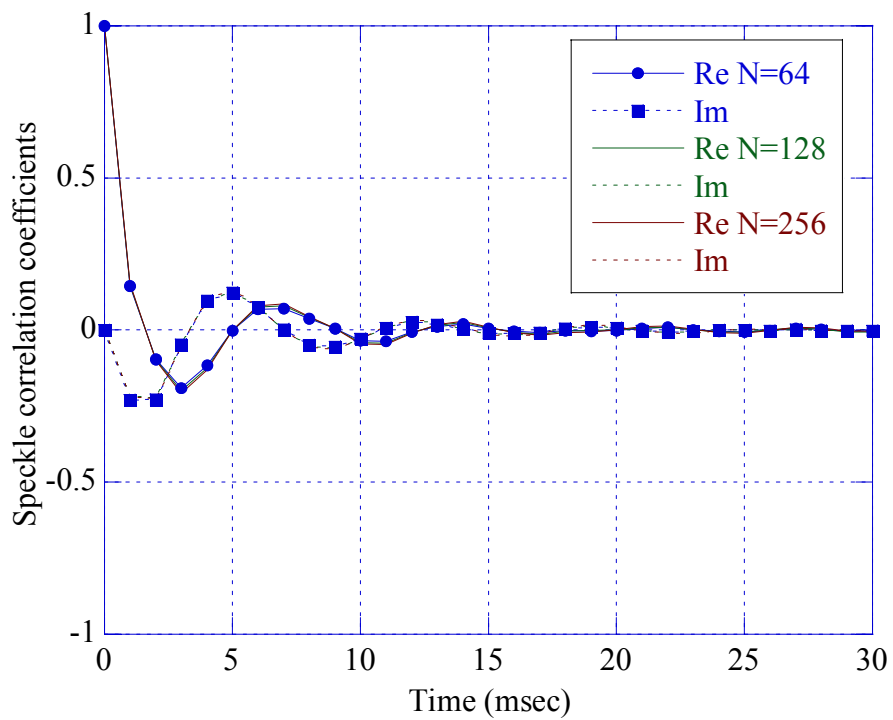


**Figure 3. 42** - Speckle correlation coefficients, HH pol., 1<sup>st</sup> cell, 9 m.

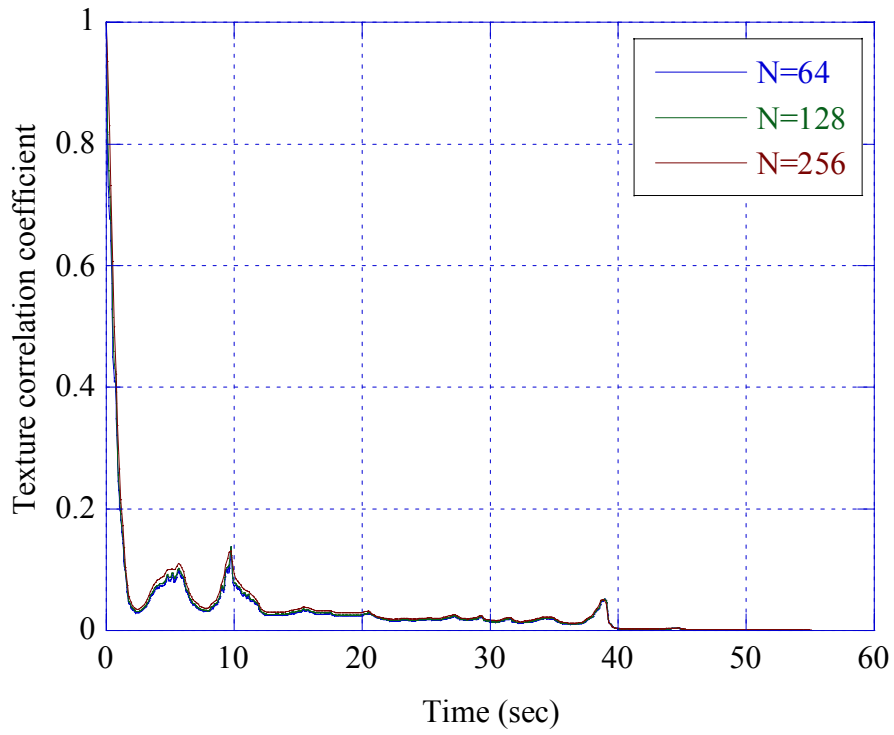


**Figure 3. 43** - Texture correlation coefficient, HH pol., 1<sup>st</sup> cell, 9 m.

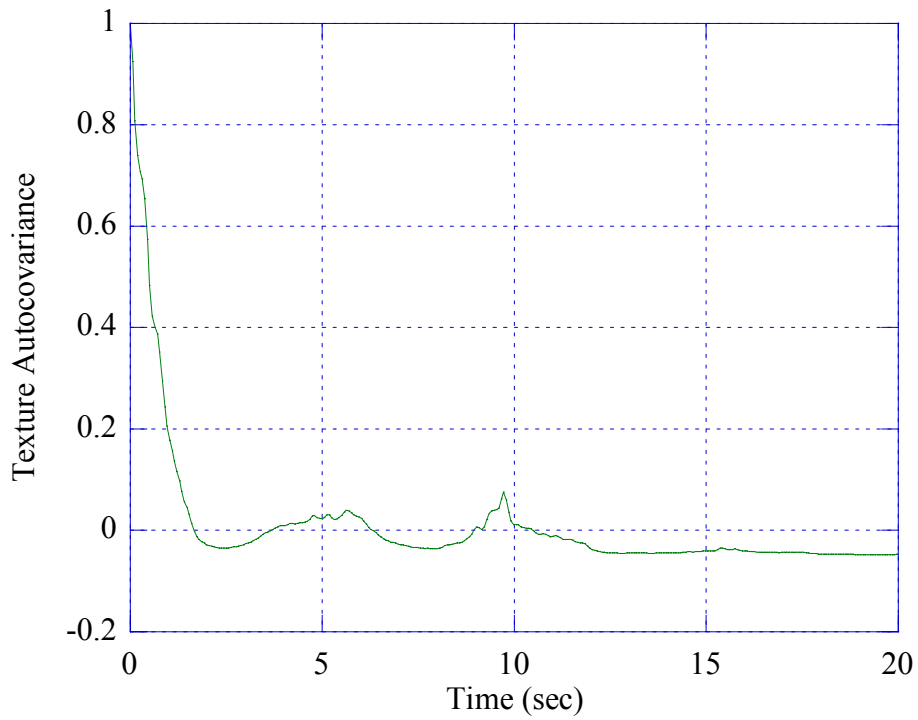


**Figure 3. 44** - Texture auto-covariance function, HH pol., 1<sup>st</sup> cell, 9 m.

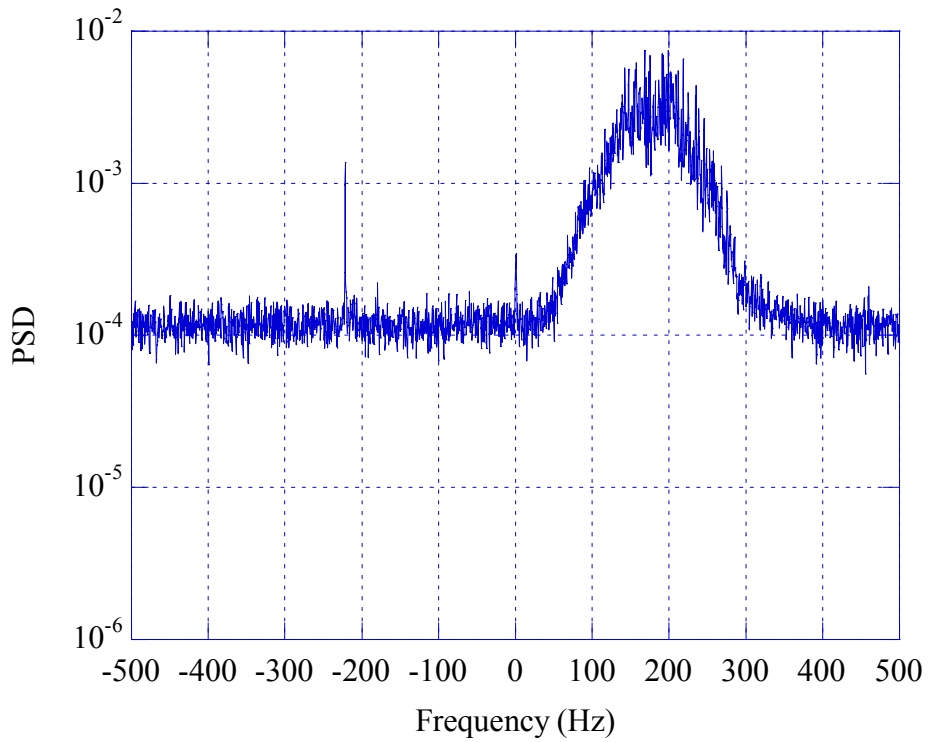


Figure 3.45 - Average Power Spectral Density, PSD, VH pol., 1<sup>st</sup> cell, 9 m,  $CNR \approx 6$  dB .

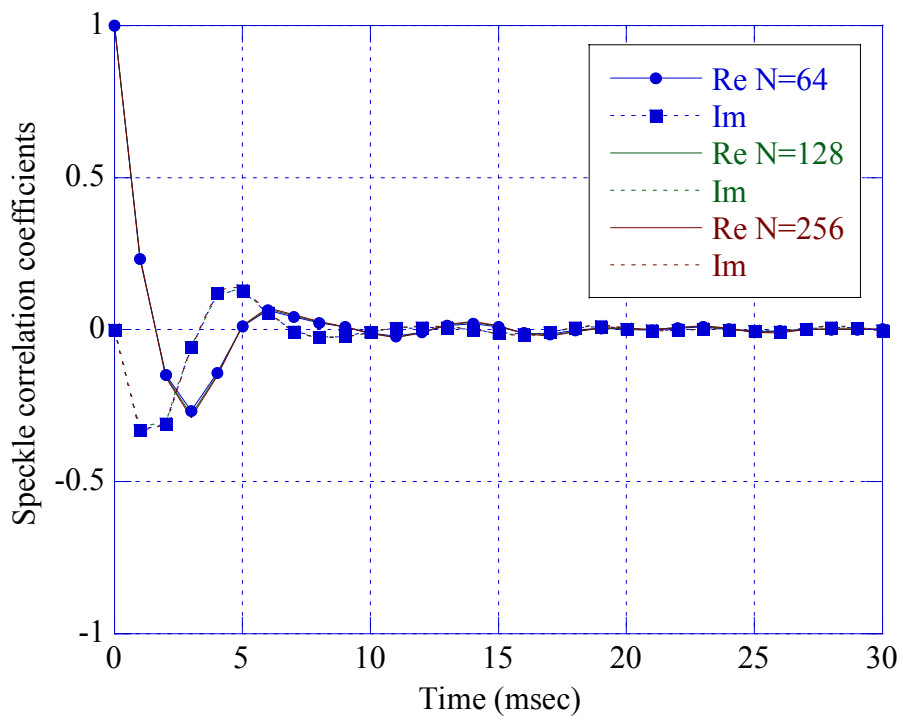
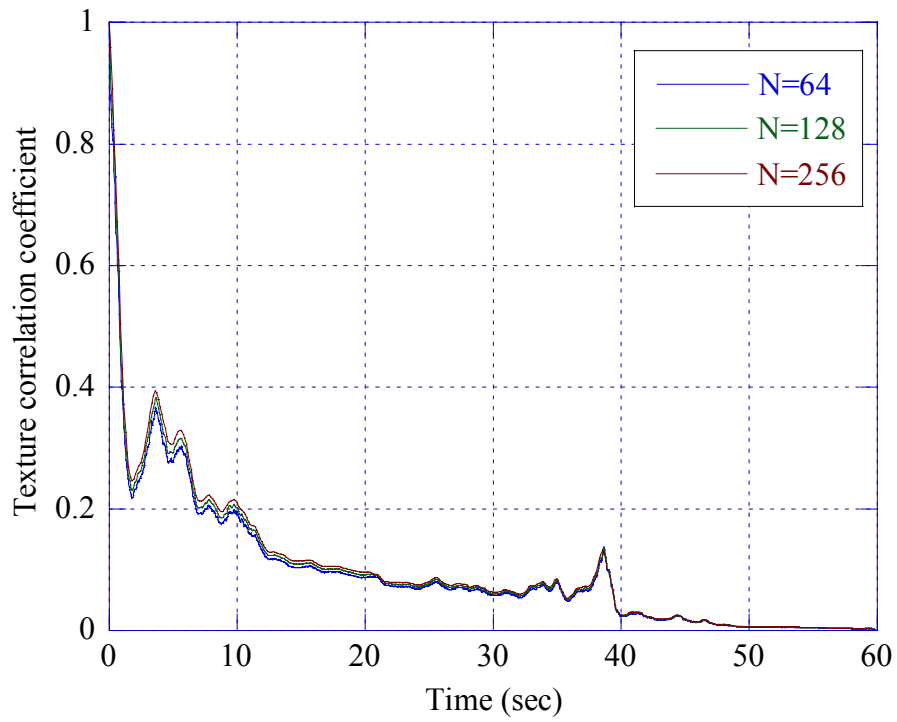
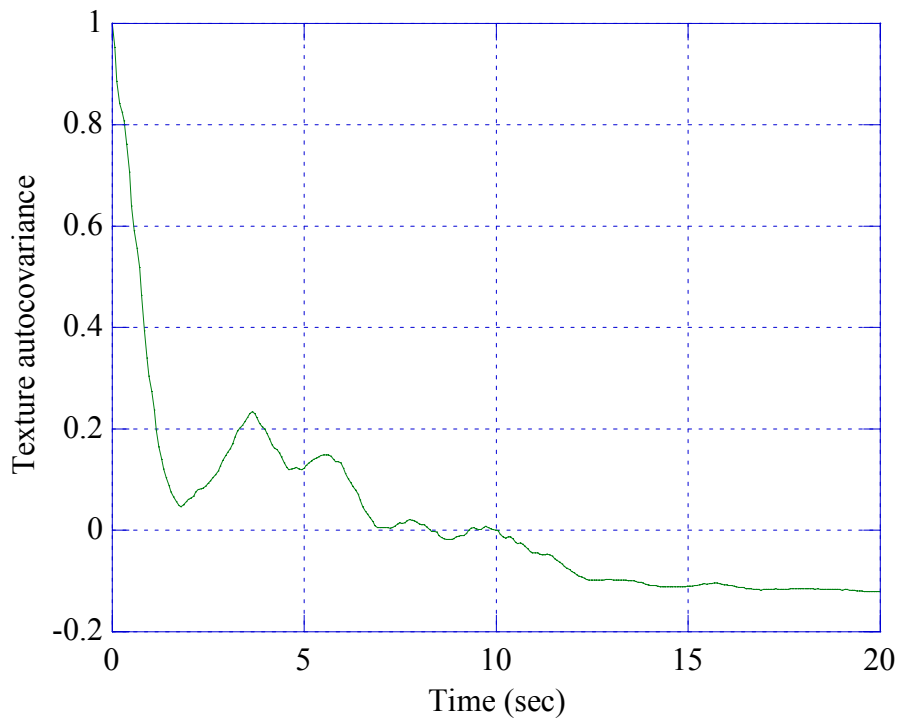


Figure 3.46 Speckle correlation coefficients, VH pol., 1<sup>st</sup> cell, 9 m.

b



**Figure 3. 47** - Texture correlation coefficient, VH pol., 1<sup>st</sup> cell, 9 m.



**Figure 3. 48** - Texture autocovariance function, VH pol., 1<sup>st</sup> cell, 9 m.

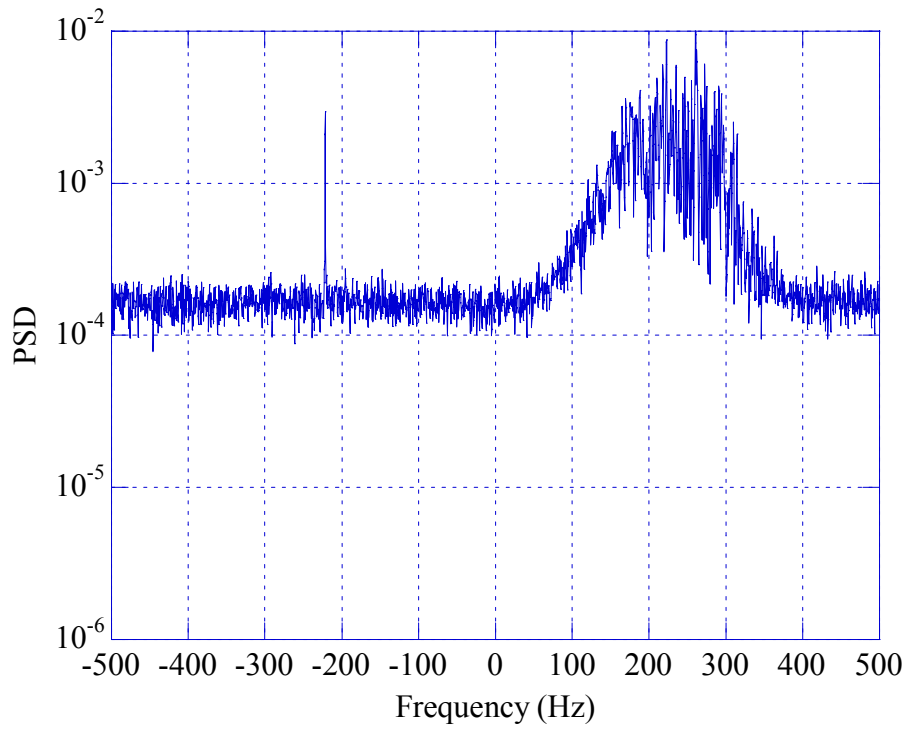


**Figure 3. 49** - Average Power Spectral Density, PSD, VV pol., 8<sup>th</sup> cell, 3 m,  $CNR \approx 4$  dB .

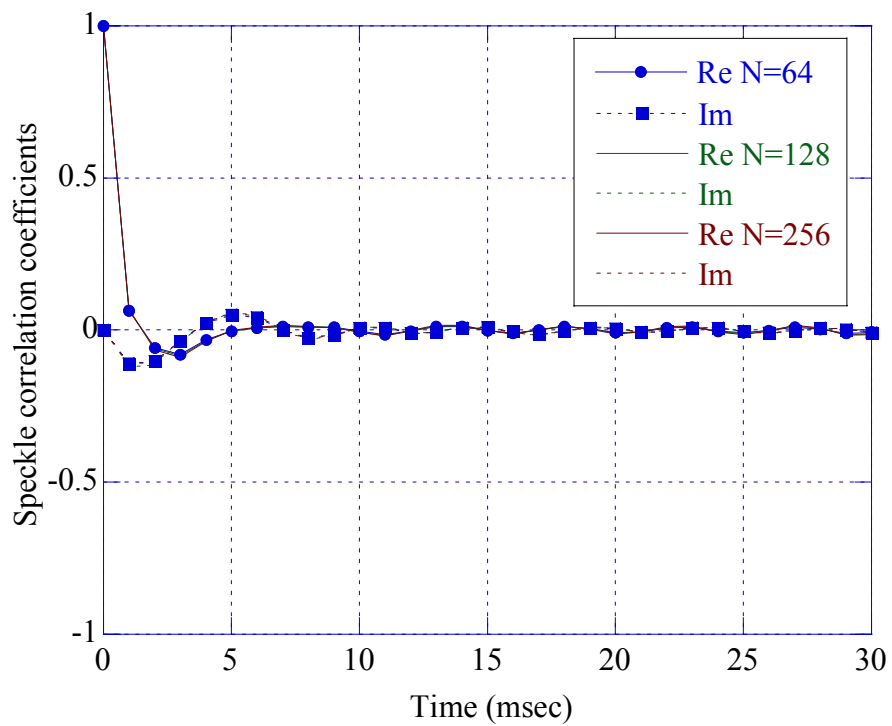


**Figure 3. 50** - Speckle correlation coefficients, VV pol., 8<sup>th</sup> cell, 3 m.

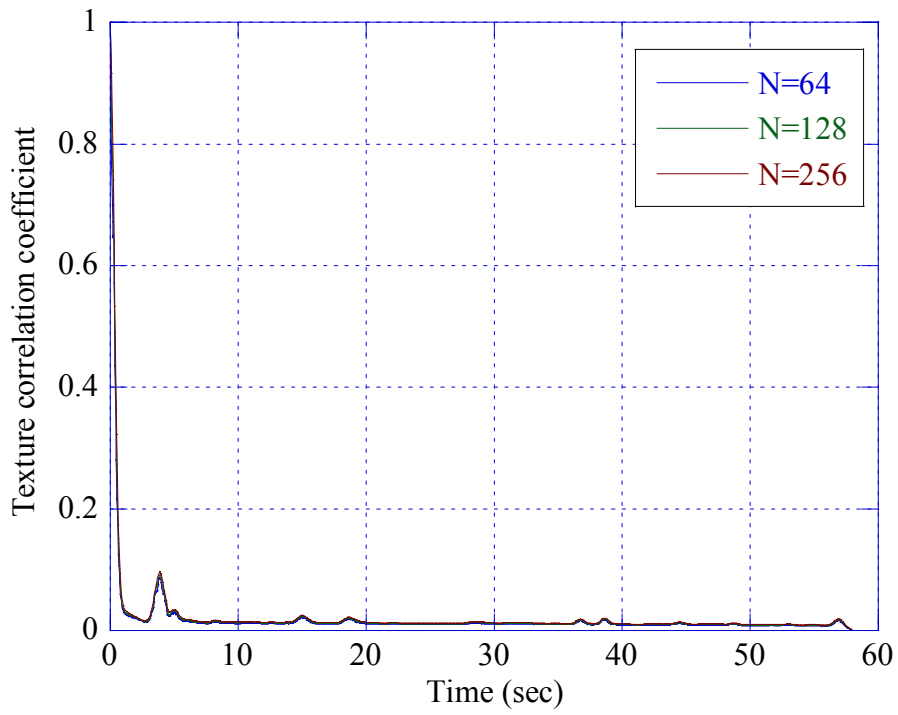


**Figure 3. 51** - Texture correlation coefficient, VV pol., 8<sup>th</sup> cell, 3 m.

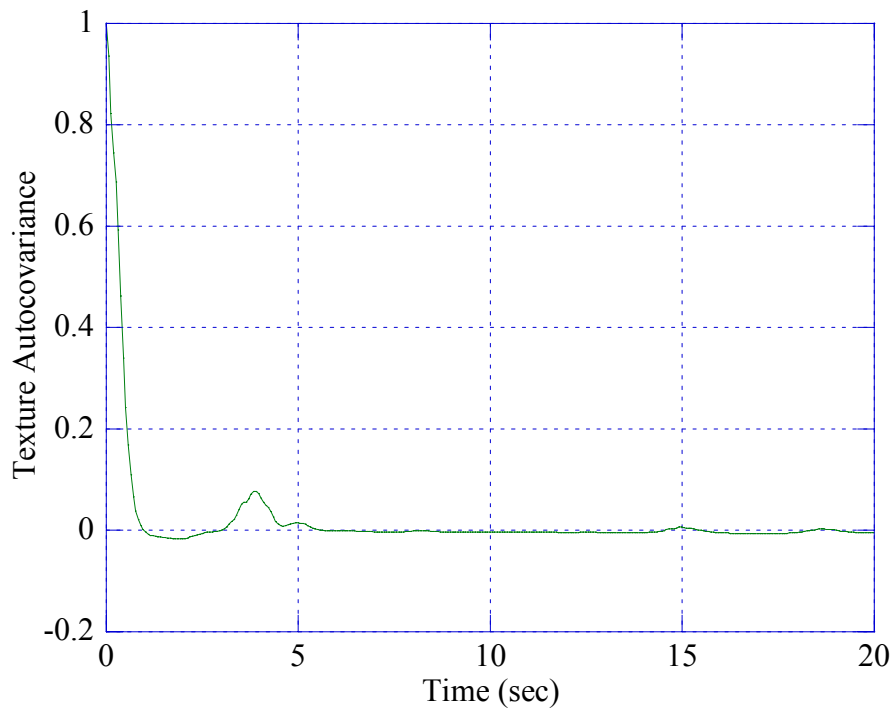


**Figure 3. 52** - Texture autocovariance function, VV pol., 8<sup>th</sup> cell, 3 m.

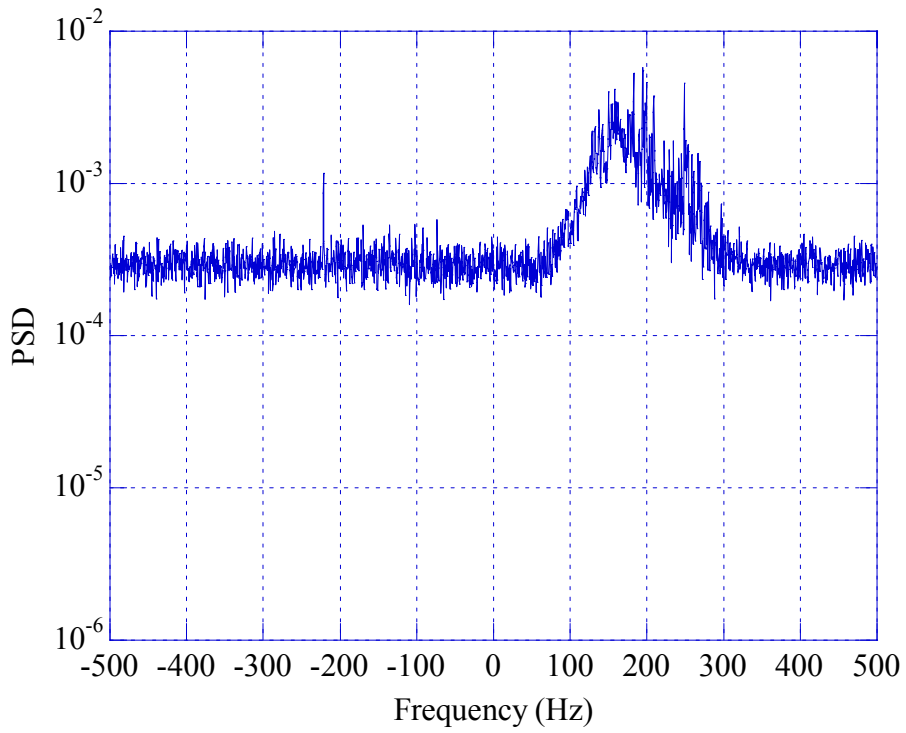


**Figure 3. 53** - Average Power Spectral Density, PSD, HH pol., 1<sup>st</sup> cell, 3 m,  $CNR = 0$  dB .

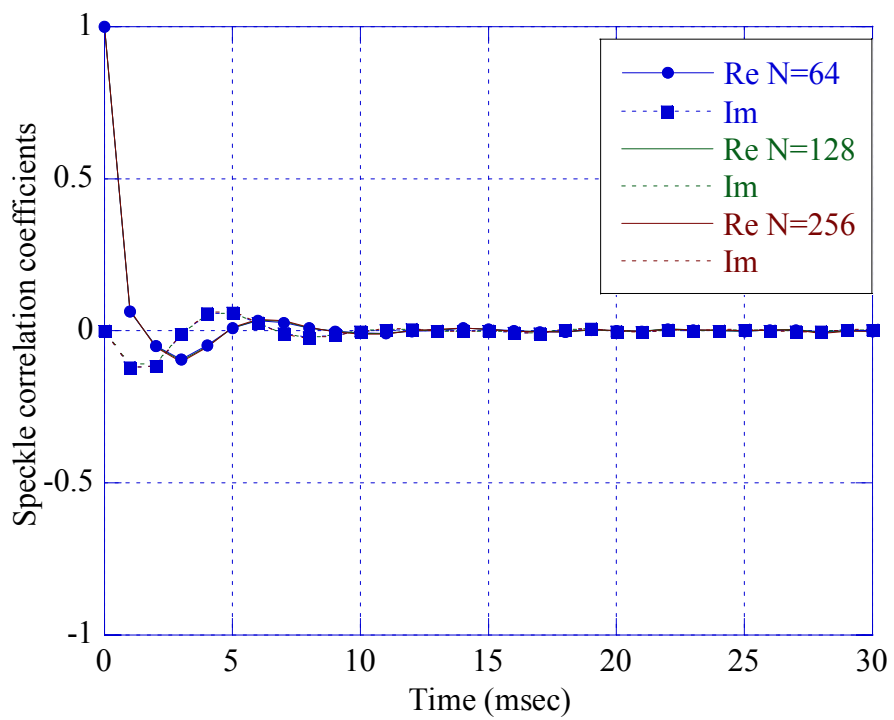


**Figure 3. 54** - Speckle correlation coefficients, HH pol., 1<sup>st</sup> cell, 3 m.

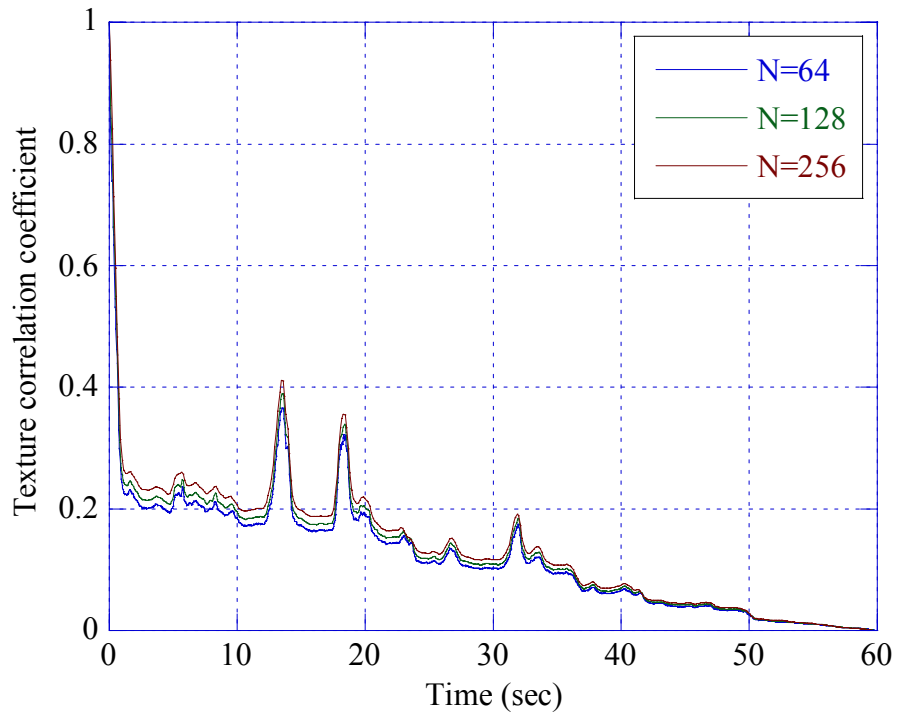


**Figure 3. 55** - Texture correlation coefficient, HH pol., 1<sup>st</sup> cell, 3 m.

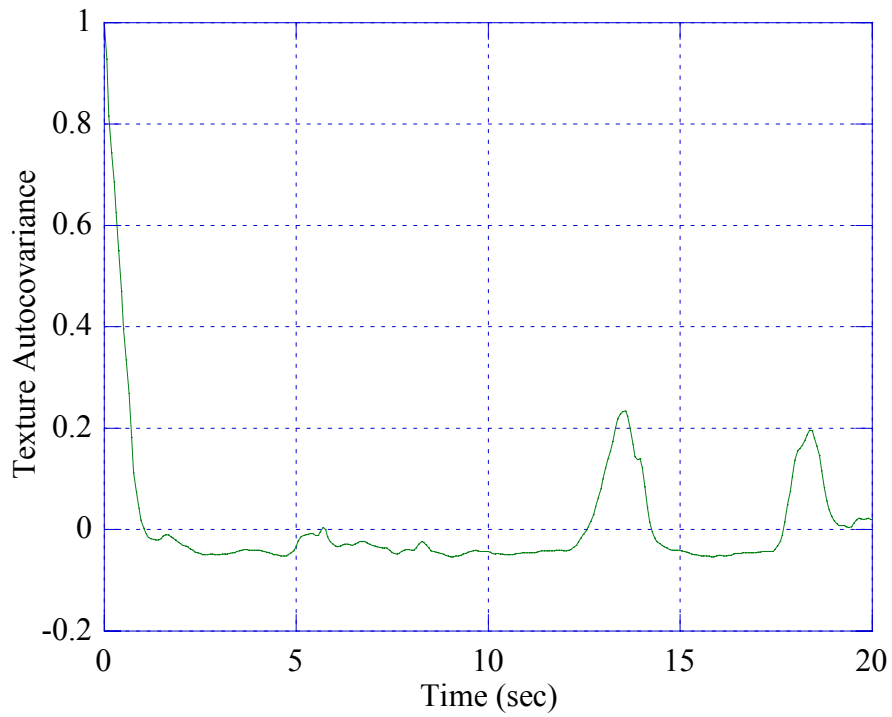


**Figure 3. 56** - Texture autocovariance function, HH pol., 1<sup>st</sup> cell, 3 m.

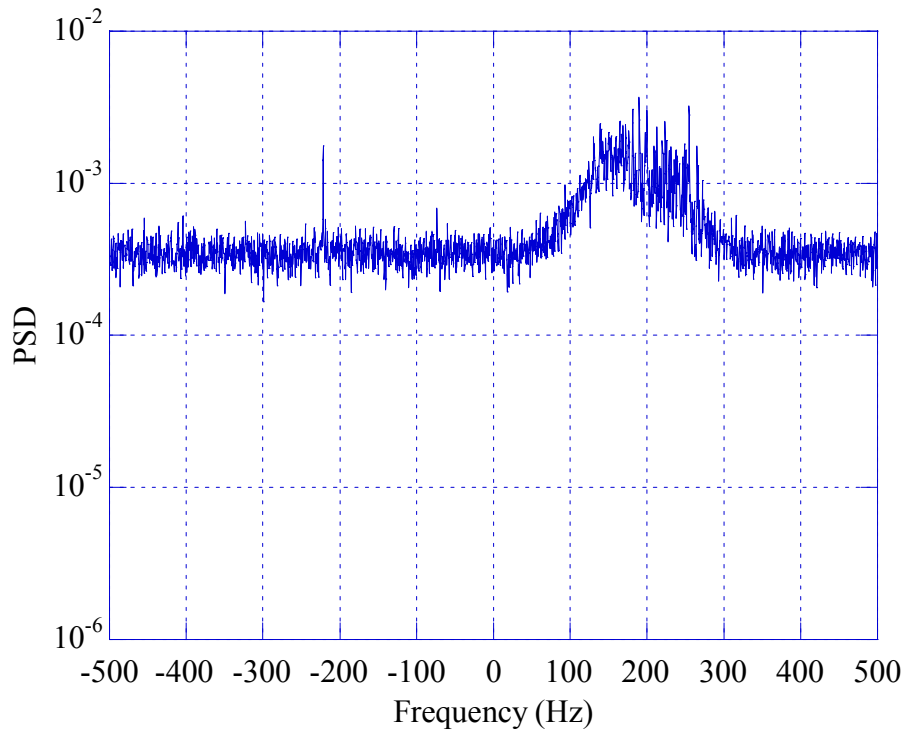


**Figure 3.57** - Average Power Spectral Density, PSD, VH pol., 1<sup>st</sup> cell, 3 m,  $CNR \approx -5$  dB

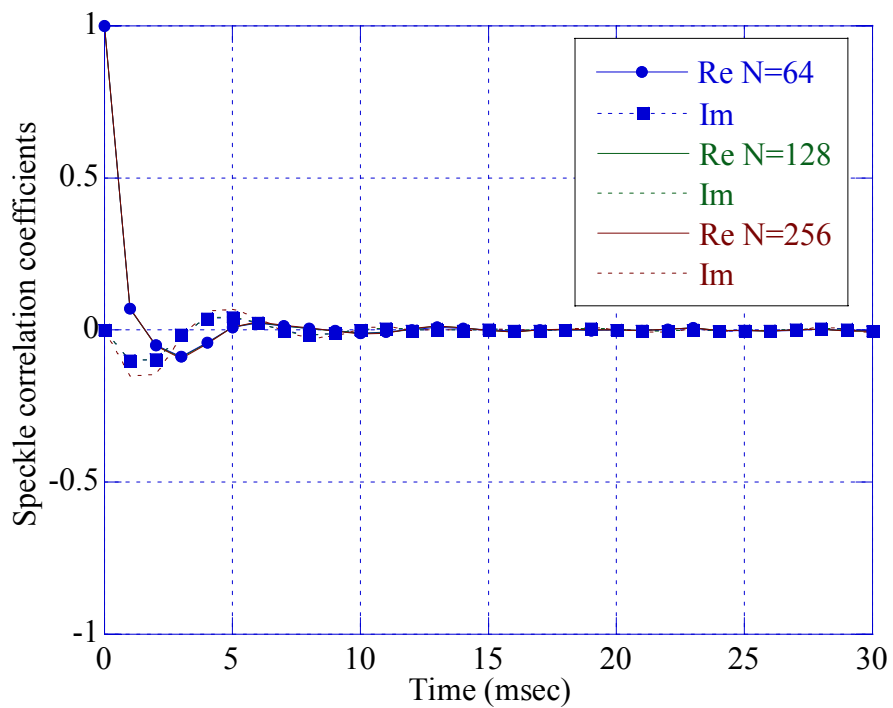


**Figure 3.58** - Speckle correlation coefficients, VH pol., 1<sup>st</sup> cell, 3 m.

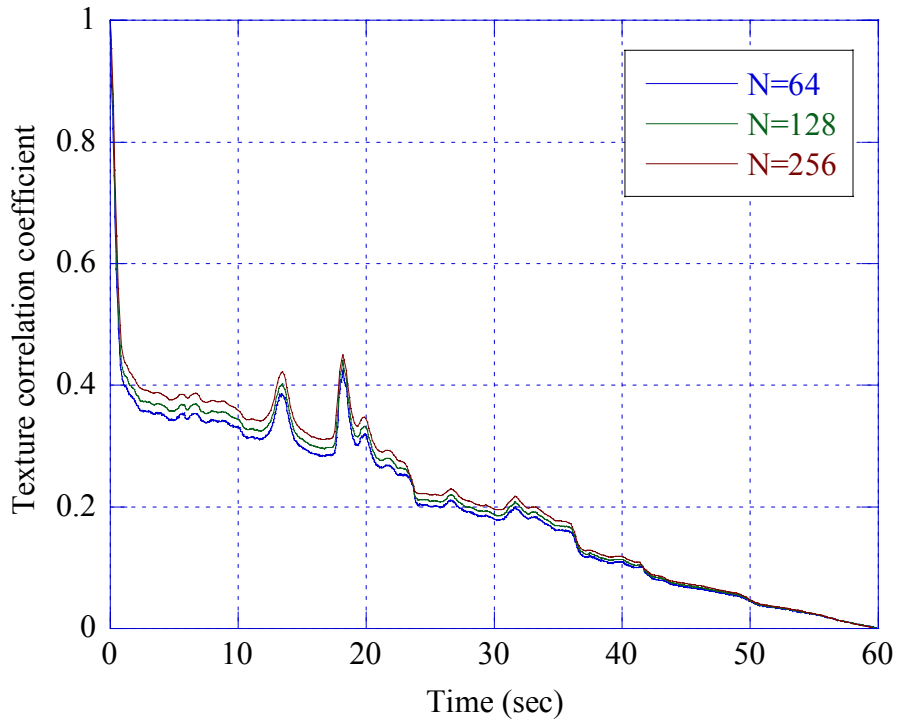


**Figure 3. 59** - Texture correlation coefficient, VH pol., 1<sup>st</sup> cell, 3 m.

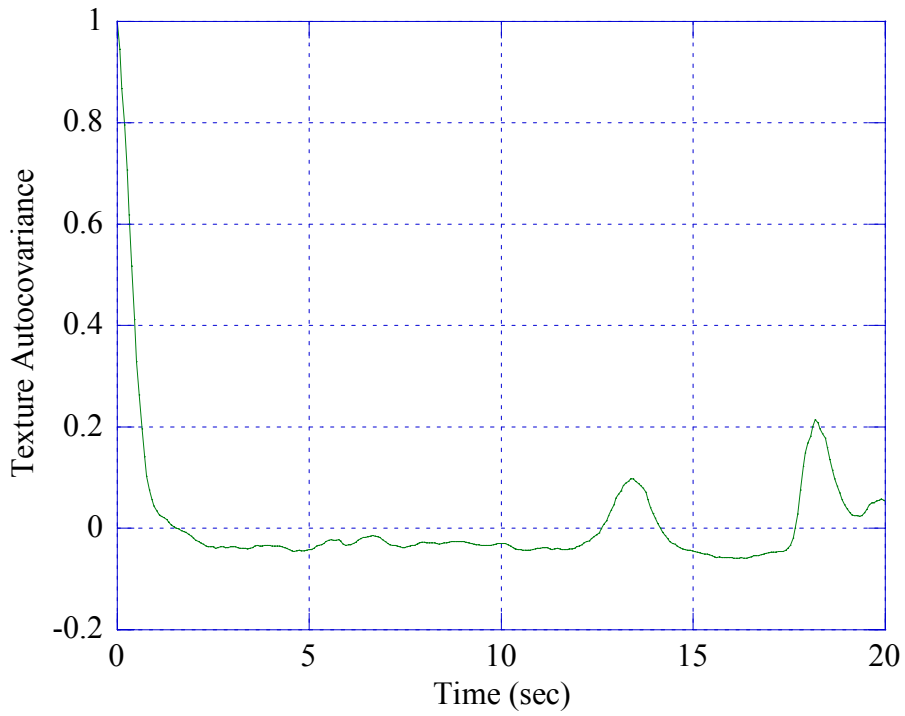


**Figure 3. 60** - Texture auto-covariance function, VH pol., 1<sup>st</sup> cell, 3 m.

### 3.1.3 Mean range texture auto-covariance

To conclude the correlation analysis, in order to highlight further differences due to the resolution, we also calculated the average range autocovariance function of the texture:

$$R_r(n) = \frac{1}{N_b} \sum_{m=1}^{N_b} R_{r_m}(n) = \frac{1}{N_b N_c} \sum_{m=1}^{N_b} \sum_{i=0}^{N_c-n-1} (\tau_m(i) - \bar{\tau}_m)(\tau_m(i+n) - \bar{\tau}_m) \quad ()$$

where  $\tau_m(i)$  is the estimate of the texture on the  $m$ th burst of the  $i$ th cell,  $N_c$  is the number of illuminated cells,  $N_b$  is the number of bursts and  $\bar{\tau}_m = \sum_{i=0}^{N_c-1} \tau_m(i)$ .

Since at 30 m range resolution the illuminated zone is different, we only compared the results found at 15 m, 9 m, e 3 m range resolutions.

Figures 3.61, 3.62, and 3.63 show the results obtained for VV, HH and VH polarizations. From the figures it seems evident that with a resolution of 3 m it is possible to highlight and resolve shorter range periodicities that are not visible in the other resolutions in all the polarizations.

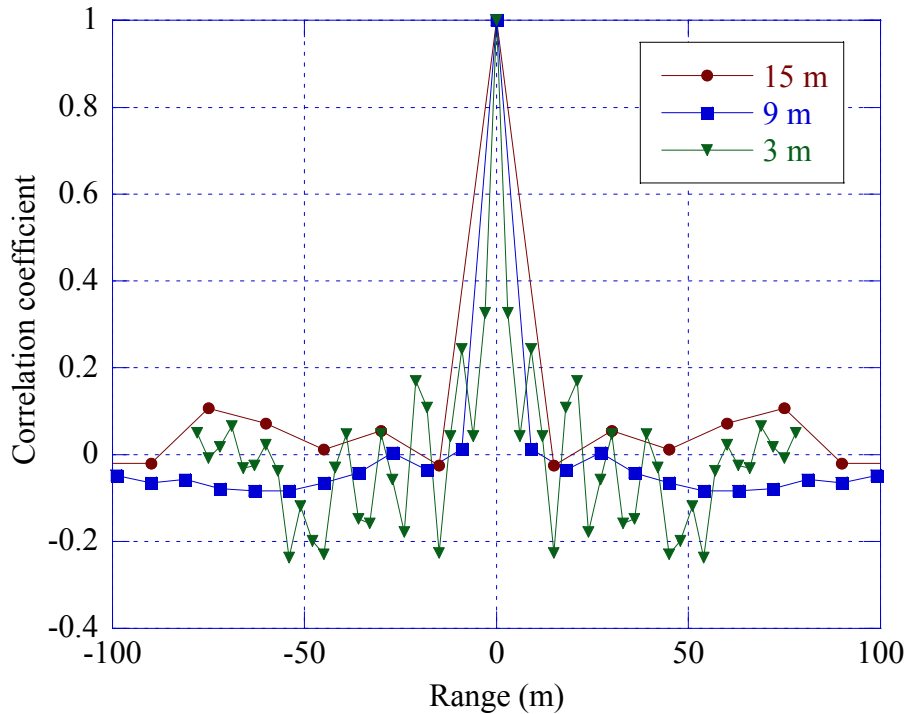


Figure 3. 61 - Mean range texture autocovariance, VV pol.

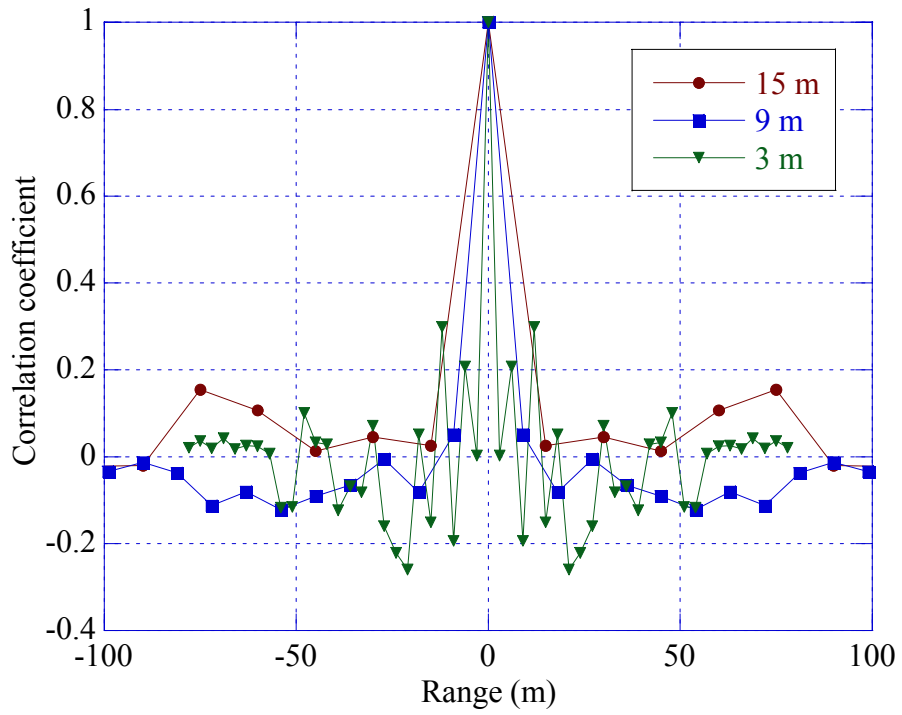


Figure 3.62 - Mean range texture auto-covariance, HH pol.

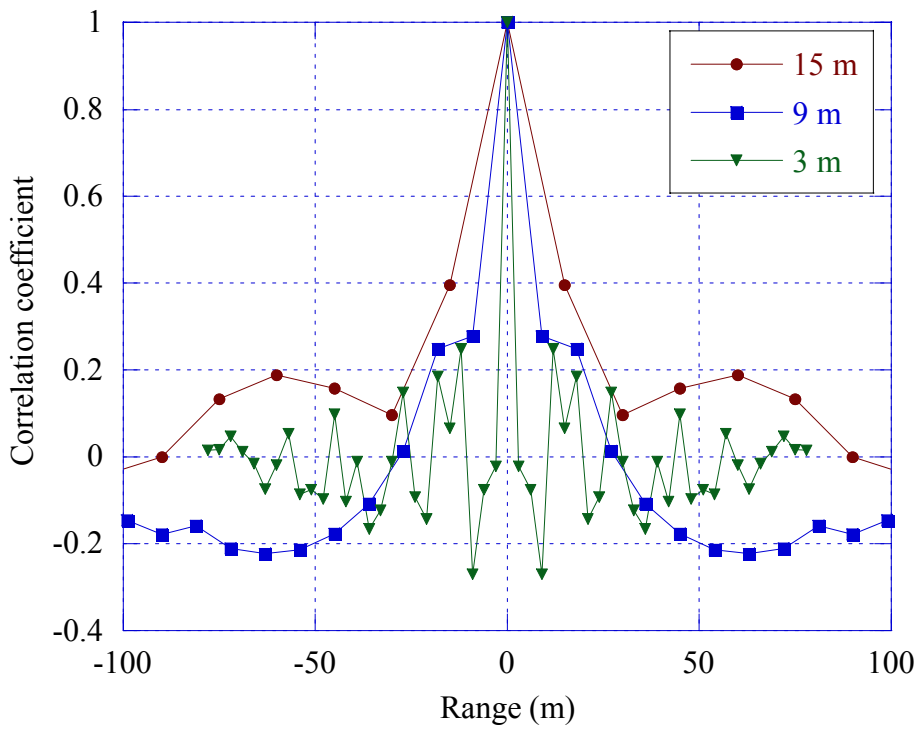


Figura 3.63 - Mean range texture auto-covariance, VH pol.

## 3.2 Conclusions

In this chapter, the goal of our analysis is the study of the clutter correlation, both in time and range, in all polarizations and different range resolutions. Based on our results, we can conclude that in all the analyzed resolutions, in each polarization, the average speckle correlation time is about 10 *msec* and the behavior is oscillatory. Moreover, without differences in the polarizations, the texture correlation time is some seconds long; texture presents periodicities with a period of 8 seconds at a range resolution of 60 m and of 3 seconds at a range resolution of 30 m. The periodicity is particularly evident in the VV polarized data for the resolution of 60 m. With increasing resolution, the texture correlation time get shorter, but still in the order of few seconds and the periodicities tend to disappear, due to the strong contribution of the thermal noise.

The analysis of the periodogram shows, for all the polarizations, for all the range resolutions, a peak located around 150 Hz.

# References

- [Bar96] Barnard T.J., Weiner D.D. “Non-Gaussian Clutter Modeling with Generalized Spherically Invariant Random Vectors,” *IEEE Trans. on Signal Processing*, Vol. 44, No. 10, October 1996.
- [Con87] Conte E., Longo M., “Characterisation of Radar Clutter as a Spherically Invariant Random Process,” *IEE Proceedings-F*, Vol. 134, No. 2, pp. 191 -197, April 1987.
- [Cur03] Currie B., *Private communications*, October 2003.
- [Fay77] Fay F. A., Clarke J., Peters R. S., “Weibull distribution applied to sea-clutter,” in *Proc. IEE Conf. Radar '77*, pp. 101-103, London, U.K., 1977.
- [Far97] Farina A., Gini F., Greco M., Verrazzani L., “High Resolution Sea Clutter Data: A Statistical Analysis of Recorded Live Data,” *IEE Proceedings-F*, Vol. 144, No. 3, pp. 121-130, June 1997.
- [Gin01] Gini F., Greco M., “Texture modeling and validation using recorded high resolution sea clutter data,” *Proc. of the 2001 IEEE Radar Conference*, pp. 387-392, May 2001.
- [Gin02] Gini F., Greco M., “Texture modelling, estimation and validation using measured sea clutter data,” *IEE Proc.-Radar Sonar Navig.*, Vol. 149, No. 3, June 2002.
- [Jak76] Jakeman E., Pusey P. N., “A model for non-Rayleigh sea echo,” *IEEE Trans. on Antennas and Propagation.*, Vol. AP-24, pp. 806-814, November 1976.
- [Ran93] Rangaswamy M., Weiner D.D., Ozturk A., “Non-Gaussian vector identification using spherically invariant random processes,” *IEEE Trans. on Aerospace and Electronic Systems*, vol. 29, No. 1, pp. 111-124, January 1993.
- [Ran95a] Rangaswamy M., Weiner D.D., Ozturk A., “Computer generation of correlated non-Gaussian radar clutter,” *IEEE Trans. on Aerospace and Electronic Systems*, vol. 31, No. 1, pp. 106-115, January 1995.
- [Ran95b] Rangaswamy M., Michels J.H., Weiner D.D., “Multichannel detection algorithm for correlated non-Gaussian random processes based on innovations,” *IEEE Trans. on Signal Processing*, vol. 43, No. 8, pp. 1915-1922, August 1995.

- [Ran97] Rangaswamy M., Michels J.H., "A parametric multichannel detection for correlated non-Gaussian random processes," *Proc. of the National Radar Conference*, pp. 349-354, Syracuse, NY, USA, May 1997.
- [Ran98] Rangaswamy M., Michels, J.H., "Adaptive signal processing in non-Gaussian noise backgrounds," *Proc. of the 9th IEEE-SSAP Workshop*, Portland, OR, September 1998.
- [Sad94] Sadler B., Giannakis G.B., Lii K.S., "Estimation and detection in the presence of non-Gaussian noise," *IEEE Trans. on Signal Processing*, Vol. 42, No. 10, pp. 2729-2741, 1994.
- [War90] Ward K. D., Baker C. J., Watts S., "Maritime surveillance radar. Part I: Radar scattering from ocean surface," *IEE Proceedings-F*, Vol. 137, No. 2, pp. 51-62, April 1990.



**UNIVERSITÀ DI PISA**  
**DIPARTIMENTO DI INGEGNERIA DELL'INFORMAZIONE**  
ELETTRONICA, INFORMATICA, TELECOMUNICAZIONI

**STATISTICAL ANALYSIS OF REAL  
POLARIMETRIC CLUTTER DATA AT DIFFERENT  
RANGE RESOLUTIONS.  
PART II: NON-STATIONARITY ANALYSIS**

*Fulvio Gini, Maria S. Greco*

*and*

*Muralidhar Rangaswamy\**

*\*collaborating engineer from the Air Force Research Laboratory*

Pisa, July 2005

This work has been funded by AFOSR grant FA8655-04-1-3059 on "High resolution clutter analysis and modelling for advanced target detection strategies".

Effort sponsored by the Air Force Office of Scientific Research, Air Force Material Command, USAF, under grant number FA8655-04-1-3059. The U.S. Government is authorized to reproduce and distribute reprints for Government purpose notwithstanding any copyright notation thereon.

Disclaimer: The views and conclusions contained herein are those of the author and should not be interpreted as necessarily representing the official policies or endorsements, either expressed or implied, of the Air Force Office of Scientific Research or the U.S. Government.

The authors certify that there were no subject inventions to declare during the performance of this grant.

## Abstract

The work developed and described in this technical report deals with the problem of providing a statistical model of the backscattering from sea surface for low-grazing angle and high resolution radar systems. Based on the electromagnetic two-scale model, we analyzed both the amplitude and frequency modulations induced on the small-scale Bragg resonant waves by the large-scale surface tilt and advection, due to the swell presence. Evidence of sea clutter non-stationarity and the relationship between the variations of clutter spectral features, like texture, Doppler centroid and bandwidth, have been investigated by processing real recorded data. The data used for the research activity have been recorded by the IPIX radar of McMaster University in Grimsby, Ontario, Canada.

In the first part of this technical report, we described our statistical analyses of high-resolution polarimetric data characterized by different range resolutions (60 m, 30 m, 15 m, 9 m, 3 m), in order to highlight possible statistical differences due to changes of both resolution and polarization.

In this second part we describe the analysis of clutter non-stationarity performed by processing the same data. The relation between texture changes, spectrum bandwidth and Doppler centroid has been highlighted with the aim of proving that a hybrid AM/FM modulated process is more suitable than a stationary process to model the sea/lake high resolution clutter.

**Keywords:** Radar clutter, non-Gaussian clutter, phenomenological modeling, statistical analysis, model parameter estimation, high-resolution radar, compound model.

This work has been funded by AFOSR grant FA8655-04-1-3059 on “High resolution clutter analysis and modeling for advanced target detection strategies.”

# CONTENTS

**ABSTRACT..... 1**

**SECTION 1 FREQUENCY ANALYSIS..... 3**

1.1 INTRODUCTION ..... 3

**1.2 NON-STATIONARITY ANALYSIS..... 6**

*1.2.1 Range resolution of 60 m..... 9*

*1.2.2 - Range resolution of 30 m ..... 23*

*1.2.3 - Range resolution of 15 m ..... 37*

*1.2.4 Range resolution of 9 m..... 51*

*1.2.6 Range resolution of 3 m..... 65*

**1.3 CONCLUSIONS..... 72**

**REFERENCES ..... 74**

# SECTION 1

## FREQUENCY ANALYSIS

### 1.1 Introduction

In the first part of this technical report, we modeled the received clutter signal as a compound process. According to this model, the received clutter signal is the product of two components (speckle and texture) that, as in many other works, are considered independent and stationary processes [Far97] [Gin95] [Gin99] [Gin02] [Gin01] [Ran93] [Ran95] [Ran97] [Ran97] [Ran98] [San99] [War90]. Focusing on the reflection phenomena that originate the received signal, we realize actually that the received clutter characteristics depend on the sea surface conditions in a certain temporal range, thus the clutter process cannot be stationary if the observation time is long.

The behavior of sea clutter signals is mainly determined by the nature of the surface roughness [Hay02], [Val78]. This is normally characterized in terms of two fundamental types of waves. The first type is represented by capillary waves with wavelengths ( $\lambda$ ) on the order of centimeters or less. The second by the longer gravity waves (sea or swell), with wavelengths ranging from a few hundred meters to less than a meter [Hay02]. In deep water, for the capillary waves we have  $\lambda < 1.73 \text{ cm}$ , whereas for the gravity waves the wavelength is  $\lambda > 1.73 \text{ cm}$ . Capillary waves are usually generated by turbulent gusts of wind near surface and their resorting force is the surface tension. On the contrary, swells are produced by stable winds and their resorting force is the force of gravity. In fact, when the wind starts to blow over a calm sea, the first waves to form are the shortest ones. As these waves build up, nonlinear interactions transfer energy to waves with larger amplitudes and longer wavelengths. This process continues until an equilibrium point is reached, at which dissipation balances the tendency for wave growth. At this point, a fully developed sea exists. Since the primary transfer of energy to the sea is at very short wavelengths, a sudden cessation of wind causes the short waves to decay rapidly, while the longer waves can last several days and propagate to great distances. Consequently, at any point on the surface the waves are complex summations of the locally generated wind

waves and waves that have propagated in from other areas and different directions, resulting in a complex interaction [Pla90].

To take into account the presence of different scales of roughness in the sea surface, Wright [Wri68] and Bass *et al.* [Bas68] developed a two-scale model of the sea surface scattering in which the surface height is partitioned into a large-scale displacement and a small-scale displacement. For this model, it is assumed that over any patch of the surface that is large compared with small-scale lengths, but small compared with large-scale lengths, the scattering can be modeled as first-order Bragg scattering from the small-scale structure. Thus, the effect of the large-scale structure is to change the distance between the antenna and each point of the considered patch, by tilting the surface and advecting the small-scale structure both vertically and horizontally. The effect of large-scale surface tilt is to introduce an effective amplitude modulation of the small-scale scattering [Pla83]. Conversely, the effect of the advection is to influence the frequency content of the overall scattering.

It is worth observing that the small-scale structure scattering of the two-scale model is what in statistical sea clutter literature is termed *speckle* ([Bar96], [Con87], [Far97], [Noh91]). The variations of the local power, due to the amplitude modulation of the speckle introduced by the tilting of the small-scale structure are modeled as the *texture* process.

The Bragg scattering is based on the principle that the return signals from scatterers that are half a radar wavelength apart, measured along the line of sight from the radar, reinforce each other since they are in phase [Hay02]. The Bragg resonant length is

$$\lambda_B = \frac{\lambda_0}{2 \cos \theta_0}, \quad (1.1)$$

where  $\lambda_0$  is the wavelength of the radar signal and  $\theta_0$  is the grazing angle. The Doppler frequency shift corresponding to this wavelength is

$$f_D = \frac{C_0}{\lambda_B} = \sqrt{\frac{g}{2\pi \lambda_B} + \frac{2\pi \gamma}{\lambda_B^3}}, \quad (1.2)$$

where  $C_0$  is the intrinsic phase speed of the Bragg wave given by the wave dispersion relation,  $g$  is the acceleration of free fall, and  $\gamma$  is the surface tension divided by the bulk

density. At microwave frequencies, the Bragg scattering is from capillary waves and the previous expression simplifies as follows:

$$f_D \cong \sqrt{\frac{g}{2\pi \lambda_B}}. \quad (1.3)$$

As a consequence, the capillary waves approaching and receding in the radar line-of-sight direction, which satisfy the condition in (1.1), give rise to two Bragg spectral lines located at  $\pm f_D$ , at least in absence of other scattering phenomena and of the long waves. The magnitude of these lines depends on the azimuth look direction of the radar relative to the wind direction. With the radar pointed in the up-wind direction, the magnitude of the approaching Bragg line is larger than that for the receding line and vice versa for down-wind look direction [Pla90]. For the crosswind direction, the magnitudes of the approaching and receding peaks are equal [Tri85].

In a real scenario, the Bragg scatterers are advected by the orbital velocity of the intermediate waves (waves with wavelengths longer than the Bragg wavelength but shorter than the radar resolution cell) and of the long waves (waves with wavelengths longer than the radar resolution cell). The sum of the orbital velocities of the unresolved intermediate scale waves causes a spectral broadening around the Bragg lines. For many ocean conditions, these orbital motions broaden the Bragg lines by more than their separation, causing the lines to be unresolved, and generating only one Doppler peak. At X-band frequencies, this is generally the case [Pla90], [Rin97].

In this technical report, we mainly investigate the non-stationarity effect due to long waves on the sea clutter returns. According to the Bragg theory, long waves that are resolved by high-resolution radars may be assumed to be constant over each illuminated cell. Consequently, their effect on the Doppler spectrum is to shift the Doppler peak according to the long wave orbital velocity. The orbital velocities are given by the simple harmonic motion  $V_0 = \pi fH = \pi H/T$ , where  $f$  is the frequency of the long gravity wave of period  $T$  and  $H$  is its height from crest to trough. The contribution of the orbital velocity to the motion of the Bragg scatterers is the horizontal component, that is  $V_{OR} = V_0 \cos(2\pi ft - Kx)$ , where  $K$  is the wave number and  $x$  the spatial position [Roz96]. It is worth noting that the velocities of the scatterers in the nodes, crests and troughs of the waves are very different. Finally, an additional Doppler shift results from any surface

currents present, including wind drift. A formula often used to represent this drift is  $D_w=0.03U_w$ , where  $U_w$  is the wind speed. Therefore, by considering the contribution of orbital velocity, current velocity  $V_c$  and wind drift, we can calculate the time-varying instantaneous Doppler shift as

$$f_D = \frac{2 \cos \theta_0}{\lambda_0} (\pm C_0 + V_{OR} + D_w + V_c). \quad (1.4)$$

Due to the periodicity of  $V_{OR}$ ,  $f_D$  as well should be periodic.

Actually, the Bragg scattering is not the only one determining the clutter return, particularly if breaking waves are present on the sea surface [Jes91]. In two recent papers Walker [Wal00], [Wal01] studied the development of the Doppler spectra for horizontal (HH) and vertical (VV) polarizations as breaking waves passed the radar illuminated area. Three types of scattering have been observed: (i) Bragg scattering, present in both HH and VV data, but stronger in VV data. (ii) Whitecaps scattering; the amplitude of both like-polarizations are roughly equal and are noticeably stronger than the background scatter, particularly in HH, in which the Bragg scattering is often weak. (iii) Spikes; absent in VV data and strong only in up-wind HH data. Therefore, to see clearly the effect of the long waves on the sea return, we should analyze dataset relating to sea surfaces where the Bragg scattering is dominant [Gre04]. As already pointed out in the previous report [Gin05], unfortunately, we have no data available regarding the wind and wave conditions for the Grimsby recording campaign. We know only the direction of the wind and the pointing direction of the radar. We have no information about the time duration of wind blowing, the speed and the fetch of the wind, then we have not enough clues to evaluate the developing of the sea surface and the dominance of the Bragg scattering. Then, in this second part of the technical report, we investigate on the non-stationarities of the clutter process and on their effect on the time-varying clutter spectrum as a function of different range resolutions, whatever the dominant scattering type. It is obvious that the clutter characteristics highlighted in the first part of the technical report have to be intended as averaged in time.

## 1.2 Non-stationarity analysis

To analyze the long-term non-stationarity of the clutter process, we supposed that the clutter is stationary on short periods of time, during which the texture can be considered constant, as well as the spectral characteristics of the overall clutter process. We tried with different burst lengths  $N$ , and we obtained very good and clear results for  $N=128$  samples, that is, for a stationarity time duration of 128 msec. Once that length was chosen, first of all, we calculated the spectrogram [The92] for each range cell, resolution and polarization, using the FFT algorithm on 512 points and using a Hanning window of  $N=128$  samples. Practically, the spectrogram is the sequence of periodograms calculated on short bursts of data with or without overlap. We used an overlap of 50% and then we normalized the spectrum of each data burst of  $N$  samples with respect to the local power (the local estimated texture), to highlight the time-varying spectral characteristics. The texture has been estimated by each  $l$ th burst of  $N$  complex data  $y[n]$  as:

$$\hat{\tau}[l] = \frac{1}{N} \sum_{n=1}^N |y[n]|^2 \quad (1.5)$$

Without normalization, all the spectrograms would show only the spectra relating to the most powerful bursts as red or light blue stripes on a dark blue background. With the normalization, the spectrum of each burst has the same weight in the image, then, the shape changes are well evident, as in Fig. 1.1.

In order to measure the temporal variation of the clutter Doppler spectra, we used the **Doppler centroid** defined as

$$f_c = \frac{\int_{-\infty}^{+\infty} f S(f) df}{\int_{-\infty}^{+\infty} S(f) df}, \quad (1.6)$$

and the Doppler bandwidth, defined as

$$B_w = \sqrt{\frac{\int_{-\infty}^{+\infty} (f - f_c)^2 S(f) df}{\int_{-\infty}^{+\infty} S(f) df}}, \quad (1.7)$$

where  $f$  is the frequency and  $S(f)$  is the clutter power spectral density (PSD). We decided to analyze the behavior of the centroid and not of the maximum because it is generally more representative of the short-time spectrum movement, especially in case of non-symmetric spectral shape. To estimate the centroid and the bandwidth for each short time interval under investigation, we calculated

$$\hat{f}_c[l] = \frac{1}{Q} \sum_{n=-N_f/2}^{N_f/2-1} f[n] P_l[n] , \quad \text{per } l=1,2,3,\dots,N_B \quad (1.8)$$

and

$$\hat{B}_w[l] = \sqrt{\frac{1}{Q} \sum_{n=-N_f/2}^{N_f/2-1} [f[n] - \hat{f}_c[l]]^2 P_l[n]} , \quad \text{for } l=1, 2, 3, \dots, N_B \quad (1.9)$$

where  $f[n] = 1000n/N_f$  is the digital frequency<sup>1</sup>,  $P_l[n]$  is the periodogram of the  $l$ th data burst composed by  $N_f = 512$  samples at the frequency  $f[n]$ , and  $Q = \sum_{n=-N_f/2}^{N_f/2-1} P_l[n]$ .

Physically, the phenomenon underlying both texture and spectral changes is the same: the presence of long waves, that amplitude and frequency modulate the clutter scattering. Then, texture, bandwidth and Doppler centroid should be correlated. In order to quantify the mutual relationship between texture, centroid, and bandwidth, we calculated the **cross-covariance functions** between texture and centroid

$$C_{\tau c}[m] = \frac{\sum_{l=1}^{N_B-|m|} (\hat{\tau}[l] - \hat{\tau}_c)(\hat{f}_c[l+m] - \hat{f}_c)}{\sqrt{\sum_{l=1}^{N_b} (\hat{\tau}[l] - \hat{\tau}_c)^2 \sum_{l=1}^{N_b} (\hat{f}_c[l] - \hat{f}_c)^2}} , \quad \text{per } m = -(N_B - 1), \dots, N_B - 1 \quad (1.10)$$

and the cross-covariance functions between texture and bandwidth:

---

<sup>1</sup> The Pulse Repetition Frequency (PRF) is 1 KHz.

$$C_{\tau B}[m] = \frac{\sum_{l=1}^{N_B-|m|} (\hat{\tau}[l] - \hat{\eta}_\tau)(\hat{B}_w[l+m] - \hat{\eta}_w)}{\sqrt{\sum_{l=1}^{N_b} (\hat{\tau}[l] - \hat{\eta}_\tau)^2 \sum_{l=1}^{N_b} (\hat{B}_w[l] - \hat{\eta}_w)^2}}, \text{ per } m = -(N_B - 1), \dots, N_B - 1 \quad (1.11)$$

where  $\hat{\tau}[l]$ ,  $\hat{f}_c[l]$ , and  $\hat{B}_w[l]$  are the estimates of the texture, Doppler centroid, and bandwidth, and

$$\hat{\eta}_\tau = \frac{1}{N_B} \sum_{l=1}^{N_b} \hat{\tau}[l] \quad (1.12)$$

$$\hat{\eta}_c = \frac{1}{N_B} \sum_{l=1}^{N_b} \hat{f}_c[l] \quad (1.13)$$

$$\hat{\eta}_w = \frac{1}{N_B} \sum_{l=1}^{N_b} \hat{B}_w[l] \quad (1.14)$$

their respective estimated mean values.

Due to large dynamic behavior of texture (3-4 orders of magnitude), we also performed some analysis on the signal  $\hat{y} = \text{Log}(\hat{\tau})$ , the logarithm of the texture. In some cases, we observed that  $\hat{y}$  has a behavior “more sinusoidal” than the estimated texture  $\hat{\tau}$ , this fact suggests that  $\hat{y}$ , more than  $\hat{\tau}$ , could be related to the periodic change of patch tilt due to the long waves. In the next subsections, together with the cross-covariances between texture, centroid and bandwidth, we will show similar results on cross-covariances between Log-texture, centroid and bandwidth (Log-covariances).

### 1.2.1 Range resolution of 60 m

In this paragraph and in the next ones, the figures show the spectrogram of the clutter amplitude, the time evolution of texture, Doppler centroid, and bandwidth, and the cross-covariance functions in some cells, for each polarization and each resolution. For each reported cell, we estimated the average clutter-to-noise power ratio (CNR) as described in the previous technical report [Gin05].

Based on the shape of cross-covariances between texture and centroid, and between texture and bandwidth we classified all the cells into three different groups. The first group is called “**periodical symmetrical**”. As suggested by the name, the cells belonging to this group exhibit periodical cross-covariance functions (texture-centroid and texture-bandwidth). Moreover, both functions present the same periodicities and are symmetrical with respect to the time (abscissa) axis.

An example of this group is the 15<sup>th</sup> range cell as shown in figures 1.3, 1.4, 1.11, 1.12, 1.19 and 1.20 for VV, HH and VH polarized data respectively. The observed period is about 7 seconds long. In all this kind of cells, the cross-covariance function between texture and centroid presents a maximum value in the origin that, on the average, is greater than 0.5 in every polarization, while, the cross-covariance function between texture and bandwidth presents a minimum value in the same point (on the average less than -0.5 in all polarizations). This means that as clutter power increases, Doppler centroid increases and bandwidth decreases. This behavior is confirmed by figures 1.2, 1.10 and 1.18, reporting the time history of texture (on an arbitrary unit scale), centroid and bandwidth in an Hz scale.

The differences between HH, VV and VH data in the 15<sup>th</sup> cell are almost negligible. We observe only clearer periodic trend of the correlation between texture and bandwidth in VV and VH data than in HH data.

The second group has been named “**aperiodical symmetrical**”. For these cells, both the cross-covariance functions do not show regular periodicities, even though they keep the property of being symmetrical. Most cells analyzed at 60 m range resolution belong to this group.

In the third group called “**periodical asymmetrical**” the cross-covariance functions are not symmetrical but show periodicities. The 1<sup>st</sup> cell (Figs.1.7, 1.8, 1.15, 1.16, 1.22, and 1.23) is an example of periodical asymmetrical cell; these periodicities are more evident between texture and centroid. In the 1<sup>st</sup> cell the differences between VV, VH and HH data are more evident. Comparing Fig. 1.7 with Fig 1.15, we observe that for VV data, when the covariance function between texture and centroid is positive generally the covariance between texture and bandwidth is negative, even if no-symmetrically. For the HH data, both covariance functions exhibit same behavior.

Concerning the covariance functions and the Log-covariances there are not meaningful differences. The classification of the cells is reported in Table 1.1.

	<b>Periodical Symmetrical</b>	<b>Periodical Asymmetrical</b>	<b>Aperiodical Symmetrical</b>
Pol. VV	28, 21, 18, 15	1	All the others
Pol. HH	28, 21	1	All the others
Pol. VH	28, 27, 26, 21, 18, 15	1	All the others

**Table 1.1** – Covariance classification, 60 m.

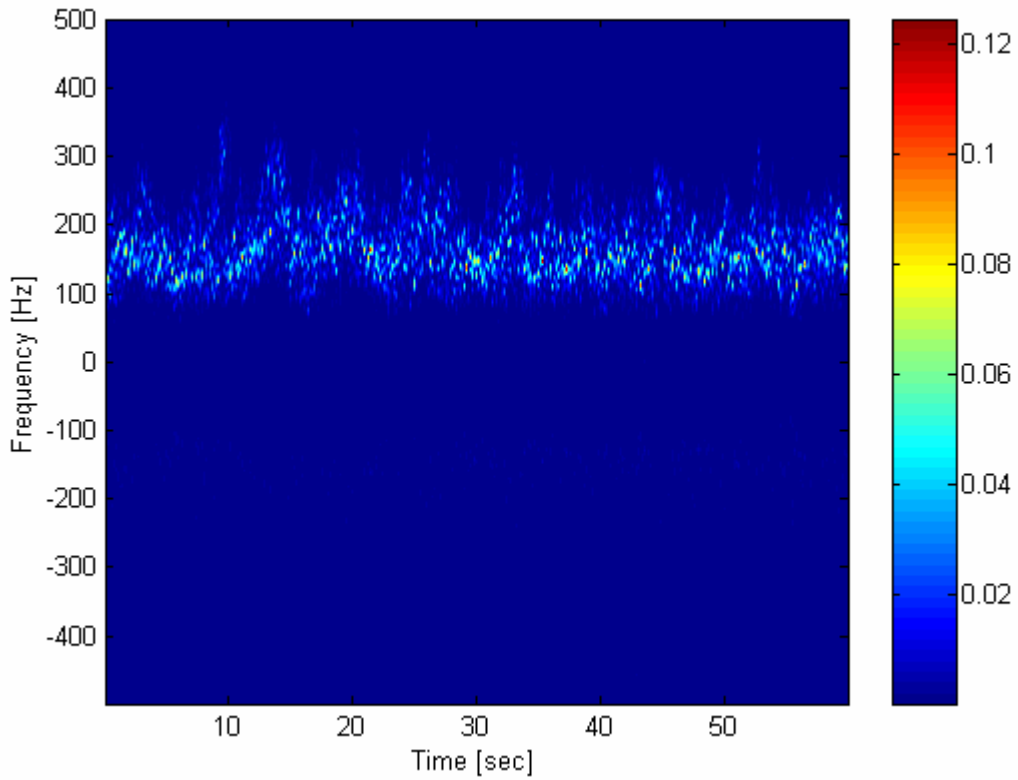


**Figure 1.1** - Normalized spectrogram, 15<sup>th</sup> range cell, VV pol. (CNR=16 dB)

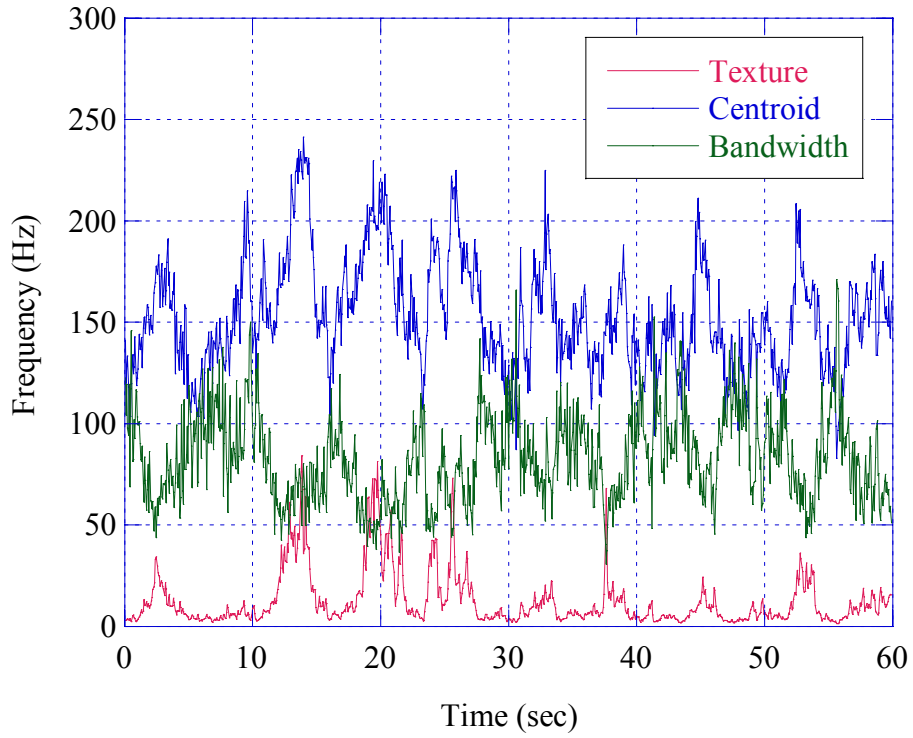


**Figure 1.2** - Time evolution of texture, centroid and bandwidth, 15<sup>th</sup> range cell, VV pol.

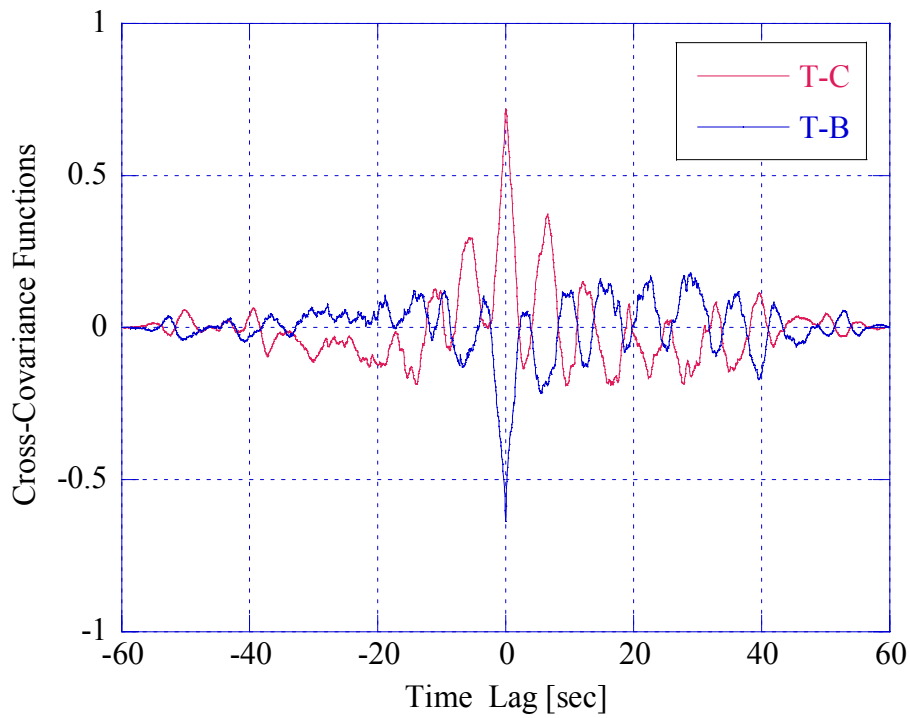


**Figure 1.3** - Texture-centroid and texture-bandwidth cross-covariance, 15<sup>th</sup> range cell, VV pol., per. sym.

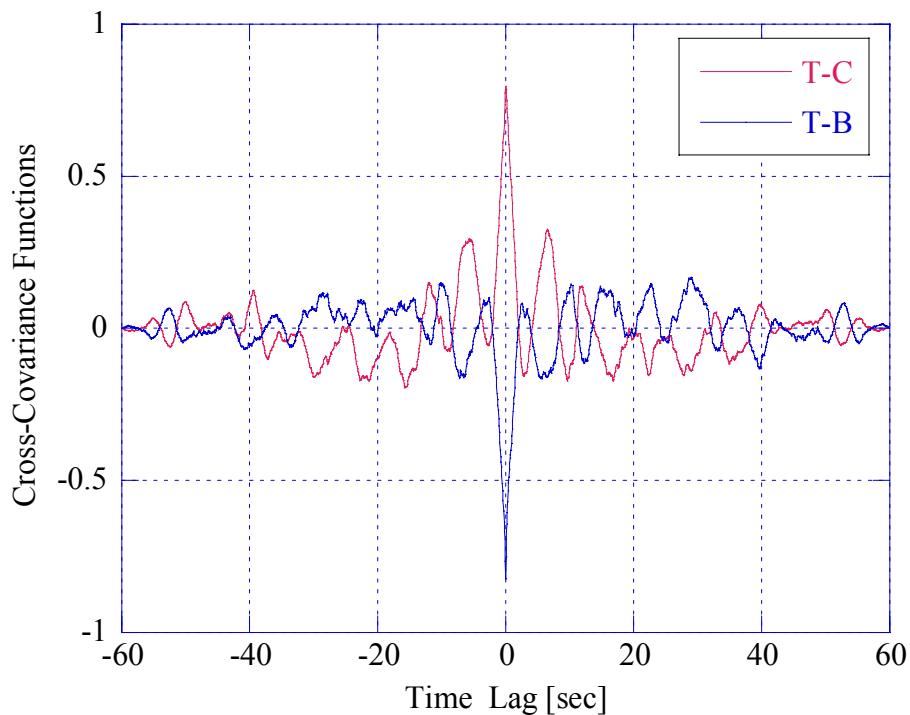


**Figure 1.4** - Log-texture-centroid and Log-texture-bandwidth cross-covariance, 15<sup>th</sup> range cell, VV pol.

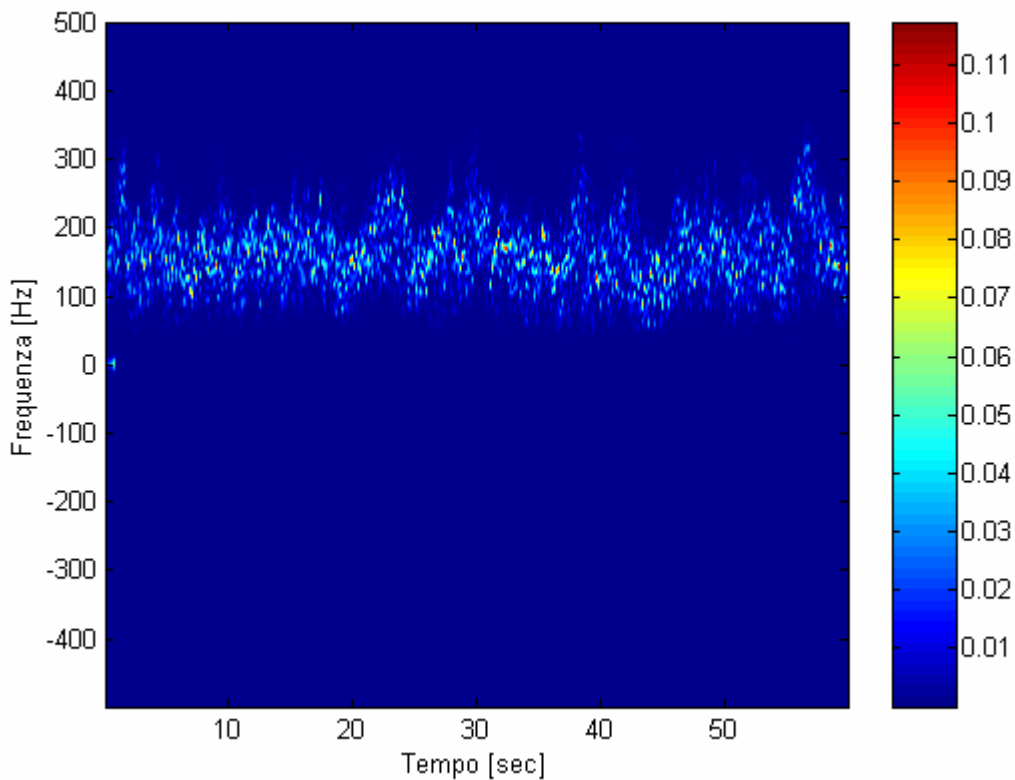


**Figure 1.5** - Normalized spectrum versus time, 1<sup>st</sup> range cell, VV pol. (CNR=23 dB).

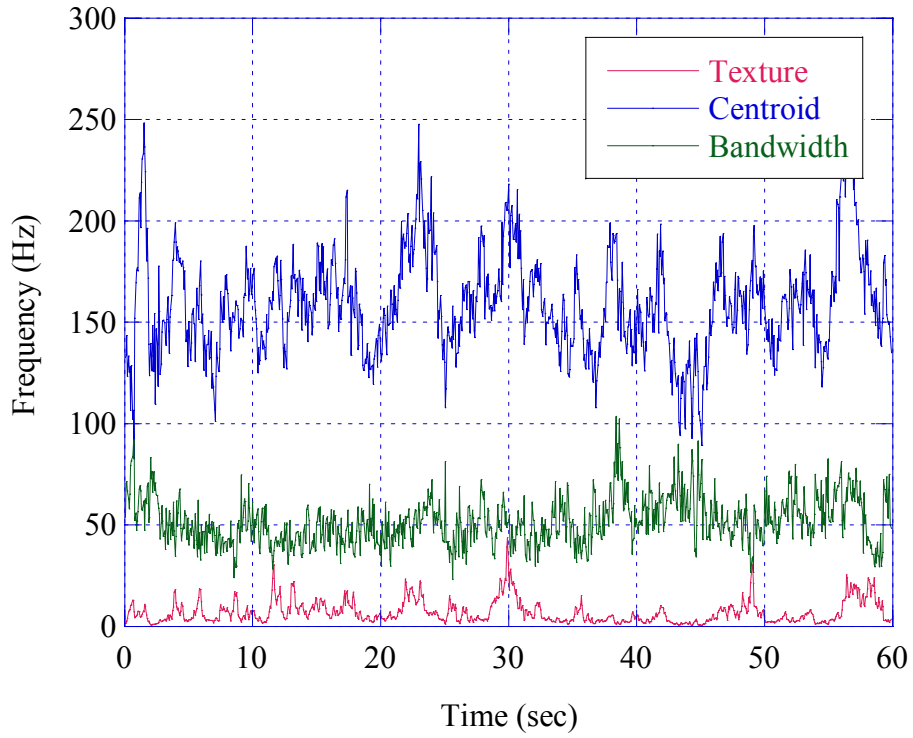


**Figure 1.6** - Time evolution of texture, centroid and bandwidth, 1<sup>st</sup> range cell, VV pol.

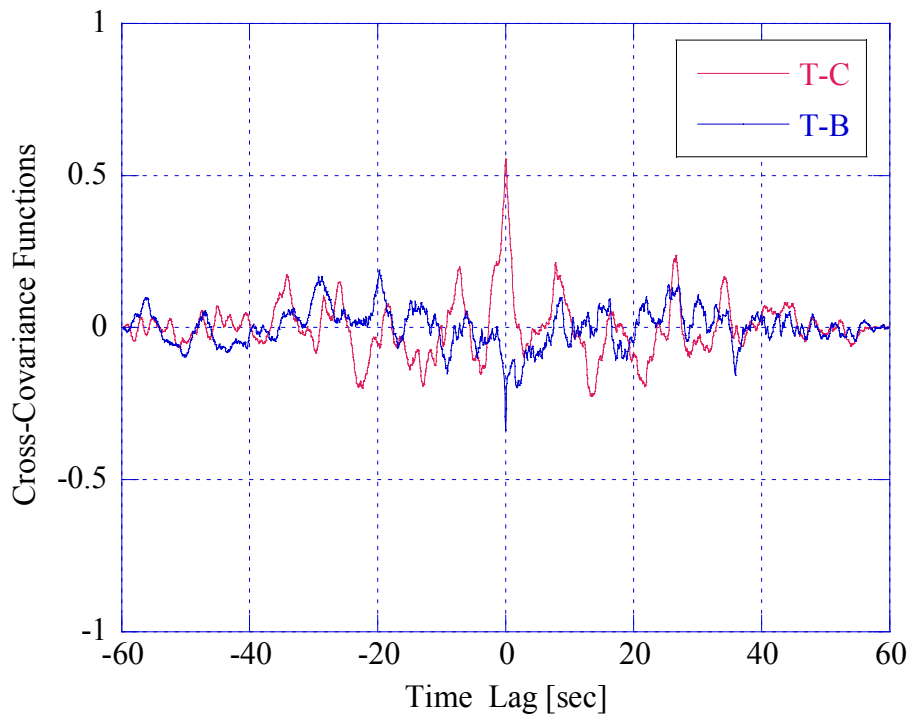


**Figure 1.7** - Texture-centroid and texture-bandwidth cross-covariance, 1<sup>st</sup> range cell, VV pol., per. asym.

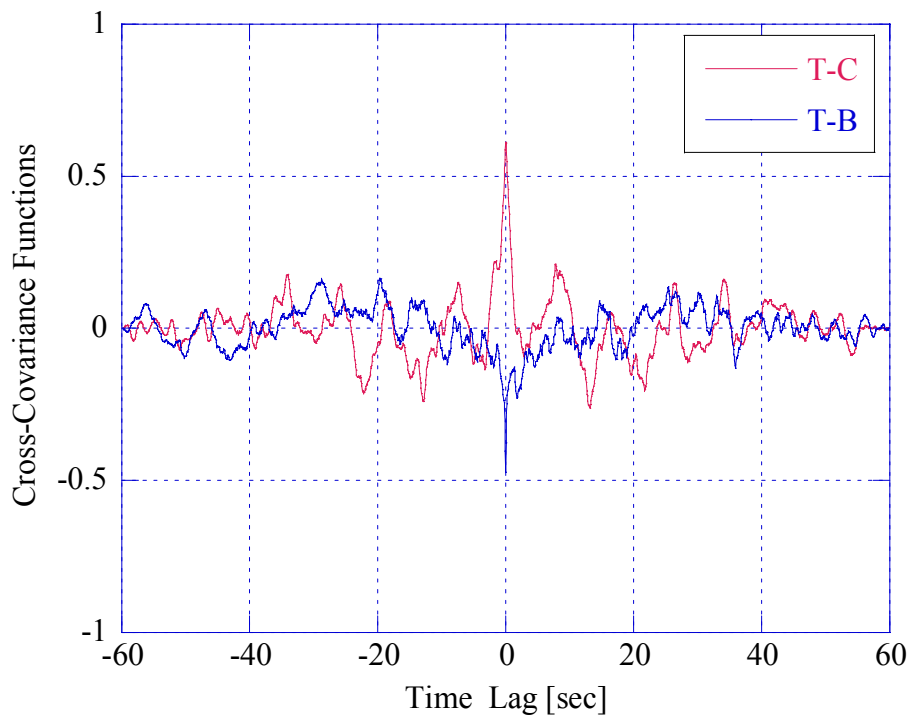


**Figure 1.8** - Log-texture-centroid and Log-texture-bandwidth cross-covariance, 1<sup>st</sup> range cell, VV pol..

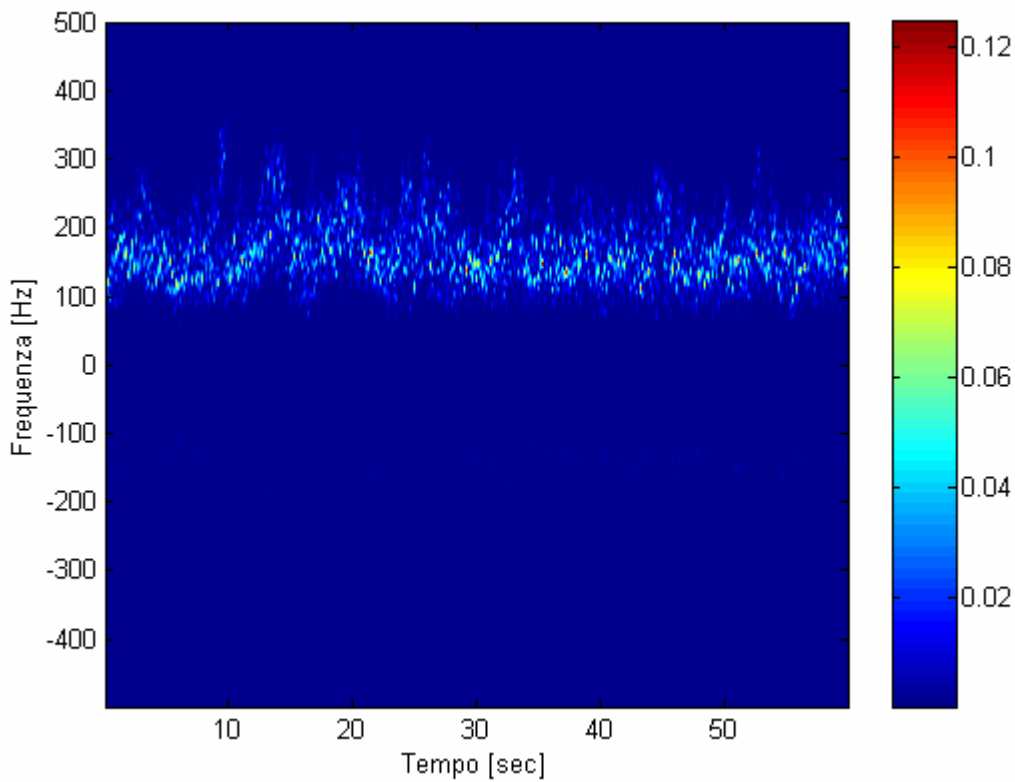


**Figure 1.9** - Normalized spectrum versus time, 15<sup>th</sup> range cell, HH pol. (CNR=16 dB)

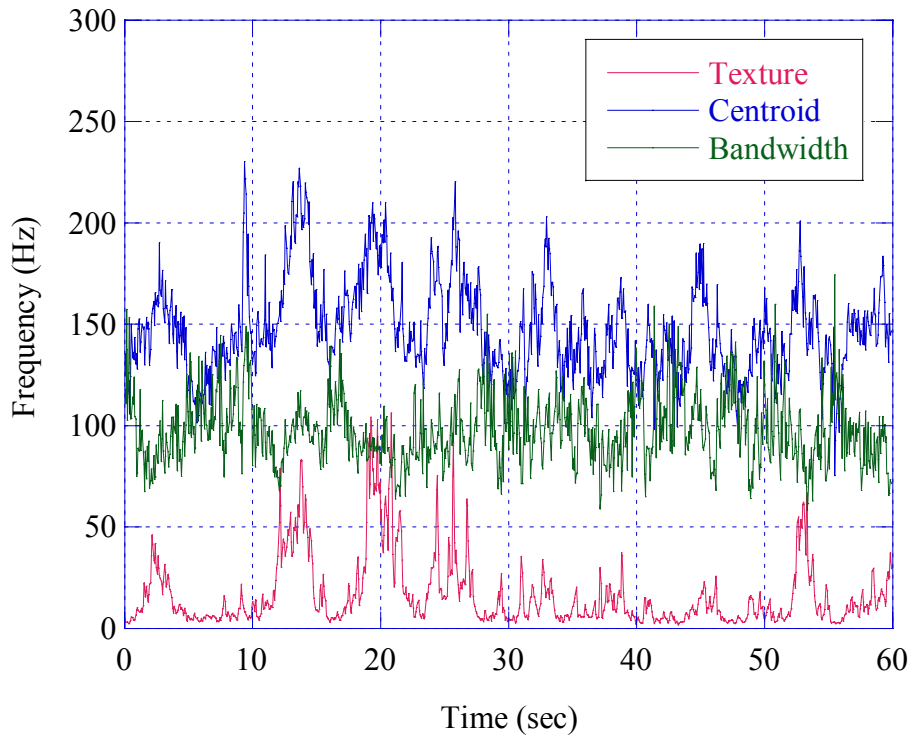


**Figure 1.10** - Time evolution of texture, centroid and bandwidth, 15<sup>th</sup> range cell, HH pol.

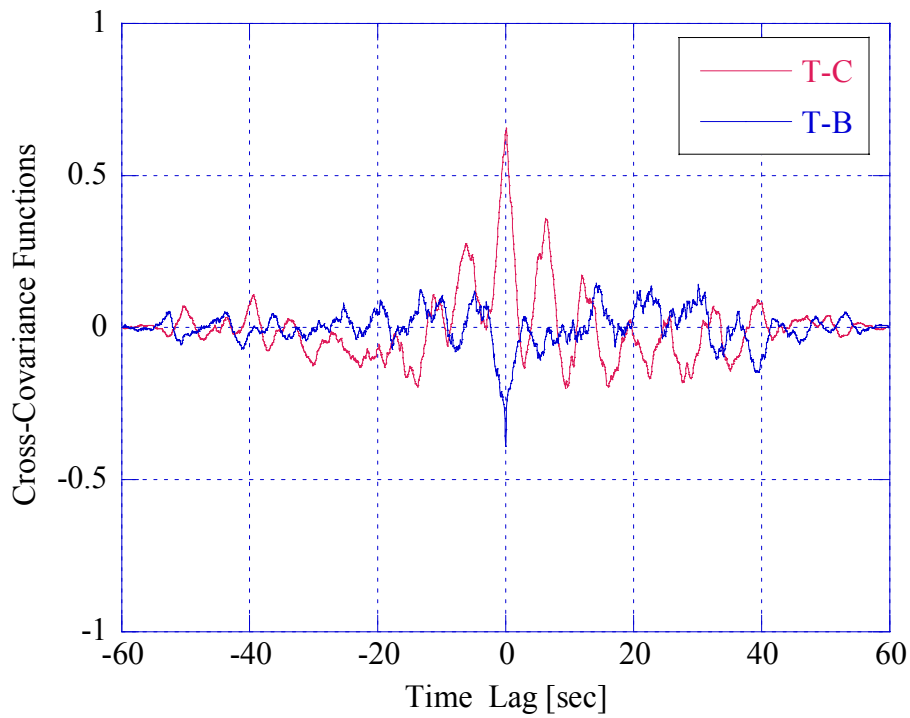


**Figure 1.11** - Texture-centroid and texture-bandwidth cross-covariance, 15<sup>th</sup> range cell, HH pol., per. sym.

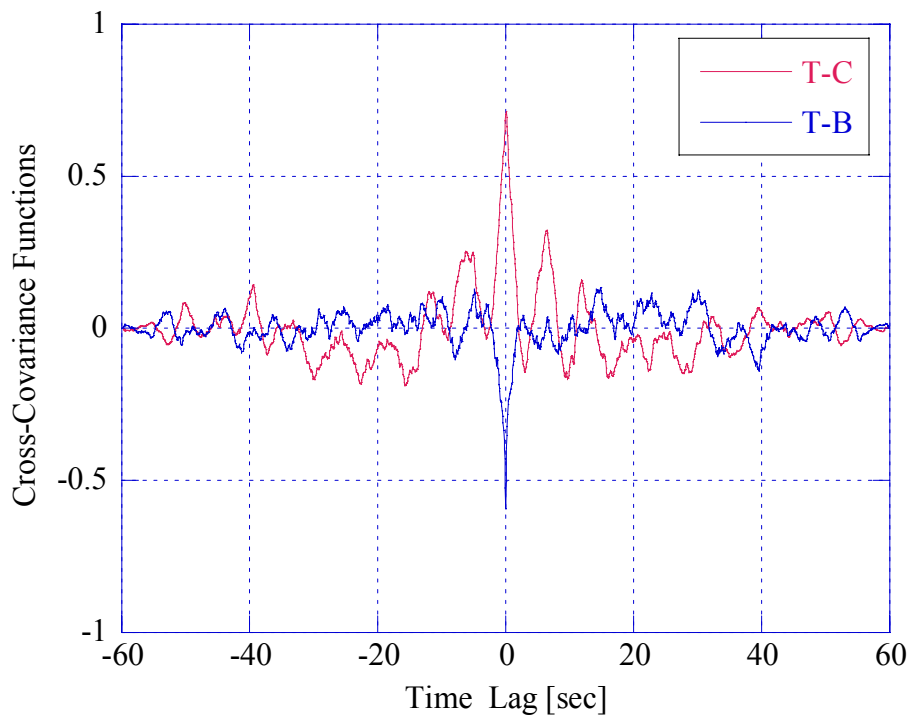


**Figure 1.12** - Log-texture-centroid and Log-texture-bandwidth cross-covariance, 15<sup>th</sup> range cell, HH pol.

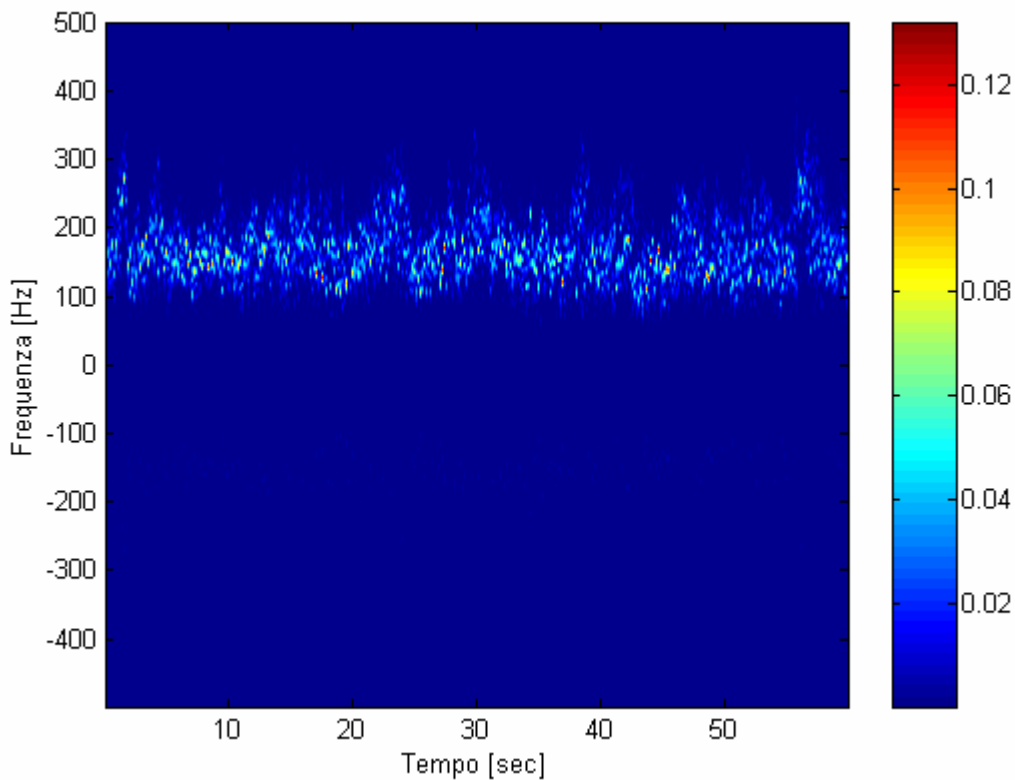


**Figure 1.13** - Normalized spectrum versus time, 1<sup>st</sup> range cell, HH pol. (CNR=22 dB)

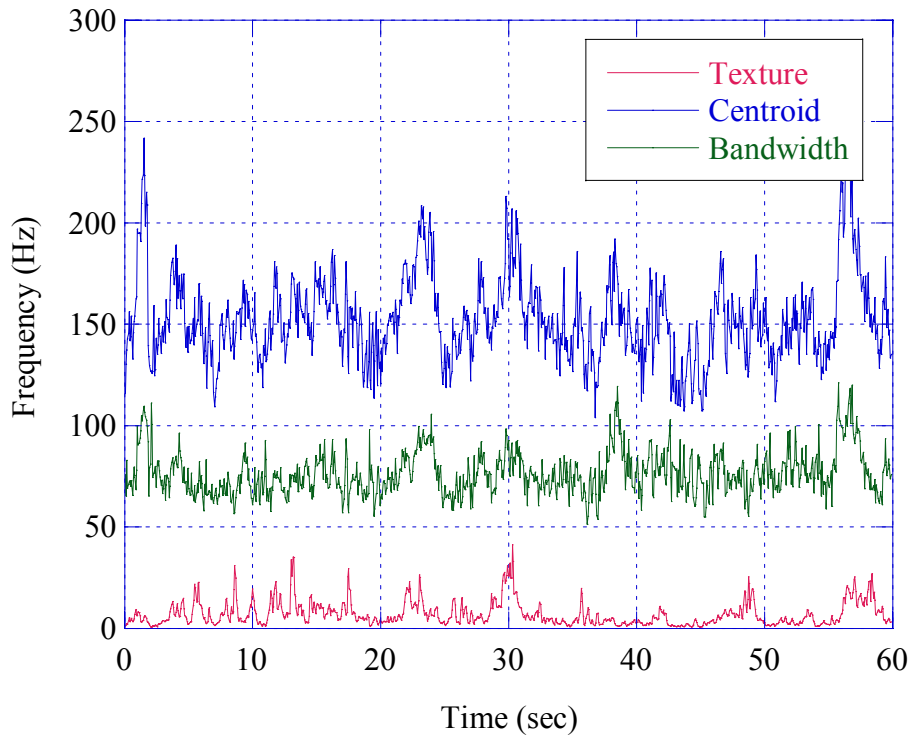


**Figure 1.14** - Time evolution of texture, centroid and bandwidth, 1<sup>st</sup> range cell, HH pol.

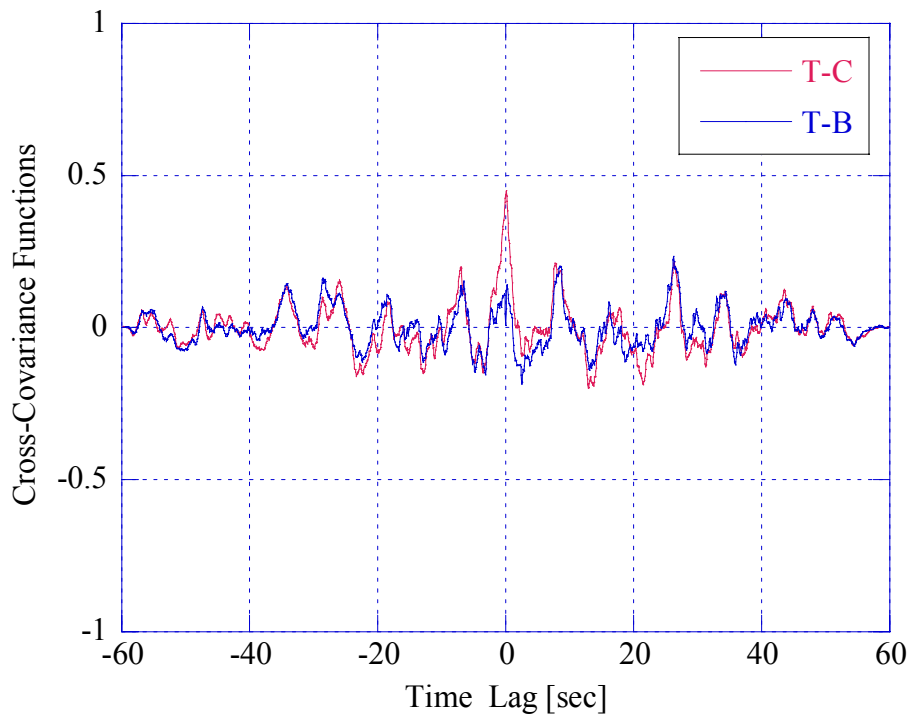


**Figure 1.15** - Texture-centroid and texture-bandwidth cross-covariance, 1<sup>st</sup> range cell, HH pol., per. asym

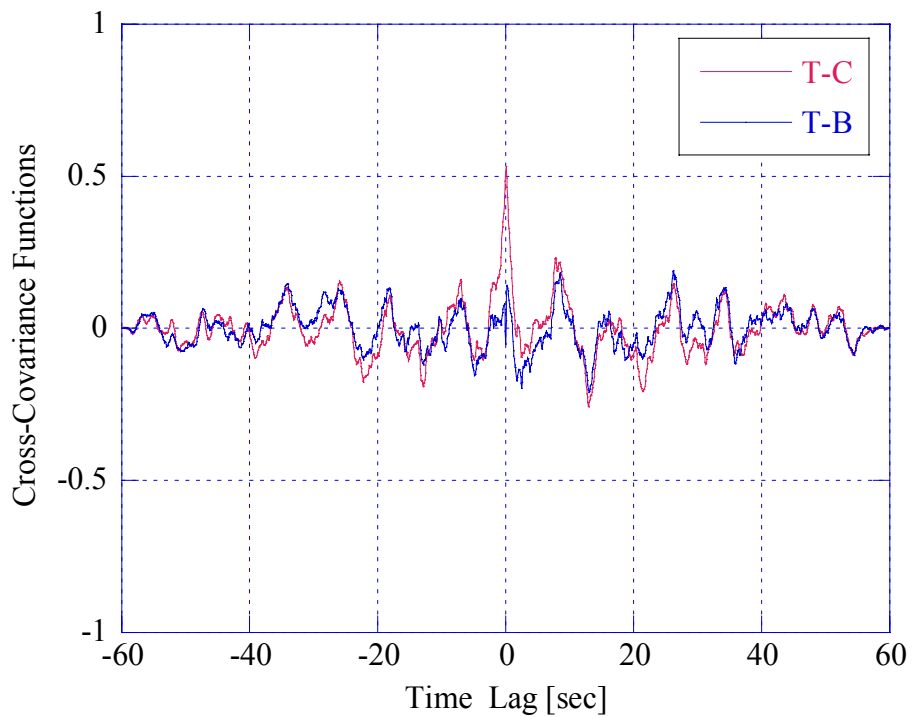


**Figure 1.16** - Log-texture-centroid and Log-texture-bandwidth cross-covariance, 1<sup>st</sup> range cell, HH pol.

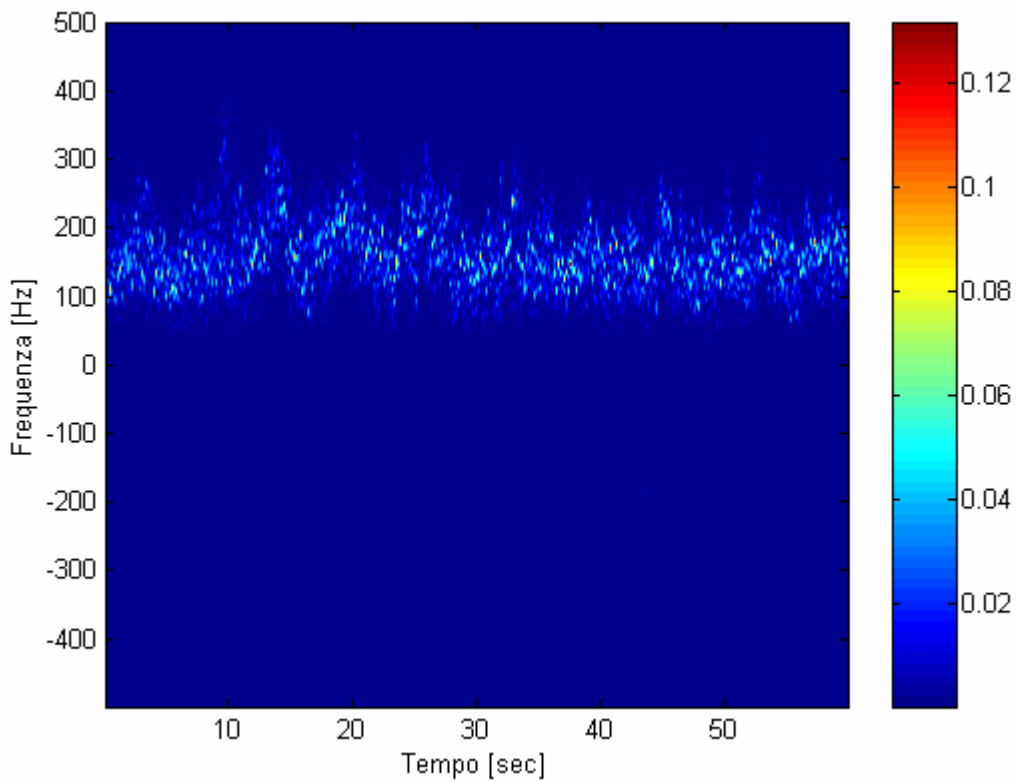


**Figure 1.17** - Normalized spectrum versus time, 15<sup>th</sup> range cell, VH pol. (CNR=16 dB)

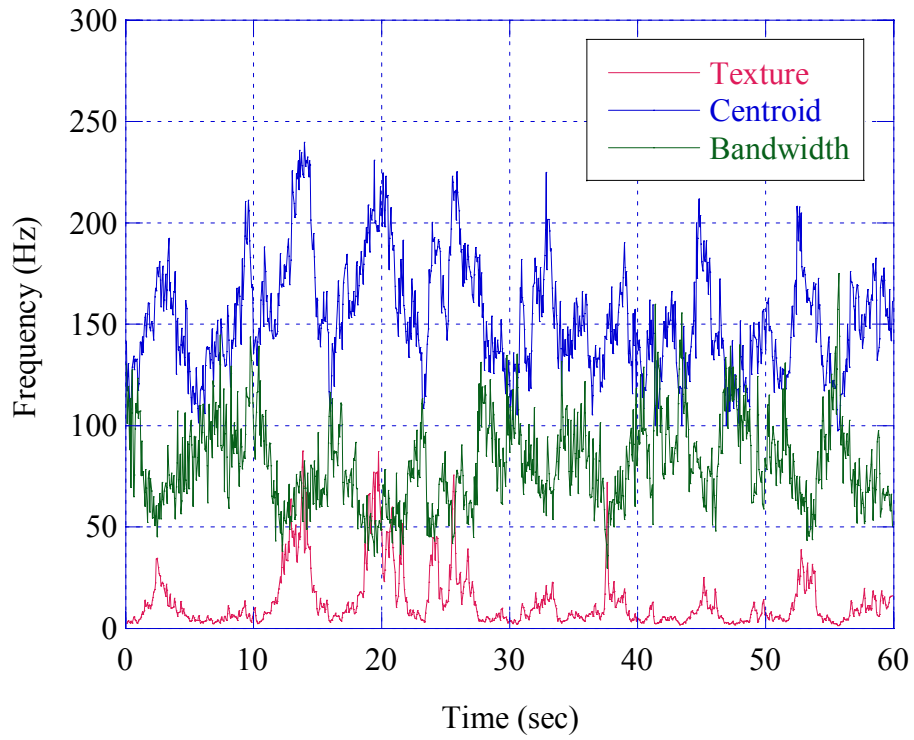


**Figure 1.18** - Time evolution of texture, centroid and bandwidth, 15<sup>th</sup> range cell, VH pol.

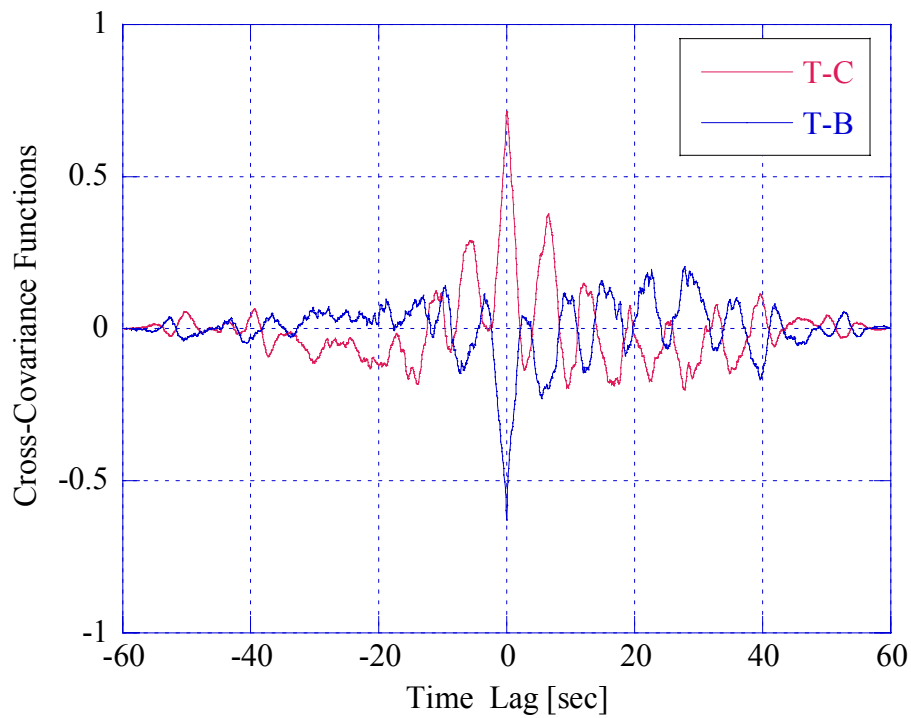


**Figure 1.19** - Texture-centroid and texture-bandwidth cross-covariance, 15<sup>th</sup> range cell, VH pol., per. sym.

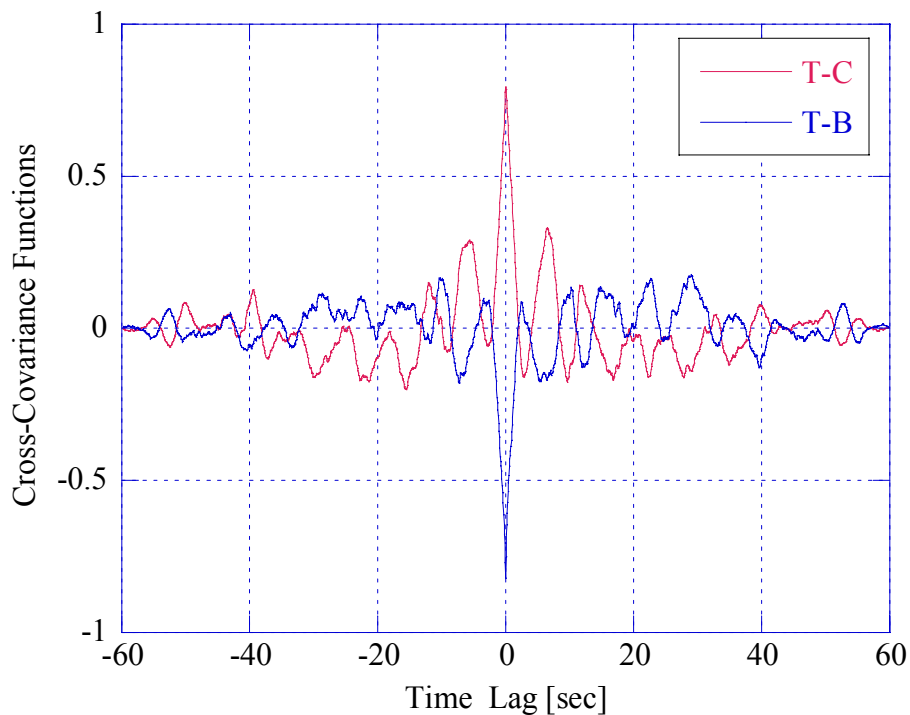


**Figure 1.20** - Log-texture-centroid and Log-texture-bandwidth cross-covariance, 15<sup>th</sup> range cell, VH pol.

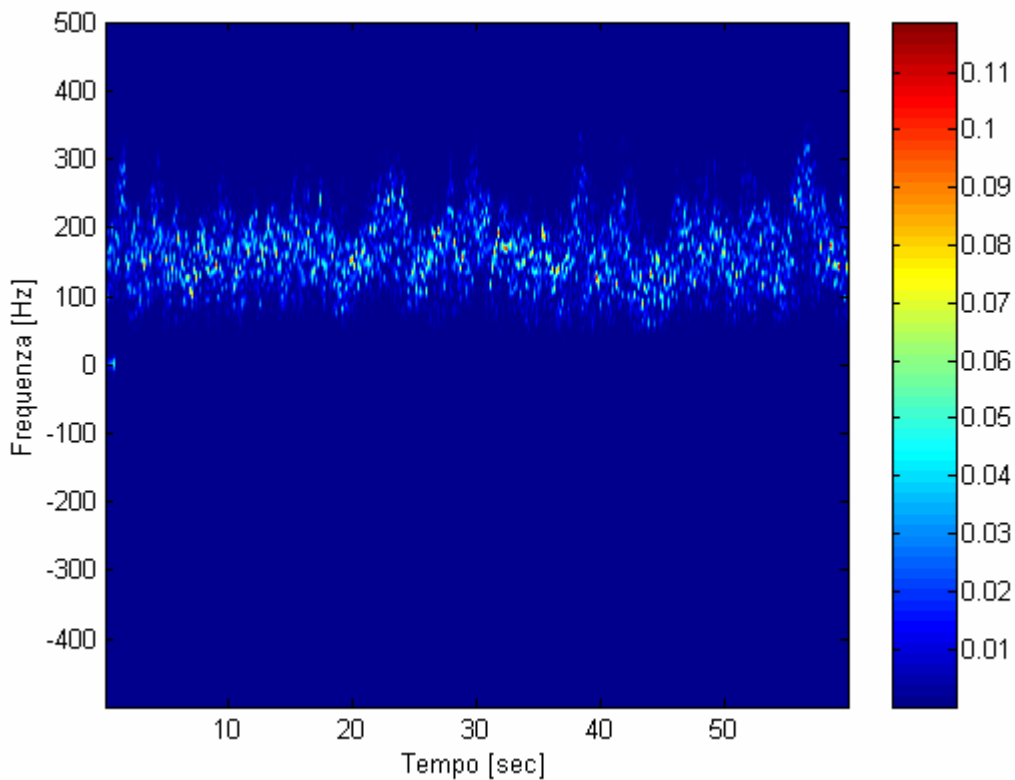


**Figure 1.21** - Normalized spectrum versus time, 1<sup>st</sup> range cell, VH pol. (CNR=23 dB)

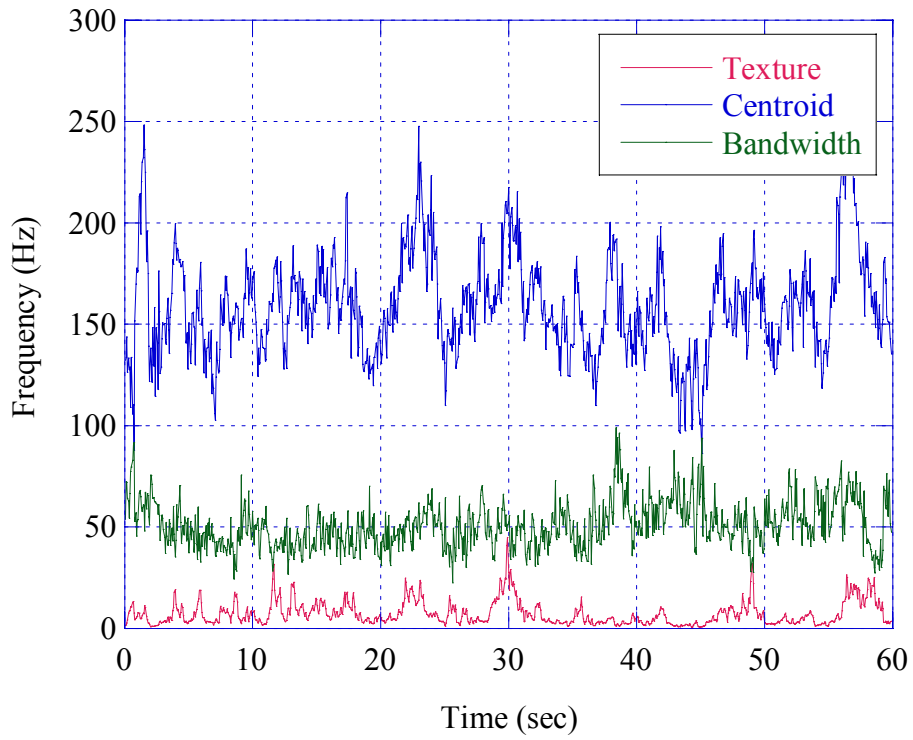


**Figure 1.22** - Time evolution of texture, centroid and bandwidth, 1<sup>st</sup> range cell, VH pol.

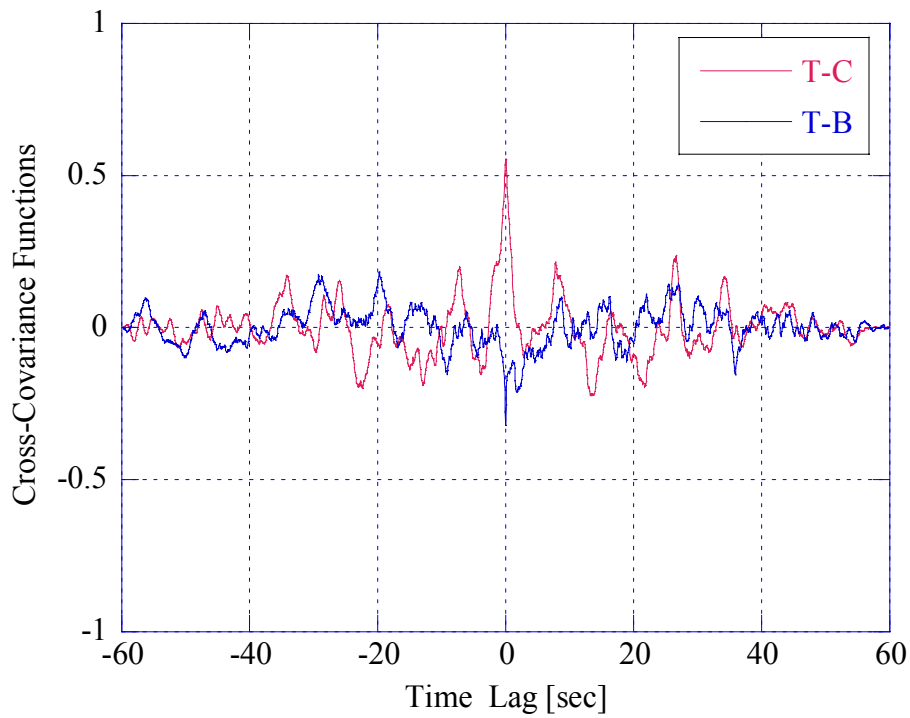


**Figure 1.23** - Texture-centroid and texture-bandwidth cross-covariance, 1<sup>st</sup> range cell, VH pol., per. asym.

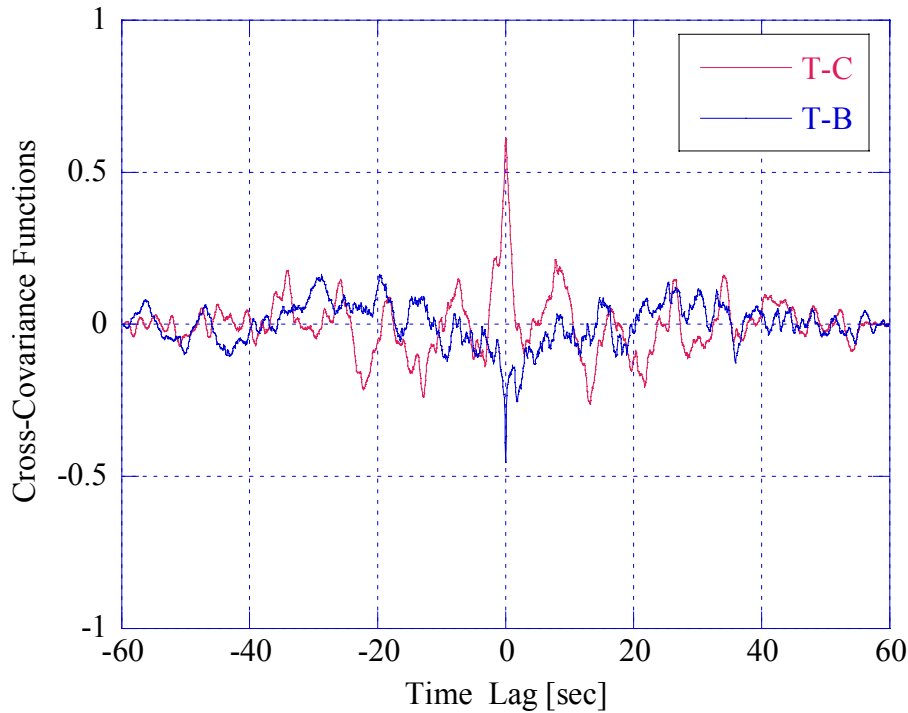


**Figure 1.24** - Log-texture-centroid and Log-texture-bandwidth cross-covariance, 1<sup>st</sup> range cell, VH pol.

### 1.2.2 - Range resolution of 30 m

Figures 1.25, 1.29, 1.33, 1.37, 1.41, and 1.45 show the normalized time varying spectrograms for the 1<sup>st</sup> and 21<sup>st</sup> cells, in all the polarizations. As for the 60 m range resolution, in most cells, the clutter power is concentrated in a narrow band at the positive frequencies between 50 and 200 Hz. Looking at the texture, centroid and bandwidth behavior versus time (Figs. 1.26, 1.30, 1.34, 1.38, 1.42, 1.46) we notice some differences with respect to lower resolution. It is evident that the variations of the bandwidth and of the centroid are larger than those presented at 60 m; Doppler centroid reaches values under 50 Hz and the bandwidth goes over 250 Hz. This phenomenon could partially depend on the thermal noise effect; some reported spectrograms show the presence of thermal noise through vertical lighter bands (thermal noise is modeled as Additive White Gaussian Noise (AWGN) process). But, more likely, it is due to a stronger non-homogeneity of the clutter relating to higher resolution. The larger the range cell, the heavier the averaging effect on time-varying phenomena. With higher resolutions, the local changes are more evident.

Cross-covariance function behaviors show that, also at 30 m range resolution for all polarizations, most cells belong to the aperiodical symmetrical group but some cell

presents clear periodicities. Figures 1.27, 1.35, 1.36, and 1.44 report the cross-covariance functions in every polarization for the 1<sup>st</sup> cell (aperiodical symmetrical) while figures 1.31, 1.32, 1.38, 1.47, and 1.48 for the 21<sup>st</sup> cell (periodical symmetrical). The periodical cell show a period of about 8 seconds. The maximum value of the cross-covariance function between centroid and texture is still in the origin in all polarizations and on the average is higher than 0.5 (sometimes it reaches 0.8). The minimum value of the cross-covariance functions between bandwidth and texture is in the origin too.

Figures 1.28, 1.32, 1.39, and 1.43 report the cross-covariance functions calculated with respect to the Log-texture; at this resolution, the logarithm highlights the correlation between texture and bandwidth and centroid, and the periodicity. Compare, as instance, Fig. 1.31 with Fig. 1.32. The maximum value of the cross-covariance between texture and centroid is 0.73, between Log-texture and centroid is 0.86, between texture and bandwidth is -0.71, between Log-texture and bandwidth -0.93.

The classification of the cells is in Table 1.2.

	<b>Periodical Symmetrical</b>	<b>Periodical Asymmetrical</b>	<b>Aperiodical Symmetrical</b>
Pol. VV	21, 20	8, 7	All the others
Pol. HH	21, 20, 18, 13, 5	8, 7	All the others
Pol. VH	21, 20	8, 7	All the others

**Table 1.2** – Covariance classification, 30 m.

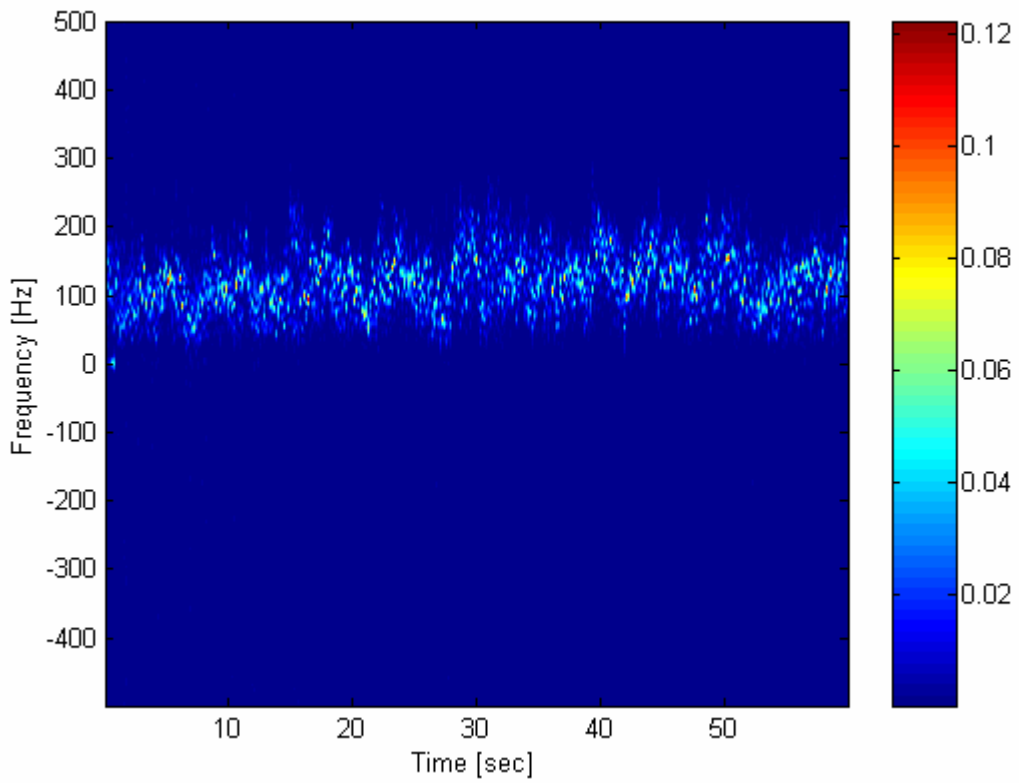


**Figure 1.25** - Normalized spectrum versus time, 1<sup>st</sup> range cell, VV pol. (CNR=16 dB).

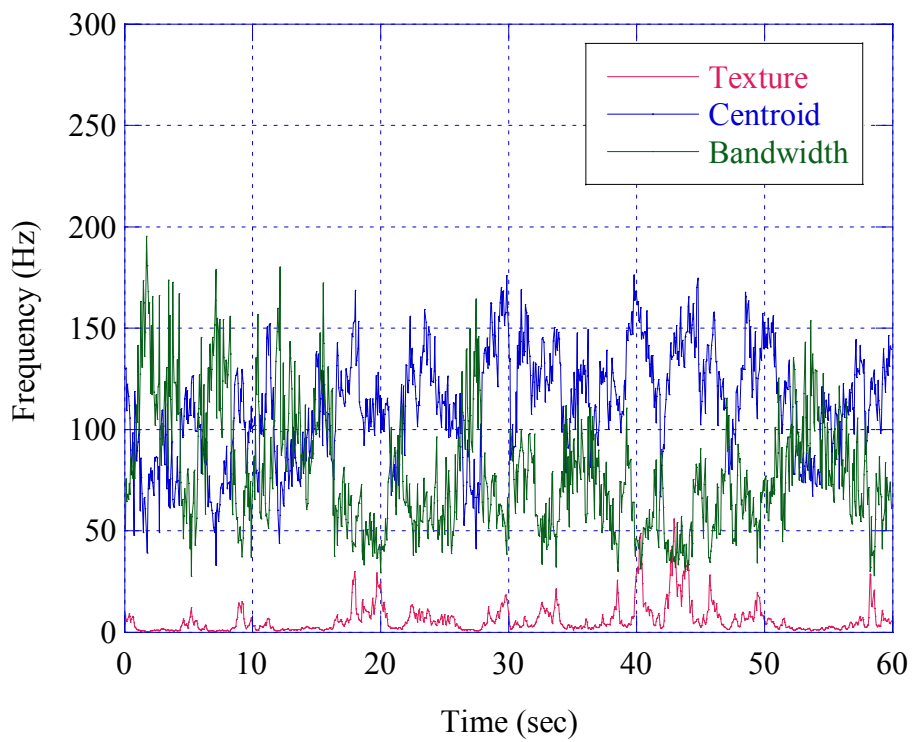


**Figure 1.26** - Time evolution of texture, centroid and bandwidth, 1<sup>st</sup> range cell, VV pol.

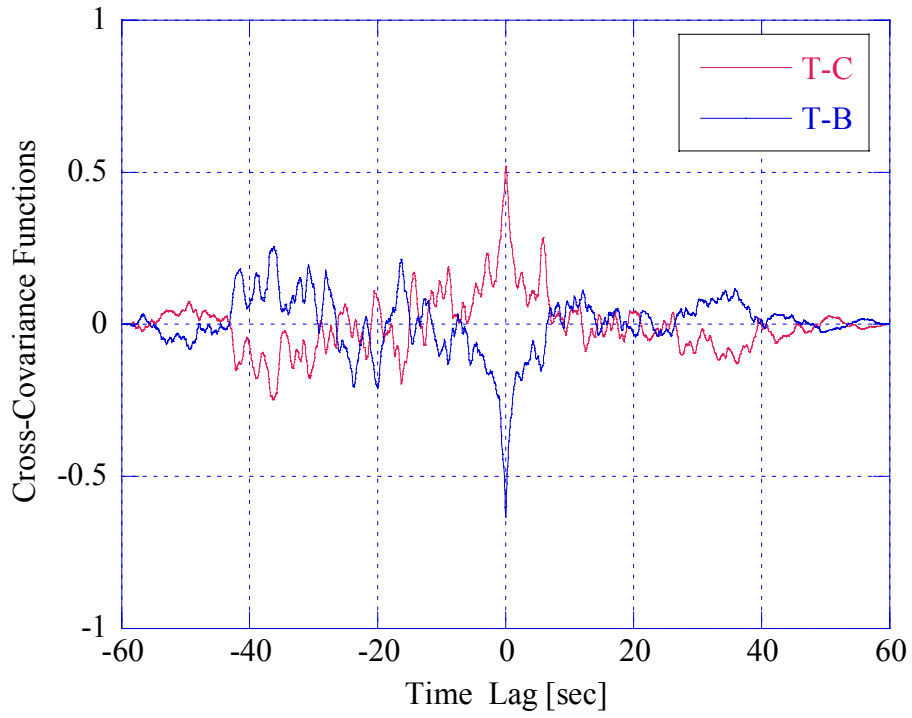


**Figure 1.27** - Texture-centroid and texture-bandwidth cross-covariance, 1<sup>st</sup> range cell, VV pol., aper. sym.

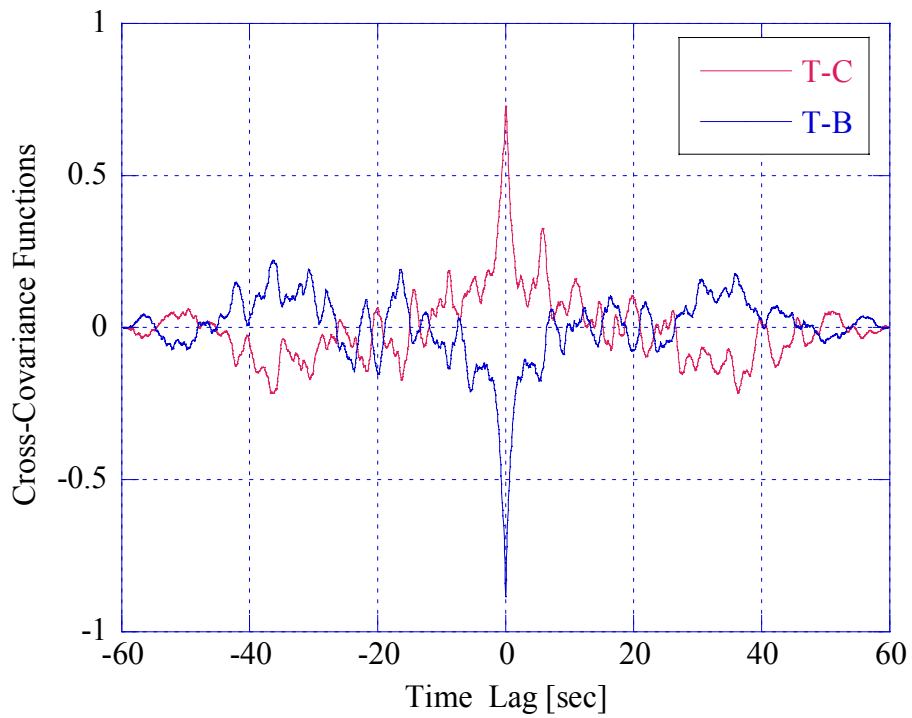


**Figure 1.28** - Log-texture-centroid and Log-texture-bandwidth cross-covariance, 1<sup>st</sup> range cell, VV pol.

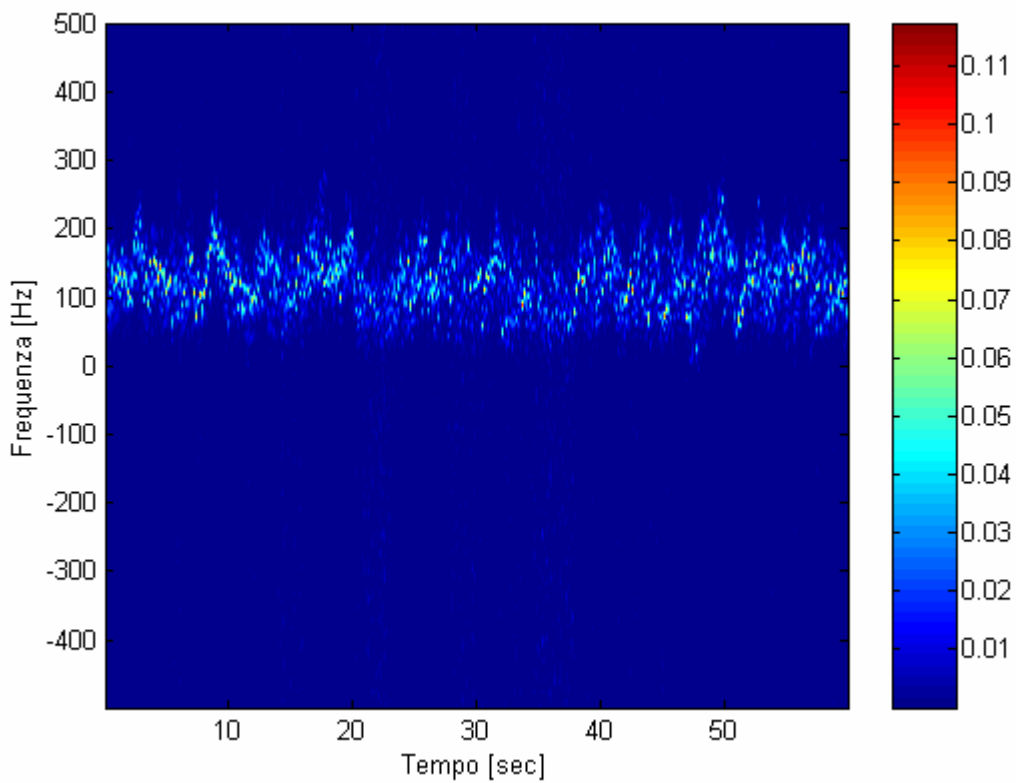


**Figure 1.29** - Normalized spectrum versus time, 21<sup>st</sup> range cell, VV pol. (CNR=12 dB)

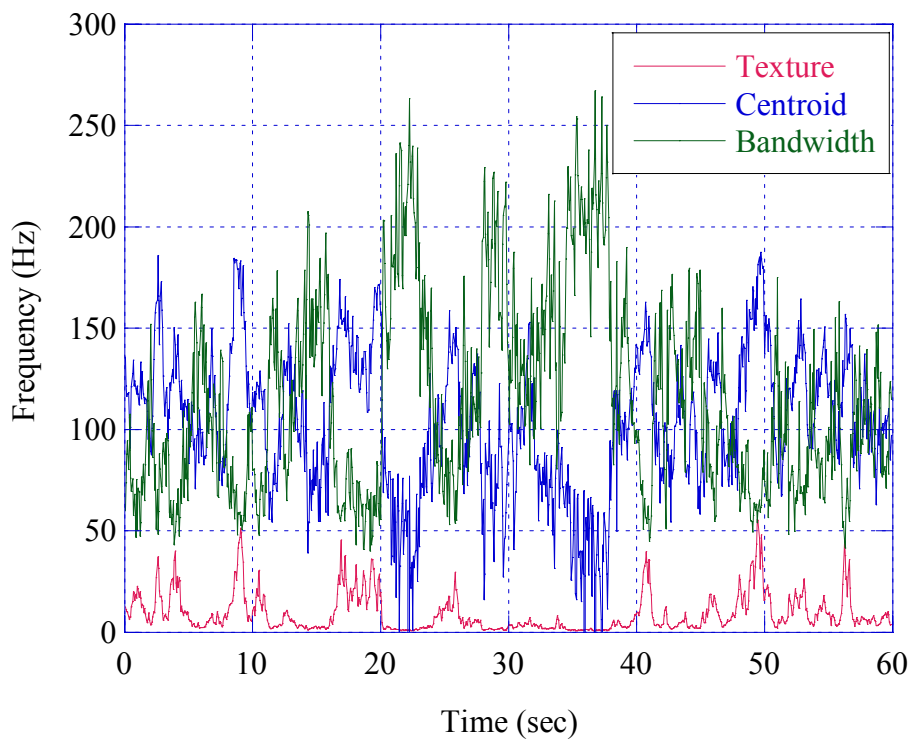


**Figure 1.30** - Time evolution of texture, centroid and bandwidth, 21<sup>st</sup> range cell, VV pol.

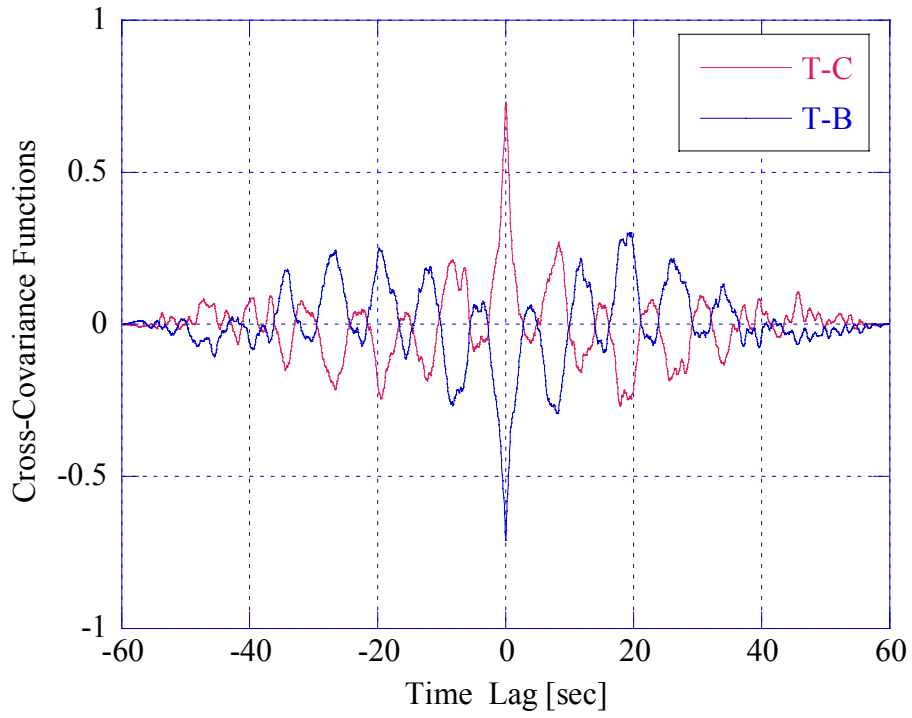


**Figure 1.31** - Texture-centroid and texture-bandwidth cross-covariance, 21<sup>st</sup> range cell, VV pol., per. sym.

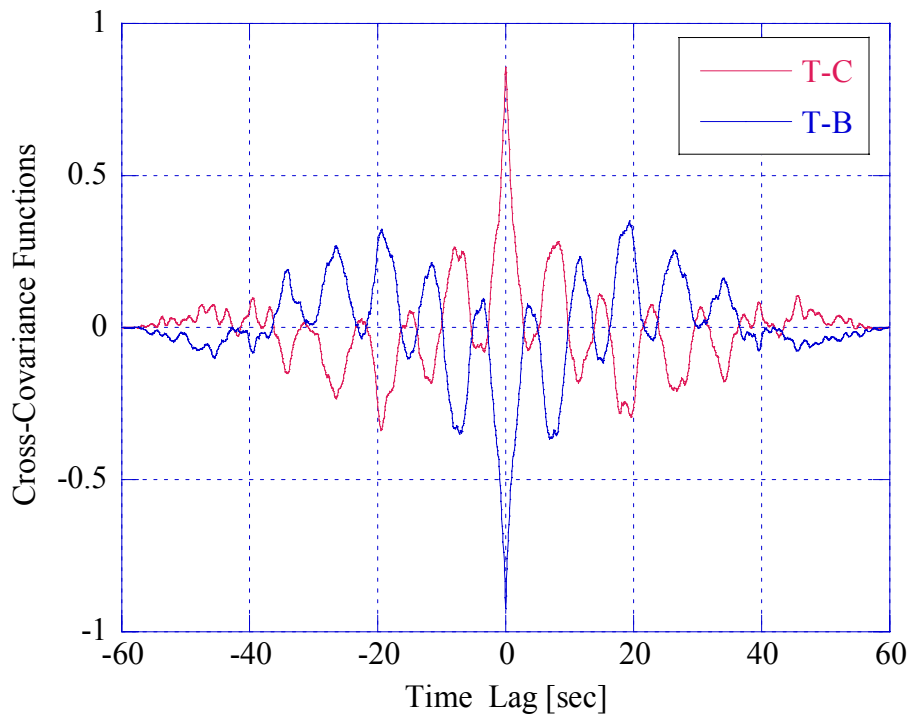


**Figure 1.32** - Log-texture-centroid and Log-texture-bandwidth cross-covariance, 21<sup>st</sup> range cell, VV pol.

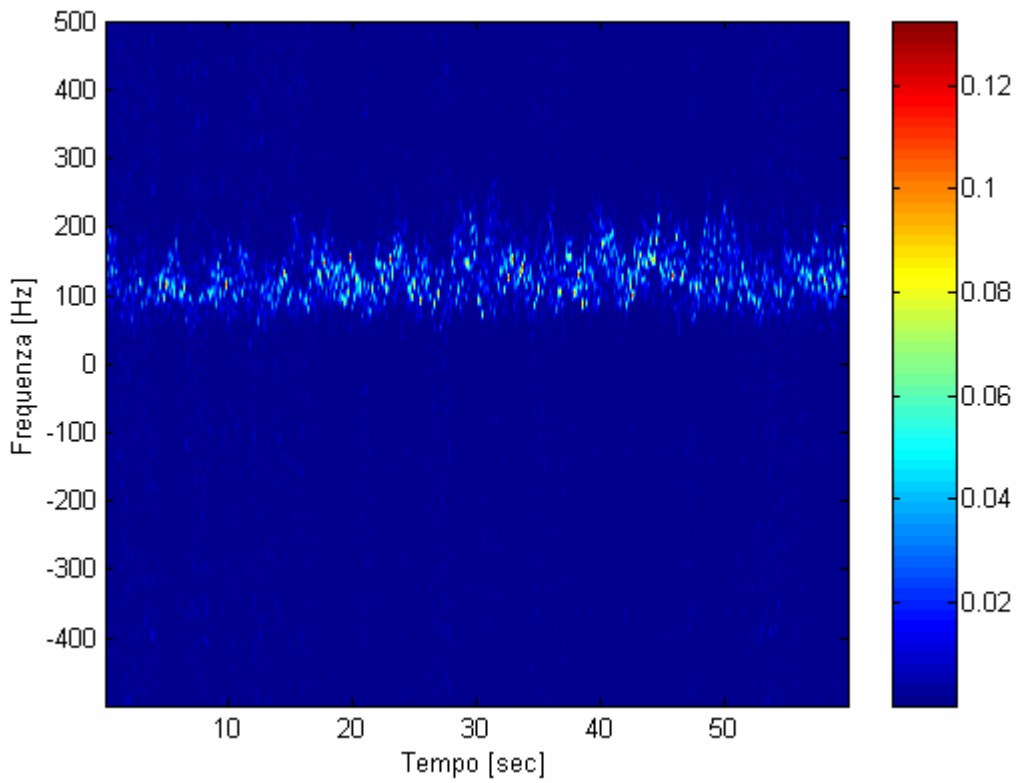


**Figure 1.33** - Normalized spectrum versus time, 1<sup>st</sup> range cell, HH pol. (CNR=7 dB)

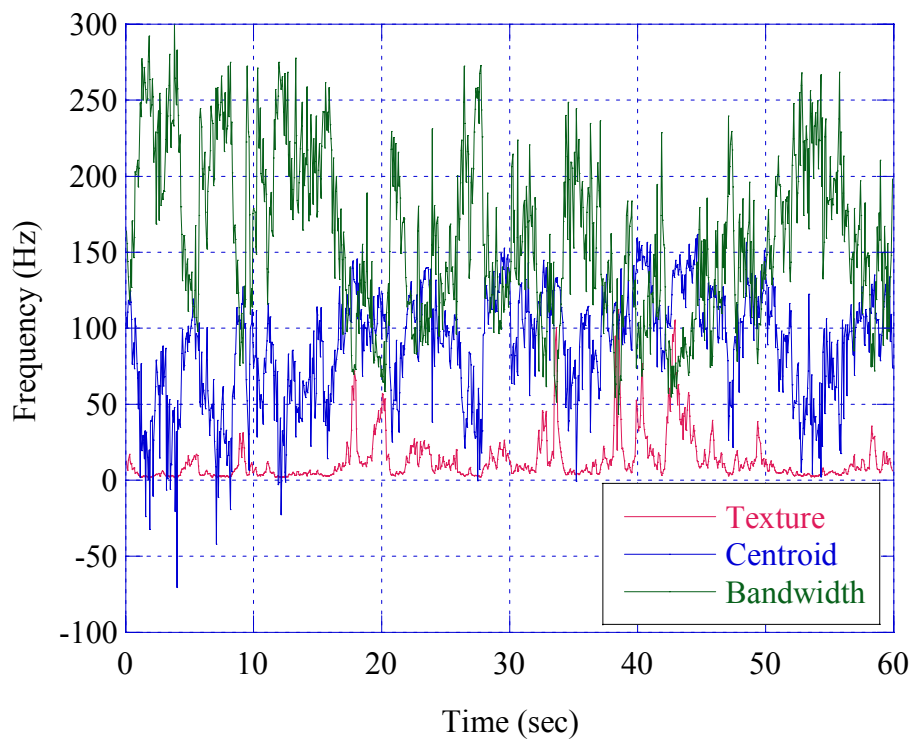


**Figure 1.34** - Time evolution of texture, centroid and bandwidth, 1<sup>st</sup> range cell, HH pol.

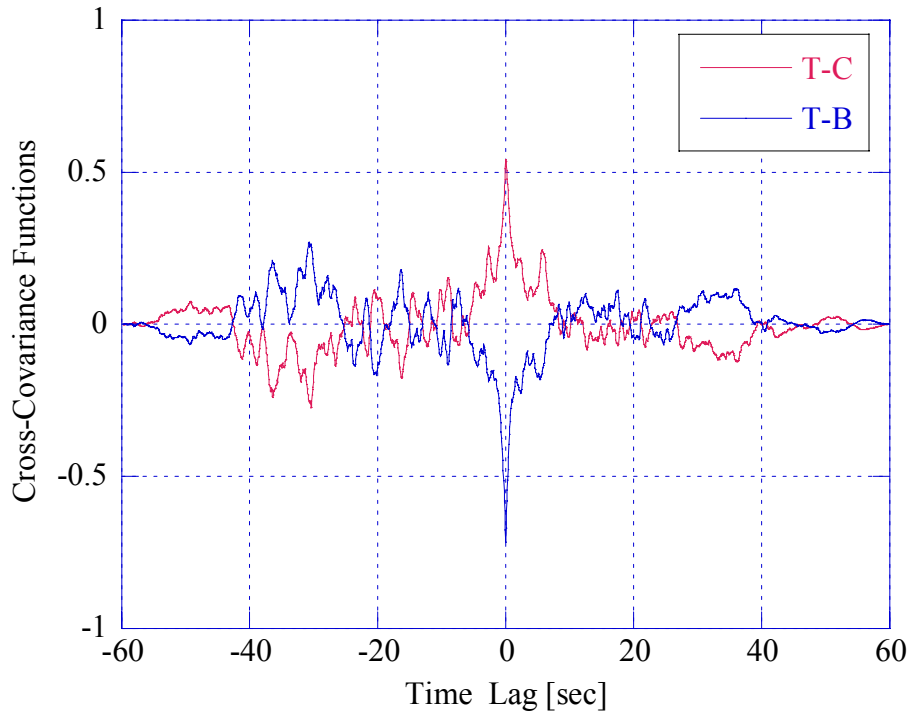


**Figure 1.35** - Texture-centroid and texture-bandwidth cross-covariance, 1<sup>st</sup> range cell, HH pol., aper. sym.

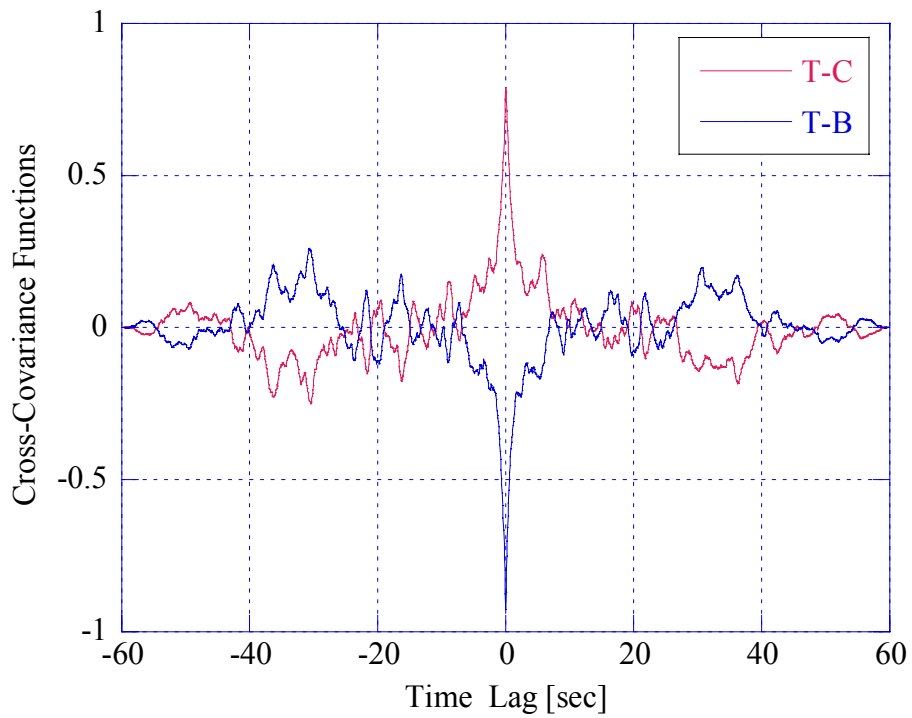


**Figure 1.36** - Log-texture-centroid and Log-texture-bandwidth cross-covariance, 1<sup>st</sup> range cell, HH pol.

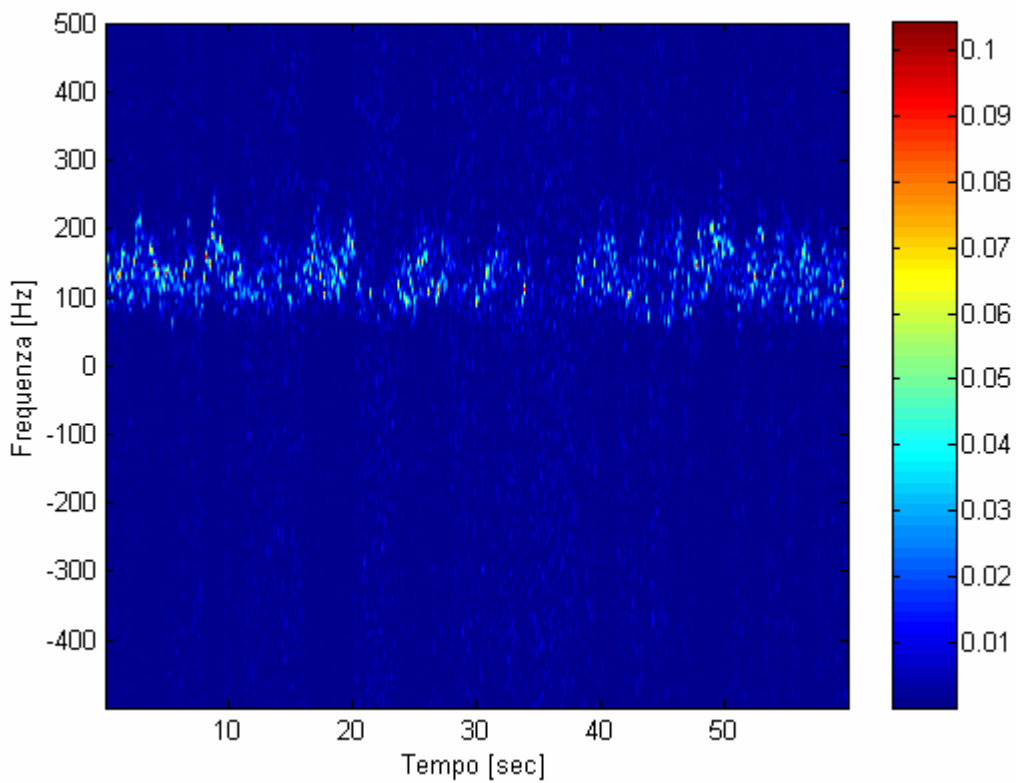


**Figure 1.37** - Normalized spectrum versus time, 21<sup>st</sup> range cell, HH pol. ( $CNR=1.5$  dB)

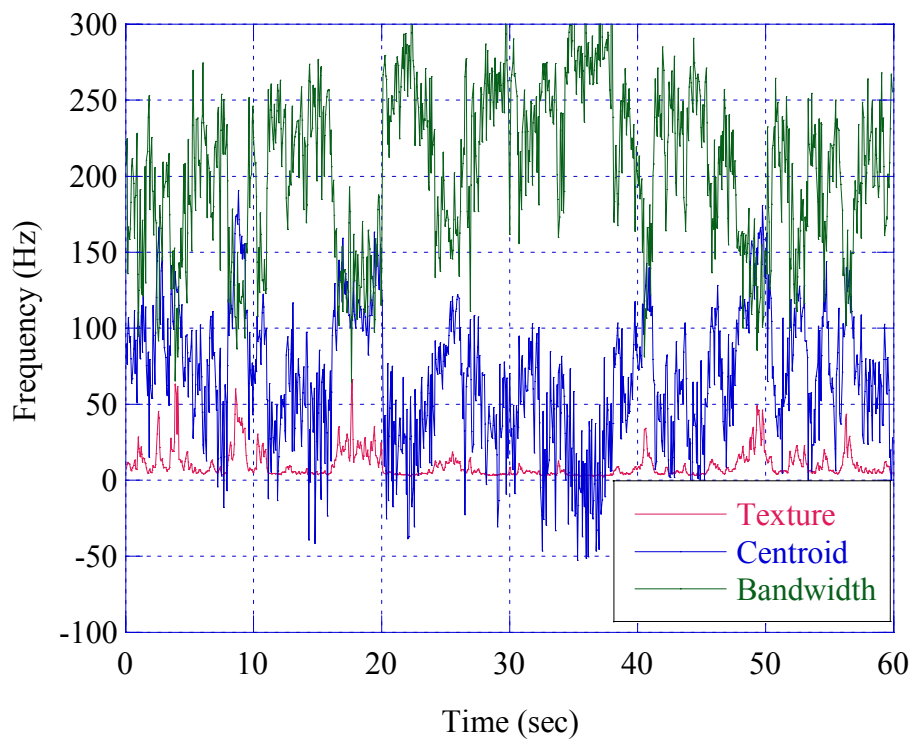


**Figure 1.38** - Time evolution of texture, centroid and bandwidth, 21<sup>st</sup> range cell, HH pol.

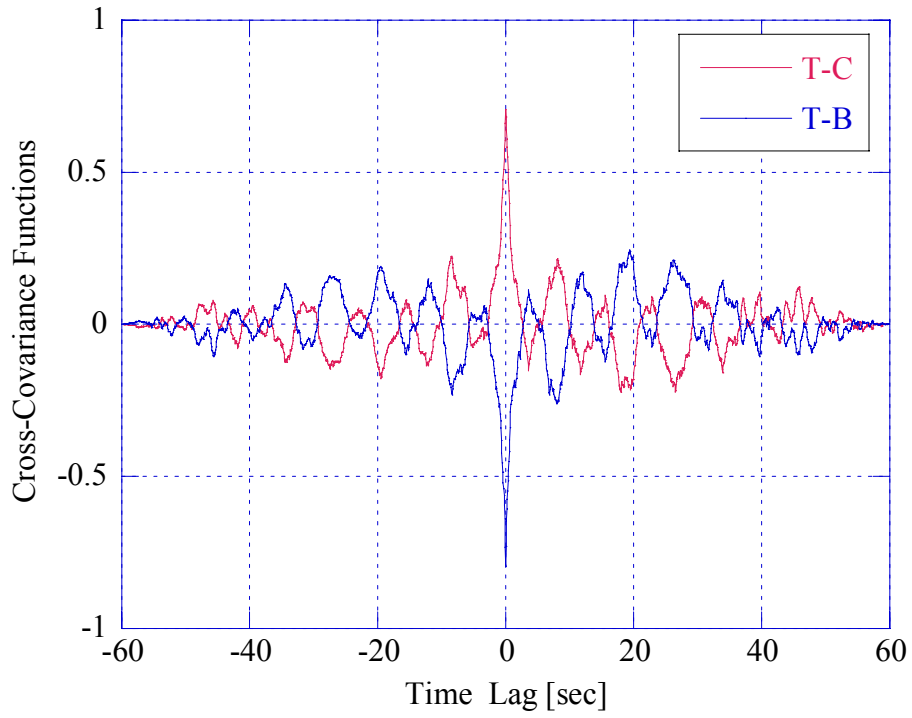


**Figure 1.39** - Texture-centroid and texture-bandwidth cross-covariance, 21<sup>st</sup> range cell, HH pol., per. sym.

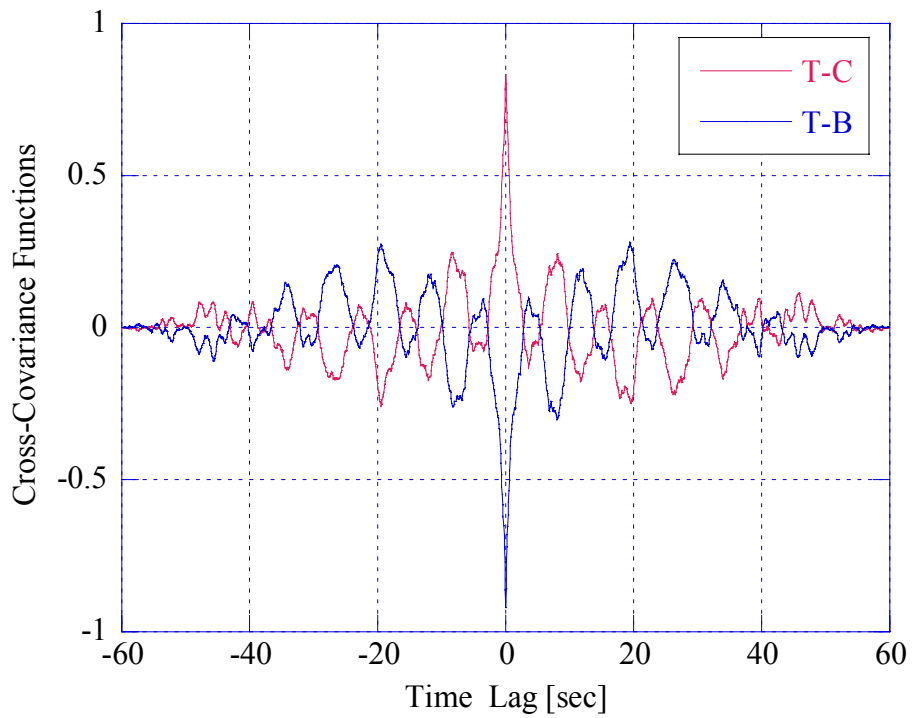


**Figure 1.40** - Log-texture-centroid and Log-texture-bandwidth cross-covariance, 21<sup>st</sup> range cell, HH pol.

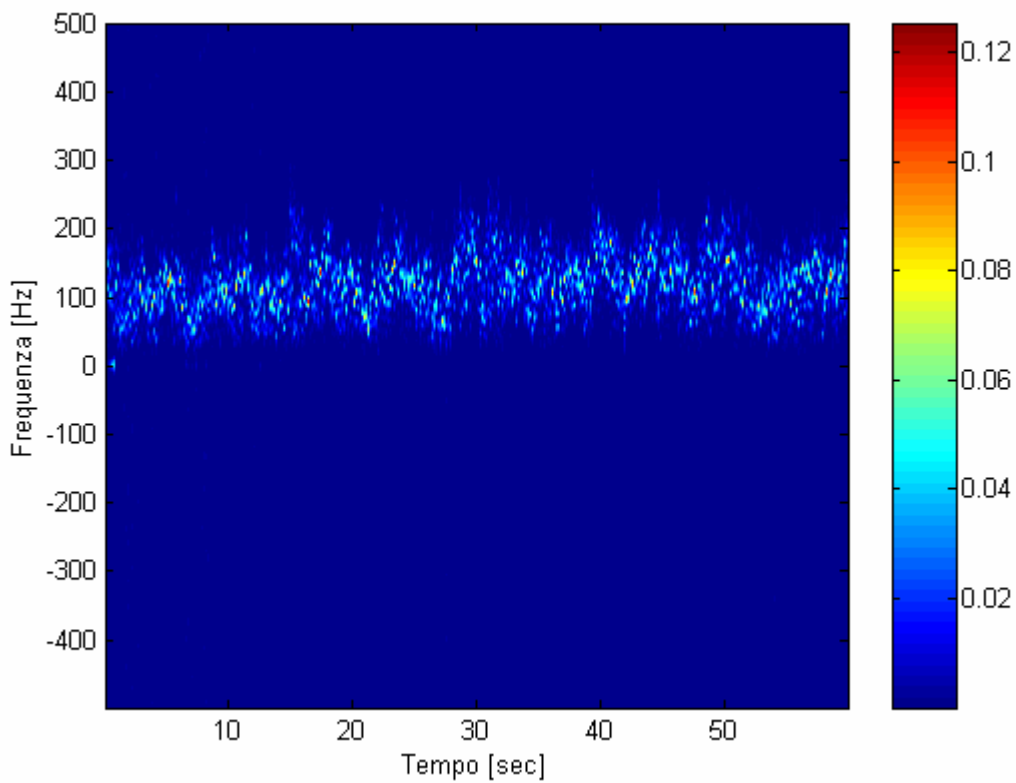


**Figure 1.41** - Normalized spectrum versus time, 1<sup>st</sup> range cell, VH pol. (CNR=16 dB)

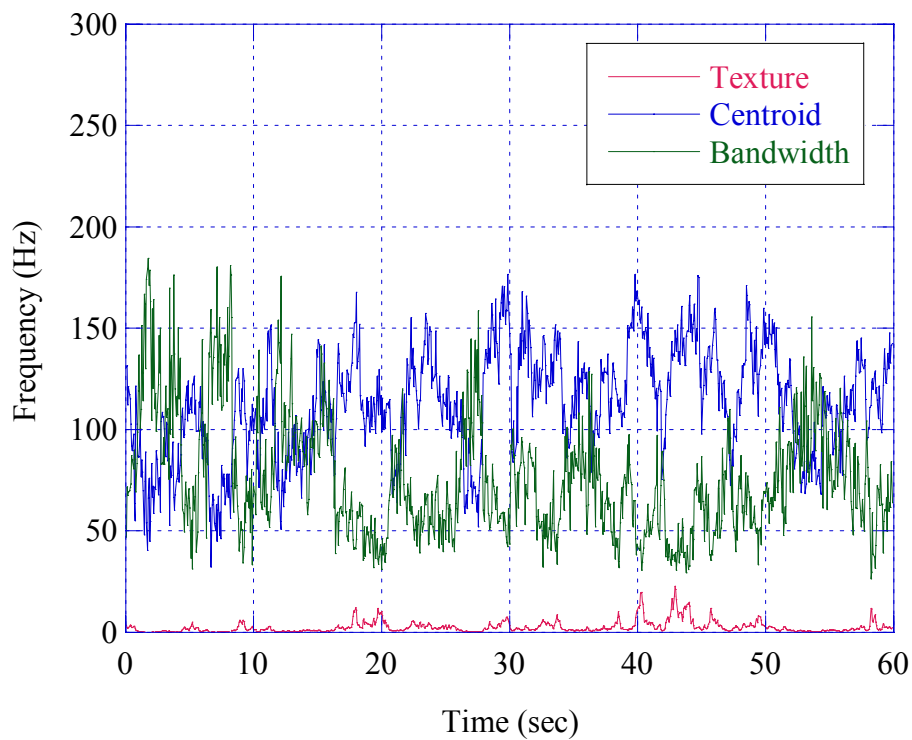


**Figure 1.42** - Time evolution of texture, centroid and bandwidth, 1<sup>st</sup> range cell, VH pol.

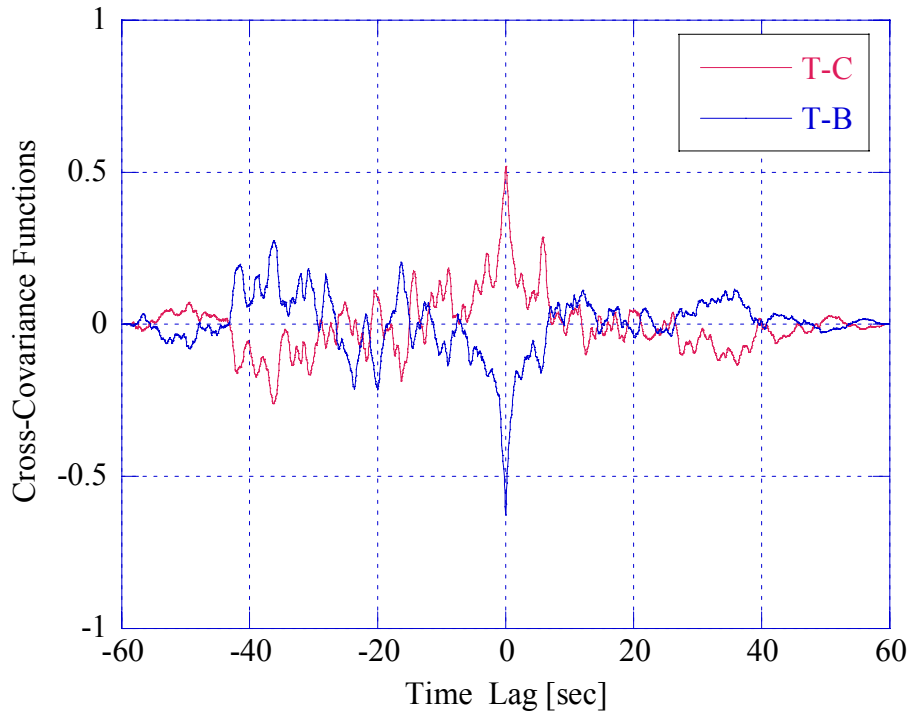


**Figure 1.43** - Texture-centroid and texture-bandwidth cross-covariance, 1<sup>st</sup> range cell, VH pol., aper. sym.

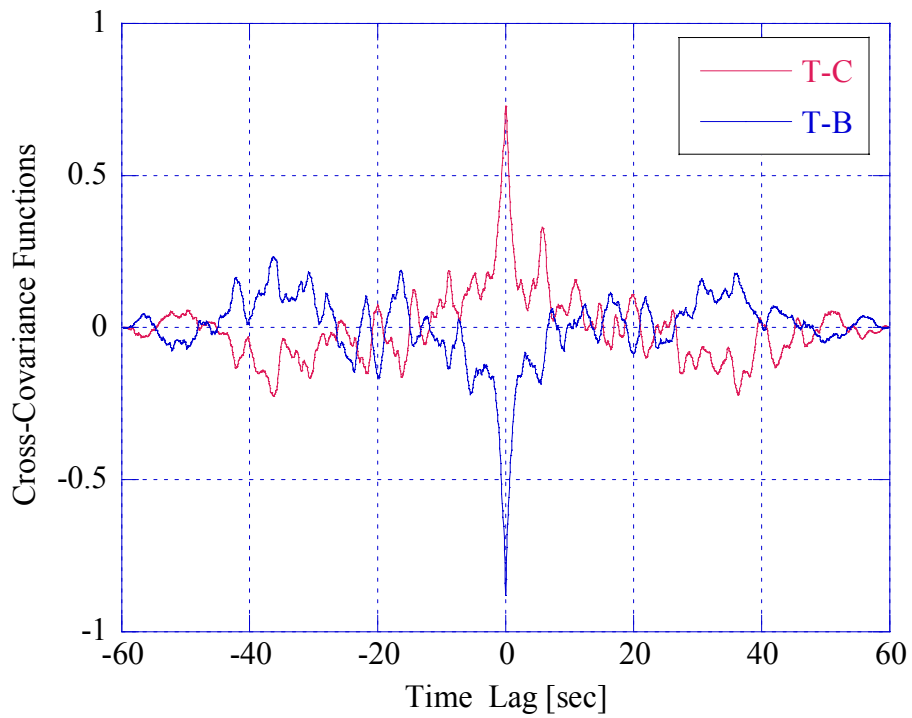


**Figure 1.44** - Log-texture-centroid and Log-texture-bandwidth cross-covariance, 1<sup>st</sup> range cell, VH pol.

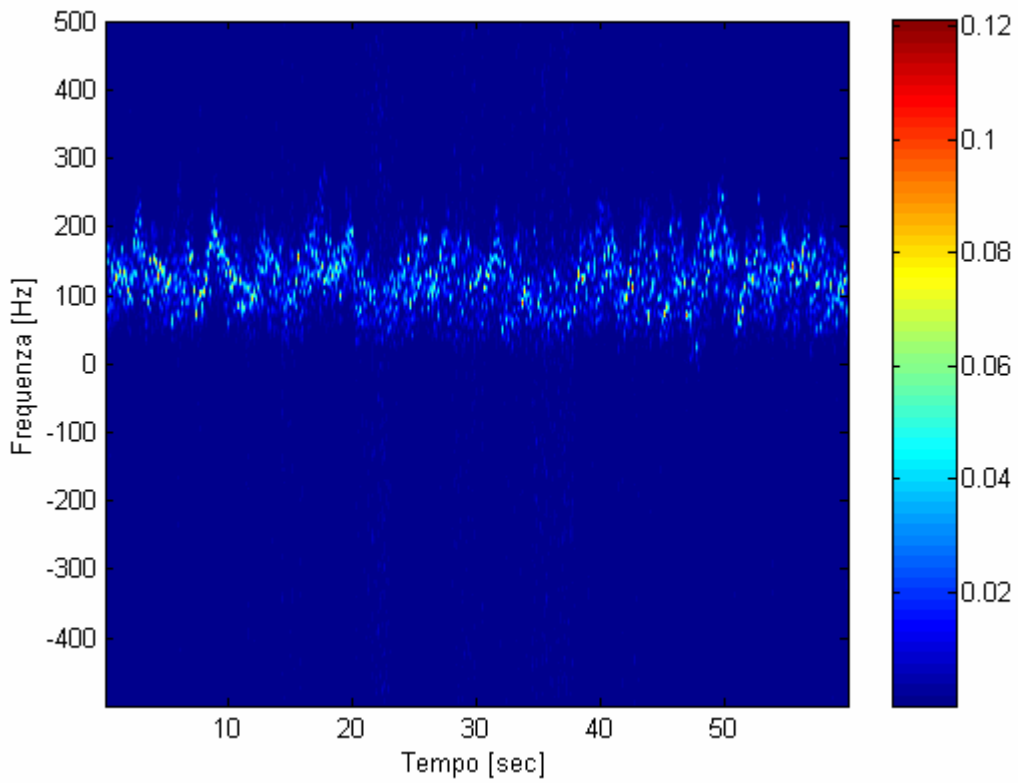


**Figure 1.45** - Normalized spectrum versus time, 21<sup>st</sup> range cell, VH pol. ( $CNR=12$  dB)

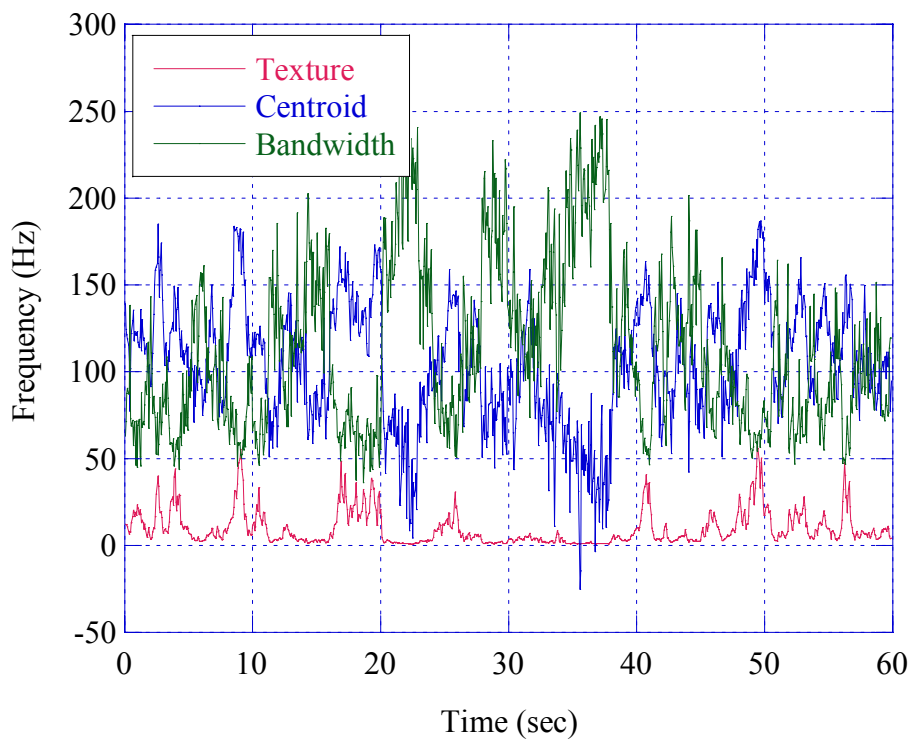


**Figure 1.46** - Time evolution of texture, centroid and bandwidth, 21<sup>st</sup> range cell, VH pol.

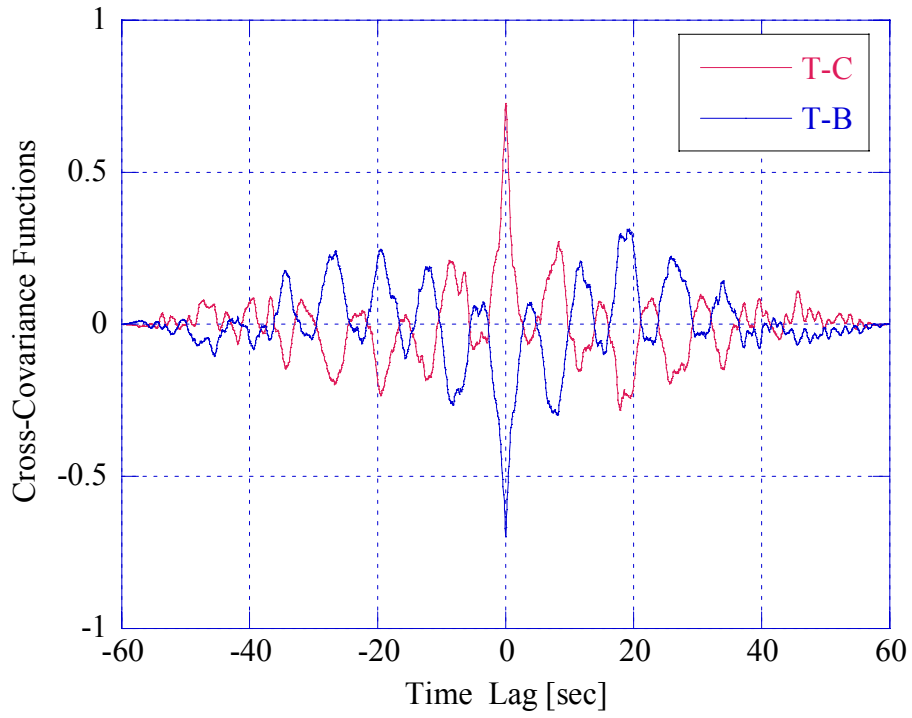


**Figure 1.47** - Texture-centroid and texture-bandwidth cross-covariance, 21<sup>st</sup> range cell, VH pol., per. sym.

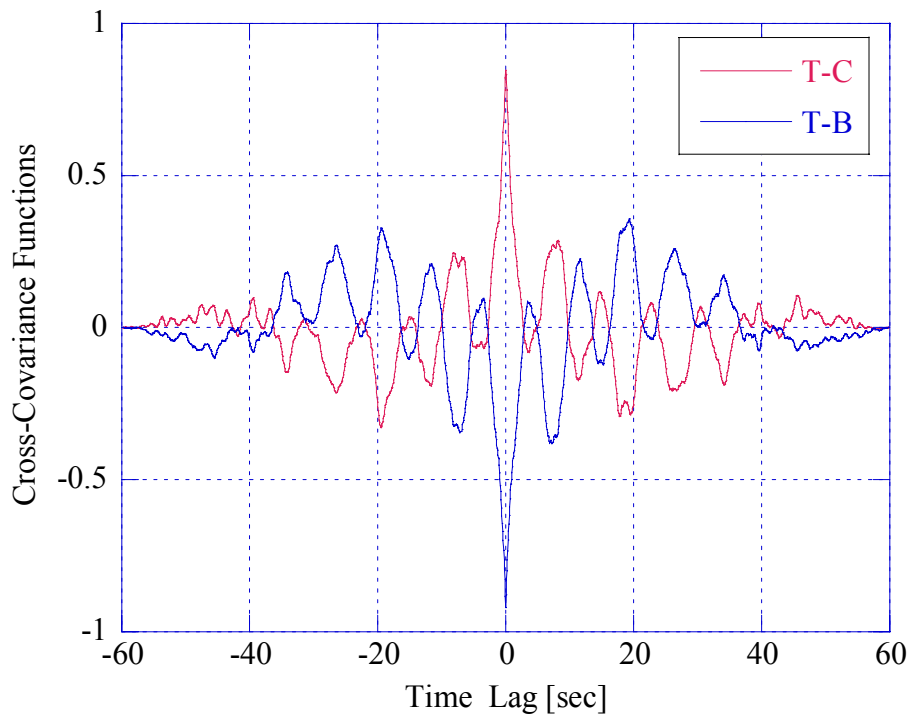


**Figure 1.48** - Log-texture-centroid and Log-texture-bandwidth cross-covariance, 21<sup>st</sup> range cell, VH pol.

### 1.2.3 - Range resolution of 15 m

The evolution of the spectrogram versus time, plotted in Figs. 1.49, 1.53, 1.57, 1.61, 1.65, and 1.69, confirms that the peaks in the spectrum due to the clutter are located between 100 Hz and 300 Hz for all polarizations, and shows that the thermal noise effect is not more negligible. Even if, in the average, the power of the clutter is greater than the power of the thermal noise, locally it is not always the case. When the texture is small, locally the *CNR* gets very small and the thermal noise overcomes the clutter. In this case the estimated Doppler centroid and bandwidth are mainly affected by the characteristics of the noise, then the centroid tend to be very small (almost zero) and the bandwidth increases, as in Figs. 1.50 and 1.54. Then, sometimes, with high resolutions, the interpretation of the spectral changes is not clear and the thermal noise presence cannot be ignored.

Cross-covariance functions between texture and bandwidth and between texture and centroid show some particularities with respect to the lower resolutions. Most cells analyzed at 15 m, show evident periodicities in both VV and HH polarization and, in some cases, less evident in VH polarization. Moreover, the period is shorter than in the lower resolutions (Figs. 1.51, 1.52, 1.59, 1.60); this period is about 4.5 seconds. This means that the radar system with higher resolution can resolve local waves with shorter periods.

No studied cell belongs to the periodical asymmetrical group.

Looking at figures 1.52, 1.56, 1.60, 1.64, 1.68, and 1.72, reporting the cross-covariance functions calculated with respect to the texture logarithm, it is apparent that these functions show periodicities that were bypassed in the cross-covariance functions calculated using the texture, particularly for the 5<sup>th</sup> range cell. In this case, the periodicities are much longer than in other cells, being the period 20 seconds long and they are maybe due to a dominant long wave with a period of 20 sec.

To highlight the similarities between Log-texture and centroid we plotted in Fig. 1.54b the centroid in Hz scale and the texture on arbitrary unit scale. They are almost superimposed. In Fig. 1.54c, instead of plotting the bandwidth as in Fig. 1.54a, we plotted the negative bandwidth shifted of 250 Hz (processed bandwidth), again to superimpose it with the texture. The similarities in the behavior are surprising. We obtained very similar results for the other cells. It seems that, the long waves modulate in frequency the amplitude of the clutter and in amplitude the logarithm of the texture more than the texture itself. The physical reasons of this phenomenon are still open questions.

The classification table is Table 1.3 below.

	<b>Periodical Symmetrical</b>	<b>Periodical Asymmetrical</b>	<b>Aperiodical Symmetrical</b>
Pol. VV	26, 23, 21, 20, 19, 18, 17, 16, 15, 14, 13, 12, 3, 1	_____	28, 27, 25, 24, 22, 11, 10, 9, 8, 7, 6, 5, 4, 2
Pol. HH	26, 23, 21, 20, 19, 18, 17, 16, 15, 14, 13, 12, 9, 1	_____	28, 27, 25, 24, 22, 11, 10, 8, 7, 6, 5, 4, 3, 2
Pol. VH	17, 15, 14, 13, 9, 8	_____	All the others

**Table 1.3** – Covariance classification, 15 m.

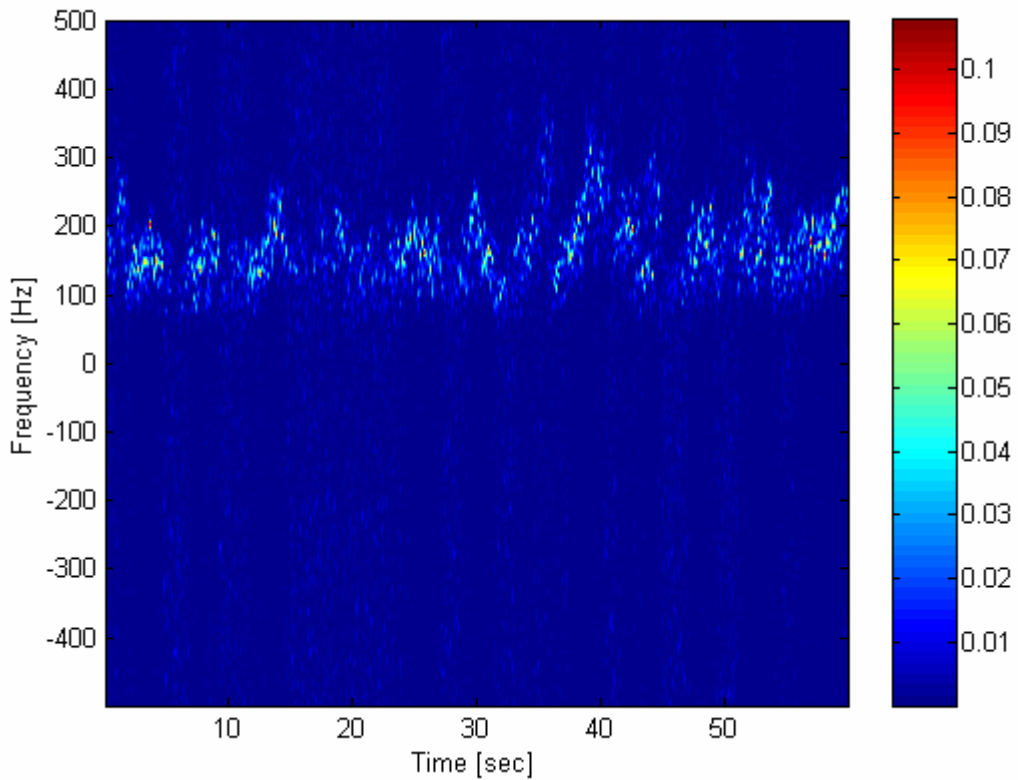


**Figure 1.49** - Normalized spectrum versus time, 15th range cell, VV pol. ( $CNR=9$  dB)

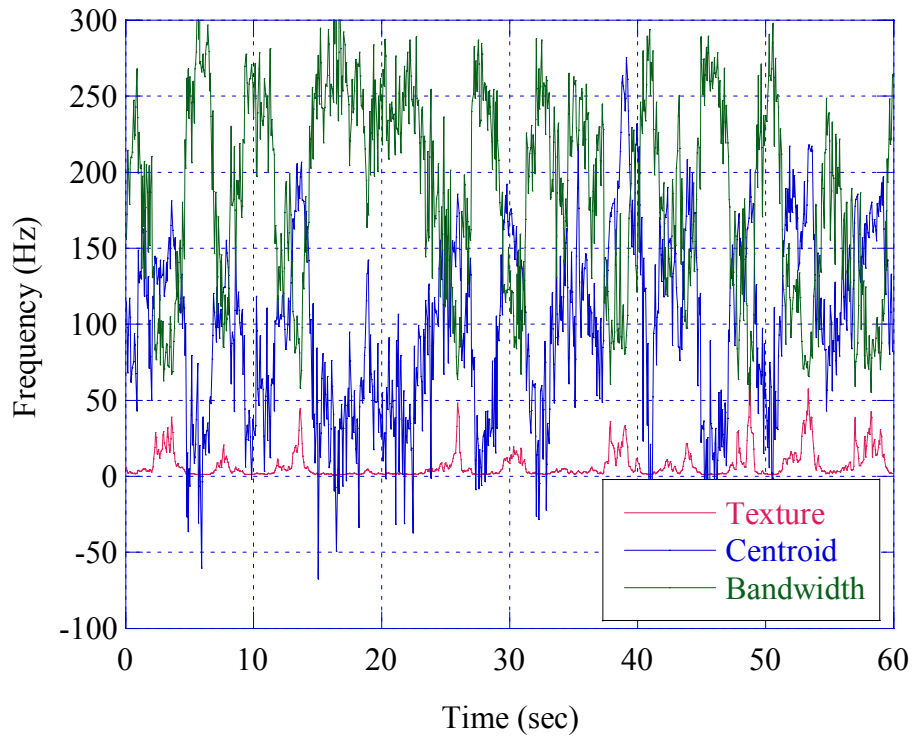


Figure 1.50 - Time evolution of texture, centroid and bandwidth, 15<sup>th</sup> range cell, VV pol.

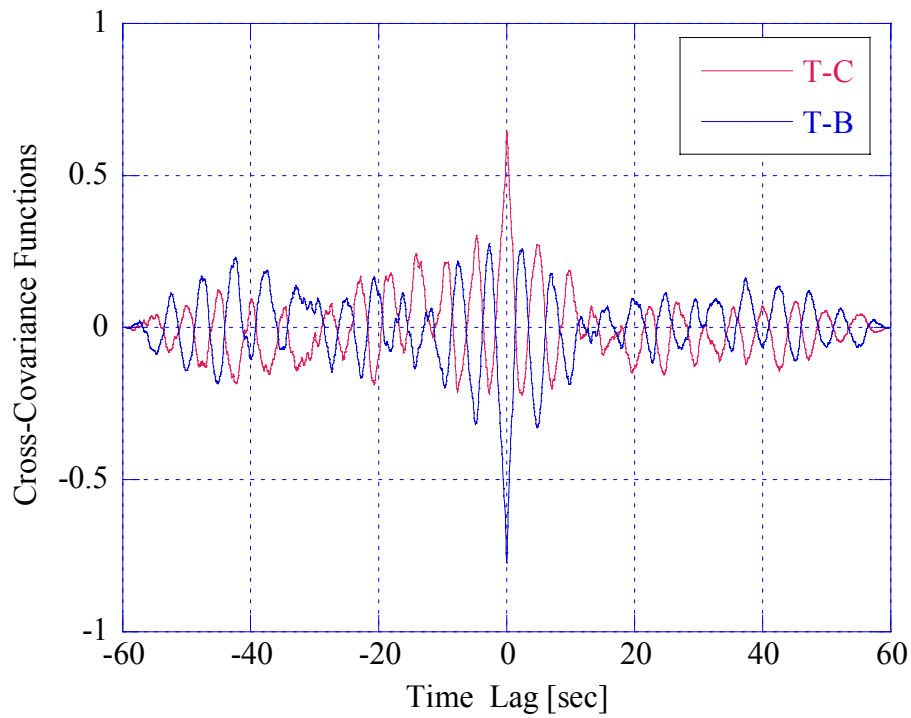
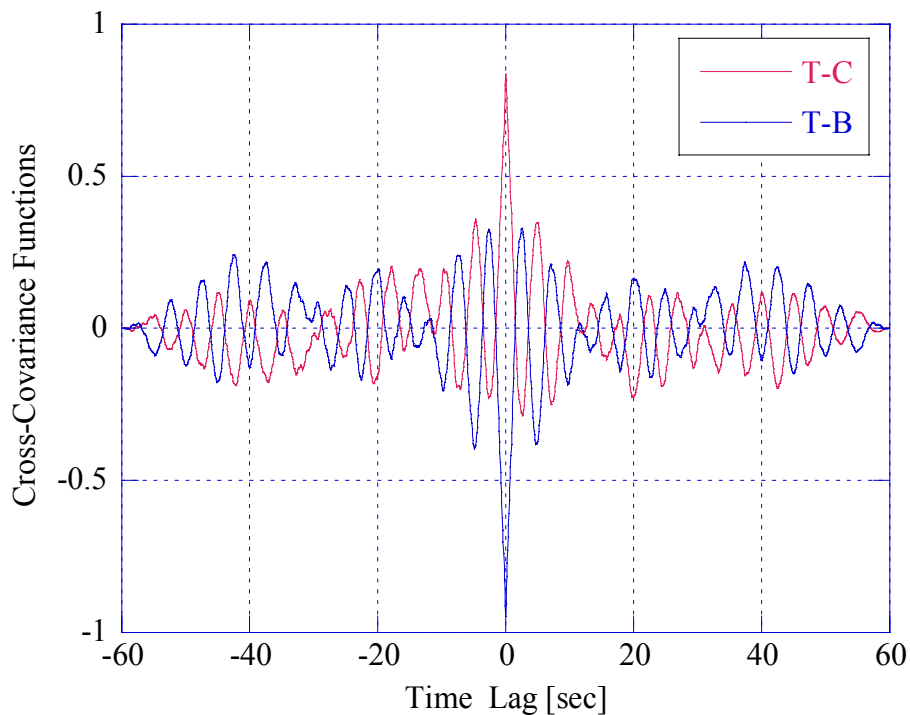
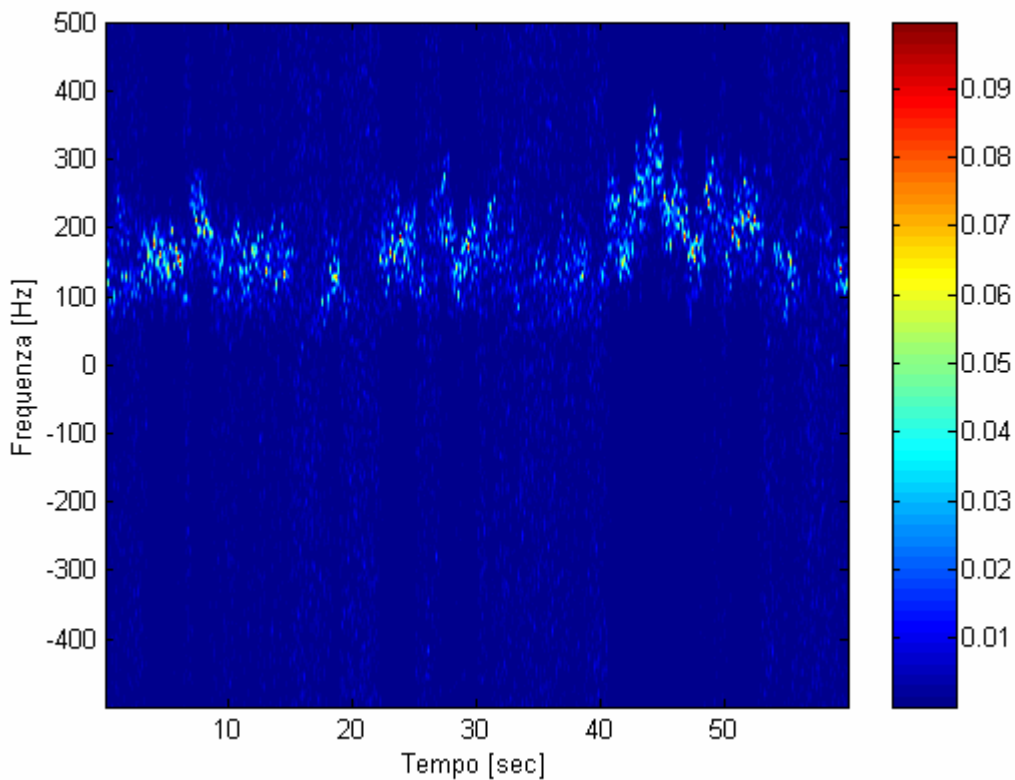


Figure 1.51 - Texture-centroid and texture-bandwidth cross-covariance, 15<sup>th</sup> range cell, VV pol., per. sym.



**Figure 1.52** - Log-texture-centroid and Log-texture-bandwidth cross-covariance, 15<sup>th</sup> range cell, VV pol.



**Figure 1.53** - Normalized spectrum versus time, 5<sup>th</sup> range cell, VV pol. (CNR=11.7 dB)

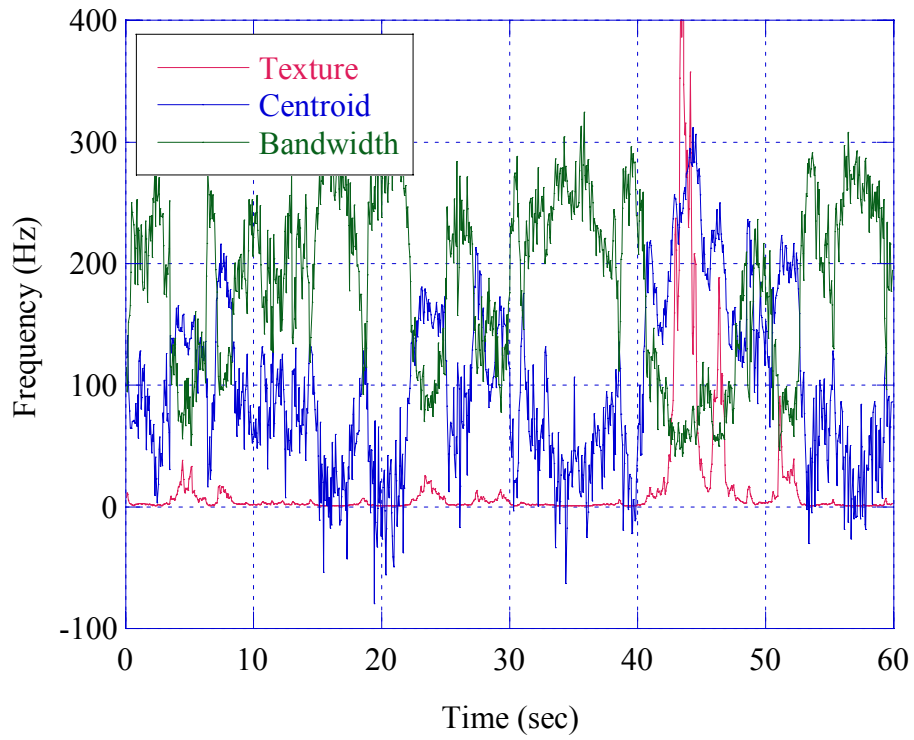


**Figure 1.54a** - Time evolution of texture, centroid and bandwidth, 5<sup>th</sup> range cell, VV pol.

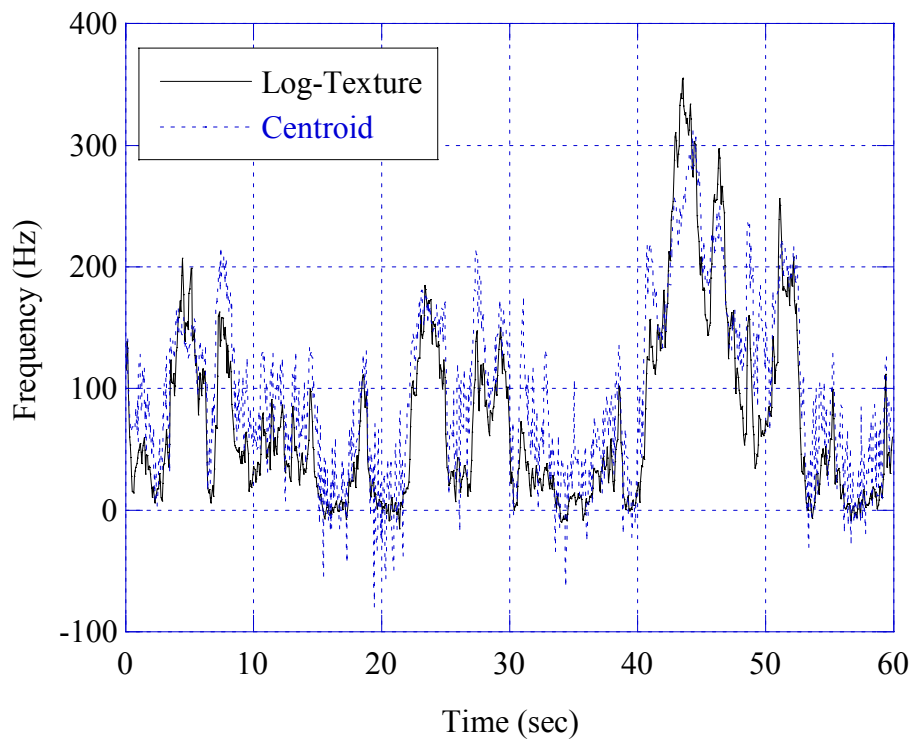


**Figure 1.54b** - Time evolution of Log-texture and centroid, 5<sup>th</sup> range cell, VV pol.

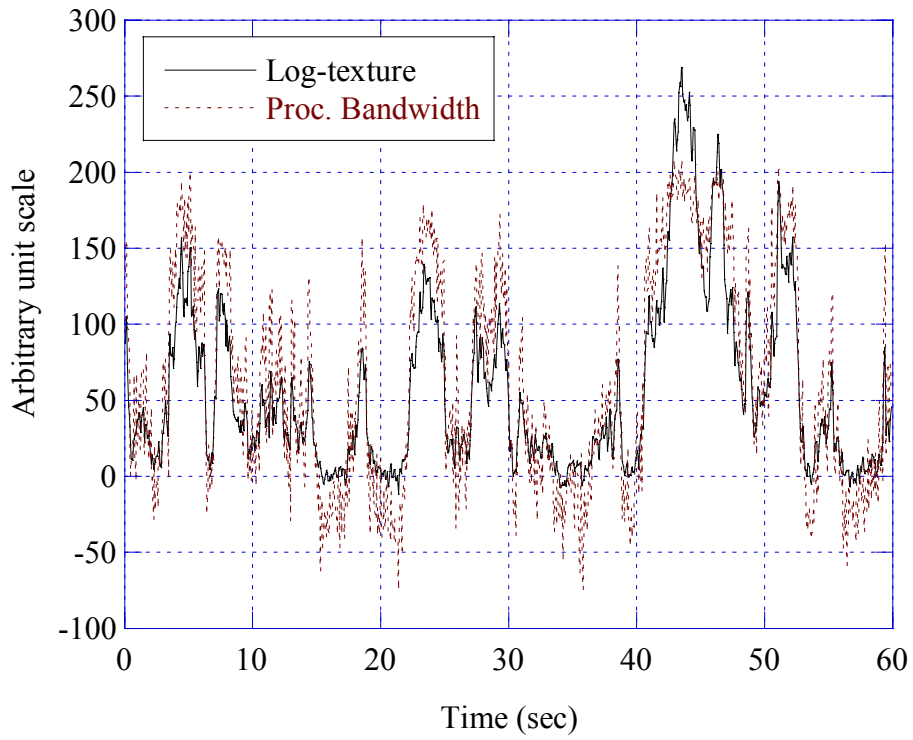


Figure 1.54c - Time evolution of Log-texture and processed bandwidth, 5<sup>th</sup> range cell, VV pol.

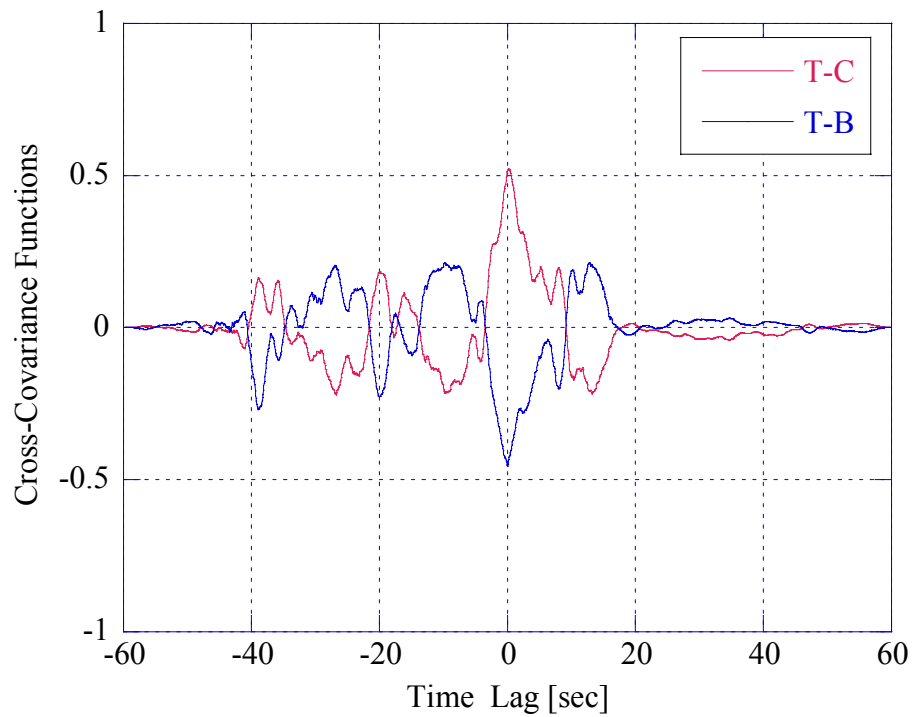


Figure 1.55 - Texture-centroid and texture-bandwidth cross-covariance, 5<sup>th</sup> range cell, VV pol., aper. sym.

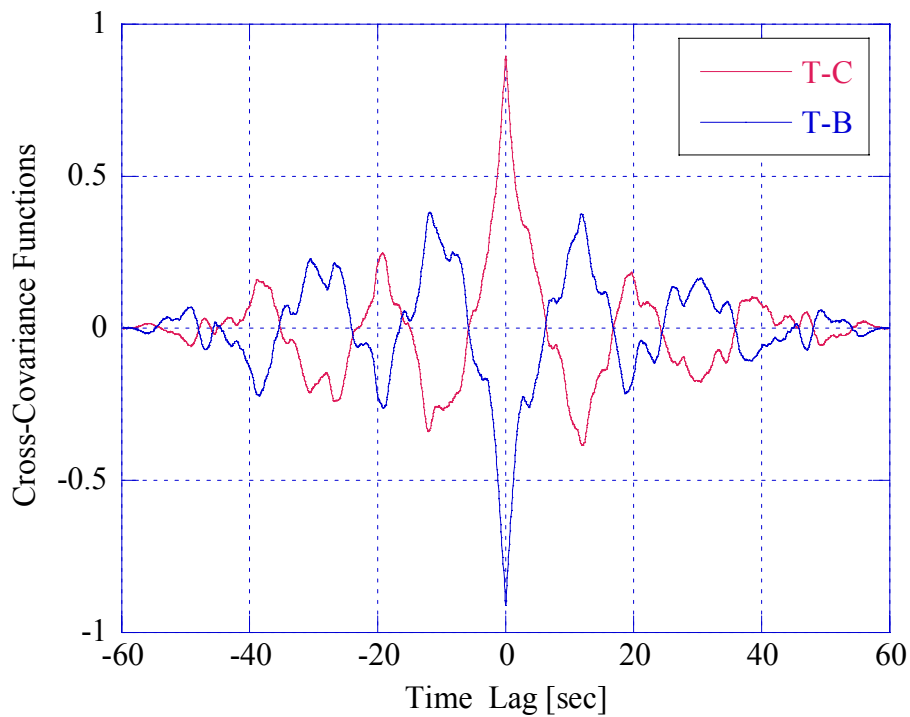


Figure 1.56 - Log-texture-centroid and Log-texture-bandwidth cross-covariance, 5<sup>th</sup> range cell, VV pol.

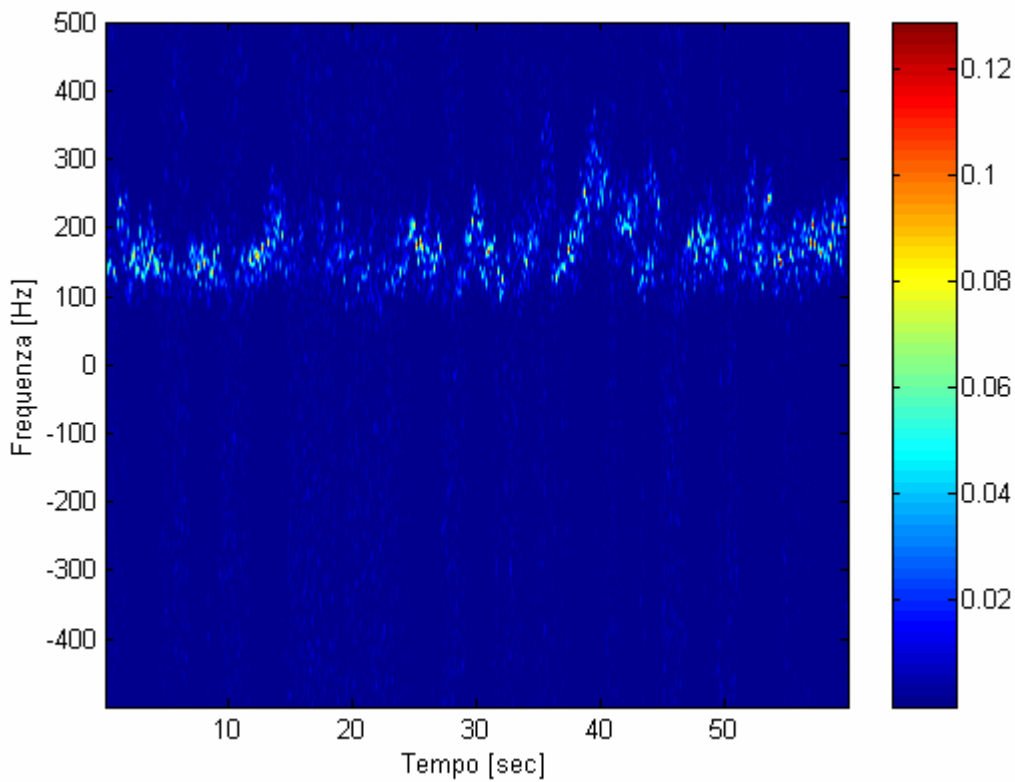


Figure 1.57 - Normalized spectrum versus time, 15<sup>th</sup> range cell, HH pol. (CNR=9 dB)

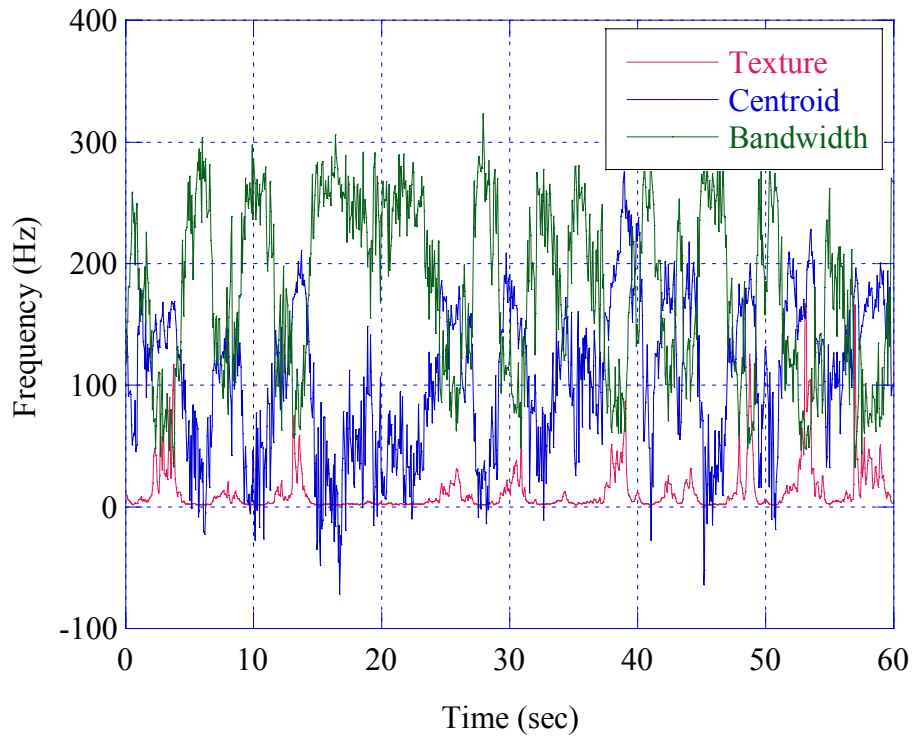


Figure 1.58 - Time evolution of texture, centroid and bandwidth, 15<sup>th</sup> range cell, HH pol.

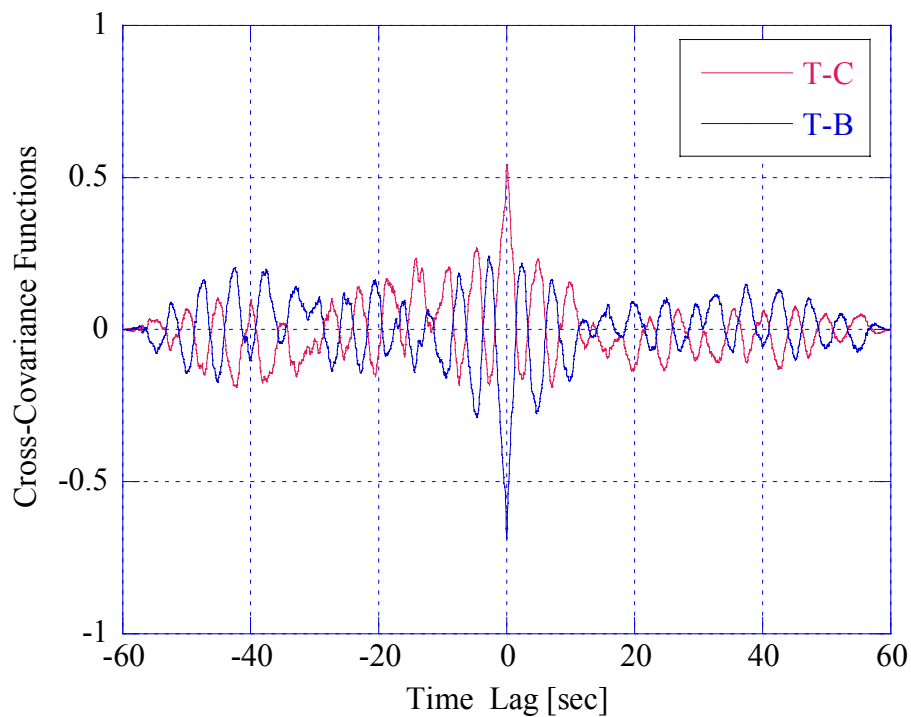
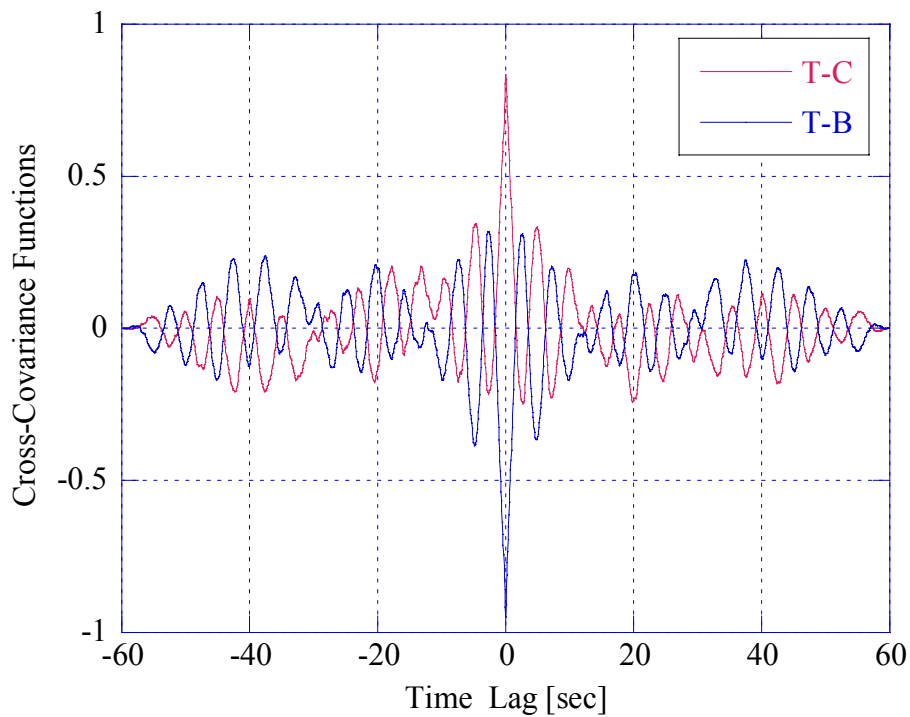
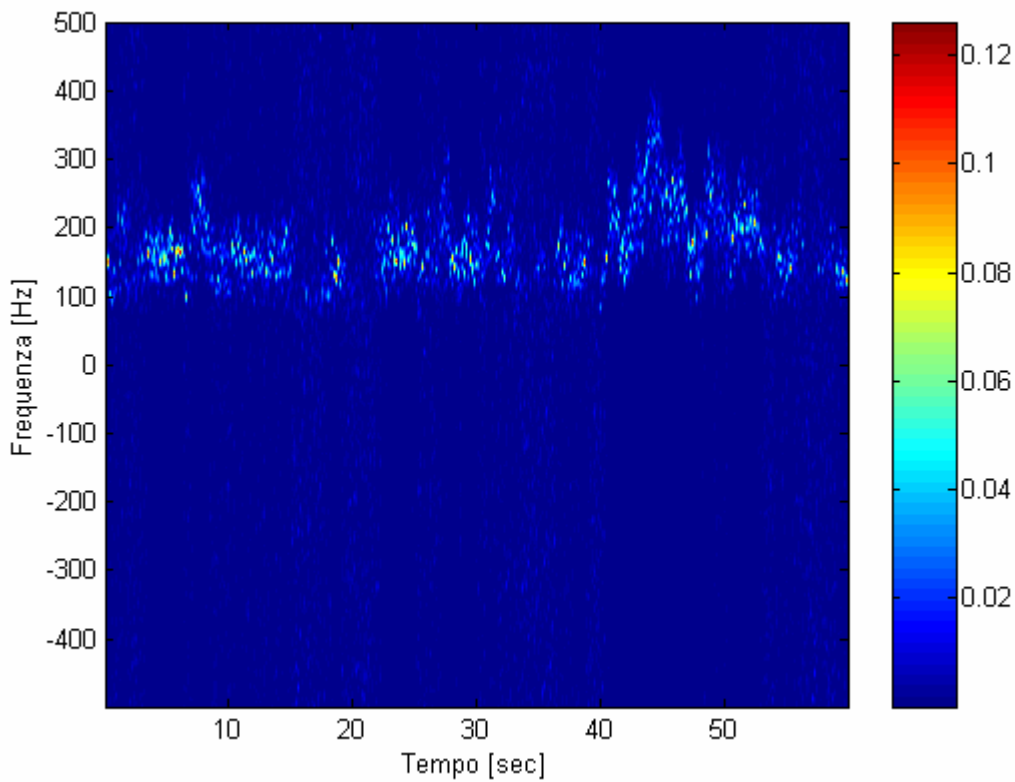


Figure 1.59 - Texture-centroid and texture-bandwidth cross-covariance, 15<sup>th</sup> range cell, HH pol., per. sym.



**Figure 1.60** - Log-texture-centroid and Log-texture-bandwidth cross-covariance, 15<sup>th</sup> range cell, HH pol.



**Figure 1.61** - Normalized spectrum versus time, 5<sup>th</sup> range cell, HH pol. ( $CNR=13$  dB)

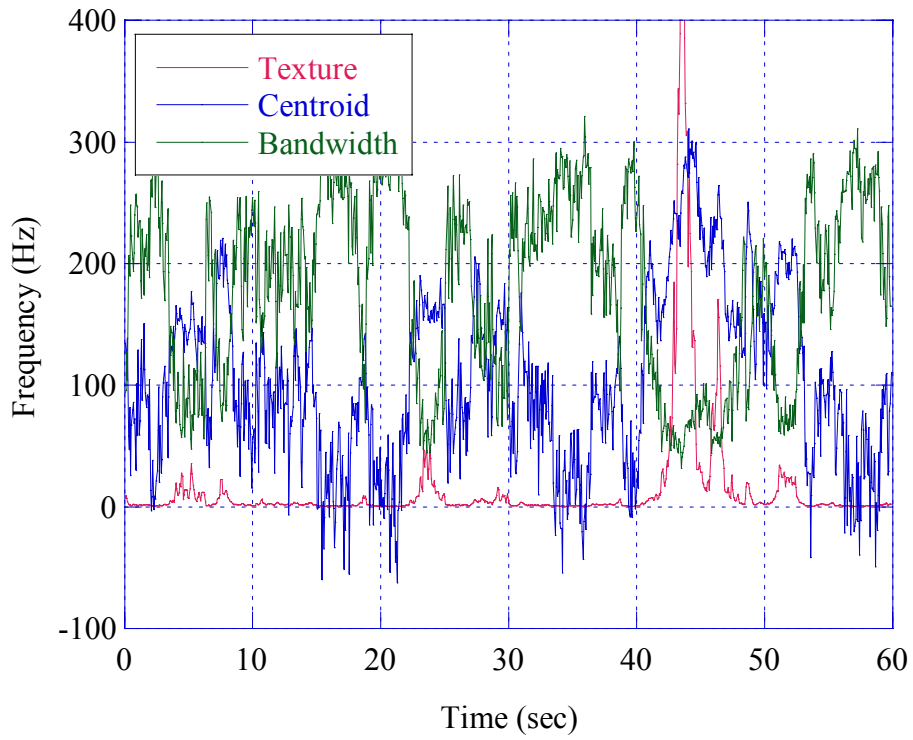


Figure 1.62 - Time evolution of texture, centroid and bandwidth, 5<sup>th</sup> range cell, HH pol.

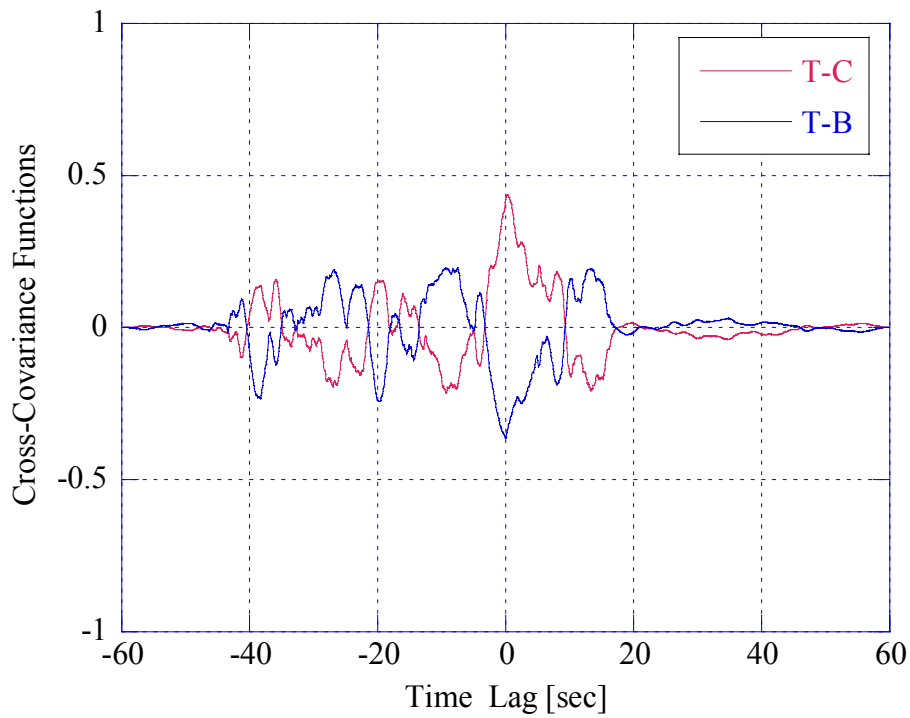


Figure 1.63 - Texture-centroid and texture-bandwidth cross-covariance, 5<sup>th</sup> range cell, HH pol., aper. sym.

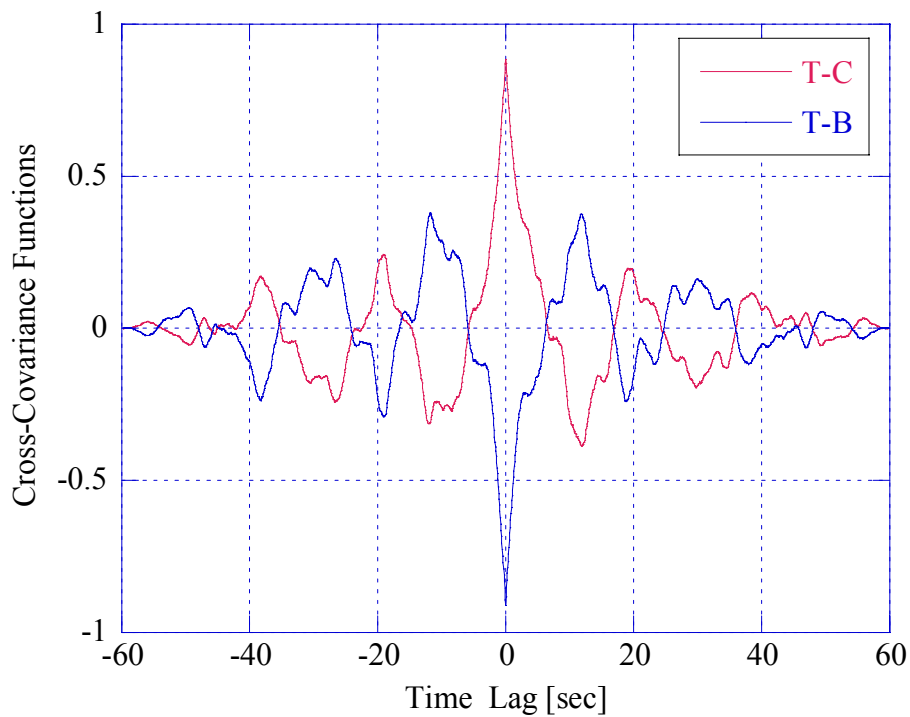


Figure 1.64 - Log-texture-centroid and Log-texture-bandwidth cross-covariance, 5<sup>th</sup> range cell, HH pol.

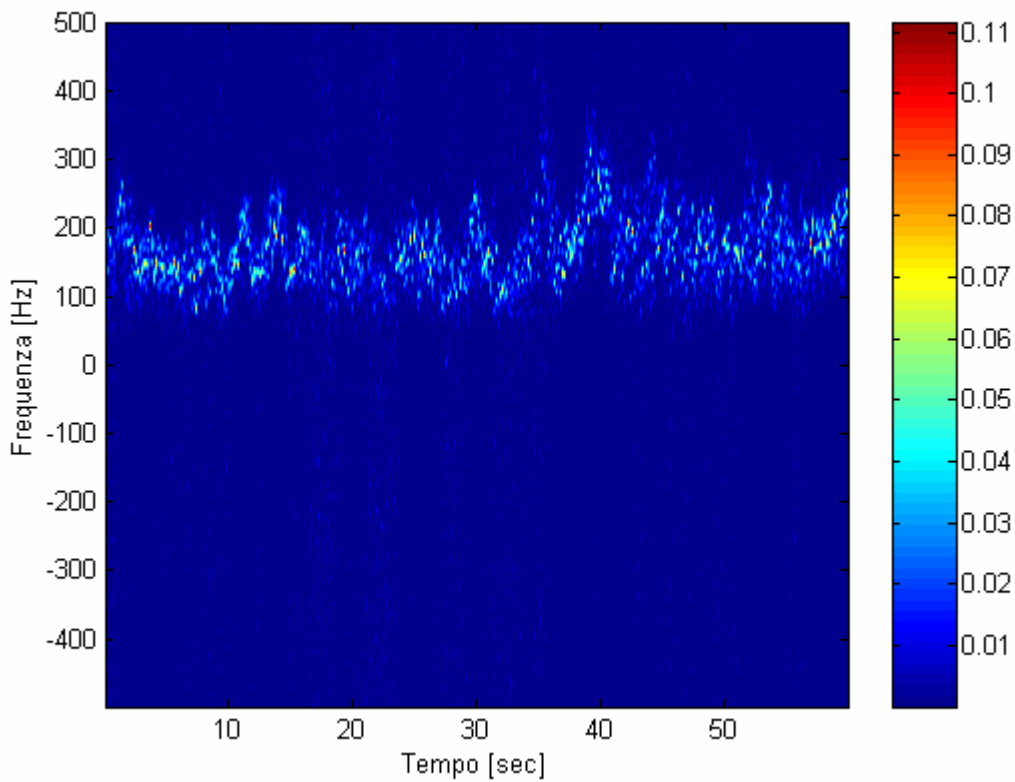


Figure 1.65 - Normalized spectrum versus time, 15<sup>th</sup> range cell, VH pol. (CNR=9 dB)

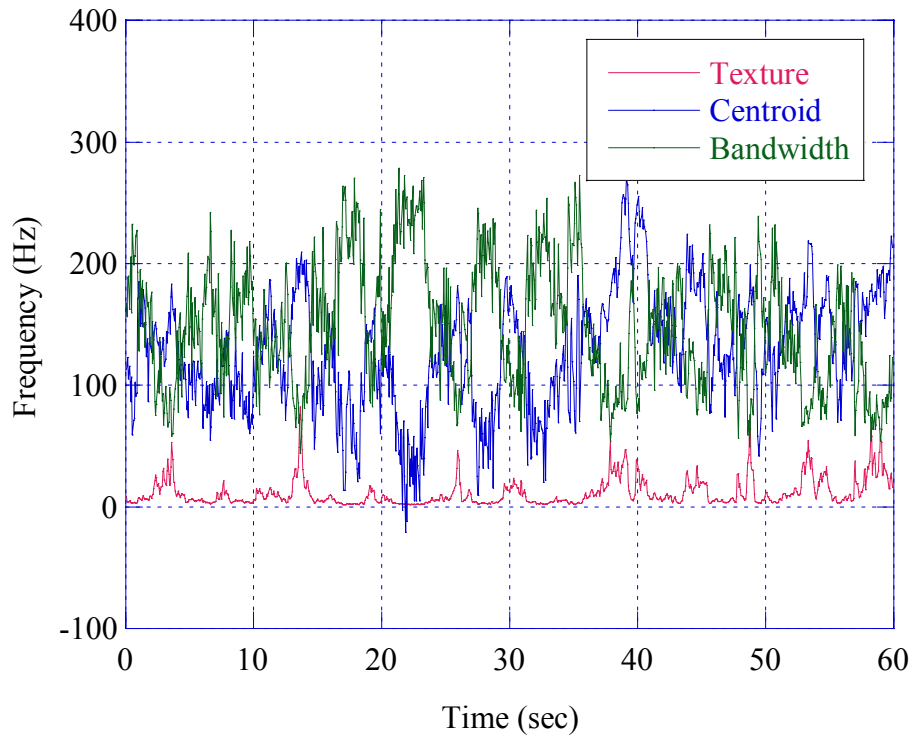


Figure 1.66 - Time evolution of texture, centroid and bandwidth, 15<sup>th</sup> range cell, VH pol.

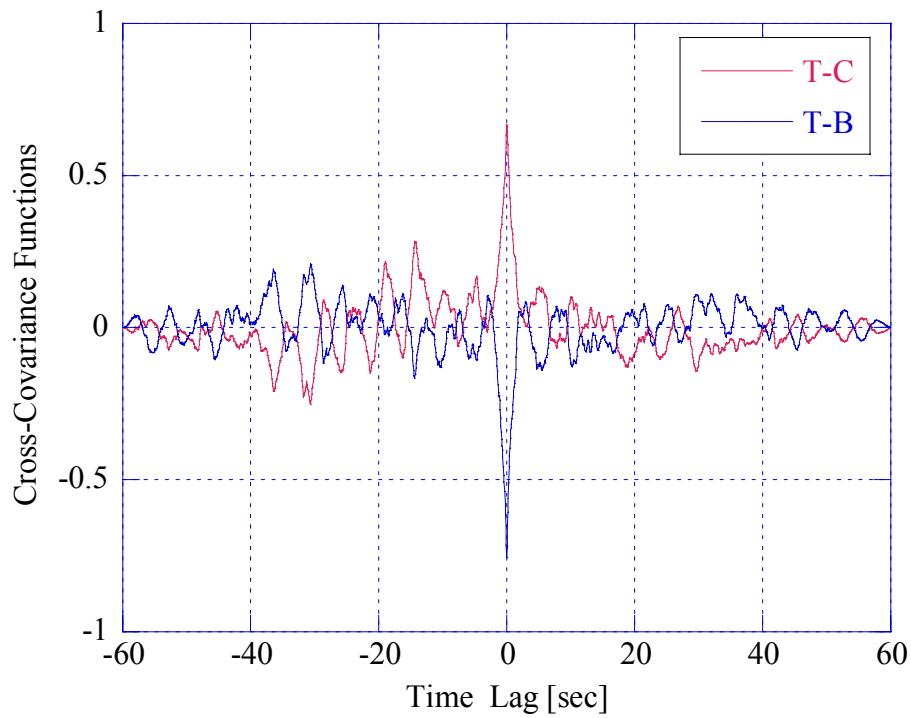
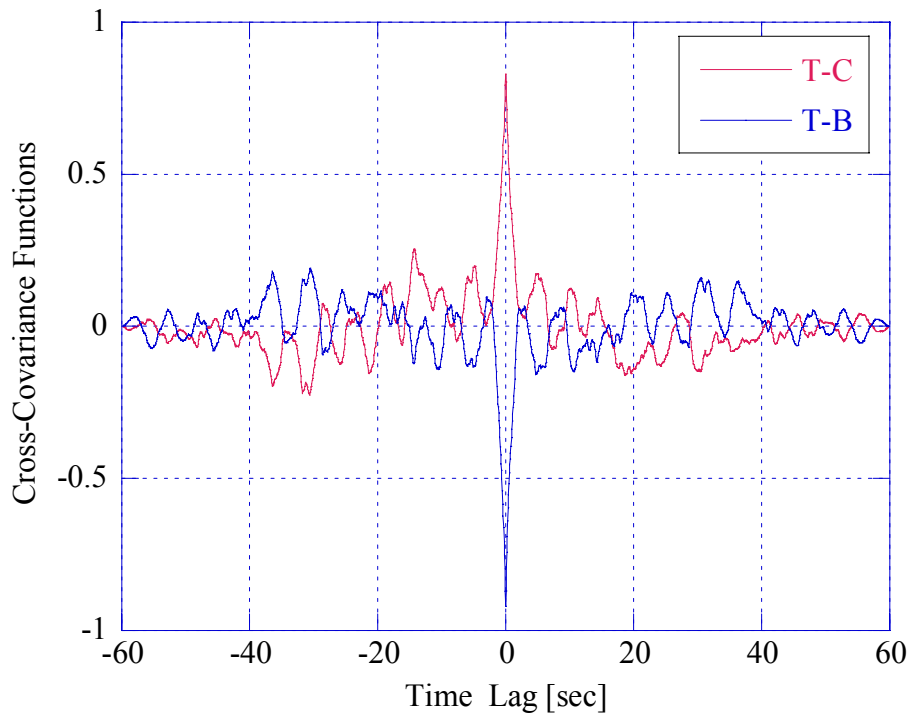
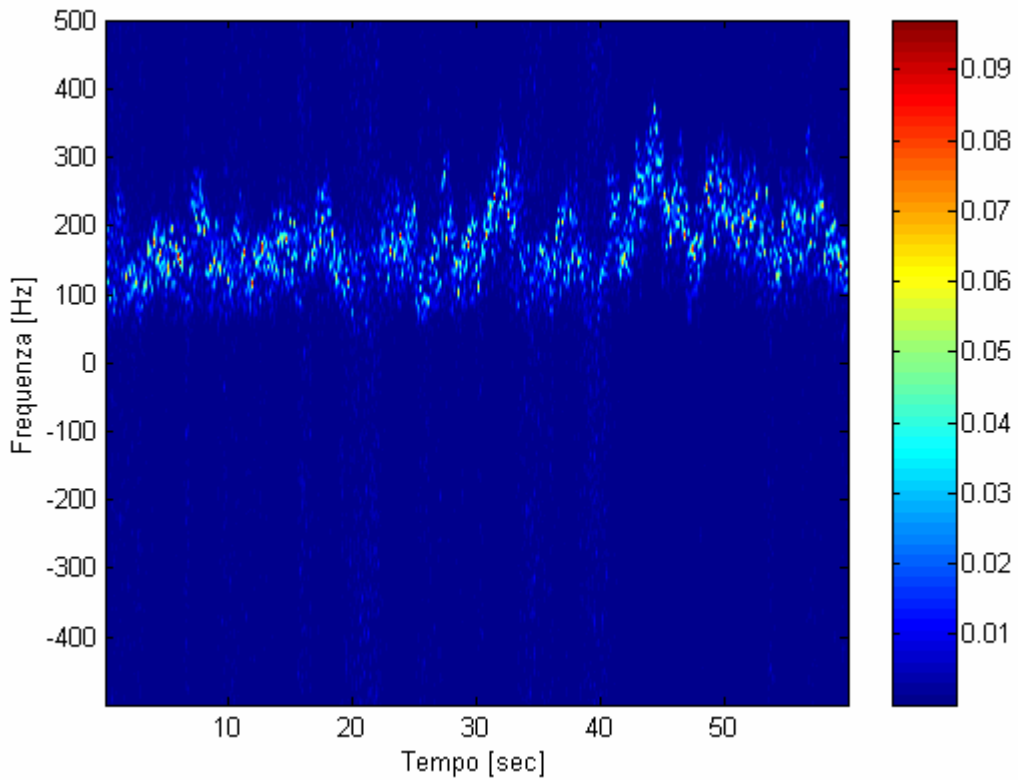


Figure 1.67 - Texture-centroid and texture-bandwidth cross-covariance, 15<sup>th</sup> range cell, VH pol., per. sym.



**Figure 1.68** - Log-texture-centroid and Log-texture-bandwidth cross-covariance, 15<sup>th</sup> range cell, VH pol.



**Figure 1.69** - Normalized spectrum versus time, 5<sup>th</sup> range cell, VH pol. (CNR=11.5 dB)

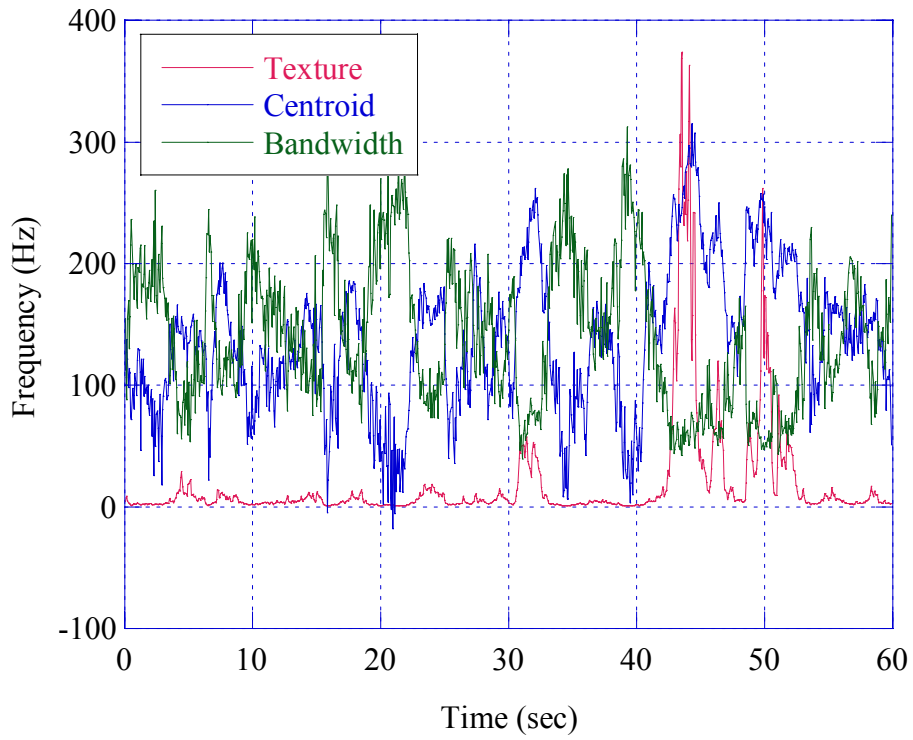


**Figure 1.70** - Time evolution of texture, centroid and bandwidth, 5<sup>th</sup> range cell, VH pol.

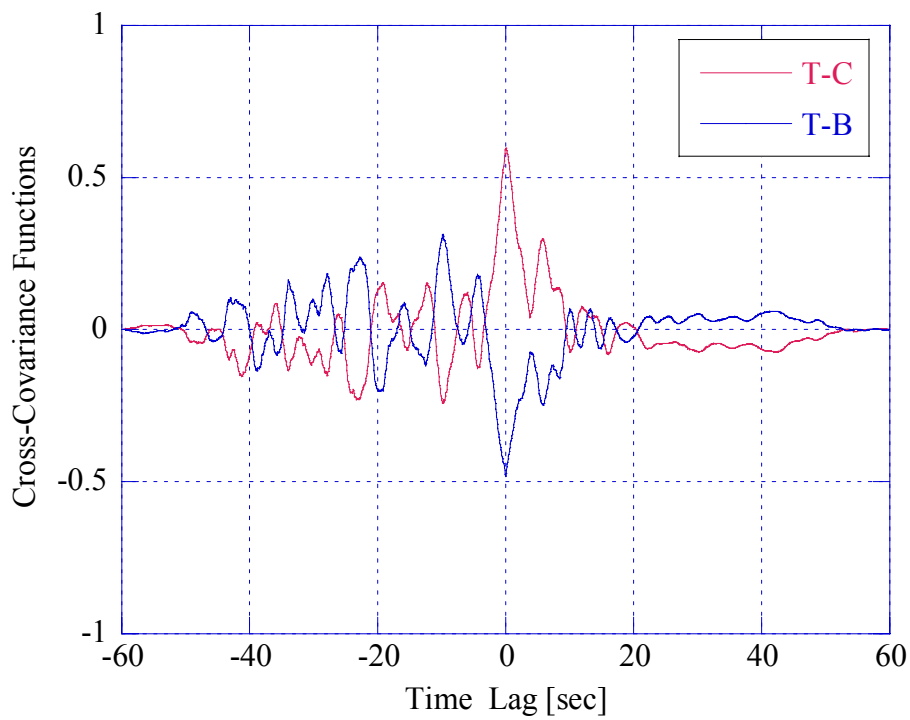


**Figure 1.71** - Texture-centroid and texture-bandwidth cross-covariance, 5<sup>th</sup> range cell, VH pol., aper. sym.

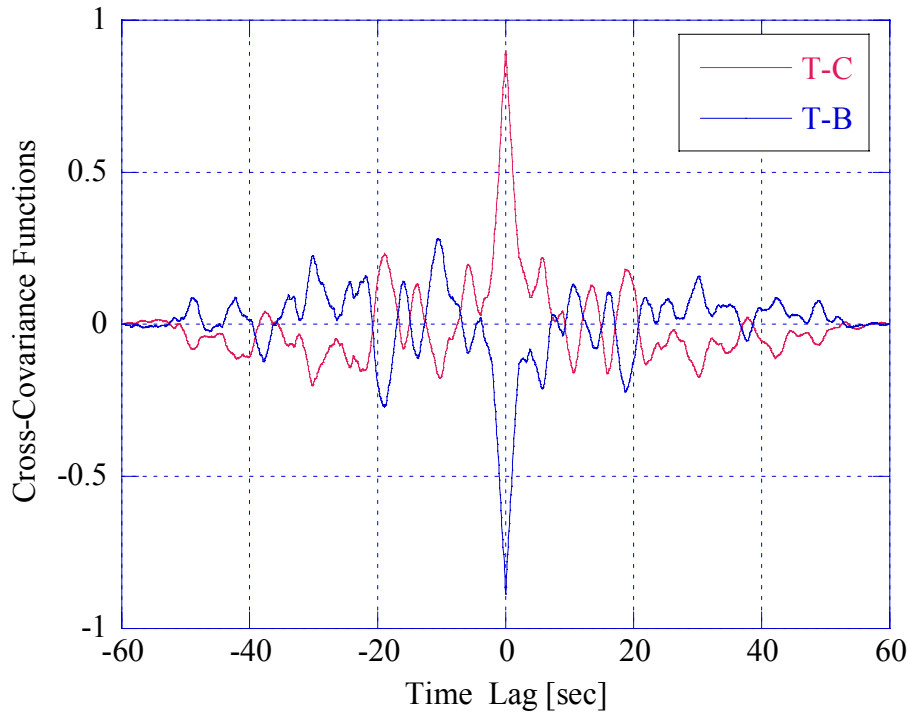


**Figure 1.72** - Log-texture-centroid and Log-texture-bandwidth cross-covariance, 5<sup>th</sup> range cell, VH pol.

### 1.2.4 Range resolution of 9 m

The results obtained at the range resolutions of 9 m in some cells confirm what was shown by previous resolutions, as for the 26<sup>th</sup> range cell, in all the polarizations (Figs. 1.73-1.1.76, 1.81-1.84 and 1.89-1.92). The period is again around 5 sec.

However, often, the thermal noise level is locally high; and the clutter behavior is not always clearly visible. Let's analyze the behavior of the 1<sup>st</sup> range cell, VV data, in the Figures 1.77-1.80. Figure 1.77 and Figure 1.78a show that in the time range [0, 25] sec the thermal noise is dominant. In the spectrogram, we see light blue stripes along the whole frequency axis and in Fig. 1.78a the Doppler centroid is close to zero and the bandwidth gets high values around 300 Hz. On the other hand, in the time interval [25, 45] sec, we observe 4 spikes, the texture and centroid increase, the bandwidth decreases as already observed in lower resolutions. It is interesting now to analyze Figs. 1.78b and 1.78c. Where the clutter is dominant ([25, 45] sec), centroid and bandwidth follow closely the behavior of the Log-texture, where the thermal noise is dominant we observe non-negligible discrepancies. That is not surprising because clutter and thermal noise are

independent processes and the behavior of the thermal noise is not affected by long-wave effect.

	<b>Periodical Symmetrical</b>	<b>Periodical Asymmetrical</b>	<b>Aperiodical Symmetrical</b>
Pol. VV	26, 24, 23, 21, 20, 19,17, 16, 14, 12	_____	28,27, 25, 22, 18, 15, 13, 11,10, 9, 8, 7, 6, 5, 4, 3, 2, 1
Pol. HH	26, 23, 22, 21, 20, 19, 16, 14, 13, 12	_____	28, 27, 25, 24, 18, 17, 15, 11, 10 9, 8, 7, 6, 5, 4, 3, 2, 1
Pol. VH	26,25,16	_____	All the others

**Table 1.4** – Covariance classification, 9 m.

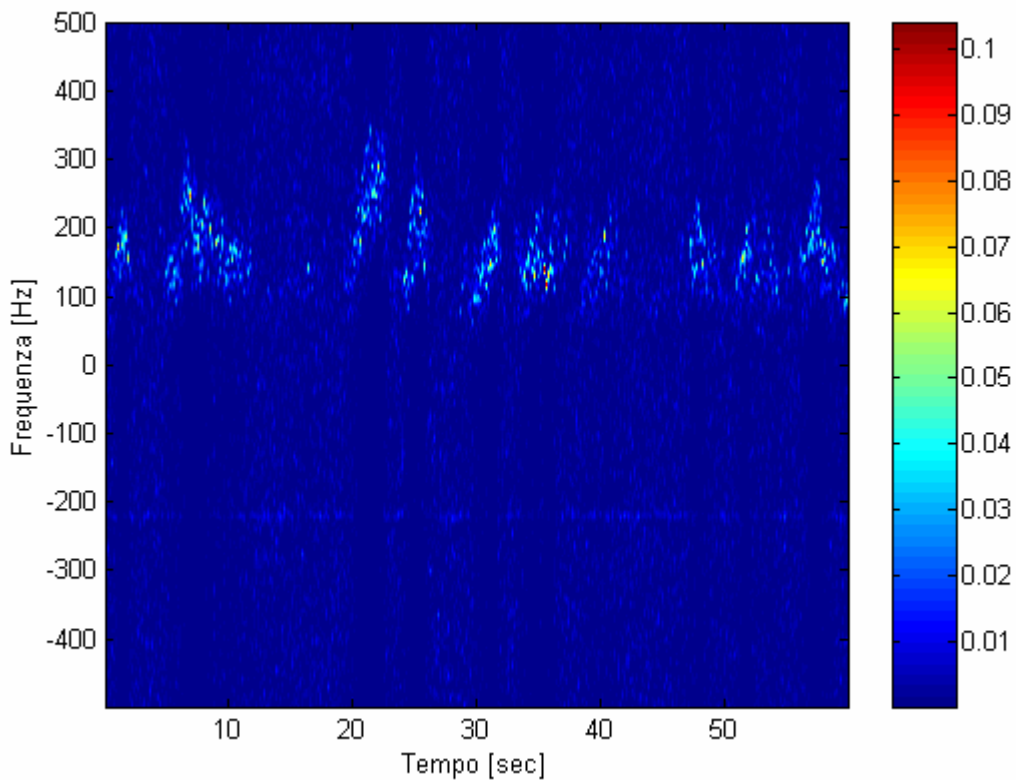


**Figure 1.73** - Normalized spectrum versus time, VV pol., 26th range cell. ( CNR=1.2 dB )

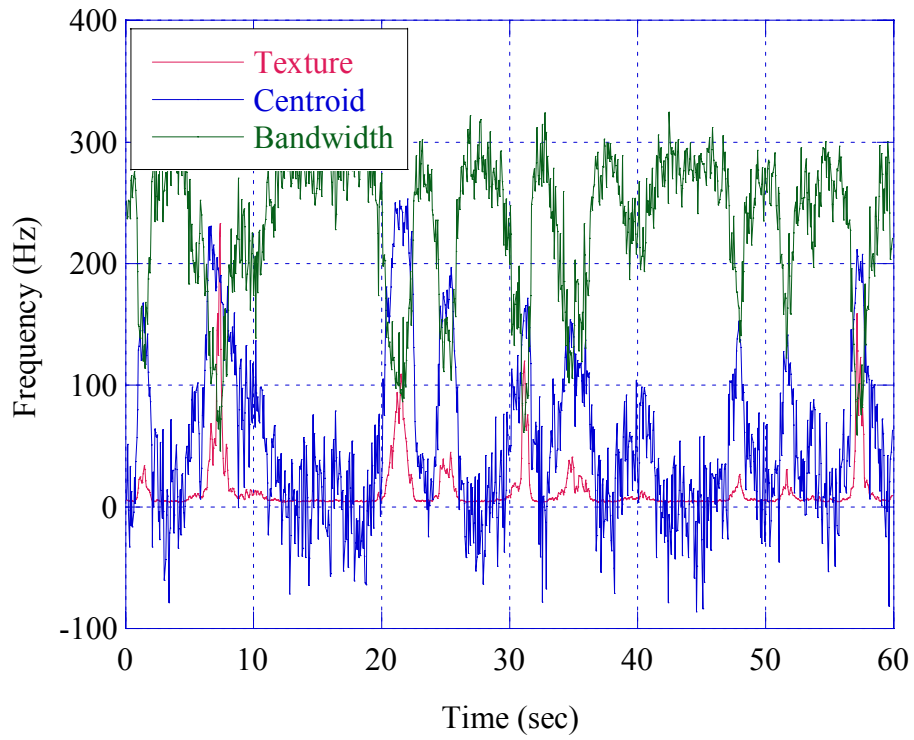


**Figure 1.74** - Time evolution of texture, centroid and bandwidth, VV pol., 26<sup>th</sup> range cell.

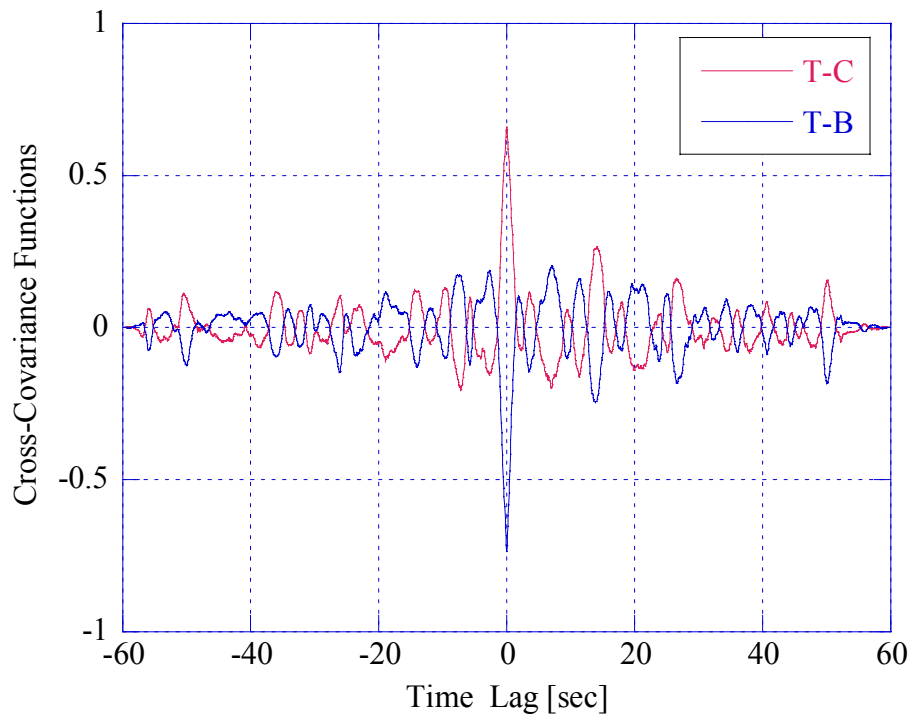


**Figure 1.75** - Texture-centroid and texture-bandwidth cross-covariance, VV pol., 26<sup>th</sup> range cell, per. sym.

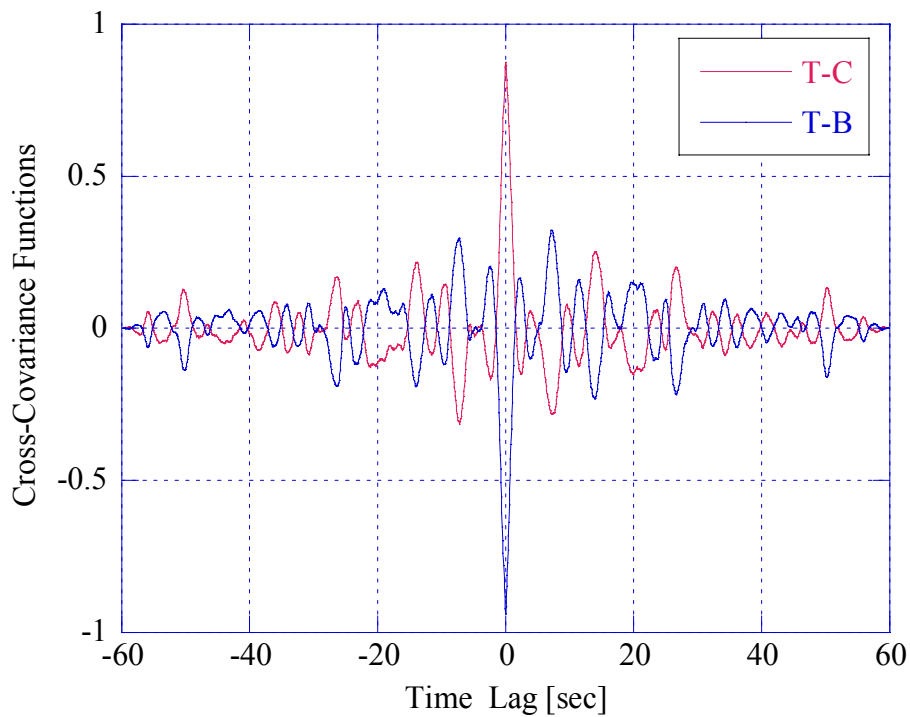


**Figure 1.76** - Log-texture-centroid and Log-texture-bandwidth cross-covariance, VV pol., 26<sup>th</sup> range cell.

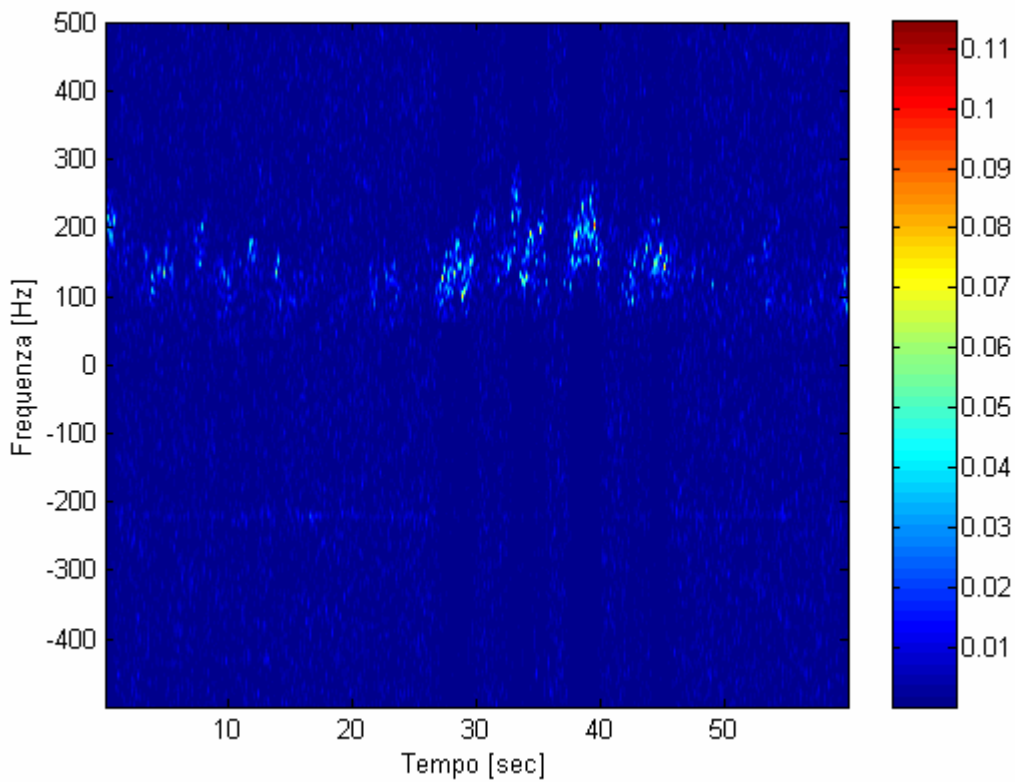


**Figure 1.77** - Normalized spectrum versus time, VV pol., 1<sup>st</sup> range cell. (CNR=3 dB)

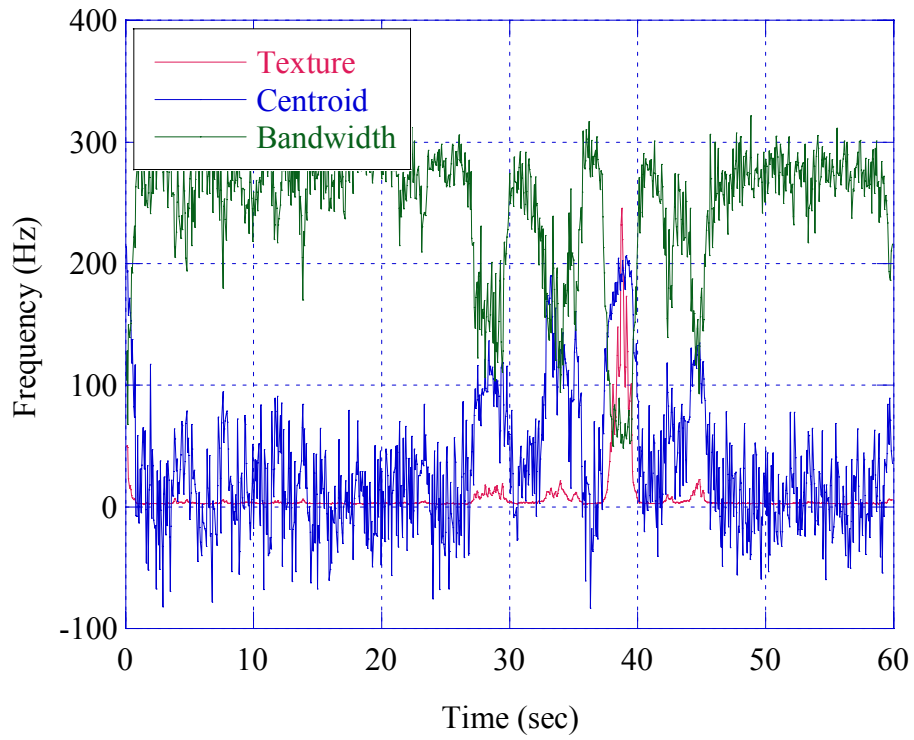


**Figure 1.78a** - Time evolution of texture, centroid and bandwidth, VV pol., 1<sup>st</sup> range cell.

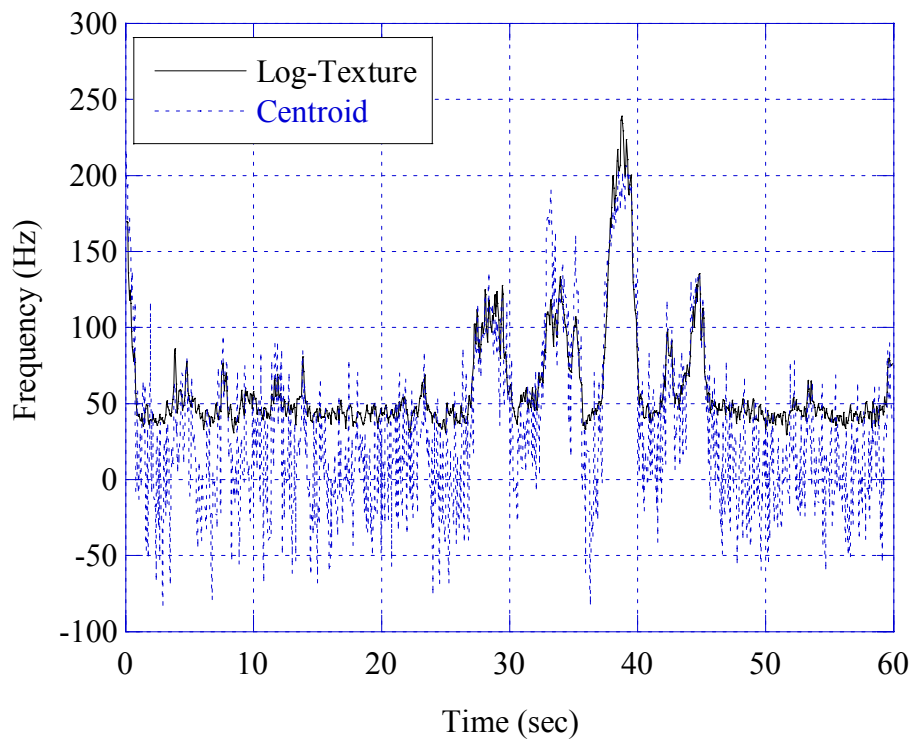


**Figure 1.78b** - Time evolution of Log-texture and centroid, VV pol., 1<sup>st</sup> range cell.

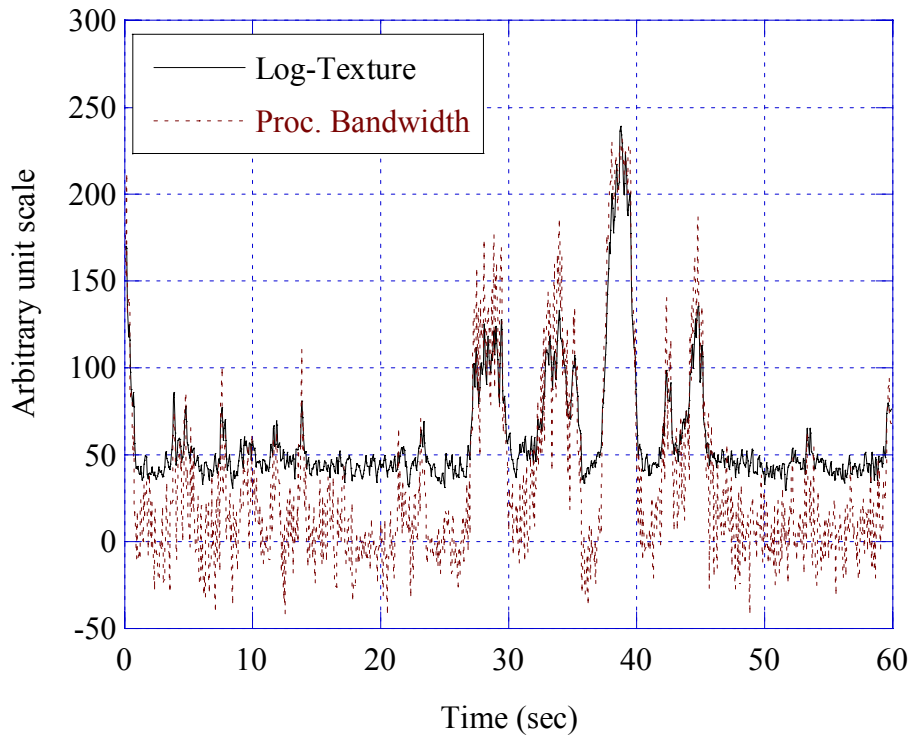


**Figure 1.78c** - Time evolution of Log-texture and bandwidth, VV pol., 1<sup>st</sup> range cell.

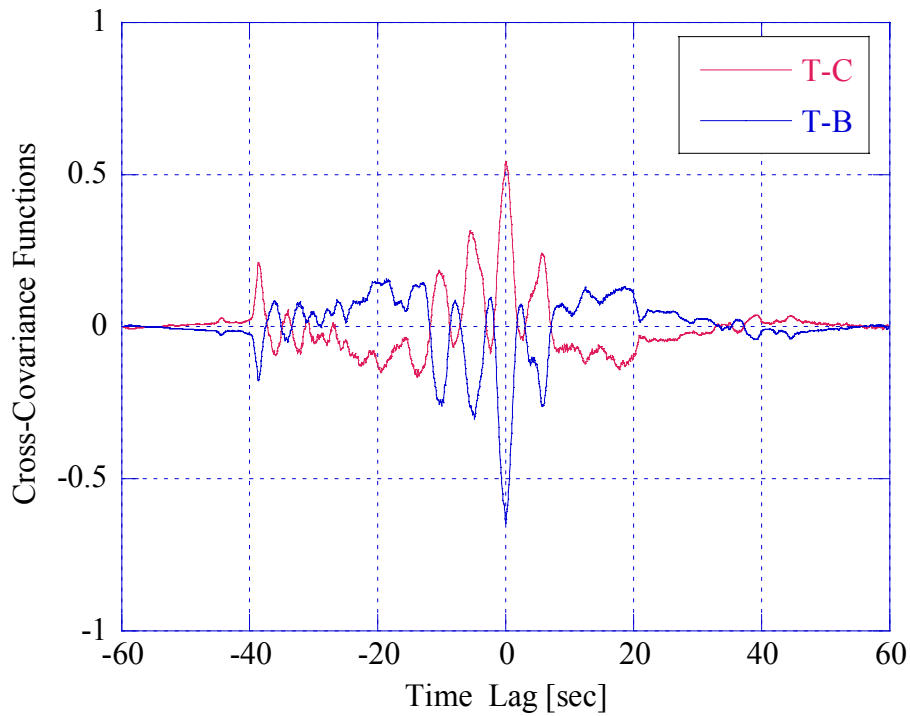


**Figure 1.79** - Texture-centroid and texture-bandwidth cross-covariance, VV pol., 1<sup>st</sup> range cell., aper., sym.

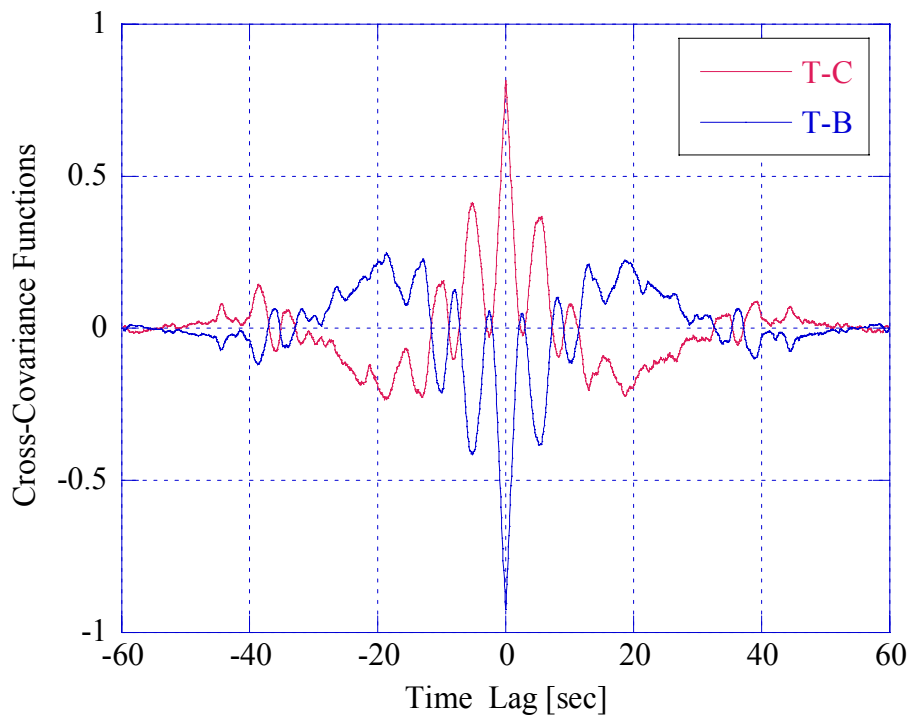


**Figure 1.80** - Log-texture-centroid and Log-texture-bandwidth cross-covariance, VV pol., 1<sup>st</sup> range cell.

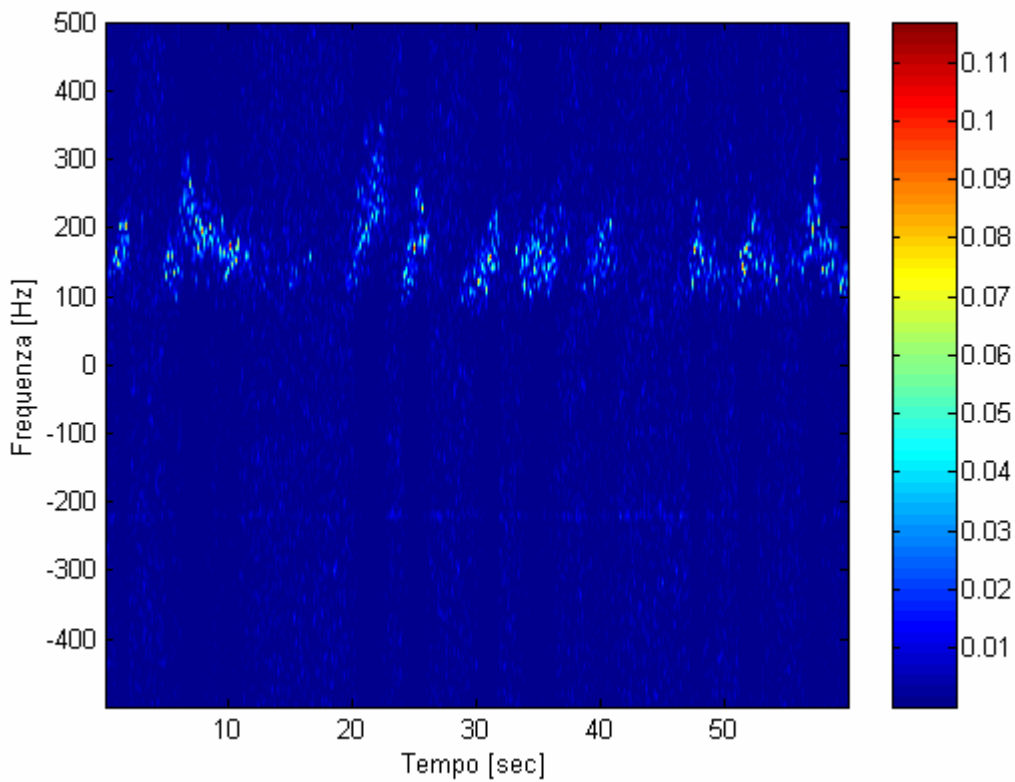


**Figure 1.81** - Normalized spectrum versus time, HH pol., 26th range cell. ( CNR=4.8 dB )

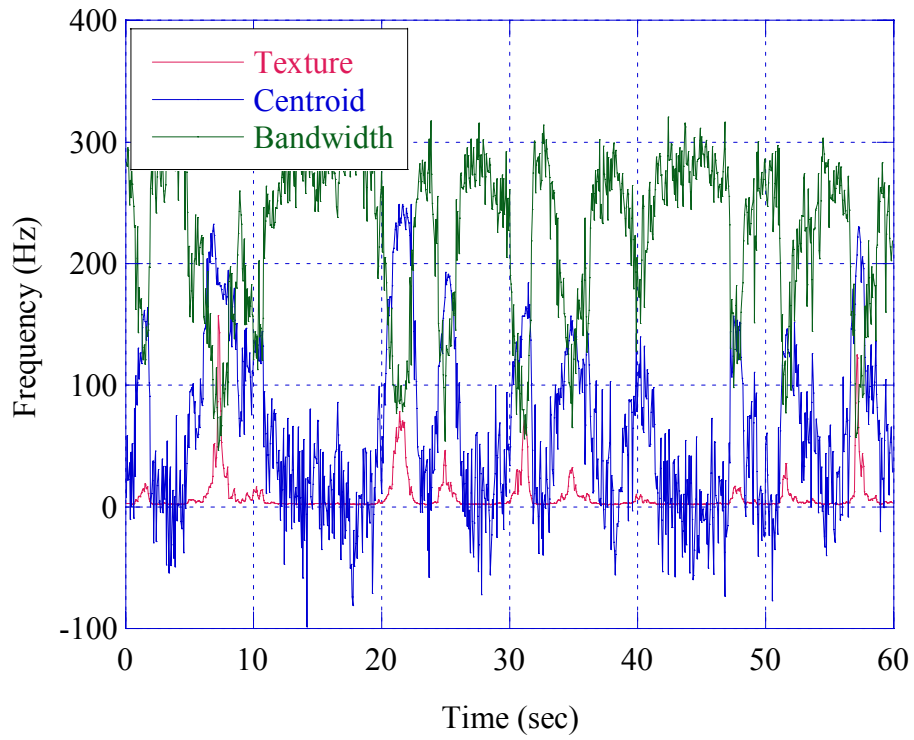


**Figure 1.82** - Time evolution of texture, centroid and bandwidth, HH pol., 26<sup>th</sup> range cell.

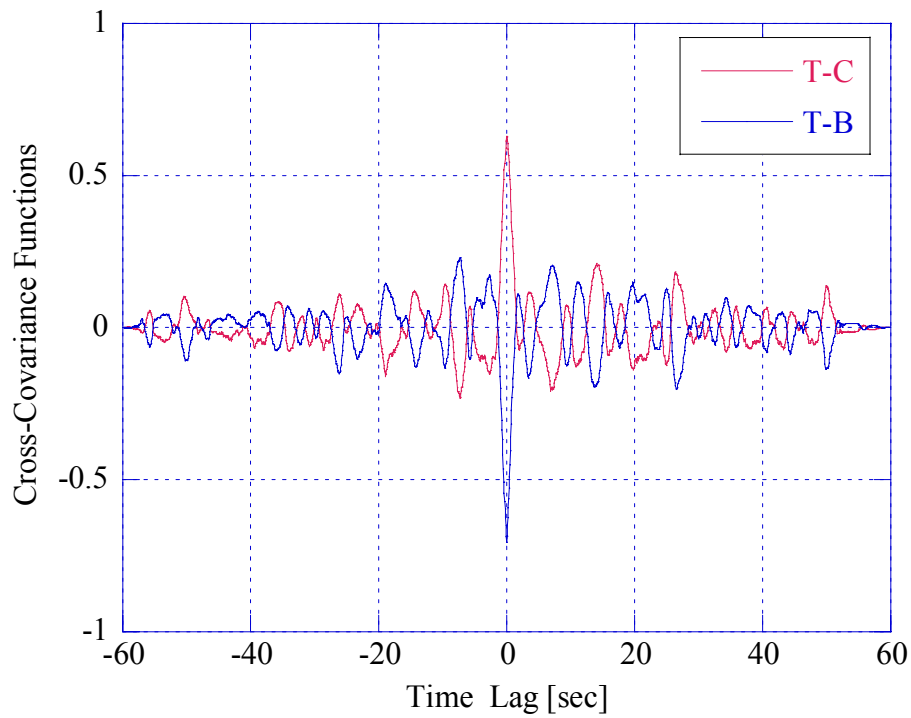


**Figure 1.83** - Texture-centroid and texture-bandwidth cross-covariance, HH pol., 26<sup>th</sup> range cell, per. sym.

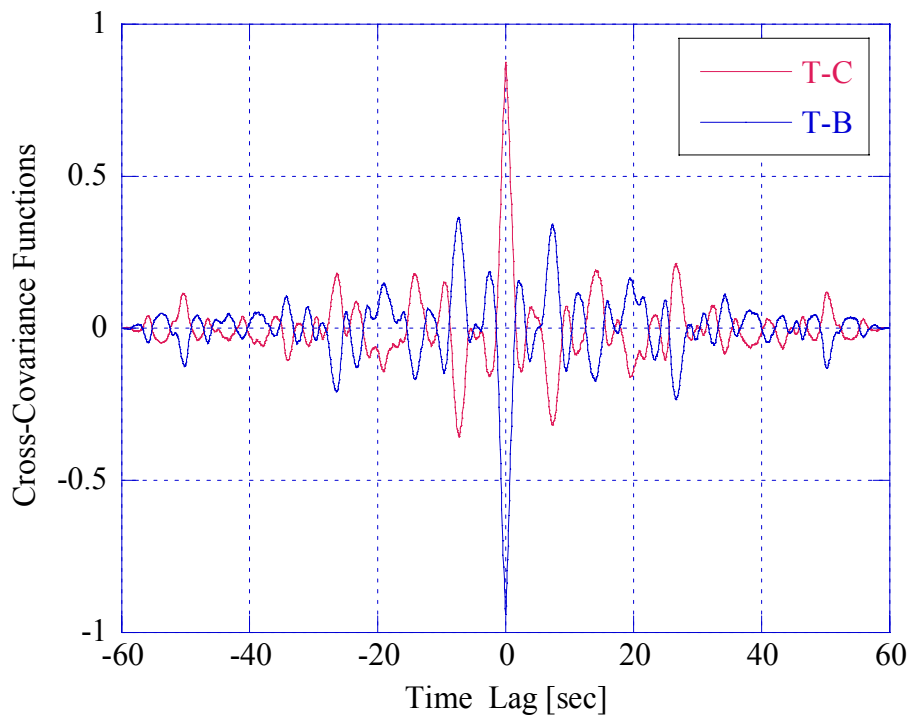


**Figure 1.84** - Log-texture-centroid and Log-texture-bandwidth cross-covariance, HH pol., 26<sup>th</sup> range cell.

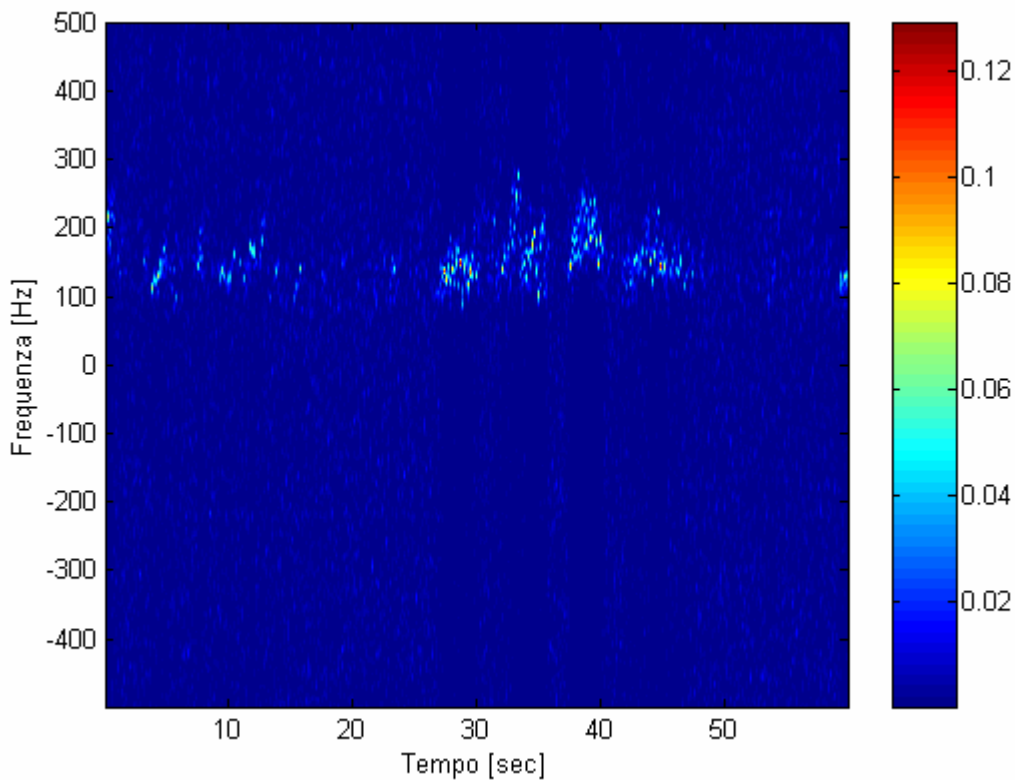


**Figure 1.85** - Normalized spectrum versus time, HH pol., 1<sup>st</sup> range cell ( $CNR=5$  dB)

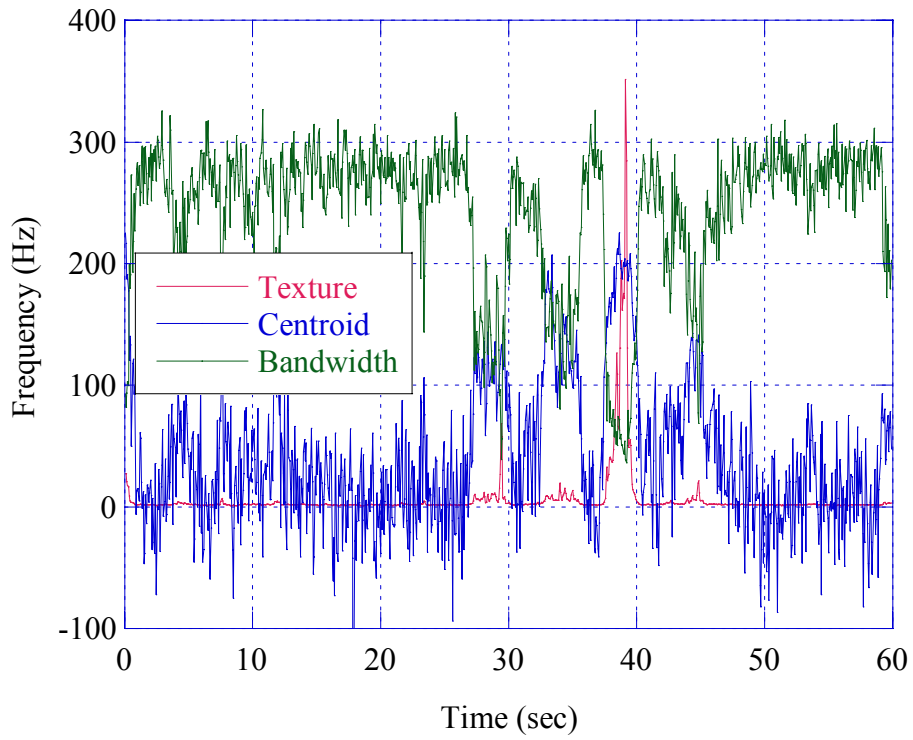


**Figure 1.86** - Time evolution of texture, centroid and bandwidth, HH pol., 1<sup>st</sup> range cell.

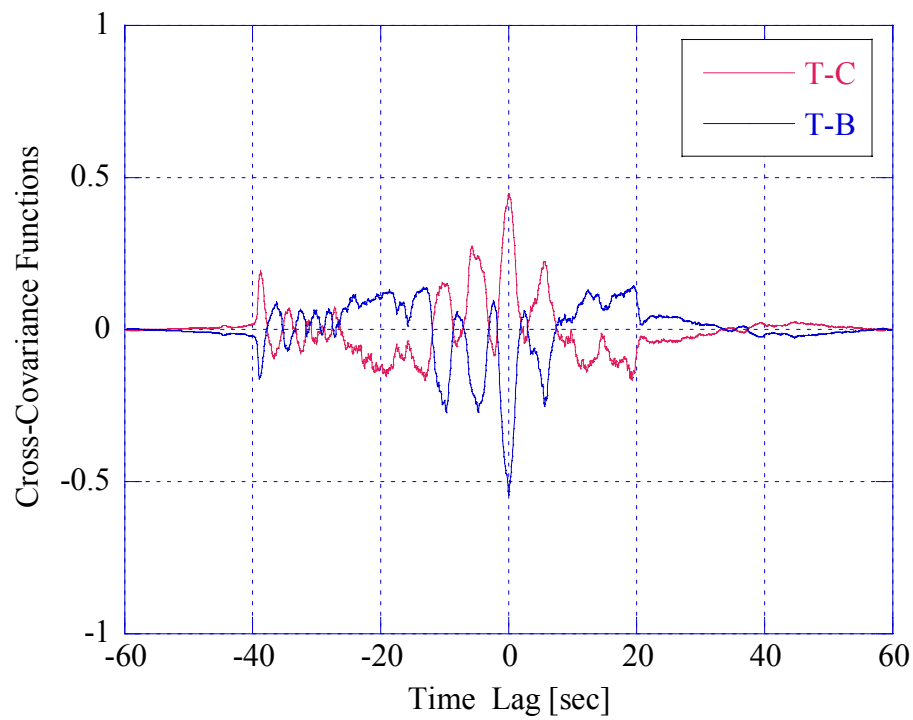


**Figure 1.87** - Texture-centroid and texture-bandwidth cross-covariance, HH pol., 1<sup>st</sup> range cell., aper. sym.

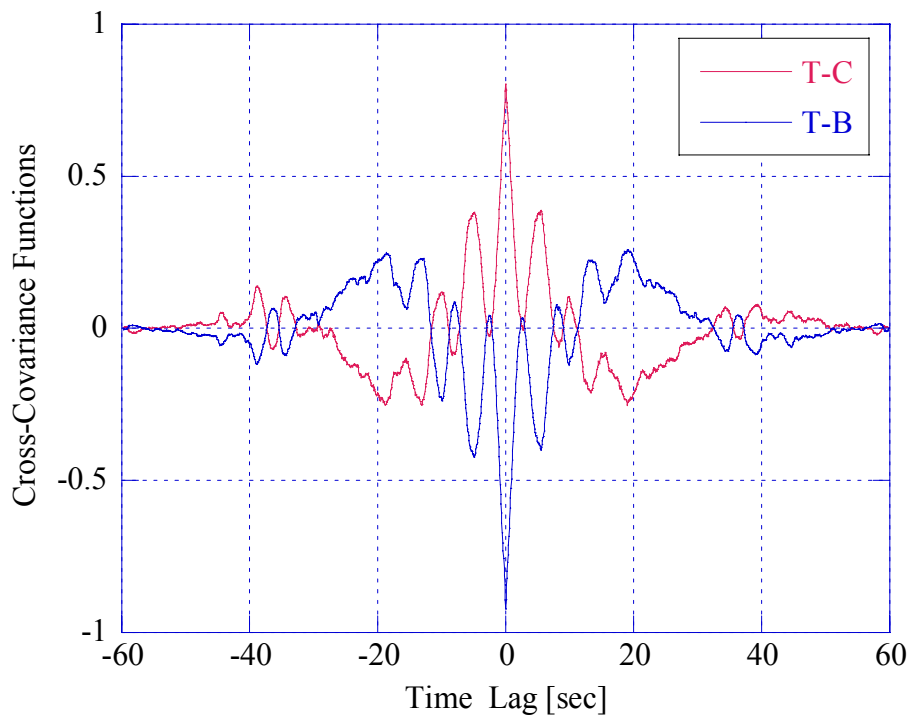


**Figure 1.88** - Log-texture-centroid and Log-texture-bandwidth cross-covariance, HH pol., 1<sup>st</sup> range cell.

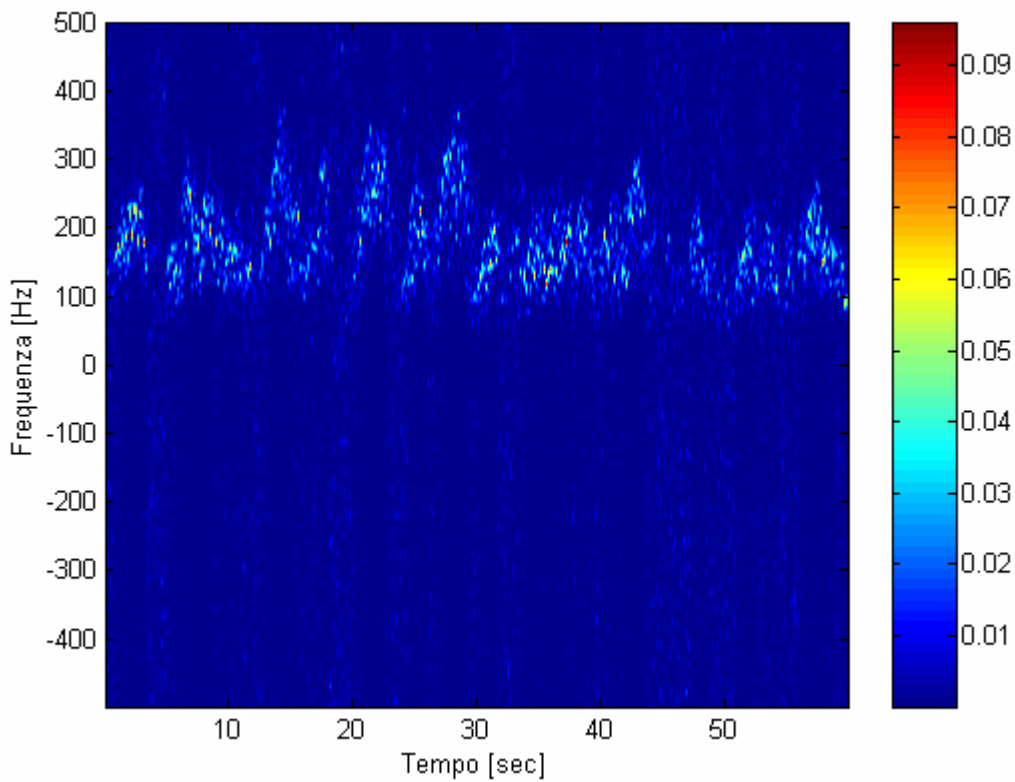


**Figure 1.89** - Normalized spectrum versus time, VH pol., 26th range cell. ( CNR=5.5 dB )

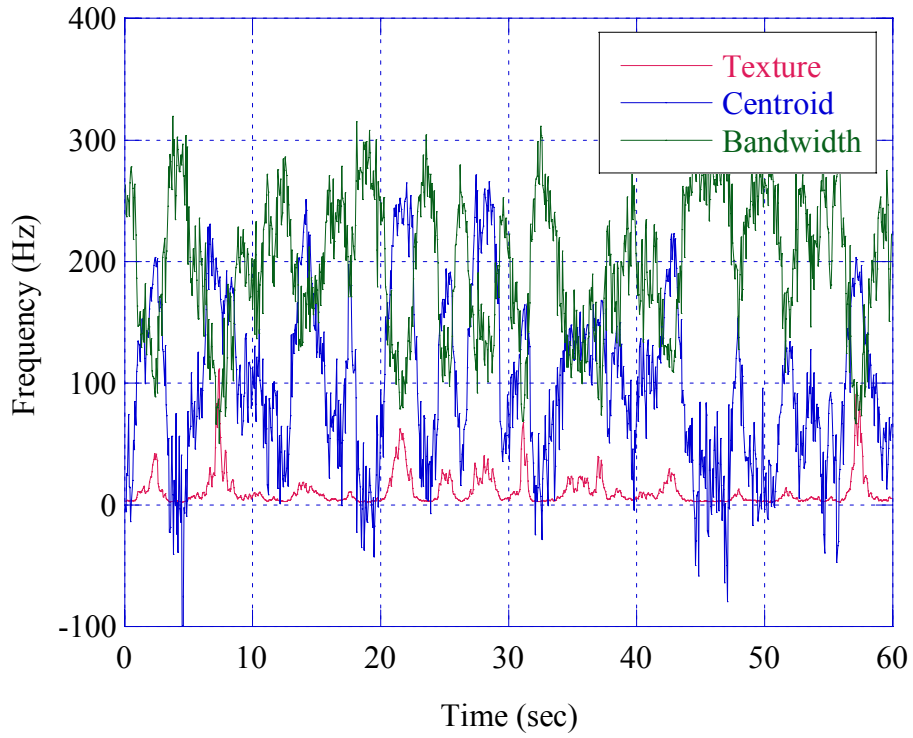


**Figure 1.90** - Time evolution of texture, centroid and bandwidth, VH pol., 26<sup>th</sup> range cell.

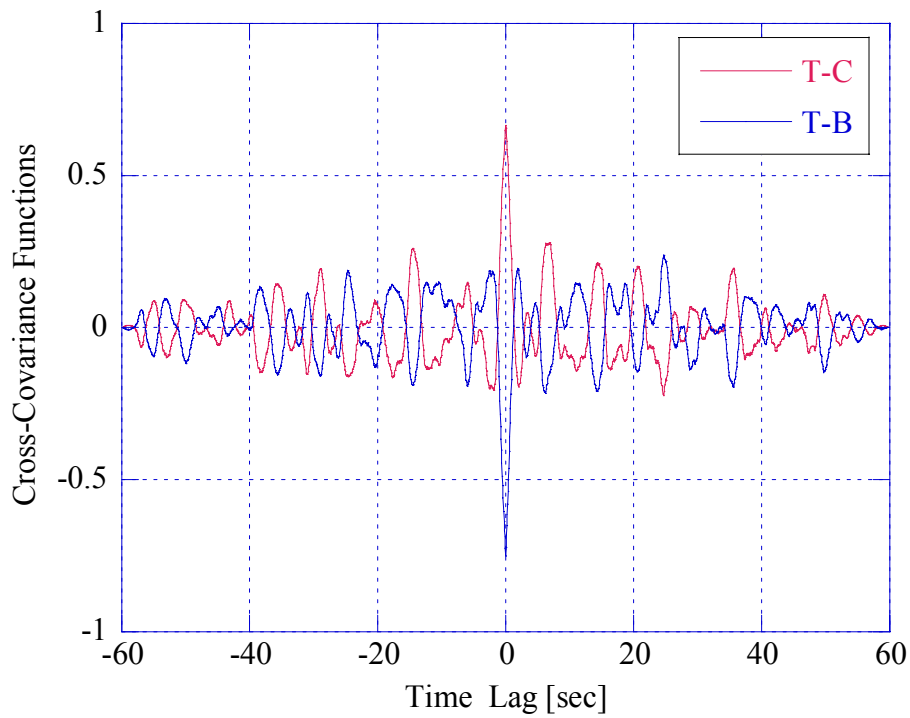


**Figure 1.91** - Texture-centroid and texture-bandwidth cross-covariance, VH pol., 26<sup>th</sup> range cell, per. sym.

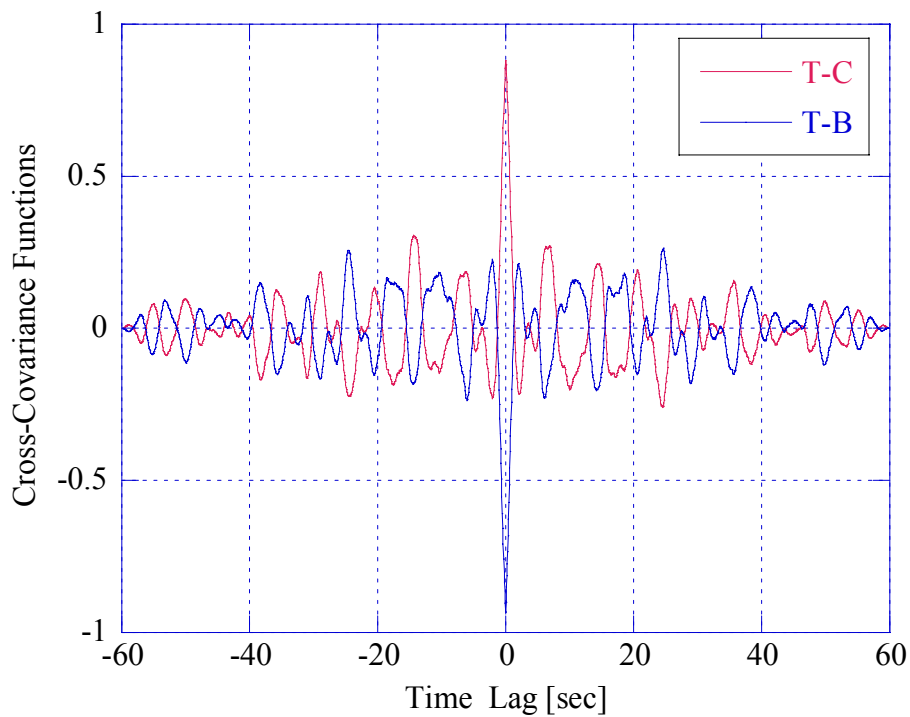


**Figure 1.92** - Log-texture-centroid and Log-texture-bandwidth cross-covariance, VH pol., 26<sup>th</sup> range cell.

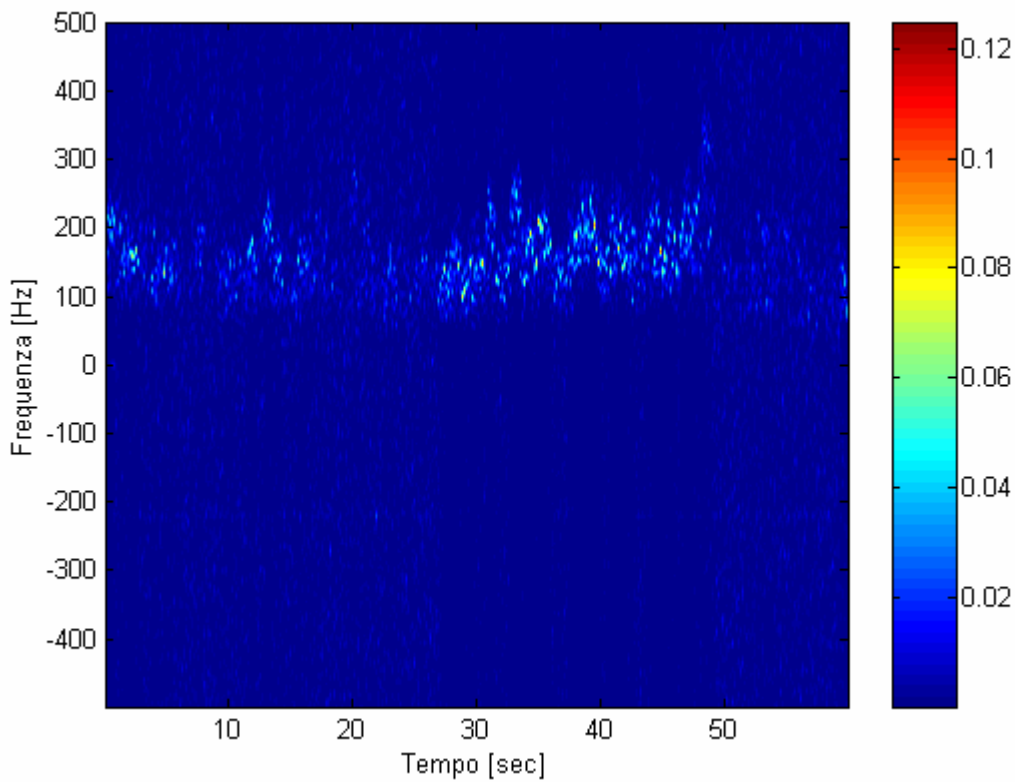


**Figure 1.93** - Normalized spectrum versus time, VH pol., 1<sup>st</sup> range cell. (CNR=5 dB)

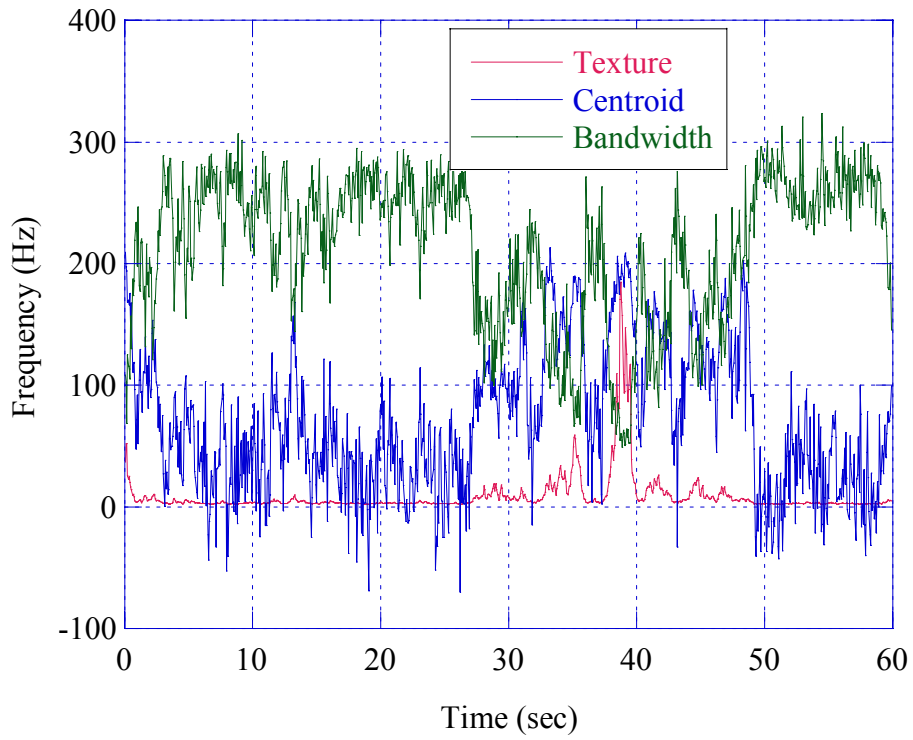


**Figure 1.94** - Time evolution of texture, centroid and bandwidth, VH pol., 1<sup>st</sup> range cell.

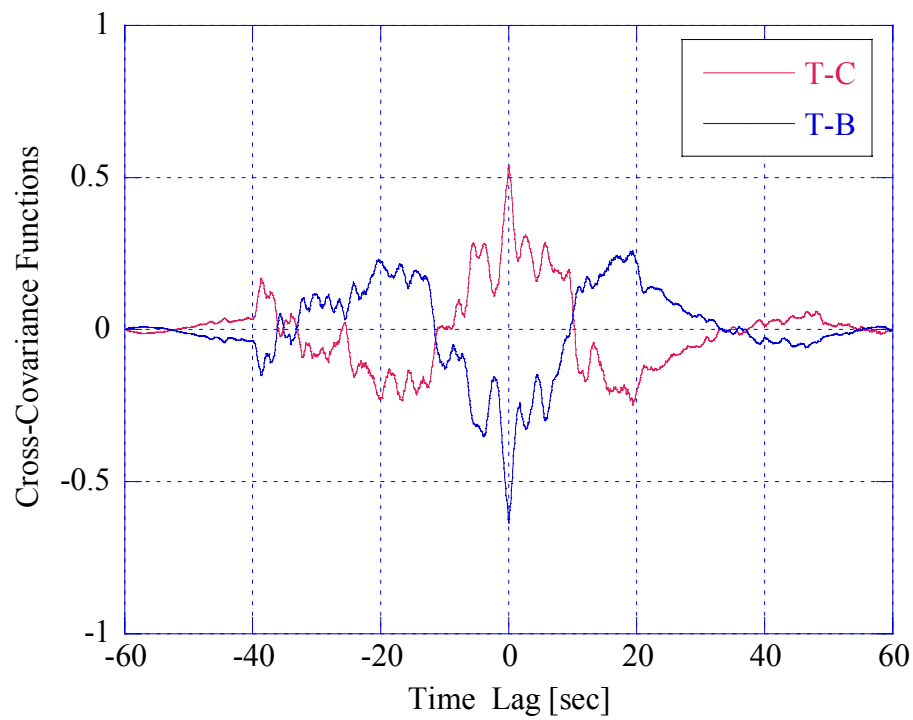


**Figure 1.95** - Texture-centroid and texture-bandwidth cross-covariance, VH pol., 1st range cell., aper. sym.

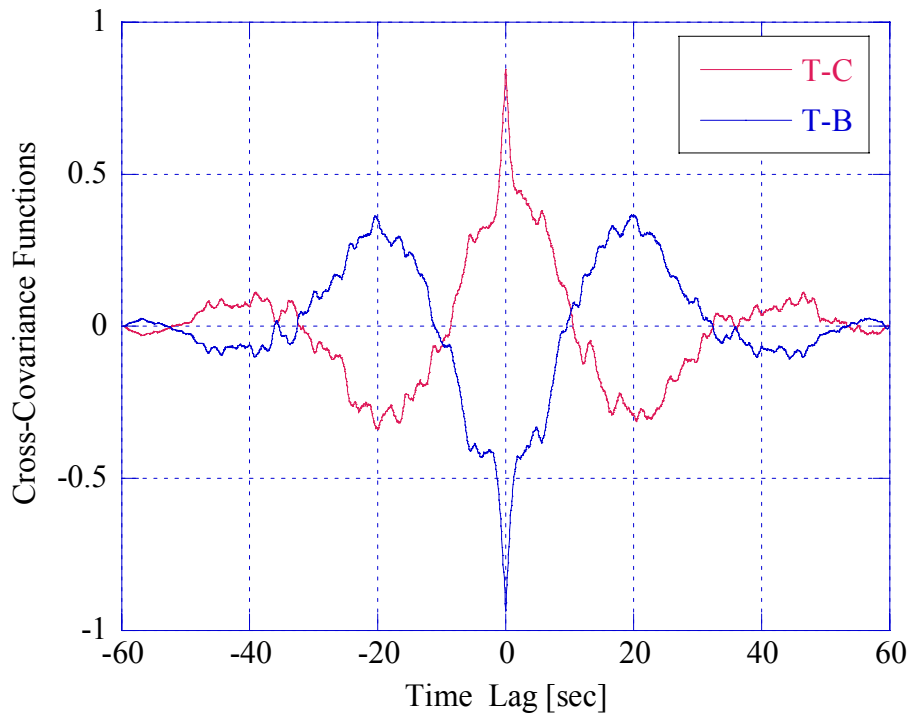


**Figure 1.96** - Log-texture-centroid and Log-texture-bandwidth cross-covariance, VH pol., 1<sup>st</sup> range cell.

### 1.2.6 Range resolution of 3 m

In this resolution, thermal noise usually overcomes the clutter, and then texture, centroid and bandwidth are almost always relating to the noise. Looking at spectrograms (Figs. 1.97, 1.101, and 1.105), we can observe that the power density is quasi-uniform on the entire frequency range; clutter contribution is sporadic and is confined in the range [100, 300] Hz. The trend in the behavior of texture, centroid, and bandwidth is the same; when texture decreases the noise is dominant then the centroid is close to zero and the bandwidth is large. In the cross-covariances the periodicities tend to disappear and their shape tends to a delta (see Figs. 1.99, 1.100, 1.104, 1.105, 1.107 and 1.108).

The cells are classified in Table 1.5. They are all aperiodical symmetrical cells.

	<b>Periodical Symmetrical</b>	<b>Periodical Asymmetrical</b>	<b>Aperiodical Symmetrical</b>
Pol. VV	—	—	All
Pol. HH	—	—	All
Pol. VH	—	—	All

**Table 1.5** – Covariance classification, 3 m.

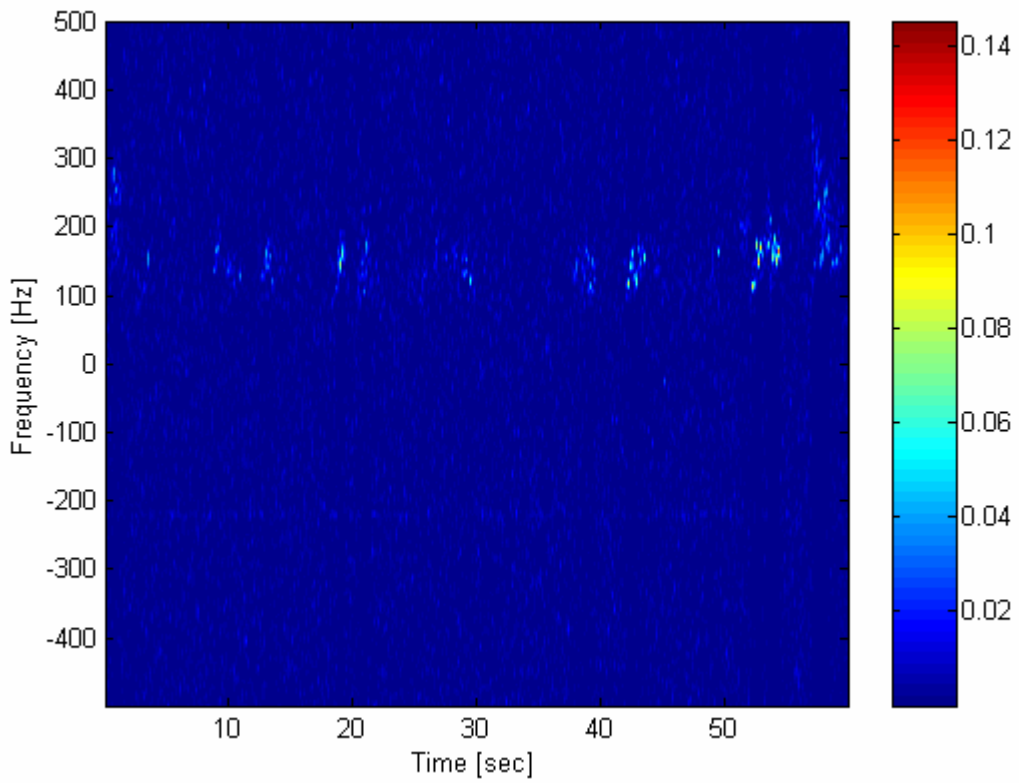


**Figure 1.97** - Normalized spectrum versus time, VV pol., 8<sup>th</sup> range cell. (CNR=3 dB)

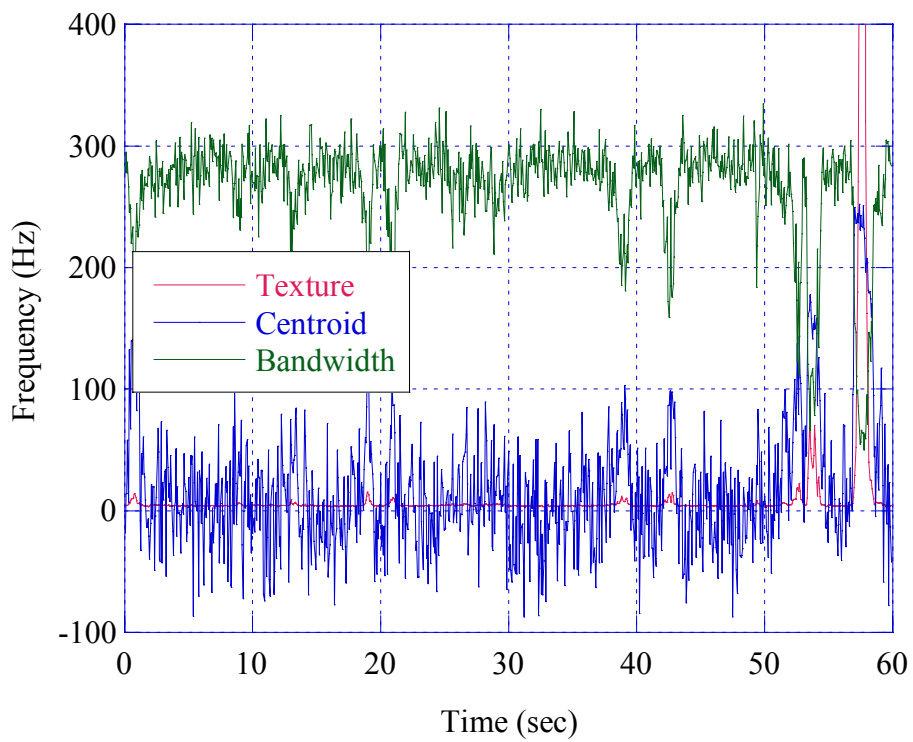


**Figure 1.98a** - Time evolution of texture, centroid and bandwidth, VV pol., 8<sup>th</sup> range cell.

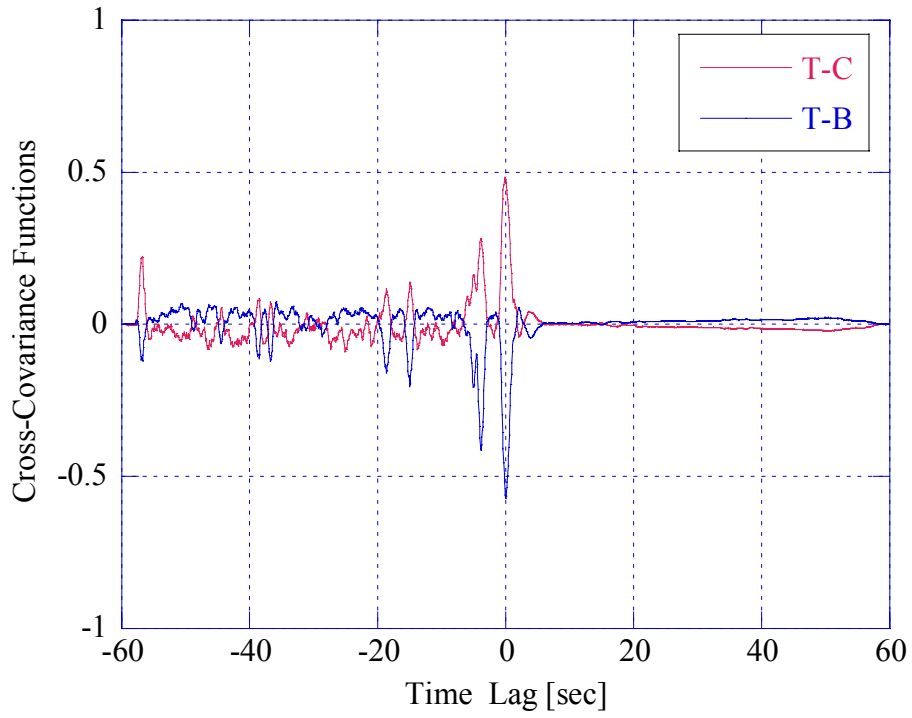


**Figure 1.99** - Texture-centroid and texture-bandwidth cross-covariance, VV pol., 8<sup>th</sup> range cell., aper. sym.

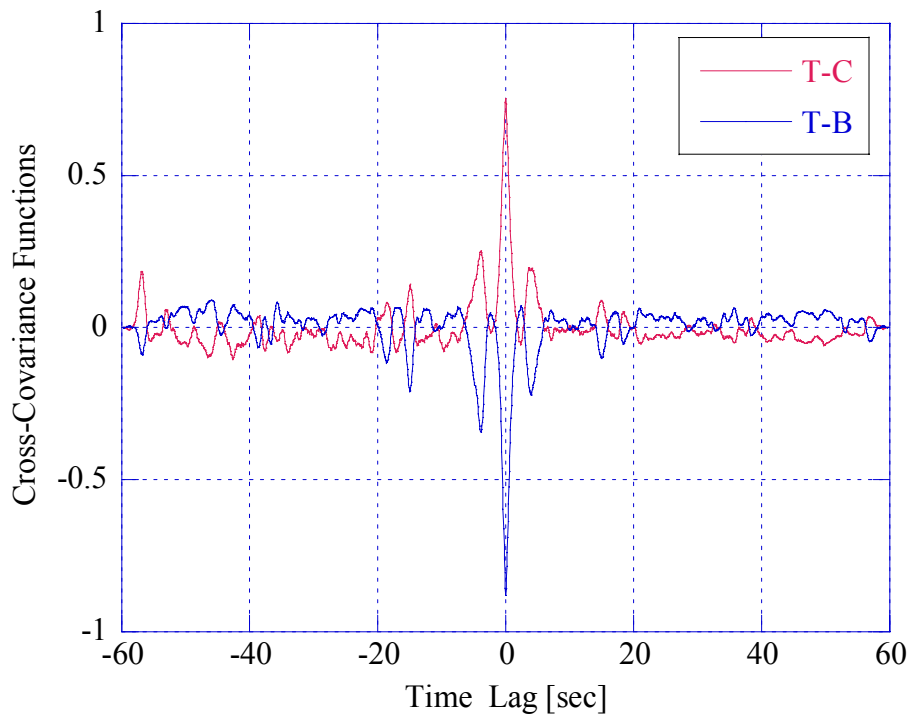


**Figure 1.100** - Log-texture-centroid and Log-texture-bandwidth cross-covariance, VV pol., 8<sup>th</sup> range cell.

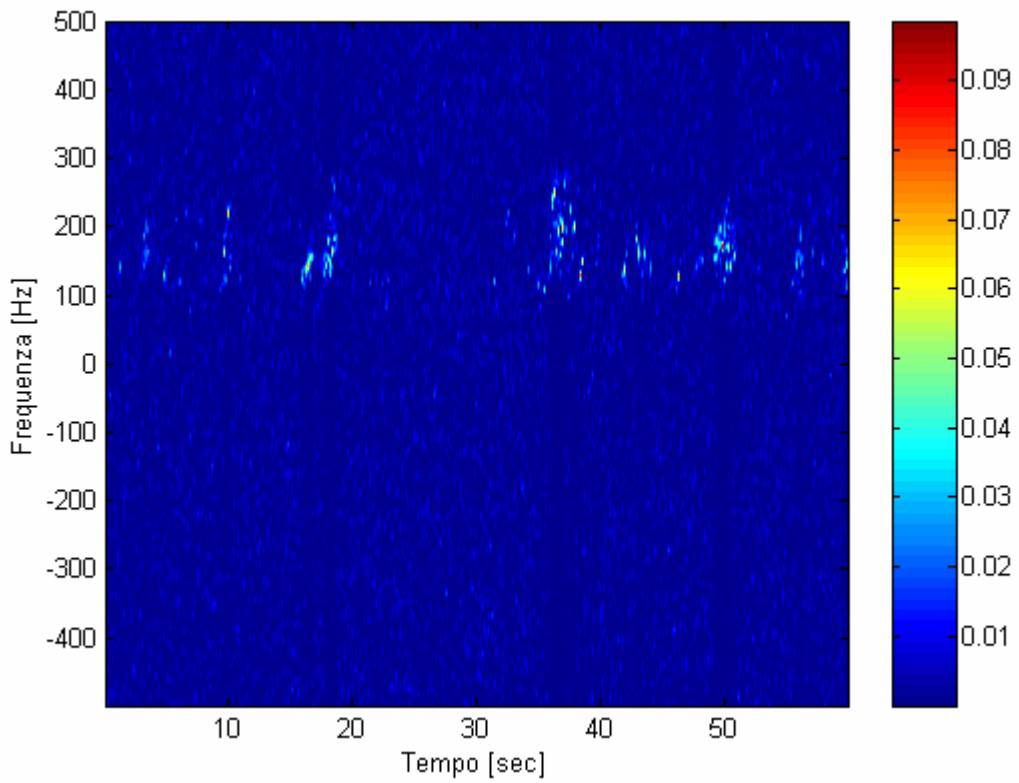


**Figure 1.101** - Normalized spectrum versus time, HH pol., 1<sup>st</sup> range cell. (CNR=-2 dB)

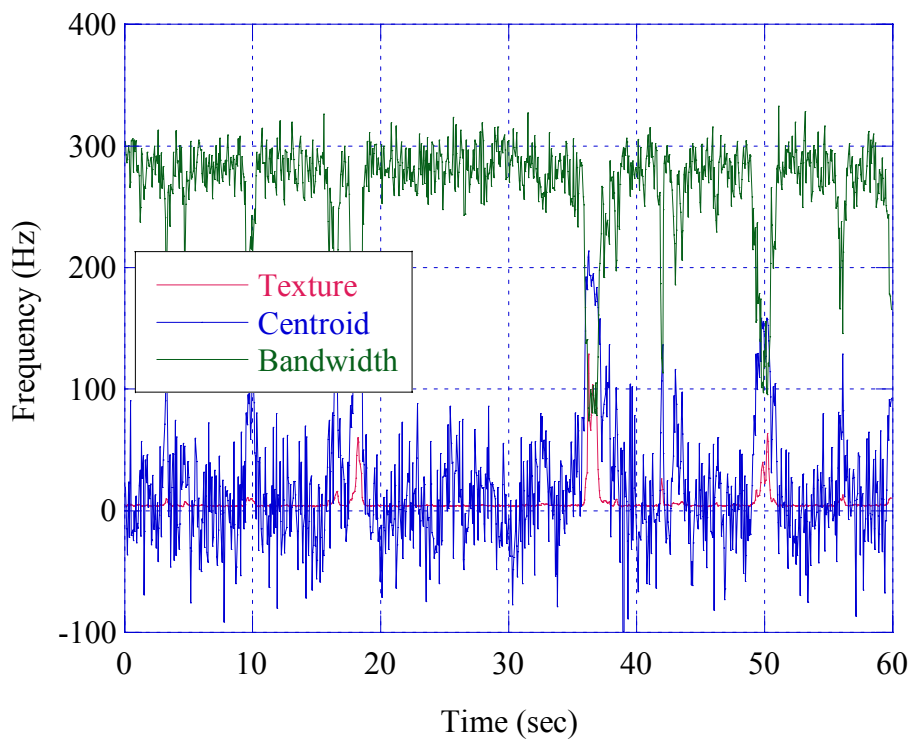


**Figure 1.102** - Time evolution of texture, centroid and bandwidth, HH pol., 1<sup>st</sup> range cell.

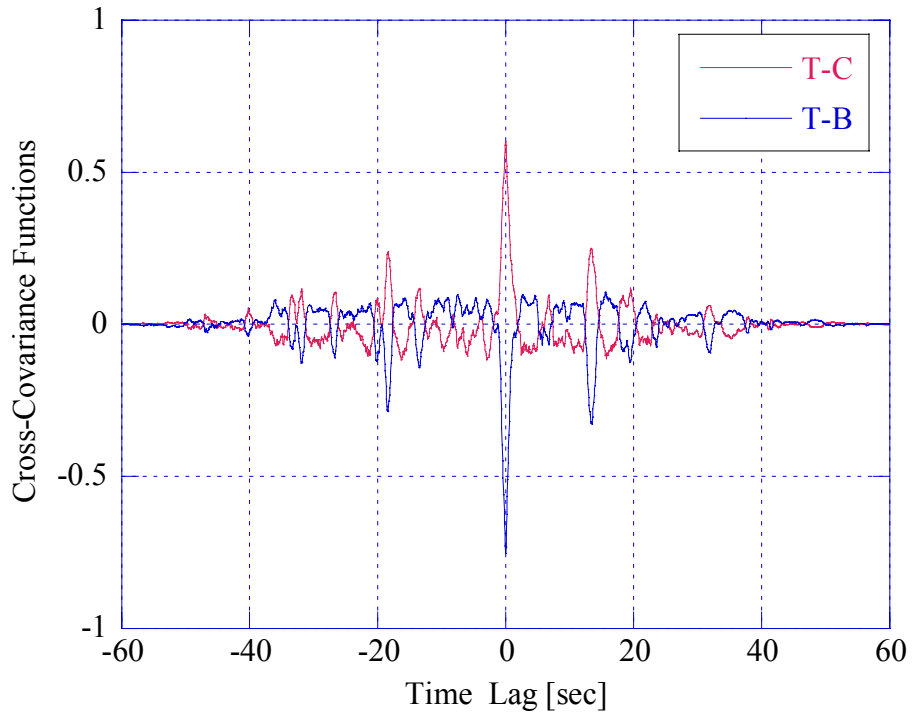


**Figure 1.103** - Texture-centroid and texture-bandwidth cross-covariance, HH pol., 1st range cell., aper. sym.

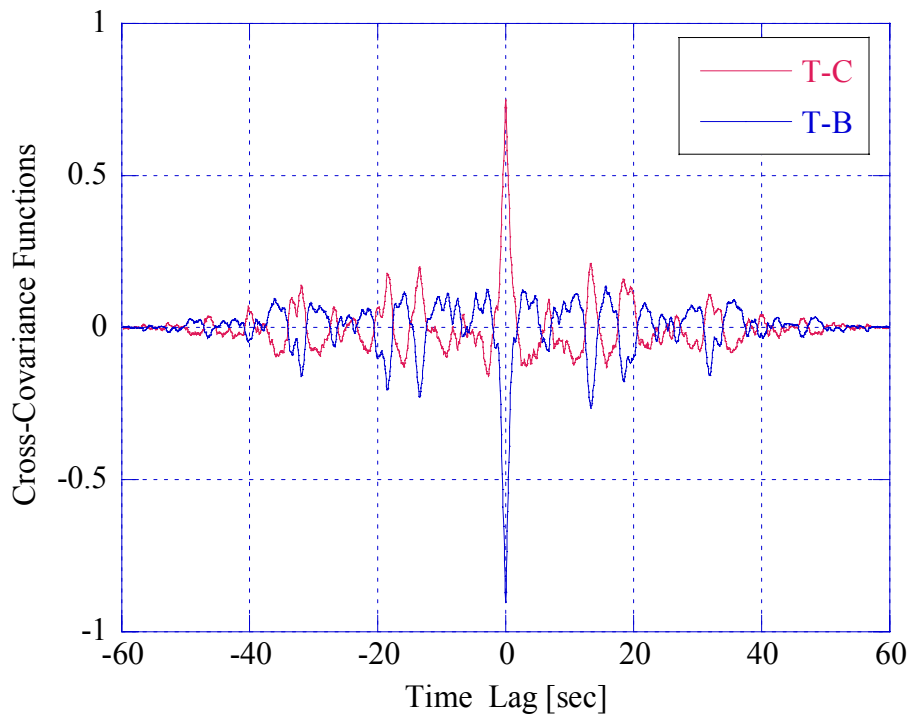


**Figure 1.104** - Log-texture-centroid and Log-texture-bandwidth cross-covariance, HH pol., 1<sup>st</sup> range cell.

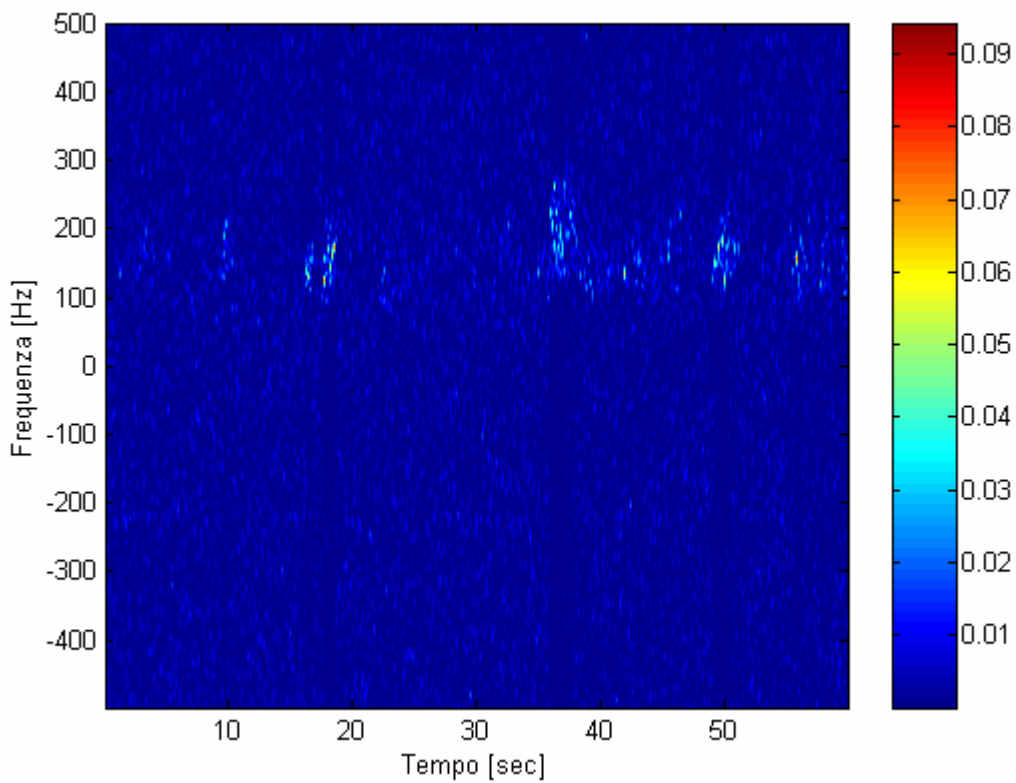


**Figure 1.105** - Normalized spectrum versus time, VH pol., 1<sup>st</sup> range cell. (CNR=-2 dB)

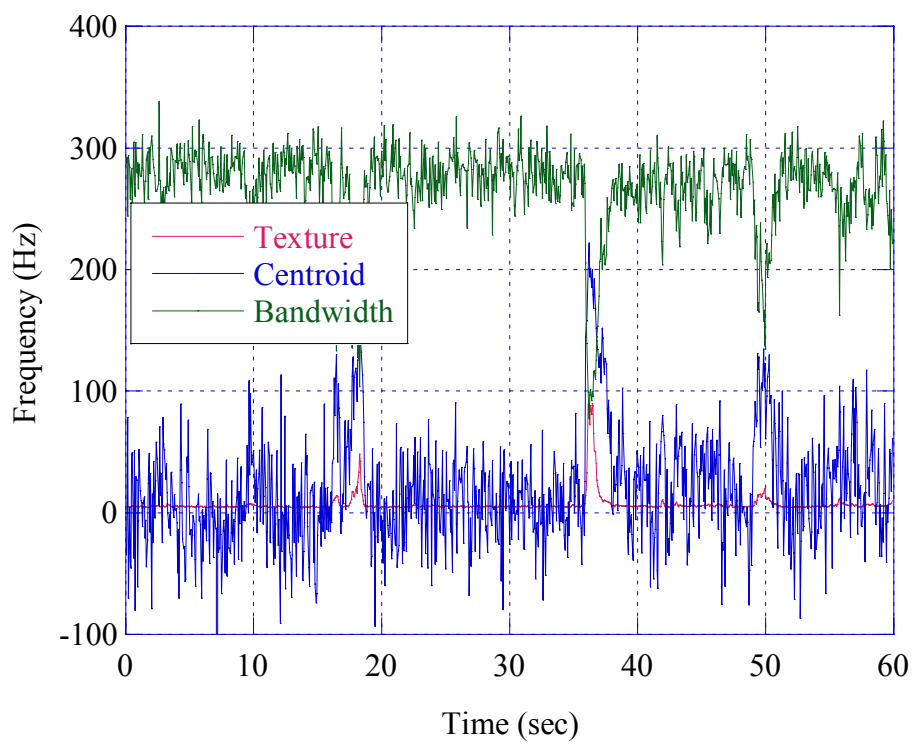


**Figure 1.106** - Time evolution of texture, centroid and bandwidth, VH pol., 1<sup>st</sup> range cell.

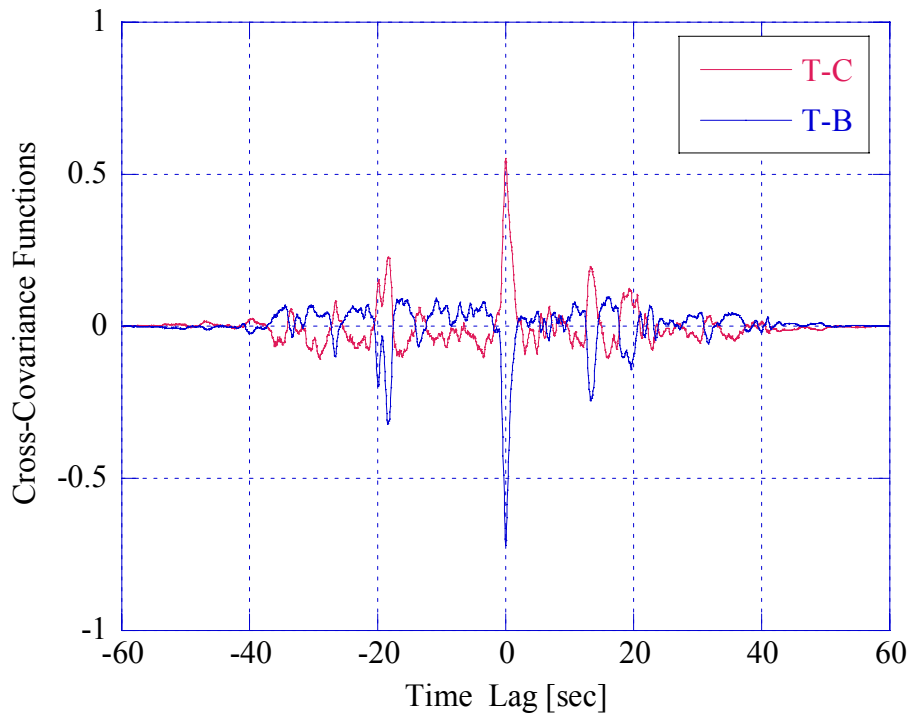


**Figure 1.107** - Texture-centroid and texture-bandwidth cross-covariance, VH pol., 1<sup>st</sup> range cell., aper. sym.

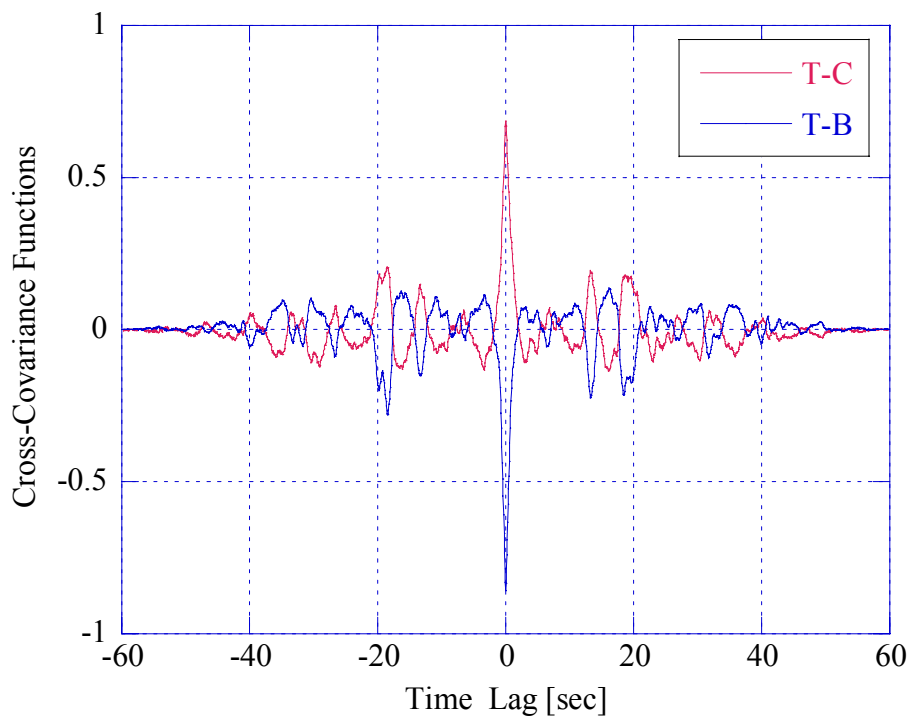


**Figure 1.108** - Log-texture-centroid and Log-texture-bandwidth cross-covariance, VH pol., 1<sup>st</sup> range cell.

### 1.3 Conclusions

In the first part of the technical report [Gin05], we modeled the received clutter signal as a compound stationary process, but thinking more deeply to the reflection phenomena that originate the received signal, it is easy to realize that the received clutter characteristics depend on the sea surface conditions in a certain temporal range, thus the clutter process cannot be stationary if the observation time is long and the resolution is high. Then, in this second part of the technical report, we investigated on the non-stationarities of the clutter process and on their effect on the time-varying clutter spectrum as a function of different range resolutions. In particular, we studied the influence of long waves on sea clutter by estimating texture, Doppler centroid and bandwidths on short time intervals. We analyzed as well the relations between texture, centroid and bandwidth by estimating their cross-covariances functions.

Figures reporting the clutter spectrograms show that the clutter is mostly concentrated between 100 Hz e 300 Hz for each polarization in each resolution. Generally, for all the estimated parameters there are not big differences among the polarizations. The differences are evident for different resolutions.

Based on the shape of the cross-correlation function between texture, centroid and bandwidth, the cells have been classified into three principal groups: **periodical symmetrical**, **aperiodical symmetrical** and **periodical asymmetrical**.

Many of the analyzed cells at **60 m** and **30 m** belong to the periodical symmetrical group and they exhibit a period of 6-7 sec. For the symmetrical cells (periodical and aperiodical) the typical behavior seems to be always the same: as clutter power increases, Doppler centroid increases and bandwidth decreases. Then we can conclude that the long-waves (with different periods) modulate in amplitude the scattering causing the changes in the texture values and modulate in frequency the clutter determining the movement of the Doppler centroid and the changes in the bandwidth. The maximum values of the texture are reached when the velocity of the sea surface is maximum (high values of the Doppler centroid), generally on the crest of the waves. On the contrary, the bandwidth is minimum. This behavior is still very clear at a resolution of **15 m** where we observe a shorter periodicity in the cross-covariances. The period is 4-5 sec long. At this resolution, we observed also larger variation of the centroid and of the bandwidth. This phenomenon could partially depend on the thermal noise effect; some reported spectrograms show the presence of thermal noise through vertical lighter bands. But, more likely, it is due to a

stronger non-homogeneity of the clutter relating to higher resolution. The larger the range cell, the heavier the averaging effect on time-varying phenomena. With higher resolutions, the local changes are more evident. Moreover, in some cell where the periodicity seems to disappear in the cross-covariances it is clear in the Log- covariances, that is the covariances with the Log-texture instead of the texture. The physical meaning of this phenomenon is not clear but seems that the periodic behavior is more related to the logarithm of the texture than to the texture itself.

For higher resolutions (**9 and 3 m**) the effect of the noise is not more negligible and usually the estimated parameters relate to the noise and not to the clutter. The periodicities tend to disappear and the cross-covariances to get lower and delta shaped.

## References

- [Bar96] Barnard T.J., Weiner D.D. "Non-Gaussian Clutter Modeling with Generalized Spherically Invariant Random Vectors," *IEEE Trans. on Signal Processing*, Vol. 44, No. 10, October 1996.
- [Bas68] Bass F.G., Fuks I.M., Kalmykov A.E., Ostrovsky I.E., Rosenberg A.D., "Very high frequency radiowave scattering by a disturbed sea surface," *IEEE Trans. on Antennas and Propagation*, AP-16, pp. 554-568, 1968.
- [Con87] Conte E., Longo M., "Characterisation of Radar Clutter as a Spherically Invariant Random Process," *IEE Proceedings-F*, Vol. 134, No. 2, pp. 191 -197, April 1987.
- [Far97] Farina A., Gini F., Greco M., Verrazzani L., "High Resolution Sea Clutter Data: A Statistical Analysis of Recorded Live Data," *IEE Proceedings-F*, Vol. 144, No. 3, pp. 121-130, June 1997.
- [Gin95] Gini F., Greco M., Verrazzani L., "Detection Problem in Mixed Clutter Environment as a Gaussian Problem by Adaptive Pre-Processing," *Electronics Letters*, Vol.31, No.14, pp. 1189-1190, July 1995.
- [Gin99] Gini F., Greco M., "A Suboptimum Approach to Adaptive Coherent radar Detection in Compound-Gaussian Clutter," *IEEE Trans. on Aerospace and Electronic Systems* Vol. 35, No. 3, pp. 1095-1104, July 1999.
- [Gin01] Gini F., Greco M., "Texture modeling and validation using recorded high resolution sea clutter data," *Proc. of the 2001 IEEE Radar Conference*, pp. 387-392, May 2001.
- [Gin02] Gini F., Greco M., "Texture modelling, estimation and validation using measured sea clutter data," *IEE Proc.-Radar Sonar Navig.*, Vol. 149, No. 3, June 2002.
- [Gin05] Gini F., Greco M., Rangaswamy M., "*Statistical analysis of real polarimetric clutter data at different range resolution. Part I: Non-Stationarity analysis*", Technical Report, AFOSR grant FA8655-04-1-3059, University of Pisa, Italy, April 2005.
- [Gre04] M. Greco, F. Bordoni, F. Gini, "X-band Sea Clutter Non-Stationarity: The influence of Long Waves," *IEEE Journal on Ocean Engineering*, Special Issue

- on “Non-Rayleigh Reverberation and Clutter”, special issue, Vol.29, No. 2, April 2004, pp.269-283.
- [Hay02] Haykin S., Bakker R., Currie B.W., “Uncovering Nonlinear Dynamics - The Case Study of Sea Clutter,” *Proceedings of the IEEE*, Vol. 90, No. 5 , pp. 860 - 881, May 2002.
- [Jes91] Jessup A.T., Melville W.K., Keller W.C., “Breaking Waves Affecting Microwave Backscatter. 1. Detection and Verification,” *J. Geophysical Research*, Vol.96, No.C11, pp. 20547-20559, November 1991.
- [Noh91] Nohara T., Haykin S., “Canadian East Coast radar trials and the K-distribution,” *IEE Proceedings-F*, Vol. F138, No. 2, pp. 80-88, 1991.
- [Pla83] Plant W.J., Keller W.C., “The Two-Scale Radar Wave Probe and SAR Imagery of the Ocean,” *Journal of Geophysical Research*, Vol.88, No. C14, pp. 9776-9784, November 20, 1983.
- [Pla90] Plant W.J., Keller W.C., “Evidence of Bragg Scattering in Microwave Doppler Spectra of Sea Return,” *Journal of Geophysical Research*, Vol.95, No. C9, pp. 16299-16310, Sept. 15, 1990.
- [Ran93] Rangaswamy M., Weiner D.D., Ozturk A., “Non-Gaussian vector identification using spherically invariant random processes,” *IEEE Trans. on Aerospace and Electronic Systems*, vol. 29, No. 1, pp. 111-124, January 1993.
- [Ran95] Rangaswamy M., Michels J.H., Weiner D.D., “Multichannel detection algorithm for correlated non-Gaussian random processes based on innovations,” *IEEE Trans. on Signal Processing*, vol. 43, No. 8, pp. 1915-1922, August 1995.
- [Ran97] Rangaswamy M., Michels J.H., “A parametric multichannel detection for correlated non-Gaussian random processes,” *Proc. of the National Radar Conference*, pp. 349-354, Syracuse, NY, USA, May 1997.
- [Ran98] Rangaswamy M., Michels, J.H., “Adaptive signal processing in non-Gaussian noise backgrounds,” *Proc. of the 9th IEEE-SSAP Workshop*, Portland, OR, September 1998.
- [Rin97] Rino C.L., Eckert E., Siegel A., Webster T., Ochadlick A., Rankin M., Davis J., “X-Band Low-Grazing-Angle Ocean Backscatter Obtained During LOGAN 1993,” *IEEE Journal of Oceanic Engineering*, Vol. 22, No. 1, pp. 18-26, January 1997.

- [Roz96] Rozenberg A.D., Quigley D.C., Melville W.K., "Laboratory Study of Polarized Microwave Scattering by Surface Waves at Grazing Incidence: The Influence of Long Waves," *IEEE Trans. on Geoscience and Remote Sensing*, Vol.34, No. 6, pp. 1331-1342, November 1996.
- [San99] Sangston K. J., Gini F., Greco M.V., Farina A., "Structures for Optimum and Suboptimal Coherent Radar Detection in Compound-Gaussian Clutter," *IEEE Trans. on Aerospace and Electronic Systems*, Vol. 35, NO. 2, pp. 445-458, April 1999.
- [The92] Therrien C.W., "*Discrete Random Signals and Statistical Signal Processing*", Prentice Hall, Englewood Cliffs, NJ 07632, 1992
- [Tri85] Trizna D.B., "A Model for Doppler Peak Spectral Shift for Low Grazing Angle Sea Scatter," *IEEE Journal of Oceanic Engineering*, Vol. 10, No. 4, pp. 368-375, October 1985.
- [Val78] Valenzula G. R., "Theories for the interaction of electromagnetic waves and oceanic waves - A review," *Bound. Layer Meteorol.*, Vol.13, No. 1-4, pp. 61-65, 1978.
- [Wal00] Walker D., "Experimentally motivated model for low grazing angle radar Doppler spectra of the sea surface," *IEE Proceedings, Radar, Sonar and Navigation*, Vol. 147, No. 3, pp. 114 -120, Jun 2000.
- [Wal01] Walker D., "Doppler modelling of radar sea clutter," *IEE Proceedings, Radar, Sonar and Navigation*, Vol. 148, No. 2, April 2001.
- [War90] Ward K. D., Baker C. J., Watts S., "Maritime surveillance radar. Part I: Radar scattering from ocean surface," *IEE Proceedings-F*, Vol. 137, No. 2, pp. 51-62, April 1990.
- [Wri68] Wright J.W., "A new model for sea clutter," *IEEE Trans. on Antennas and Propagation*, Vol. AP-16, pp. 217-223, 1968.